



# Otx2-glycosaminoglycan interaction to regulate visual cortex plasticity

Clémence Françoise Bernard

## ► To cite this version:

Clémence Françoise Bernard. Otx2-glycosaminoglycan interaction to regulate visual cortex plasticity. Neurons and Cognition [q-bio.NC]. Université Pierre et Marie Curie - Paris VI, 2014. English. NNT : 2014PA066228 . tel-01084780

**HAL Id: tel-01084780**

**<https://theses.hal.science/tel-01084780>**

Submitted on 20 Nov 2014

**HAL** is a multi-disciplinary open access archive for the deposit and dissemination of scientific research documents, whether they are published or not. The documents may come from teaching and research institutions in France or abroad, or from public or private research centers.

L'archive ouverte pluridisciplinaire **HAL**, est destinée au dépôt et à la diffusion de documents scientifiques de niveau recherche, publiés ou non, émanant des établissements d'enseignement et de recherche français ou étrangers, des laboratoires publics ou privés.

# THÈSE DE DOCTORAT DE L'UNIVERSITÉ PARIS VI ÉCOLE DOCTORALE CERVEAU-COGNITION-COMPORTEMENT

présentée par Mlle Clémence BERNARD

---

## Otx2-GLYCOSAMINOGLYCAN INTERACTION TO REGULATE VISUAL CORTEX PLASTICITY

---

soutenance le 26 septembre 2014

### COMPOSITION DU JURY

Pr Alain Trembleau  
Pr Thomas Bourgeron  
Dr Sonia Garel  
Dr Michela Fagiolini  
Dr Alberto Bacci  
Dr Fabienne Poulain  
Pr Alain Prochiantz  
Dr Ariel Di Nardo

Président  
Rapporteur  
Rapporteur  
Examineur  
Examineur  
Examineur  
Examineur  
Directeur de thèse



*We are yet but young in deed.*  
Shakespeare



## MANY MANY THANKS TO...

... all the members of my thesis defense committee for having accepted to be part of this board of examiners, especially my two rapporteurs Sonia Garel and Thomas Bourgeron for taking time to read and evaluate my thesis.

... Alain Prochiantz, for believing in my GAG enthusiasm - thank you for having given me the opportunity to work on this deliciously sweet project! Your unfailing optimism is probably the best thing you taught me. Working with you has confirmed my aspiration to work in research, especially on this monstrous organ with its “900 cm<sup>3</sup> de trop”!

... Ariel Di Nardo, for his constant kindness and enthusiasm. Thank you for teaching me so much and advising and supporting me in the sugar struggle! I really enjoyed working with you during these 4 years, and I am glad we still have one more year to plot many other cool experiments!

... our collaborators: Takao Hensch and Hing Cheong Lee, Jin Woo Kim and Hyoun-Tai Kim, Serge Picaud and Manuel Simonutti, Jean-Maurice Mallet and Guillaume Despras, James Fawcett and Jessica Kwok, Linda Hsieh-Wilson and Greg Miller, and Antonio Simeone and Dario Acampora.

... all the people in the lab I have closely worked with: Anthony, a great team-mate in the sugar project, Raoul for the retina work, Clémentine and Eva for the scFv study and Marine for her help when I arrived in the lab.

... all the team leaders of the lab for fruitful scientific discussions: Ken Moya, Alain Joliot, Rajiv Joshi, Sophie Vriz, with special thanks to Michel Volovitch, for his constant thoughtfulness.

... all current and former members of the bureau C1.10, for the laughter, the indignation, all the craziness and of course for helping with the dilutions!

... all current and former members of the Prochiantz, Joliot and Vriz labs, for making work in the lab a real pleasure, especially my Zig-Zag partners: Thibault, Raoul, Anabelle, Clémentine, Anne-Cécile, François-Xavier, Tiphaine, Valérie, François, ...

... my parents, for their love and permanent support. And other members of my family: all the MDs and PhDs for paving my way into research; and especially my great-aunt Pierrette Rosset for her indescribable kindness.

... my dear friends, Delphine, Marie, Gratiannie; and Yijie, Agnès, Camille, Lise, Jules, Yohann, Agathe and Clémence, for ensuring my survival outside the lab!

... Ludwig, Richard, Wolfgang, Franz, Gustav, Robert, Gioacchino, Giuseppe, Jacques, Henry and Claudio, for so many great evenings!

... and a very special thanks to Otx2, for actually being in the cerebral cortex :)



# SUMMARY

LIST OF ILLUSTRATIONS	1
<b>INTRODUCTION</b>	<b>5</b>
I. Homeoproteins	9
A. Homeoproteins as classical transcription factors	9
B. Homeoproteins Otx1 and Otx2 and their roles in brain and eye development	10
C. Homeoproteins unconventional intercellular transfer	11
D. Homeoproteins as signaling proteins with <i>in vivo</i> roles	16
II. Glycosaminoglycan	17
A. Glycosaminoglycan structures	17
B. Glycosaminoglycan biosynthesis	19
C. Glycosaminoglycan interaction with morphogens and growth factors	22
D. Glycosaminoglycans in the postnatal brain	25
III. Critical period plasticity	27
A. Critical periods	27
B. Cellular and molecular mechanisms of cortical plasticity	29
C. Reopening plasticity in the adult	33
IV. Otx2 homeoprotein and visual cortex plasticity	35
A. Otx2 transfer in the visual cortex during the critical period	35
B. Otx2 transfer in the adult consolidated visual cortex	37
<b>MATERIALS AND METHODS</b>	<b>43</b>
I. Plasmid and proteins	45
II. Animals	45
III. Cell culture	48
IV. Animal experiments	49
V. Cerebrospinal fluid sampling	51
VI. Cell surface biotinylation	51
VII. Western blot	53
VIII. RNA extraction and deep sequencing	53
IX. Immunohistochemistry	53
X. Glycosaminoglycan experiments	54
XI. Statistical analysis	58



<b>RESULTS AND DISCUSSION</b>	<b>61</b>
I. Otx2 transgenic mice to investigate Otx2 transfer roles in the visual system	63
A. Otx2-AA protein activity	63
B. Otx2 activity in eye development and maintenance	65
C. Otx2 GAG-binding motif has a role in critical period timing	77
D. Towards the identification of targets of Otx2 in the visual cortex	85
Discussion	89
II. Identifying Otx2-binding GAGs	97
A. Otx2-binding GAGs in the cortex	97
B. GAG-binding homeoproteins: Engrailed2 versus Otx2	105
Discussion	107
III. Tools for disrupting Otx2 transfer in the visual cortex	113
A. A synthetic CS-E hexasaccharide interferes with Otx2 cortical transfer	113
B. Blocking Otx2 transfer in vivo in a single chain antibody mouse	116
Discussion	123
<b>CONCLUSION AND PERSPECTIVES</b>	<b>129</b>
I. Otx2, a master regulator of cortical plasticity?	131
II. Otx2-GAG interaction, from the source to the cortex?	136
<b>REFERENCES</b>	<b>141</b>





## LIST OF ILLUSTRATIONS

Figure 1. Antennapedia mutation in <i>Drosophila</i>	8
Figure 2. Homeodomain - DNA interaction	8
Figure 3. Otx2 homeoprotein in the adult retina	12
Figure 4. Engrailed2 homeoprotein is transferred between cells <i>in vitro</i>	12
Figure 5. Model for homeoprotein intercellular transfer	14
Figure 6. Typical glycosaminoglycan disaccharide units	18
Figure 7. Heparan sulfate and chondroitin sulfate chain modifications	18
Figure 8. Typical sulfation pattern of chondroitin sulfate disaccharides	20
Figure 9. Perineuronal net model	24
Figure 10. Ocular dominance and monocular deprivation in the binocular visual cortex	28
Figure 11. Maturation of inhibition controls critical period timing	28
Figure 12. Local GABA circuits and molecular factors for critical period plasticity	30
Figure 13. Otx2 regulates PV-cell maturation	34
Figure 14. Otx2 regulates the timing of the critical period for ocular dominance plasticity	34
Figure 15. The capture of Otx2 by PV-cells involves PNNs	36
Figure 16. A GAG-binding motif within Otx2 sequence	36
Figure 17. A two-threshold model for Otx2 regulation of cortical plasticity	38
Figure 18. Construct for single chain antibody knock-in mouse	46
Figure 19. Assessment of the transcriptional activity of Otx2-AA protein	62
Figure 20. <i>Otx2</i> mutants gross head and eye phenotypes	64
Figure 21. <i>Otx2</i> mutants visual acuity	66
Figure 22. <i>Otx2</i> mutants show functional deficits of photoreceptors and bipolar cells	66
Figure 23. <i>Otx2</i> mutants show functional deficits in the cone pathway	68
Figure 24. Eye and retina defects in <i>Otx2<sup>AA/AA</sup></i> mice	68
Figure 25. Otx2 dose- and age-related retinal thickness differences	70
Figure 26. Cell loss in the retina of <i>Otx2</i> mutants	72
Figure 27. Overall phenotype ranking	74
Figure 28. Mis-localisation of Otx2 protein in the visual cortex of <i>Otx2-AA</i> mice	76
Figure 29. Visual acuity of <i>Otx2-AA</i> mutants	78
Figure 30. Delayed PV and PNN expression in the visual cortex of <i>Otx2<sup>+/AA</sup></i> mice	78
Figure 31. Delayed onset and closure of critical period for plasticity in <i>Otx2<sup>+/AA</sup></i> mice	80
Figure 32. Critical period for tonotopic plasticity in auditory cortex of <i>Otx2<sup>+/AA</sup></i> mice	82
Figure 33. General information of layer IV deep sequencing in <i>Otx2</i> mutants	84
Figure 34. Examples of differentially regulated genes at P30 and P100 in <i>Otx2</i> mutants	84
Figure 35. Delayed PNN expression in the visual cortex of <i>Otx2<sup>+GFP</sup></i> mice	88
Figure 36. Critical period model for <i>Otx2</i> mutants	88
Figure 37. Both the RK-peptide and NterOtx2 protein bind to commercial CS-E	98
Figure 38. Full-length Otx2 binds preferentially to commercial CS-E	98
Figure 39. Full-length Otx2 binds to purified cortical GAGs	100
Figure 40. RK motif in homeoproteins	102
Figure 41. NterOtx2- and Engrailed2-binding GAGs on glycan microarrays	104
Figure 42. Homeoprotein-binding protects GAGs from digestion	106

Figure 43. CS-E analog synthesis plan	112
Figure 44. Otx2 binds to synthetic CS-E hexasaccharide	114
Figure 45. Otx2 binding to hexasaccharide interferes with Otx2 transfer <i>in vivo</i>	114
Figure 46. <i>scFvOtx2</i> and <i>scFvPax6</i> ear fibroblasts express and secrete scFv <i>in vitro</i>	118
Figure 47. Both scFv are expressed and secreted upon recombination <i>in vivo</i>	120
Figure 48. Anti-Otx2 scFv interferes with Otx2 transfer in visual cortex	122
Figure 49. Otx2 transfer, from choroid plexus to cortex, to regulated cortical plasticity	130
Figure 50. Tools and techniques to block Otx2 transfer	134
Table 1. Genotyping protocol	46
Table 2. Antibodies for Western blot, Dot blot and immunohistochemistry	52
Table 3. List of differentially regulated genes at P30 and P100 in <i>Otx2</i> mutants	86





# **INTRODUCTION**





Homeoproteins are a major class of transcription factors that exert some of their functions through non-cell autonomous activity, due to their ability to transfer between cells. Homeoprotein transfer has been demonstrated *in vivo* in various model systems, from drosophila to mice, for the homeoproteins Engrailed, Pax6 and Otx2. During mouse embryonic development, Otx2 is fundamental in controlling specification, maintenance and regionalization of the brain. In the postnatal and adult nervous system, Otx2 expression remains in choroid plexuses and along the visual system.

In the mouse postnatal brain, two types of glycosaminoglycans, heparan sulfates and chondroitin sulfates, are part of the perineuronal nets, a condensed extracellular matrix surrounding fast-spiking inhibitory parvalbumin interneurons. These interneurons mature during a critical period of postnatal development during which the cerebral cortex is "plastic". Cortical plasticity, which corresponds to a remodeling of connections in response to changes in the environment, is very limited outside critical periods. Among the identified molecular factors for plasticity in the visual cortex, Otx2 acts as a major extra-cortical signal for the maturation of inhibitory circuits: Otx2 transfer into the parvalbumin interneurons is necessary and sufficient to open the critical period at postnatal day 20 and close it 20 days later. Otx2, through its glycosaminoglycan-binding motif, binds the perineuronal nets at the surface of the parvalbumin cells to preferentially enter this sub-class of interneurons.

The arrival of Otx2 in the visual cortex throughout adulthood is needed to maintain its consolidated, non-plastic state. Plasticity can be reactivated in the adult by reducing inhibition or by lifting molecular brakes that limit excessive rewiring. Blocking Otx2 transfer in the adult visual cortex reopens a window of plasticity in the adult and this allows functional recovery of visually impaired mice. Previous studies in the laboratory on Otx2 and cortical plasticity are the foundation of my thesis project, which aims to understand how Otx2 interacts with the complex sugars at the surface of parvalbumin cells for critical period regulation. In this introduction I will first present homeoproteins and their unconventional intracellular transfer. I will then describe the diversity of glycosaminoglycans, their interactions with proteins and their roles in postnatal brain. The third and fourth parts of the introduction will report our current understanding of cortical plasticity during critical periods and Otx2 role in regulating this plasticity.

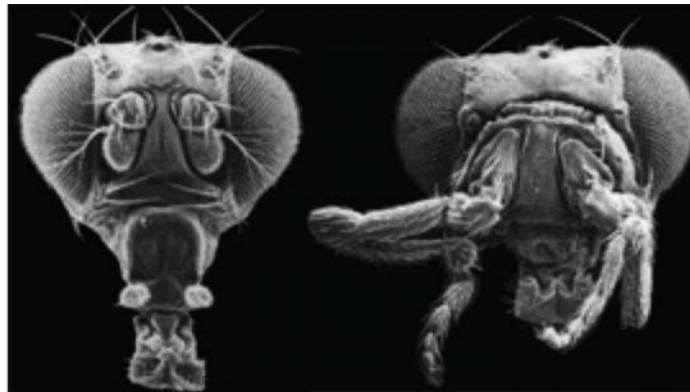


**Figure 1. Antennapedia mutation in Drosophila**

On the right panel is shown a Drosophila with the homeotic Antennapedia mutation: ectopic legs replace the antennae (compared to a normal Drosophila on the left).

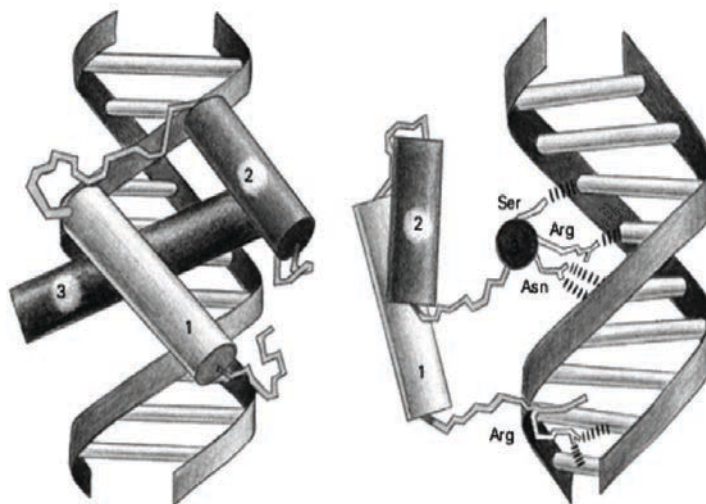


**Figure 2. Homeodomain - DNA interaction**

The homeodomain contains three well-defined  $\alpha$ -helices (represented by cylinders 1, 2 and 3). The third helix of the homeodomain contacts the major groove of the DNA. There are two additional sites of contact, between the first helix and the DNA backbone and between the flexible amino-terminal arm and bases in the minor groove.

## **I. HOMEOPROTEINS**

### **A. Homeoproteins as classical transcription factors**

Homeobox genes encode homeoproteins, a major class of transcription factors active throughout development and in the adult. Homeoproteins are key players within the genetic networks that lay out the body plan and regulate morphology and physiology at the cellular and multicellular levels.

In 1967, Gehring described in *Drosophila* the Antennapedia homeotic mutation in which antennae are replaced by ectopic legs (Figure 1) (Gehring, 1967). Homeotic mutations transform a body segment or part of this segment into the corresponding structures of another segment (Lewis, 1978). This dramatically modifies the body plan of the organism, indicating that the mutated elements probably represent regulator genes involved in the control of development. The structural analysis of the gene Antennapedia led to the identification of the homeobox, a small DNA fragment (180 base pairs long) characteristic of homeotic genes. The homeobox encodes a 60 amino acids domain called the homeodomain (McGinnis et al., 1984b). This homeodomain is highly conserved among pluricellular species, in metaphtyes and metazoans (Carrasco et al., 1984; Laughon and Scott, 1984; McGinnis et al., 1984a; Shepherd et al., 1984). The homeodomain is the DNA-binding domain of homeoprotein transcription factors. The homeodomain structure, first described for Antennapedia (Qian et al., 1989), is a compact globular structure and contains an unstructured N-terminal arm and three well-defined  $\alpha$ -helices arranged in a helix-loop-helix-turn-helix manner (Gehring et al., 1994). Helices 1 and 2 are anti-parallel and helix 3 is virtually perpendicular to the axis established by the first two helices (Billeter et al., 1993; 1990; Wolberger et al., 1991). Helix 3 is called "recognition helix" and contacts the major groove of the DNA (Figure 2). Other sites of contact with the DNA include one between helix 1 and the DNA backbone, and one between the flexible amino-terminal arm and bases in the minor groove (Otting et al., 1990).

During development, homeoproteins exert a wide array of functions, from embryonic polarity to cell migration and differentiation. They are of primary importance in the developing nervous system, which requires orchestrated morphogenetic events leading to stereotypic specification and patterning of the neuroectoderm. In mouse, most of the genes that regulate

developmental programs for brain morphogenesis are vertebrate homologs of *Drosophila* genes coding for signaling pathway molecules and transcription factors (Rubenstein et al., 1998; Tam and Behringer, 1997). Among them are the *Otx* genes (*Otx1* and *Otx2*), the murine homologs of *Drosophila* homeobox-containing gene orthodenticle (*Otd*) (Simeone et al., 1992; 1993). *Otx* homeoproteins are fundamental in controlling specification, maintenance and regionalization of the vertebrate brain.

### **B. Homeoproteins *Otx1* and *Otx2* and their roles in brain and eye development**

In *Drosophila*, mutations in *Otd* lead to the loss of anterior head segments where *Otd* is expressed (Cohen and Jürgens, 1991; Finkelstein and Perrimon, 1990; Hirth et al., 1995). In some cases, certain sensory structures are also lost, including the light sensing organs ocelli. In mouse embryos, *Otx1* and *Otx2* have a similar expression pattern to *Otd* and they are both expressed in sensory organs during development.

*Otx2* is transcribed in the entire visceral endoderm and epiblast before the onset of gastrulation (embryonic day (E) 5.5). As the primitive streak progresses, *Otx2* expression is gradually restricted to the anterior third of the embryo. At the end of gastrulation (E7.5), it is expressed in all three germ layers, especially the rostral neural plate which will give rise to the telencephalon, diencephalon and mesencephalon (Acampora et al., 2001). In the mouse embryo, *Otx1* is first expressed at E8.5 throughout the presumptive forebrain and midbrain epithelium (Simeone et al., 1992). During brain regionalization, *Otx1* and *Otx2* expression domains largely overlap. But while the expression of *Otx2* disappears from the dorsal telencephalon at E10.5, *Otx1* expression is maintained across the ventricular zone of the cortical anlagen from the onset of corticogenesis up to mid-late gestation stages (Simeone et al., 1993), in precursors of deep layers neurons (Frantz et al., 1994). This pattern coincides with *Otx1* postnatal expression in a subset of neurons located in cortical layers V and VI (Weimann et al., 1999). By late embryonic and early postnatal stages, *Otx2* expression becomes predominant in choroid plexuses and in areas of the brain involved in visual information processing: the retina, the lateral geniculate nucleus of the thalamus and the superior colliculus (Nothias et al., 1998).

Null mice for these two genes have been generated. *Otx1* null mice are viable, suffer from spontaneous epileptic seizures and exhibit abnormalities affecting primarily the telencephalic

cortex and the development of the visual and auditory sensory organs (Acampora et al., 1995). Brains from adult *Otx1*<sup>-/-</sup> mice show a dramatic reduction in cortical thickness and in cortical cell number, further underscoring a role for *Otx1* in forebrain development. During gastrulation, *Otx2* is expressed both in the cells producing signals that drive early specification and patterning of the neural plate (anterior visceral endoderm and axial mesendoderm) and in the cells responding to these instructive signals (epiblast and anterior neuroectoderm) (Ang et al., 1994; Simeone et al., 1993). *Otx2* null embryos therefore die early in embryogenesis because of their lack of rostral neuroectoderm. They also exhibit major defects in their body plan (Acampora et al., 1995; Ang et al., 1996; Matsuo et al., 1995). This illustrates the multifunctional role of Otx2 homeoprotein in gastrulation and in the regionalization of the rostral brain.

If *Otx2* complete deletion is lethal, *Otx2* heterozygous mice are viable and fertile and often present no gross abnormalities (Koike et al., 2007; Martinez-Morales et al., 2001). However, depending on the genetic background, retinal functions of *Otx2*<sup>+/-</sup> mice can be affected (Hide et al., 2002; Matsuo et al., 1995). Mutations in human *Otx2* cause severe ocular and retinal diseases such as microphthalmia and anophthalmia, with incomplete penetrance (Ragge et al., 2005; Schilter et al., 2011). Indeed, Otx homeoproteins play a major role in eye development. Retinal tissue derives from the neuroectoderm and, during embryonic and postnatal development (from E9 to postnatal day (P) 14), the multipotent retinal progenitor cells will give rise to the different cell types of the adult retina: photoreceptors, bipolar, horizontal, amacrine and retinal ganglion cells (Figure 3) (Bassett and Wallace, 2012). Among other transcription factors, many homeoproteins play a part in controlling these differentiation programs (Reese, 2011). *Otx2* is expressed in the mouse optic vesicle as early as E9 and overlapping expression of *Otx1* and *Otx2* is required to specify the retinal pigment epithelium at E9.5 (Martinez-Morales et al., 2001). At E12.5, photoreceptor and bipolar cell fates are determined by the expression of *Otx2* in retinal progenitor cells (Nishida et al., 2003). Expression of *Otx2* is then maintained throughout life in both photoreceptors and bipolar cells (Figure 3) (Fossat et al., 2007; Sugiyama et al., 2008).

### **C. Homeoproteins unconventional intercellular transfer**

Homeoproteins are traditionally defined as DNA-binding transcription factors but they also share activities that extend beyond their classical transcriptional role, especially intercellular

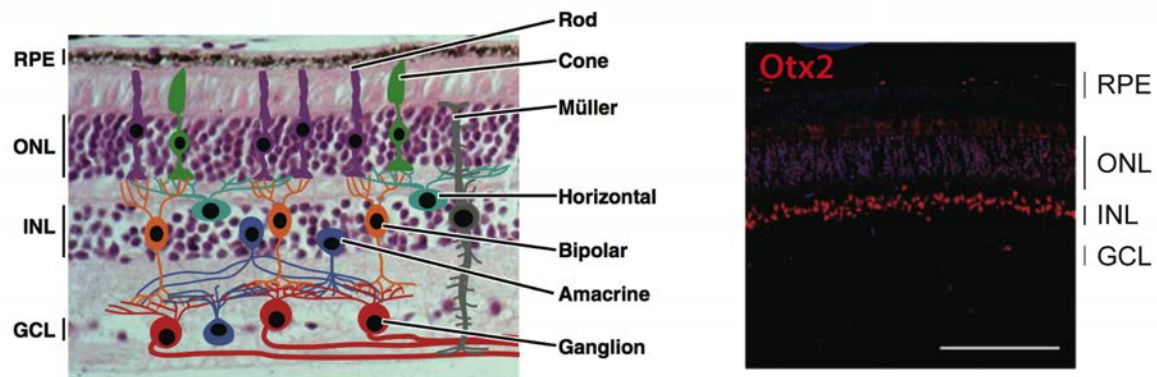


**Figure 3. Otx2 homeoprotein in the adult retina**

On the left panel are illustrated the layers and cell types of the mouse adult retina. The photoreceptor outer segments associate with the retinal pigmented epithelium (RPE), whereas their cell bodies reside in the outer nuclear layer (ONL). The inner nuclear layer (INL) contains the cell bodies of horizontal, bipolar, and amacrine cells, as well as Müller glia. The ganglion cell layer (GCL) contains the cell bodies of both ganglion and displaced amacrine cells (adapted from Bassett and Wallace, 2012).

The right panel presents the distribution of Otx2 immunostaining in the layers of adult mouse retina (scale bar: 100µm).

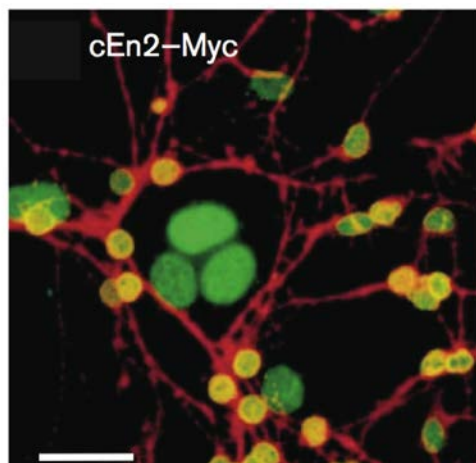


**Figure 4. Engrailed2 homeoprotein is transferred between cells *in vitro***

COS-7 cells expressing full-length Engrailed2 tagged with Myc (cEn2-Myc, stained for Myc in green) are co-cultured with E15 neurons (stained for NCAM in red). After 48h, the tagged protein is found in the neurons (scale bar: 10µm, adapted from Joliot et al., 1998).

signaling. In the early 1990s, Alain Prochiantz's group discovered the ability of homeodomains and homeoproteins to translocate across biological membranes. The first observation of this unconventional role of homeoproteins was that the homeodomain of Antennapedia could spontaneously enter live neurons *in vitro*, without altering the plasma membrane (Joliot et al., 1991b; Le Roux et al., 1993). Once internalized, the homeodomain retains its DNA-binding activity, leading to neurite outgrowth (Joliot et al., 1991b). A minimal domain (16 amino acids long), called penetratin (Derossi et al., 1994), is necessary and sufficient for translocation and matches exactly the homeodomain third helix (Le Roux et al., 1993).

Penetratin internalization properties have been extensively studied and are now well described. Internalization occurs at 4°C as well as at 37°C, supporting an energy-independent capture of the peptide. The tryptophan residue in position 48 of the homeodomain is indispensable for penetratin translocation, suggesting that internalization cannot be due only to penetratin general hydrophobicity or charge content (Derossi et al., 1994). Penetratin does not bind a chiral receptor and internalization is not believed to be receptor dependent (Derossi et al., 1996). However, negative charges at the cell surface are important for internalization, as Antennapedia homeodomain is preferentially captured *in vitro* by neurons expressing  $\alpha 2,8$ -polysialic acid (Joliot et al., 1991a).

As penetratin is a most conserved sequence among homeoproteins and is sufficient for homeodomain internalization, its discovery led to the deciphering of unconventional mechanisms for the internalization of many members of the homeoprotein family. Most homeoproteins tested so far can be internalized by live cells and addressed to their cytoplasm and nucleus, including Engrailed1/2, Emx1/2, Hoxa5, Hoxb4, Hoxc8, Pax6 and Otx2 (Chatelin et al., 1996; Joliot et al., 1998; Prochiantz and Joliot, 2003; Volovitch et al., 1993). Certain aspects of internalization, such as the energy-independence and the tryptophan residue in position 48 seem to be shared between penetratin and full-length homeoproteins (Brunet et al., 2005; Chatelin et al., 1996; Joliot et al., 1998; Torero Ibad et al., 2011). A two-step model for internalization has been proposed. The first step is the binding of the peptide to the negative charges of the membrane (sugars and/or lipids), demonstrated by the requirement of cell-surface carbohydrates and negatively charged lipids for the interactions of penetratin with live cells and artificial vesicles, respectively (Christiaens et al., 2002; Jiao et al., 2009;



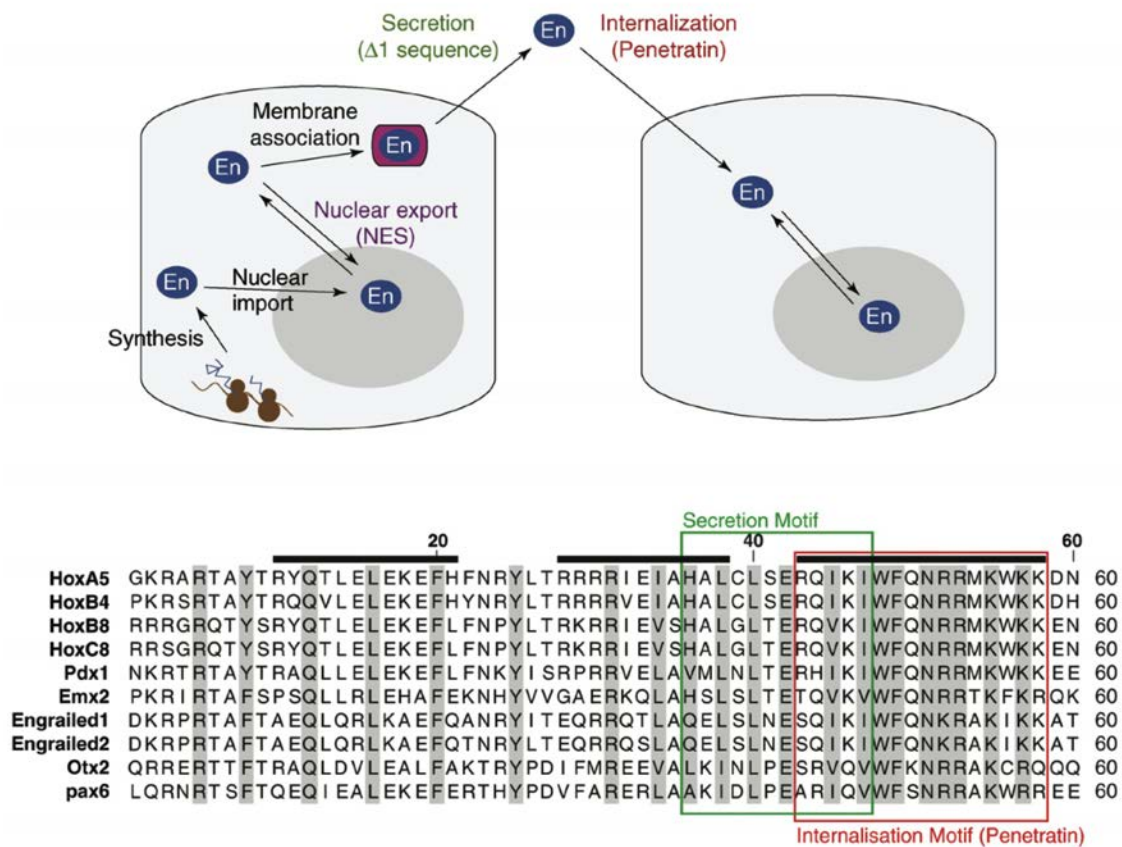


**Figure 5. Model for homeoprotein intercellular transfer**

The upper panel is a diagram for intercellular transfer of homeoproteins involving unconventional secretion and internalization.

The lower panel shows homeodomain sequence alignments for 10 homeoproteins verified for intercellular transfer. The internalization sequence (in red) corresponds to the third helix of the homeodomain and the secretion sequence (in green) includes the end of helix 2, the beginning of helix 3 and the  $\beta$ -turn between the two helices (adapted from Brunet et al., 2007 and Spatazza et al., 2013a).

Lensink et al., 2005). A second step consists of a transient destabilization of the membrane induced by the insertion of tryptophan 48 into the acyl core of the lipid bilayer, which sometimes leads to the formation of inverted micelles (Berlose et al., 1996; Christiaens et al., 2002; Dupont et al., 2007).

Similarly to its internalization, homeoprotein secretion is not canonical. Most of the secretion studies have been done on the Engrailed2 homeoprotein. In a co-culture assay, Engrailed2 expressed by Cos7 cells is secreted in the culture medium and then internalized by neighboring neurons (Figure 4) (Joliot et al., 1998). The small sequence (11 amino acids long) necessary for Engrailed2 secretion, called  $\Delta 1$ , is also part of the homeodomain. It spans part of the second and third helix and the entire  $\beta$ -turn, is distinct from classical secretion signals and is highly conserved among homeoproteins. In the absence of  $\Delta 1$ , Engrailed2 is not secreted (Joliot et al., 1998). Homeoproteins do not seem to have the same mechanisms for entering and exiting (Joliot and Prochiantz, 2004). Engrailed2 is devoid of any signal sequence recognized by the endoplasmic reticulum and its secretion is not blocked by Brefeldin A, therefore demonstrating a reticulum/Golgi-independent non-conventional mechanism. The  $\Delta 1$  domain overlaps with a nuclear export sequence, suggesting a link between secretion and nuclear export (Nakielnny and Dreyfuss, 1997). Indeed, secretion requires a passage of Engrailed2 through the nucleus. Engrailed2 probably shuttles between the nucleus and the cytoplasm and has to be exported from the nucleus to be secreted. Engrailed2 is found associated with cholesterol- and glycosphingolipid-rich caveolae or caveolae-like vesicles, suggesting that these vesicles participate in Engrailed2 secretion (Joliot et al., 1997). The regulation of secretion can occur at several levels, but the phosphorylation of a serine-rich domain within Engrailed2 by the serine/threonine protein kinase 2 specifically inhibits its secretion *in vitro* (Maizel et al., 2002). *In vitro* and *in vivo*, ~5% of the total amount of homeoprotein is present at the cell surface (Di Lullo et al., 2011; Joliot et al., 1997; Wizenmann et al., 2009). Ten homeoproteins (out of 10 tested) can pass between cells *in vitro*: Hoxa5, Hoxb4, Hoxb8, Hoxc8, Engrailed1/2, Otx2, Pax6, Pdx1 and Emx2 (Spatazza et al., 2013a). A model for homeoprotein intercellular transfer is presented in Figure 5.

#### **D. Homeoprotein as signalling proteins with *in vivo* roles**

Intercellular transfer has been demonstrated *in vivo* for Engrailed1, Engrailed2, Pax6 and Otx2 (Spatazza et al., 2013a). This non-cell autonomous activity of homeoproteins has now been studied in various model systems: drosophila (Layalle et al., 2011), xenopus (Brunet et al., 2005; Yoon et al., 2012), zebrafish (Lesaffre et al., 2007), chick (Di Lullo et al., 2011; Wizenmann et al., 2009) and mouse (Beurdeley et al., 2012; Miyata et al., 2012; Spatazza et al., 2013b; Stettler et al., 2012; Sugiyama et al., 2008).

Axon guidance has been the first model clearly demonstrating homeoprotein non-cell autonomous activity in metazoans. The patterning of the retinal ganglion cell axons in the optic tectum (chick) and superior colliculus (mouse) includes the projection of the nasal-temporal axis of the retina onto the posterior-anterior axis of the tectum, classically explained by the graded expression of ephrins and their receptors (McLaughlin and O'Leary, 2005). Engrailed homeoproteins also show a graded intracellular and extracellular expression in the tectum and the exogenous application of Engrailed2 can differentially guide temporal versus nasal retinal growth cones (Brunet et al., 2005). Blocking extracellular Engrailed in the developing chick and frog interferes with a proper patterning of the tectum (Wizenmann et al., 2009). This guidance effect requires the internalization of Engrailed2 in growth cones and subsequent local protein synthesis, with no transcription involved (Brunet et al., 2005).

The best *in vivo* model would of course be a genetic animal model in which transport sequences would be mutated, leaving only the cell autonomous functions intact. Unfortunately, these sequences (penetratin and  $\Delta 1$ ) are located within the homeodomain and mutating them also interferes with cell autonomous functions (Joliot and Prochiantz, 2004). Other strategies have been developed, in particular the cloning of mini-genes encoding single chain antibodies (scFv) directed against specific homeoproteins. Indeed, the expression of such antibodies and their addressing to the extracellular space by the addition of a classic secretion signal ensure that they only interfere with the homeoprotein non-cell autonomous activities. This scFv strategy was tested in the early development of the drosophila wing disc and the zebrafish eye (Layalle et al., 2011; Lesaffre et al., 2007). For the latter case, the expression of a secreted anti-Pax6 scFv in the developing zebrafish leads to a reduced eye field, demonstrating a non-cell autonomous role for Pax6 homeoprotein in eye development (Lesaffre et al., 2007).

This extracellular neutralization of homeoproteins with single chain antibodies takes place in the extracellular space. This raises the question of homeoprotein partners outside the cell: while inside the cell, its partners are protein co-factors and nucleic acids, the extracellular partners may include the glycosaminoglycans of the extracellular matrix.

## II. GLYCOSAMINOGLYCANS

### A. Glycosaminoglycan structures

Complex polysaccharides are primary constituents of the eukaryotic extracellular matrix and, more generally of extracellular environment. Glycosaminoglycans (GAGs) are a major class of extracellular complex polysaccharides. GAGs are unramified acidic polymers constituted of 20 to more than 100 repeats of variably sulfated disaccharide blocs. These disaccharides are composed of an uronic acid linked to a *N*-acetyl-hexosamine, both of which possibly sulfated at different positions. They have molecular masses ranging from a few kDa to  $2 \times 10^4$  kDa. These linear sulfated GAGs are classified into four types of GAG chains based on their different chemical structures: chondroitin sulfate/dermatan sulfate (CS/DS), heparin/heparan sulfate (HS), keratan sulfate and hyaluronan (Figure 6). Hyaluronan consists of  $\beta$ -D-glucuronic acid (1 $\rightarrow$ 3)-linked to 2-acetamido-2-deoxy- $\beta$ -D-glucopyranose (linkages between disaccharide units are 1 $\rightarrow$ 3). It is the only GAG incorporated in the extracellular matrix as a core protein-free GAG. In CS, the disaccharide unit is a  $\beta$ -D-glucuronic acid (1 $\rightarrow$ 3)-linked to a 2-acetamido-2-deoxy- $\beta$ -D-galactopyranose (linkages between disaccharide units are 1 $\rightarrow$ 4). The glucuronic acid can be sulfated on the C-2 and the galactosamine on the C-4 and/or C-6 positions.  $\beta$ -D-glucuronic acid in CS is converted to  $\alpha$ -L-iduronic acid in DS by C-5 epimerization. Repeating disaccharide units in heparin and HS are either  $\alpha$ -L-iduronic acid (1 $\rightarrow$ 4)-linked to glucosamine or  $\beta$ -D-glucuronic acid (1 $\rightarrow$ 4)-linked to glucosamine. The glucosamine is either N-sulfated or N-acetylated and can be ester-O-sulfated at the C-3 or C-6 position while the uronic acid can be sulfated at the C-2 position (Bülow and Hobert, 2006; Mikami and Kitagawa, 2013).

HS and CS are major components of the extracellular matrix in the central nervous system.

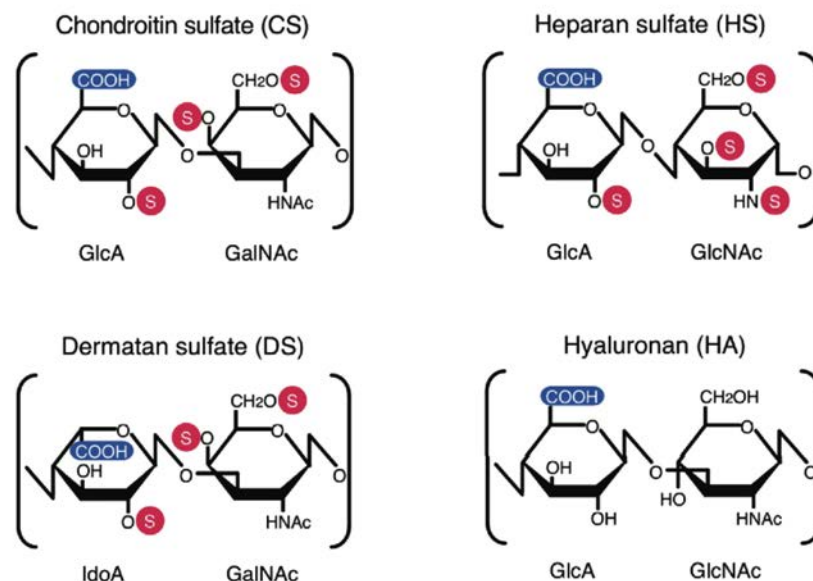


**Figure 6. Typical glycosaminoglycan disaccharide units**

Chondroitin sulfate (CS) chains are made of glucuronic acid and N-acetyl-galactosamine residues. Dermatan sulfate (DS) is a stereoisomer of chondroitin sulfate including iduronic acid instead of glucuronic acid. Heparan sulfate (HS) chains comprise glucuronic acid and N-acetyl-glucosamine residues. Hyaluronan (HA) is a linear polymer similar in structure to non-sulfated chondroitin sulfate (adapted from Mikami and Kitagawa, 2013).

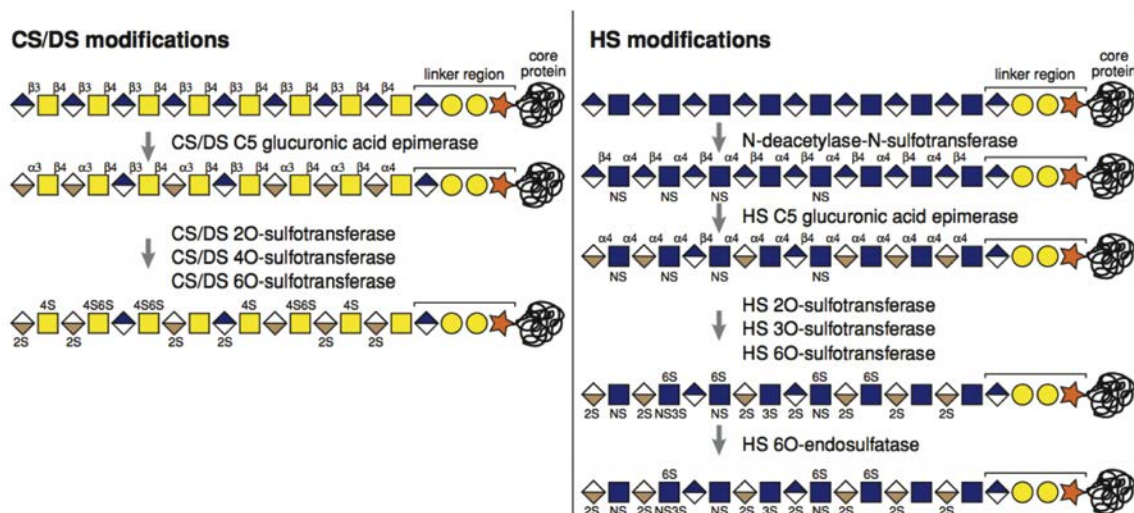


**Figure 7. Heparan sulfate and chondroitin sulfate chain modifications**

During the last steps of glycosaminoglycan chain biosynthesis, chondroitin sulfate (CS) and heparan sulfate (HS) chains are modified by a number of epimerases and sulfotransferases that are specific to chondroitin or heparan sulfate. This creates a remarkable molecular diversity (individual sugar units and linkages are shown according to convention, adapted from Bülow and Hobert, 2006).

These GAG chains are usually found linked to a core protein and proteins with covalently attached GAGs are named proteoglycans. They are separated between heparan sulfate proteoglycans (HSPGs) and chondroitin sulfate proteoglycans (CSPGs). The core proteins, as well as the characteristic disaccharides, differ between HSPGs and CSPGs. More than 30 proteoglycan core proteins have been isolated so far with sizes ranging from 10 kDa to 500 kDa (Silbert and Sugumaran, 2002). In the central and peripheral nervous system, HSPGs are diverse and can be transmembrane (syndecans), bound by a glycosyl phosphatidylinositol linkage to plasma membrane lipids (glypicans) or secreted into basement membranes (perlecan, agrin) (Iozzo, 1998). In the brain, the main CSPGs are the proteins of the lectican family (neurocan, brevican, aggrecan and versican), also called hyalectans for their interaction with hyaluronic acid and lectins. Among other CSPGs are NG2, expressed mainly by oligodendrocyte progenitor cells, phosphacan/RPTP $\zeta\beta$ , expressed predominantly in the central nervous system and decorin, a small proteoglycan that bears both DS and CS chains (Yamaguchi, 2000).

## **B. Glycosaminoglycan biosynthesis**

The assembly of GAG chains occurs in the endoplasmic reticulum and Golgi. It is initiated by the synthesis of the so-called GAG-protein linkage region tetrasaccharide, common to both HS and CS chains, and covalently linked to specific serine residues in different core proteins. This tetrasaccharide comprises a xylose (from precursor uridine diphosphate (UDP)-xylose), two galactose (Gal) units and a glucuronic acid (GlcA) (Sugahara et al., 2003). After this first step, monosaccharide units Gal, GlcA, N-acetylglucosamine (GlcNAc) and N-acetylgalactosamine (GalNAc) are transferred from sugar nucleotide precursors (UDP-Gal, UDP-GlcA, UDP-GlcNAc and UDP-GalNAc) to the linkage region leading to chain elongation. The transfer of GalNAc or GlcNAc to the linkage oligosaccharide is the first step that provides the corresponding specificity for CS or HS formation (Silbert and Sugumaran, 2002). HS and CS then differentiate into mature chains after various modification reactions, mainly epimerization and sulfation, and this chemical combination can give rise to a large number of highly diverse structures (Figure 7). Unlike nucleic acids and proteins, the biosynthesis of complex sugars is a non-template-driven process involving several enzymes and their tissue-specific isoforms. The list of these enzymes goes from glycosyltransferases

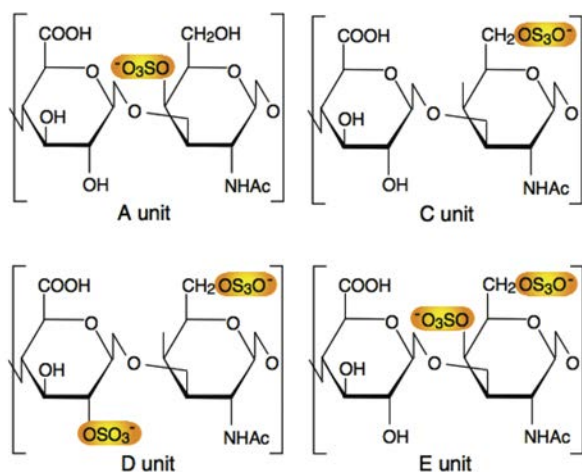


**Figure 8. Typical sulfation pattern of chondroitin sulfate disaccharides**

The disaccharide units of chondroitin sulfate (CS) chains are classified into

CS-O (unsulfated),  
 CS-A (GlcA-GalNAc(4S)),  
 CS-C (GlcA-GalNAc(6S)),  
 CS-D (GlcA(2S)-GalNAc(6S))  
 and CS-E (GlcA-GalNAc(4S,6S)) units

on the basis of their sulfation patterns  
 (adapted from Sugahara et al., 2003).

that participate in the elongation and polymerization of GAG chains to sulfotransferases and epimerases that modify the glycan backbone.

Sulfotransferases add sulfate groups from 3'-phosphoadenosine-5'-phosphosulfate to the growing GAG chains. In HS, sulfation modifications occur in restricted domains of about 5-10 disaccharides that are hyper variable and interspersed within poorly sulfated regions. The modifications in HS biosynthesis are initiated with the N-deacetylation and subsequent N-sulfation of selected GlcNAc residues, where both reactions are carried out by a bifunctional enzyme called N-deacetylase-N-sulfotransferase. Four mammalian N-deacetylase-N-sulfotransferases have been identified, with different substrate specificities (Grobe et al., 2002). After N-sulfation, C5-epimerization of GlcA into iduronic acid can occur and can be followed by 2-O-sulfation (1 enzyme), 6-O-sulfation (three enzymes) and/or 3-O-sulfation (7 enzymes). 2-O-sulfated hexuronic acids are almost exclusively found in contiguous N-sulfated domains of the GAG chain. Similarly, CS chains are composed of several types of disaccharide units that differ in their sulfation pattern. To date, seven sulfotransferases responsible for the sulfation of CS/DS chains have been identified (Kusche-Gullberg and Kjellén, 2003). A non-sulfated unit serves as a common acceptor substrate for two types of sulfotransferases, one catalyzing the 4-O-sulfation and the other the 6-O-sulfation of GalNAc residues. Subsequent sulfation on the C-2 position of the GlcA or on the C-6 position of the GalNAc can occur, forming disulfated disaccharides. The typical disaccharide units found in CS chains are named A, C, D and E, according to their sulfation pattern (Figure 8).

The redundancy of the biosynthetic machinery based on different enzyme isoforms (Esko and Lindahl, 2001) makes it challenging to take a genetic approach by knocking in or out specific enzymes. However, most critical functions of GAGs in development have been revealed by analyses of mutants defective in GAG biosynthesis enzymes. For instance, exostosin glycosyltransferase 1 homozygous mutant mice, in which only short stubs containing the linkage region are attached to the protein, fail to gastrulate and generally lack organized mesoderm and extraembryonic tissues (Lin et al., 2000). Mutants lacking both N-deacetylase-N-sulfotransferase 1 and N-deacetylase-N-sulfotransferase 2 die during early embryogenesis (Forsberg and Kjellen, 2001). In *C. elegans*, animals lacking one of the three HS-modifying enzymes, glucuronyl C5-epimerase, 6O-sulfotransferase or 2O-sulfotransferase, exhibit distinct as well as overlapping axonal and cellular guidance defects in specific neuron classes (Bülow and Hobert, 2004). *C. elegans* mutants for the nematode orthologs of chondroitin



sulfate synthase and chondroitin polymerizing factor show cytokinetic regression in early embryogenesis (Hwang et al., 2003; Izumikawa et al., 2004; Mizuguchi et al., 2003). In mouse, knockout of  $\beta$ -1,3-glucuronyltransferase 1 encoding gene also results in embryonic lethality due to cytokinetic failure (Izumikawa et al., 2010). These studies show the crucial roles of GAG chains in metazoan embryonic development, from worms to mammals.

### **C. Glycosaminoglycan interaction with morphogens and growth factors**

Disruption of genes involved in the synthesis of HSPG and CSPG core proteins also results in physiological defects (Lamanna et al., 2007). But although the core proteins alone can display some activity, mounting evidence indicates that most functions of CSPGs and HSPGs are largely exerted through their GAG moiety. GAG moieties vary considerably in the size and number of CS or HS per core protein and in the position and degree of modifications, primarily sulfation, which create huge molecular diversity and structural complexity. For instance, an octasaccharide can have over 1,000,000 different sulfation patterns (Sasisekharan and Venkataraman, 2000). This structural heterogeneity of GAG chains is thought to promote specific interactions with a variety of bioactive molecules such as growth factors and morphogens in the extracellular environment. As mentioned earlier, genetic studies on GAG biosynthetic enzymes have provided direct functional evidence for the involvement of GAGs in cell growth and developmental processes based in particular on Wnt, Hedgehog, bone morphogenetic protein (BMP), transforming growth factor and fibroblast growth factor (FGF) signaling pathways (Lin, 2004). For instance, in *Drosophila* embryos with mutations in *sulfateless*, the N-deacetylase-N-sulfotransferase homolog, the signaling pathways involving either Wingless (a member of the Wnt family), FGF or Hedgehog are completely silenced (Lin and Perrimon, 1999). Reduction of 3O-sulfotransferase activity in *Drosophila* results in compromised Notch signaling with neurogenic phenotypes (Kamimura et al., 2004). In mice lacking exostosin glycosyltransferase 1, Indian Hedgehog is not correctly distributed in the gastrulating embryo (Lin et al., 2000). GAGs can participate in growth factor signaling by assembling protein-protein complexes on the cell surface. The best example is the well-studied affinity of HS for FGFs and FGF receptors. FGF signals through cell surface tyrosine kinase receptors and its oligomerization leads to receptor oligomerization, phosphorylation of other signaling molecules and initiation of signaling cascades (Raman et al., 2005). HSPGs directly interact with FGFs and their receptors to form a ternary complex at the cell surface thus facilitating FGF interaction with its receptor and/or stabilizing FGF oligomerization (Lin,

2004). Similarly, HS chains bind to both the axon guidance molecule Slit2 and its receptor Robo1 to facilitate the ligand-receptor interaction (Zhang et al., 2013).

X-ray crystal structures of GAG-protein complexes have provided information on the structural features required for GAG-protein interaction. The specificity of GAG-protein interactions is governed by the ionic interactions of the sulfate and carboxylate groups in the GAG chains with the basic amino acids on the protein, as well as by the optimal fit of the GAG chain into the binding site of the protein. The topology and distribution of basic amino acids on the protein sequence influences the specificity of its recognition of GAG sequences. Two principal consensus sequences have been presented as potential binding sites for GAG interaction: XBBXBX and XBBBXXBX, where B is a basic residue (lysine or arginine, sometimes histidine) and X is a hydrophilic residue (Cardin and Weintraub, 1989). Despite their identical charges, arginine residues bind more tightly to GAGs than lysine residues. The spacing of these residues may determine protein-GAG interaction affinity and specificity: GAG binding sites can be formed by basic amino acids distant in sequence but brought close together in the folded protein (Gandhi and Mancera, 2008). The binding affinity of GAGs depends on the ability of their oligosaccharide sequence to provide optimal charge interaction with the protein. Under physiological conditions, all carboxylic acid and sulfate groups are deprotonated, giving a very high negative charge to GAG chains (Capila and Linhardt, 2002). These negatively charged groups form ion pairs with the clusters of positively charged basic amino acids on proteins. However, ionic interactions contribute only in part to the GAG-protein interaction (30% for FGF-2 and heparin (Gandhi and Mancera, 2008)) as other types of interaction are also involved: van der Waals forces, hydrogen bonds and hydrophobic interactions.

Conformation studies have shown that variations in the primary sequence (chain length and sulfation pattern) are crucial for protein binding. The minimum GAG chain length required for binding is typically 4-12 monosaccharide units (Gandhi and Mancera, 2008). Binding affinity increases with the size of the oligosaccharides (Rusnati et al., 1999). Tetra- and hexasaccharides of HS are sufficient to bind FGF1 and FGF2 with high affinity. However, octosaccharides or longer sugar chains are required for bridging a dimeric FGF2 along with its receptor to form the ternary signaling complex (Pellegrini et al., 2000; Schlessinger et al., 2000). The relative proportions of N- and O-sulfation in HS chains impact on their interaction with proteins. FGF1 and FGF2 interactions with HS oligosaccharides require 2-O- and -N-

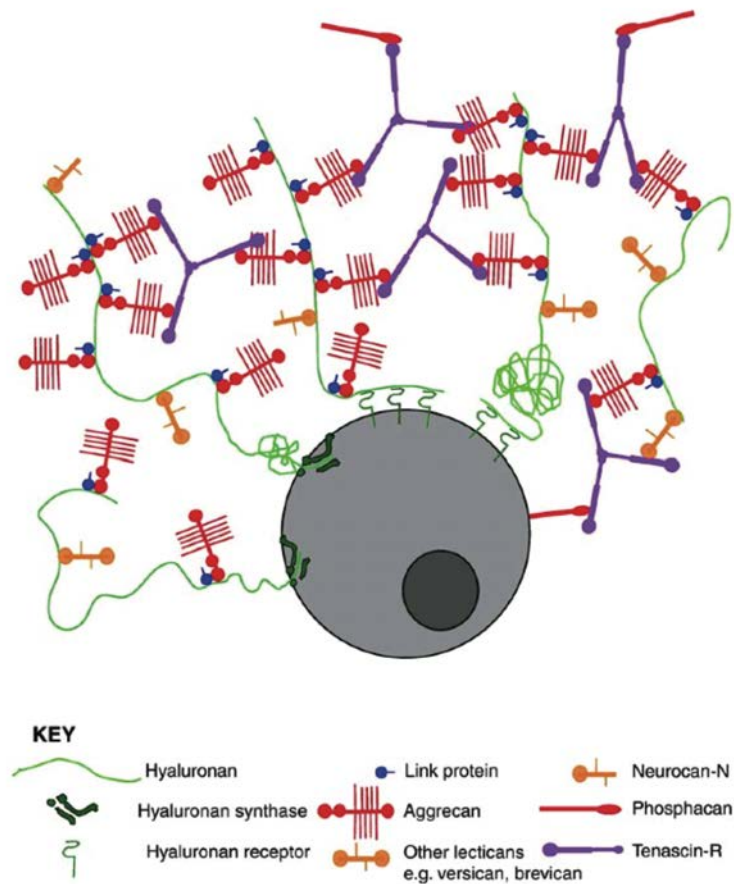


### Figure 9. Perineuronal net model

Hyaluronan is attached to the cell surface and provides a scaffold for the perineuronal net. The lectican family of chondroitin sulfate proteoglycans (aggrecan, neurocan, phosphacan, versican, brevican, ...) bind hyaluronan through their N-terminal domain (interaction stabilized by link proteins) and tenascin-R via their C-terminal domain (adapted from Galtrey and Fawcett, 2007).

sulfate groups. However, the 6-O sulfation is critical for FGF1 signaling, but not completely necessary for FGF2 signaling (Guerrini et al., 2002). CS chains with disulfated disaccharides (CS-D and/or CS-E) bind with high affinity to midkine, pleiotrophin, FGF, hepatocyte growth factor and brain-derived growth factor (BDNF) (Tamura et al., 2012). CS-A chains negatively regulate axon guidance (Wang et al., 2008), while CS-C chains appear to be relatively permissive for neurite regeneration (Lin et al., 2011). CS-E, but not CS-A, CS-C nor HS, binds to contactin-1 and leads to neurite outgrowth (Mikami et al., 2009). The oligosaccharide motif that is recognized by a protein is often found in low abundance which, given the diversity of GAG sequences, supports the idea of a specificity in GAG-protein interactions (Raman et al., 2005).

#### **D. Glycosaminoglycans in the postnatal brain**

Complex sugars are precisely distributed in the developing and adult brain and the spatiotemporal expression and composition of GAGs changes throughout development. GAG-protein interactions in the central nervous system have been shown to play critical roles in proliferation and differentiation of neural progenitor cells, neuronal migration, axon guidance, synaptogenesis, neural plasticity and regeneration (Maeda et al., 2011). Sulfation patterns of GAG chains change dramatically during brain development. In the adult brain, the content of CS/DS is about 9 times higher than the HS one. The proportion of 6-O-sulfated CS decreases and that of 4-O-sulfated CS progressively increases (Kitagawa et al., 1997; Mitsunaga et al., 2006). Furthermore, while during embryonic development, GAGs are diffusely distributed in the extracellular matrix, they gradually accumulate around subsets of neurons during postnatal development.

In the postnatal and adult brain, CSPGs are the major components of a form of condensed extracellular matrix called perineuronal nets (PNNs) (Galtrey and Fawcett, 2007). PNNs surround cell soma and proximal dendrites of distinct neuron subpopulations in the brain (Celio and Blümcke, 1994). PNNs constitute a highly organized complex composed of HA, link proteins, CSPGs (mainly lecticans) and tenascin-R (Figure 9) (Carulli et al., 2007; Köppe et al., 1997b). Hyaluronan synthases, located on the plasma membrane, anchor the PNN structure to the cell surface (Carulli et al., 2007). They synthesize and secrete hyaluronan in the extracellular space. There are three hyaluronan synthase isoforms that synthesize hyaluronan chains of various lengths and at different speeds (Itano et al., 1999; Spicer et al.,

1997). Hyaluronan synthase isoforms have different spatiotemporal expressions and confer different structure and mechanical strength to the PNNs (Carulli et al., 2006; Galtrey et al., 2008). The lecticans (aggrecan, neurocan, versican and brevican), bind to hyaluronan through the N-terminal domain of their core protein (Iozzo, 1998). Aggrecan, which is necessary for PNN formation (Giamanco et al., 2010; Kwok et al., 2010), is present on almost all PNN-positive neurons, while other lecticans are found only in subpopulations of PNN-bearing neurons (Galtrey et al., 2008). Furthermore, glycosylation of aggrecan in PNNs varies between different areas of the nervous system (Matthews et al., 2002). The differential distribution of lecticans in PNNs probably affects their properties and functions (Kwok et al., 2011). Some CSPGs of the PNNs are produced by neurons, some by glia and some by both cell types (Carulli et al., 2006; Giamanco and Matthews, 2012). However, cortical neurons in culture are able to construct PNN-like structures without glial cells (Miyata et al., 2005). The interaction between hyaluronan and lecticans is stabilized by link proteins (Binette et al., 1994), which belongs to a family of proteins that bind to both hyaluronan and CSPGs (Kwok et al., 2011). Crtl1 and Bral2 are the two members of this family that colocalize with PNNs; they are expressed exclusively by PNN-bearing neurons (Bekku et al., 2003; Rauch, 2004). Link proteins are crucial for the condensed nature of the PNNs (Kwok et al., 2010). Indeed, mice lacking Crtl1 in the central nervous system show reduced PNNs throughout the nervous system, with no dendritic staining and a faint staining around neuronal soma (Carulli et al., 2010). Bral2-deficient mice also have attenuated PNNs (Bekku et al., 2012). To complete the formation of the PNNs, the lecticans bind tenascin-R through their C-terminus. *Tenascin-R* knock-out mice exhibit abnormal PNN staining (Weber et al., 1999).

The sulfation pattern of PNNs differs from the sulfation pattern of GAGs of the diffuse matrix (Deepa et al., 2006). The proportion of CS/DS (71%) is higher than that of HS (29%). In PNNs, unsulfated CS and 4-O-sulfated CS disaccharides are predominant, while the disulfated CS-D and CS-E only represent 1.2% and 2.1% of the CS GAGs, respectively. Unsulfated HS disaccharide is the major disaccharide in the PNNs, followed by 2-N-sulfated HS disaccharide units. Di- and tri-sulfated HS disaccharides represent about 15% of the PNN HS GAGs (Deepa et al., 2006).

Immunohistochemistry with Wisteria floribunda agglutinin (WFA), one of the established markers for PNNs that binds the N-acetylgalactosamine residue on the CS chains of PNNs, allows one to estimate PNN density and to visualize their morphology. Staining with this

lectin shows that PNNs surround neurons throughout the central nervous system, including the visual cortex, barrel cortex, frontal cortex, amygdala, striatum, substantia nigra, hippocampus, cerebellum and spinal cord (Brückner et al., 2008; Carulli et al., 2006; Galtrey et al., 2008; Gogolla et al., 2009; Lee et al., 2012; McRae et al., 2007; Ohira et al., 2013; Pizzorusso et al., 2002; Yamada and Jinno, 2013). PNNs are particularly abundant in the visual and somatosensory cortices, especially in layer IV (Karetko and Skangiel-Kramska, 2009). The formation of PNNs is activity-dependent (Ye and Miao, 2013). Sensory-deprivation by dark-rearing (visual cortex, (Pizzorusso et al., 2002)) or whisker trimming (barrel cortex, (McRae et al., 2007)) decreases the number of PNN-bearing neurons. PNNs are found mainly around parvalbumin-positive interneurons (PV-cells) (Härtig et al., 1992; Morris and Henderson, 2000), although they are sometimes localized to certain pyramidal cells in structures such as the parietal cortex (Härtig et al., 2001; Wegner et al., 2003). The PV-cells surrounded by PNNs are fast-spiking, highly active neurons: PNNs probably provide a suitable microenvironment around these neurons for their high activity, possibly through their buffering capacity of local cations. Indeed, due to the GAGs highly negative charge, PNNs bind to various cations (e.g. calcium), thus controlling their diffusion (Härtig et al., 2001; 1999). CS moieties in the PNNs have also been shown to interact with proteins: semaphorin3A, an axon guidance molecule, binds to PNNs by interacting with CS-E (Dick et al., 2013). But PNNs are most highly involved in synaptic stabilization to limit plasticity. Indeed, the formation of PNNs begins during postnatal development, at periods of synaptic refinement called critical periods (Köppe et al., 1997a).

### **III. CRITICAL PERIOD PLASTICITY**

#### **A. Critical periods**

The potency of the environment to shape brain function changes dramatically across lifespan. During postnatal development, anatomical and functional plasticity of neural circuits allows the cerebral cortex to adapt to the environment as cortical connections can be remodeled by physiological activity. These windows of learning are called critical periods and their duration (from weeks to years) is proportional to the expected lifespan of a given species (Berardi et al., 2000). Such periods are needed to establish an optimal neural representation of (and adaptation to) the surrounding environment: several sensory, motor, linguistic and

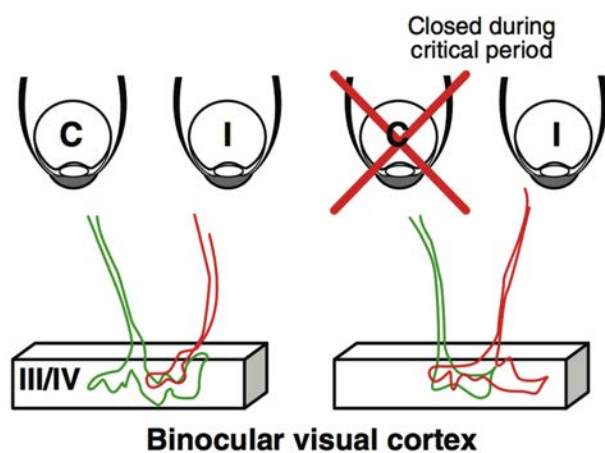


**Figure 10. Ocular dominance and monocular deprivation in the binocular visual cortex**

The left side presents the normal situation when the two eyes are competing during the critical period. In the mouse, the contralateral eye (C, in green) is dominant and occupies more space than the ipsilateral eye (I, in red) in layers III/IV of the binocular visual cortex.

The right side illustrates the shift in ocular dominance when the contralateral eye is closed during critical period (adapted from Prochiantz, 2013).

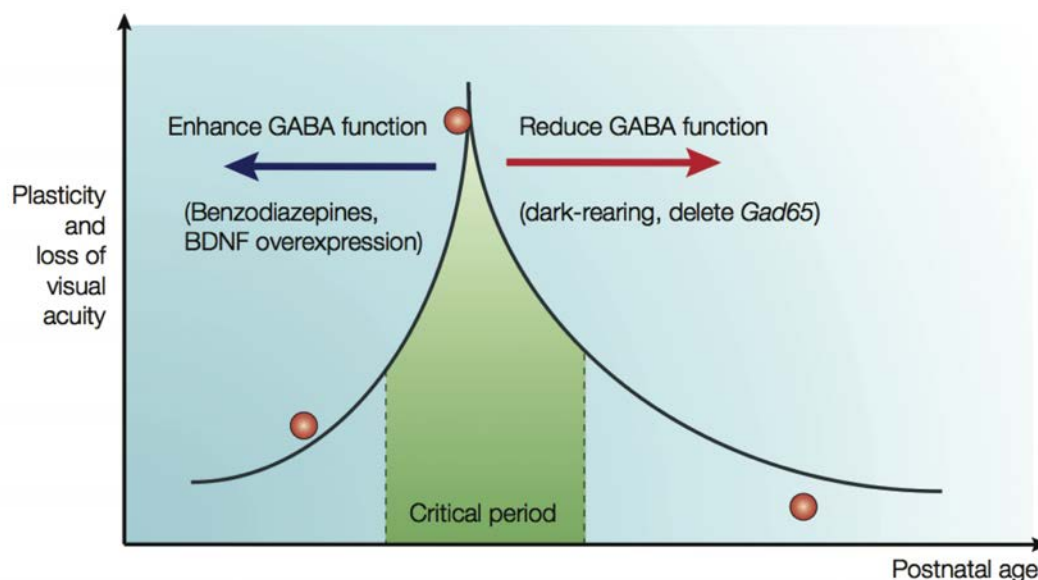


**Figure 11. Maturation of inhibition controls critical period timing**

Sensitivity to monocular deprivation (and therefore cortical plasticity) is restricted to ocular dominance critical period. The onset of plasticity can be delayed by directly preventing the maturation of GABA-mediated transmission (dark-rearing from birth or deletion of *Gad65*, red arrow). Conversely, the critical period can be brought forward by enhancing GABA transmission (benzodiazepines just after eye opening or excess BDNF expression, blue arrow) (adapted from Hensch, 2005).

psychological abilities can only be acquired during critical periods. Plasticity is very limited outside these critical periods, as the circuits and synapses mature and the whole system eventually becomes consolidated.

Critical periods have been observed in various systems and across species (Hensch, 2004). But since the pioneering work of Hubel and Wiesel 50 years ago in cats, the critical period has been primarily studied in the binocular visual cortex. Hubel and Wiesel have shown that the inputs from the two eyes compete when they first converge onto individual neurons in the binocular zone of the primary visual cortex (Wiesel and Hubel, 1963). This leads to an ocular dominance, representing the relative anatomical and physiological strengths of the connections contributed by either eye (Hensch, 2005). Unmatched inputs from the two eyes early in life disrupt the typical binocular organization of thalamo-cortical afferents and produce a permanent deficit in visual acuity, known as amblyopia (Lewis and Maurer, 2009). In the rodent, the ocular dominance shows a typical bias towards the contralateral eye. During the critical period, monocular deprivation (the closure of one eye) produces a loss of response to the deprived eye and a gain in the input of the open eye. Ocular dominance then shifts towards the open ipsilateral eye (Figure 10) (Shatz and Stryker, 1978; Wiesel and Hubel, 1963). Sensitivity to monocular deprivation is restricted to the critical period that begins at P20 in rodents (about 1 week after eye opening), peaks at P30 and rapidly declines over the next days (Fagiolini et al., 1994; Gordon and Stryker, 1996). Before and after this critical period, the response to monocular deprivation is very limited.

## **B. Cellular and molecular mechanisms of cortical plasticity**

Binocular interactions are detected by the integrated action of local excitatory and inhibitory connections in the visual cerebral cortex. This excitatory/inhibitory balance is dynamically adjusted by the cortical layer circuits where inhibitory connections develop later than the excitatory ones (Turrigiano and Nelson, 2004). An optimal excitatory/inhibitory balance is required for plasticity and critical period onset is determined by the maturation of local inhibitory circuits (Fagiolini and Hensch, 2000; Hensch, 2005). Consequently, directly manipulating inhibitory transmission shifts the timing of the critical period for ocular dominance plasticity (Figure 11). Developing inhibitory cells are susceptible to early life sensory experience. Partial or total loss of activity in a sensory cortex – dark-rearing from birth (Morales et al., 2002) but also whisker trimming during the critical period (Jiao et al., 2006) and early hearing loss (Kotak et al., 2008; Takesian et al., 2010) – generally leads to a



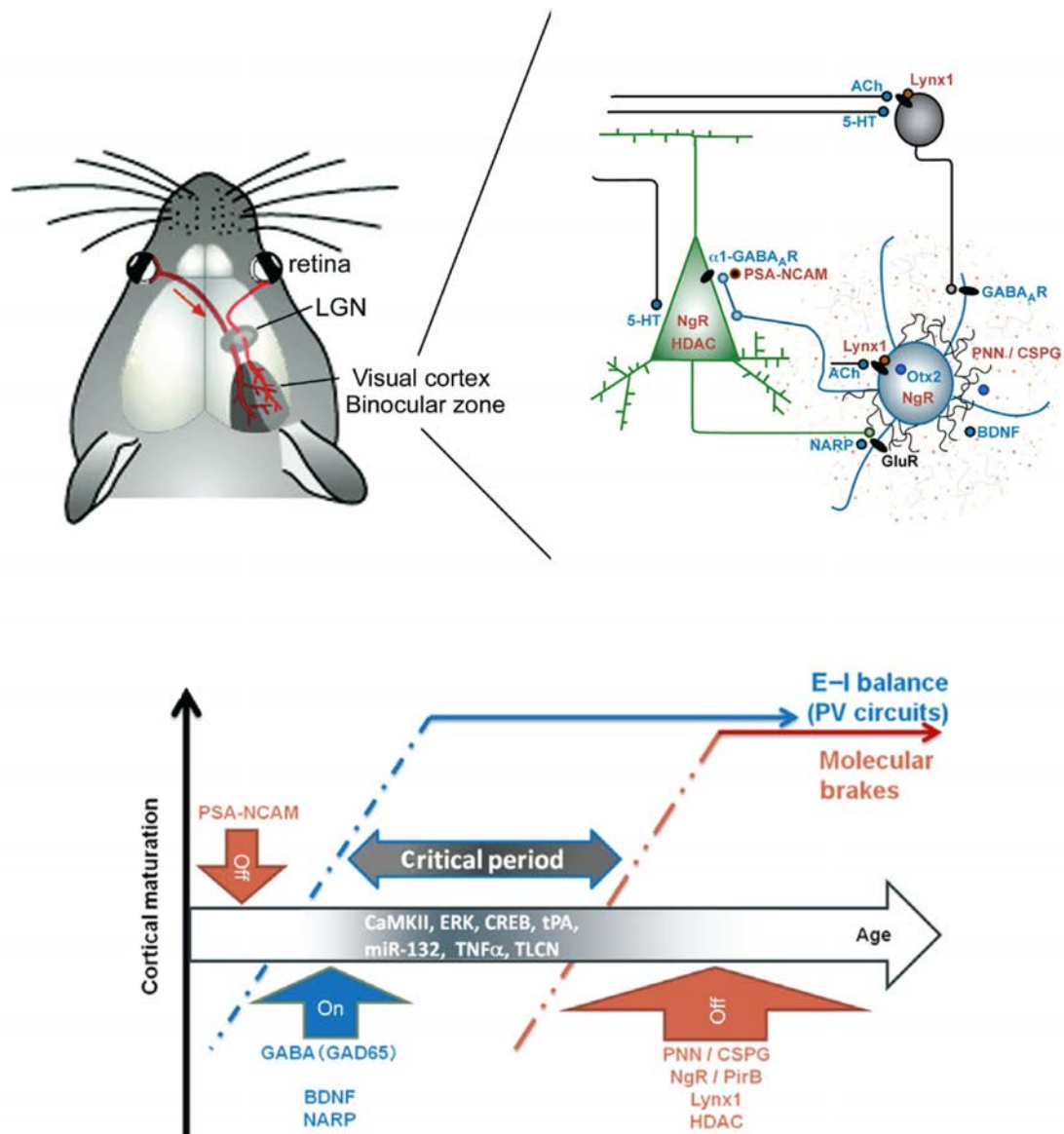


**Figure 12. Local GABA circuits and molecular factors for critical period plasticity**

In the upper panel, inputs from the eyes converge in the binocular zone of the primary visual cortex. The right scheme illustrates the cortical microcircuits between excitatory pyramidal cells (green), parvalbumin inhibitory cells (blue) and non-parvalbumin inhibitory cells (grey). GABA<sub>A</sub> receptors containing the  $\alpha 1$ -subunit are enriched at somatic synapses from large basket PV-cells onto pyramidal cells. Many factors controlling plasticity are found within the extracellular matrix surrounding PV-cells.

The lower panel presents the mechanisms controlling the onset and closure of the critical period. Early factors (PSA-NCAM) prevent precocious plasticity. Critical period onset is triggered when factors (BDNF, NARP, GAD65) promote PV-cell maturation. This triggers a sequence of molecular events (CaMKII, ERK, protein synthesis), which ultimately induce structural changes. The critical period closes when molecular brakes (PNN, PirB, NgR and epigenetic changes) gradually emerge to dampen plasticity (adapted from Sugiyama et al., 2009 and Takesian and Hensch, 2013).

down-regulation of inhibitory transmission. The primary inhibitory neurotransmitter in the brain,  $\gamma$ -aminobutyric acid (GABA), is synthesized by glutamic acid decarboxylase produced by two distinct genes, *Gad65* and *Gad67*. Mice lacking the synaptic isoform of the GABA-synthetic enzyme, *Gad65*, as well as immature wild-type animals just after eye opening, exhibit weak GABA release and no loss of visual responsiveness to an eye deprived of vision (Hensch et al., 1998). Weak GABAergic signaling inhibition in the visual cortex before P20 prevents experience-dependent plasticity. These mice show no response to monocular deprivation until inhibitory transmission is restored by enhancing the postsynaptic sensitivity to GABA with benzodiazepines (Fagiolini and Hensch, 2000; Iwai et al., 2003). These agonists of GABA, such as diazepam, effectively compensate for poor presynaptic GABA release.

GABA inhibitory interneurons account for nearly 20% of cortical neurons, but not all GABA circuits are involved in critical period regulation. Critical period onset corresponds closely to the emergence of parvalbumin inhibitory interneurons (PV-cells) (del Río et al., 1994). Parvalbumin is one of the three calcium-binding proteins which, together with calretinin and calbindin, are expressed in most GABA-producing neurons in the cortex in largely non-overlapping groups. PV-cells are fast-spiking interneurons, which means that they can fire non-adapting action potentials at rates of up to several hundred of Hertz, due in part to unique potassium conductances (Kv3 class) (Hensch, 2005). The specific blockade of the potassium channel Kv3.1 leads to impaired ocular dominance plasticity, thus mimicking the *Gad65* knock-out phenotype but in a cell type-specific manner (Hensch, 2005). There are two types of PV interneurons: the chandelier cells which form synapses onto the initial segment of excitatory pyramidal cell axons and the large basket cells that mostly contact excitatory pyramidal cell soma. PV-cell induced-inhibition triggers cortical plasticity through GABA<sub>A</sub> receptors containing  $\alpha 1$  subunit (Fagiolini et al., 2004). These receptors are located on excitatory pyramidal cell soma and preferentially targeted by large basket PV-cells (Figure 12) (Ali and Thomson, 2008). PV-cell maturation thus leads to an optimal ratio of excitatory and inhibitory circuit activity.

Precocious plasticity is prevented during the pre-critical period by factors such as alpha 2,8-polysialic acid (PSA) bound to the neural cell adhesion molecule (PSA-NCAM) (Figure 12). PSA expression in the mouse primary visual cortex declines shortly after eye opening and

premature PSA removal promotes the maturation of GABAergic innervation and triggers a precocious critical period for ocular dominance (Di Cristo et al., 2007).

Critical period onset is triggered when factors such as BDNF and neuronal activity-regulated pentraxin (NARP) promote PV-cell maturation (Figure 12). Genetic enhancement of BDNF triggers an early critical period in the visual cortex by promoting PV inhibitory circuit maturation (Hanover et al., 1999; Huang et al., 1999). Instead, blocking of BDNF signaling prevents the development of ocular dominance in the kitten primary visual cortex (Cabelli et al., 1997). BDNF production is activity-dependent (Greenberg et al., 2009) and BDNF is kept at immature levels in the visual cortex by dark-rearing (Castren et al., 1992). NARP is also an activity-regulated protein that regulates the expression of a class of glutamate receptor in PV-cells (Chang et al., 2010) and *NARP* knock-out mice fail to install ocular dominance plasticity throughout life (Gu et al., 2013). PV-cell maturation is accompanied by a sequence of structural and molecular events that lead to circuit rewiring and physiological consolidation (Hensch, 2005). Tissue-type plasminogen activator is a major serine protease, which, upon release, cleaves the physical connections between pre- and postsynaptic partners and induces dendritic spine motility (Mataga et al., 2004; 2002; Oray et al., 2004). The deprivation-induced increase in tissue-type plasminogen activator, along with spine pruning, fails to occur in mice lacking *Gad65* (Mataga et al., 2002; 2004). Multiple protein kinases (CaMKII, PKA, ERK (Antonini et al., 1999; Di Cristo et al., 2001; Taha and Stryker, 2002; Trachtenberg and Stryker, 2001)) and homeostatic regulators (TNF (Kaneko et al., 2008)) eventually converge on gene transcription programs mediated by CREB to ultimately strengthen open eye connections.

The critical period closes as molecular brakes that dampen plasticity gradually emerge (Figure 12). The brake factors include structural brakes, which physically prevent neurite pruning and outgrowth (PNNs, myelin factors) and functional brakes acting on neuromodulatory systems. PNNs gradually enwrap PV-cell cell bodies and proximal dendrites (Härtig et al., 1999). In the visual cortex, the progressive increase in PNNs across postnatal development coincides with PV-cell maturation and is thought to contribute to the closure of the critical period (Pizzorusso et al., 2002; Sur et al., 1988). Mice lacking the *Crt11* link protein show extended plasticity into adulthood (Carulli et al., 2010). Myelin and myelin-associated inhibitors have also been shown to control critical period: proteins found in myelin (Nogo, myelin-associated glycoprotein, myelin oligodendrocyte glycoprotein) limit axonal sprouting by their binding to

Nogo receptor and paired immunoglobulin-like receptor B complex (PirB) (Atwal et al., 2008). Nogo receptor knock-out mice exhibit ocular dominance plasticity beyond the critical period. In mice lacking functional PirB, ocular dominance plasticity is more robust at all ages (Syken et al., 2006). Developmental changes in DNA methylation and histone modifications may also be involved in critical period transitions. DNA methylation represses transcription by interfering with transcription factors binding or by recruiting repressor complexes containing histone deacetylases to condense chromatin structures (Fagiolini et al., 2009). Closure of the critical period for ocular dominance is associated with a downregulation of visual experience-induced histone acetylation and phosphorylation (Putignano et al., 2007). Windows of plasticity therefore arise between the maturation of an optimal excitatory/inhibitory balance and a later set of emerging brake factors that persistently offset the synaptic pruning machinery.

### **C. Reopening plasticity in the adult**

Targeting excitatory/inhibitory balance or the molecular brakes using pharmacological or genetic approaches (as the *Gad65* knock-out mouse) can accelerate or delay plasticity onset and even open windows of plasticity in the adult cortex. Indeed, the emerging view is that the brain is intrinsically plastic; adult brain plasticity is dampened (reversibly) by molecular brakes that limit excessive rewiring after critical period closure (Takesian and Hensch, 2013).

Plasticity can be reopened after the critical period by reinstalling immature lower levels of inhibition. Intracortical infusion of a Gad inhibitor or of a GABA<sub>A</sub> receptor antagonist promotes plasticity in adult primary visual cortex (Berardi et al., 2003). Exposure of adult rats to complete darkness enhances visual cortex plasticity, due to reduced expression of GABA<sub>A</sub> receptors relative to AMPA receptors that alters the excitatory/inhibitory balance in the visual cortex (He et al., 2007). Transplantation of embryonic inhibitory neurons in the postnatal visual cortex also promotes ocular dominance plasticity after critical period closure (Southwell et al., 2010). Raising adult amblyopic rats (rats monocularly deprived during the critical period) in an enriched environment also restores normal visual acuity and ocular dominance (Sale et al., 2007). A similar effect is obtained when animals are treated with fluoxetine, a selective serotonin recapture inhibitor (Maya Vetencourt et al., 2008). Both treatments reduce GABAergic inhibition in the visual cortex, accompanied by an increased expression of BDNF.

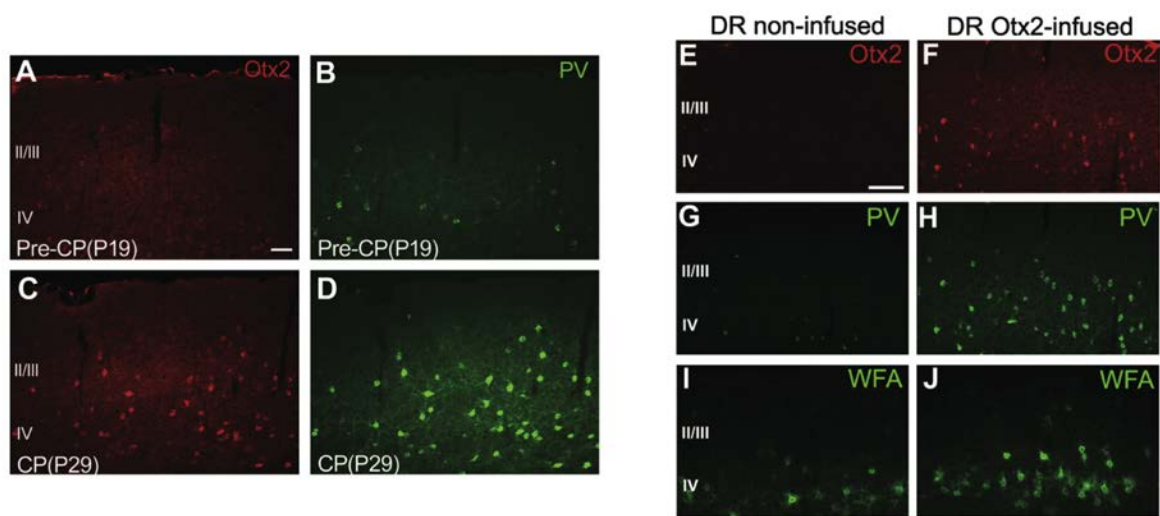


**Figure 13. Otx2 regulates PV-cell maturation**

The left panel shows Otx2 and PV distribution in the supragranular layers of the binocular zone of the mouse visual cortex, before the critical period (pre-CP, P19) and at the peak of plasticity (CP, P29) (scale bar: 50μm).

On the right panel, Otx2 infusion rescues PV-cell maturation after dark-rearing (DR) from birth. The maturation of PNN assembly, stained with the lectin WFA, is also regulated by Otx2 arrival (scale bar: 100μm, adapted from Sugiyama et al., 2008).

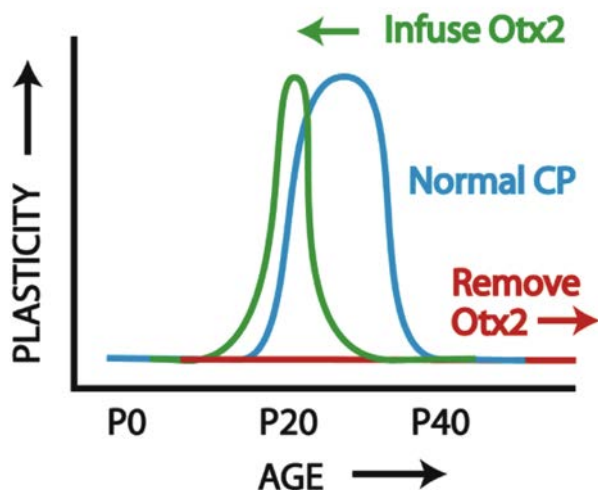


**Figure 14. Otx2 regulates the timing of the critical period for ocular dominance plasticity**

Otx2 gain of function (infusion of Otx2 in the visual cortex) before the normal critical period (CP) accelerates the onset and the closure of the critical period. Otx2 removal (through infusion of anti-Otx2 antibody in the visual cortex or deletion of *Otx2*) delays the onset of the critical period.

Plasticity in adulthood can also be induced by lifting the molecular brakes. Chondroitinase ABC (ChABC) is a bacterial enzyme that catalyzes the removal of CS chains (Prabhakar et al., 2005). Digestion of the PNNs using ChABC reactivates ocular dominance plasticity after critical period closure (Pizzorusso et al., 2002). Furthermore, ChABC treatment can rescue cortical acuity in adult amblyopic rats with a complete recovery of ocular dominance, visual acuity and dendritic spine density (Pizzorusso et al., 2006). PNNs assemble at the closure of critical periods also for other regions of the cerebral cortex, such as the mouse barrel cortex (McRae et al., 2007), the zebrafish HVC nucleus for song learning (Balmer et al., 2009), and the mouse amygdala for fear extinction (Gogolla et al., 2009). Whereas young mice can permanently erase an acquired fear memory by extinction training, adult animals exhibit fear behaviors that are resistant to erasure. In the adult basolateral amygdala, PNN degradation by ChABC reopens a critical period during which fear memories are fully erased by extinction training (Gogolla et al., 2009). On the epigenetic side, histone deacetylase inhibitors that increase histone acetylation can reactivate ocular dominance plasticity after critical period closure (Putignano et al., 2007) and enable recovery from amblyopia in adulthood (Silingardi et al., 2010). Therefore, most of these manipulations restore enough plasticity in the adult to reverse amblyopia (Bavelier et al., 2010).

#### **IV. Otx2 HOMEOPROTEIN AND VISUAL CORTEX PLASTICITY**

##### **A. Otx2 transfer in the visual cortex during the critical period**

Homeoproteins are not only expressed early in development, but also postnatally and in the adult. During postnatal development, the homeoprotein Otx2 is found at several levels of the optic trail, in the retina, in the dorsal lateral geniculate nucleus of the thalamus and in the visual cortex. While Otx2 mRNA is found in the retina and the thalamus, the Otx2 locus is silent in the visual cortex. Thus the Otx2 protein must be transported from extra-cortical sources. Among possible sources for cortical Otx2, plausible candidates are the eye and the choroid plexus, two established sites of Otx2 expression (Spatazza et al., 2013b; Sugiyama et al., 2008). Otx2 protein is clearly reduced in the visual cortex after dark-rearing, indicating that the presence of this protein in the cortex is experience-dependent (Sugiyama et al., 2008). This reduction is also observed after surgical removal of the eyes (Sugiyama et al., 2008).

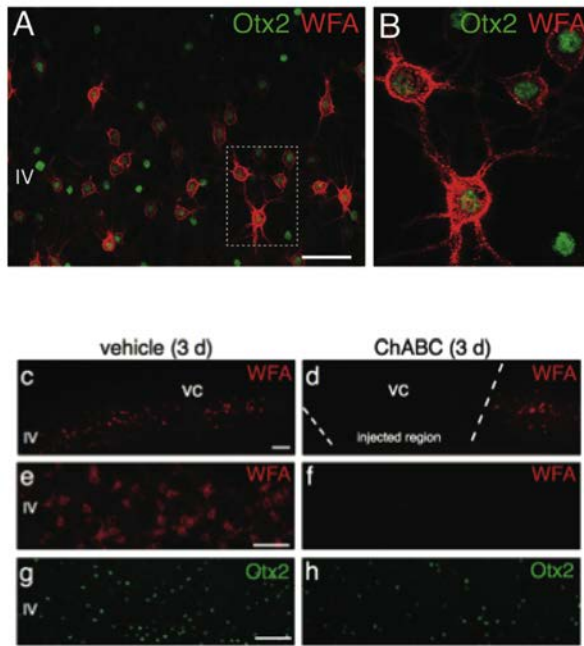


**Figure 15. The capture of Otx2 by PV-cells involves PNNs**

On the top panel, Otx2 is found preferentially in cells surrounded by PNNs (stained with WFA) in the layer IV of the visual cortex (scale bar: 50μm).

The lower panel shows that chondroitinase ABC injection into adult visual cortex disrupts PNNs and decreases the number of Otx2-positive cells (scale bar: 100μm; adapted from Beurdeley et al., 2012).

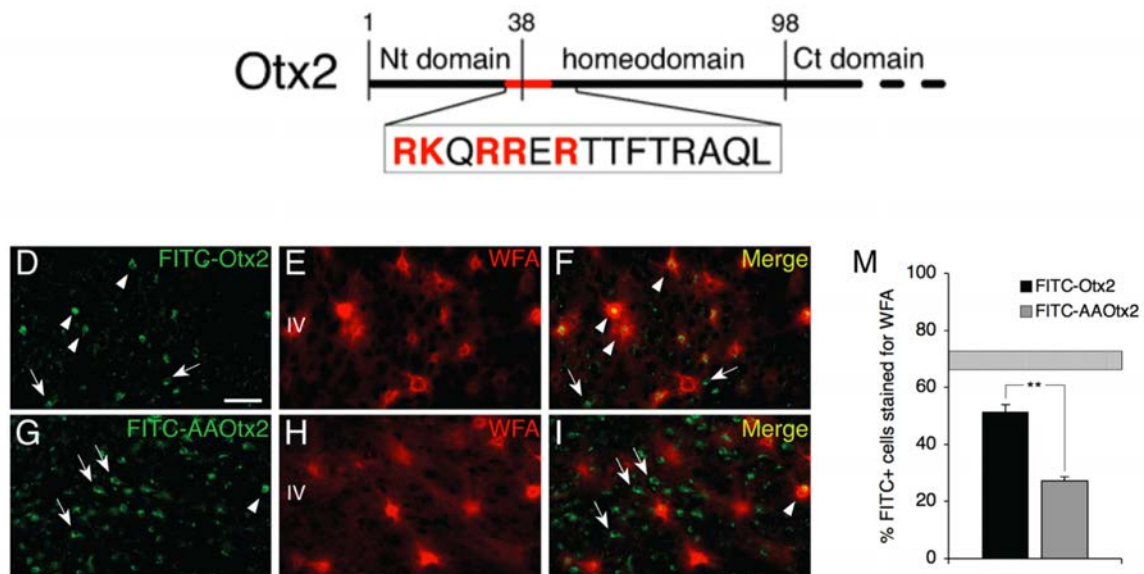


**Figure 16. A GAG-binding motif within Otx2 sequence**

The top panel shows the GAG-binding motif of Otx2, with the RK doublet located just before the beginning of the homeodomain.

The lower panel illustrates the importance of the RK doublet for PNN recognition. Exogenous FITC-Otx2 shows a preference towards PNN-surrounded cells, while FITC-AAOtx2 (in which the RK doublet has been replaced by two alanines) is internalized by a larger range of cells (scale bar: 50μm; arrow heads: double-stained cells; arrows: FITC-positive cells not stained with WFA; adapted from Beurdeley et al., 2012).

In the visual cortex, the majority of neurons containing Otx2 protein are GABAergic interneurons and over 70% of them are PV-cells. The time-course of Otx2 accumulation in PV-cells parallels that of PV expression: Otx2 protein is barely detected in the primary visual cortex prior to critical period onset, is increasingly concentrated by PV-cells during the critical period and persists in adulthood (Sugiyama et al., 2008). Otx2 not only accumulates in PV-cells but also promotes their maturation (Figure 13). Early Otx2 infusion increases PV-cell expression of molecular components such as PV, Kv3.1b potassium channel, Gad65 and the  $\alpha 1$ -subunit of GABA<sub>A</sub> receptors (Sugiyama et al., 2008). The opposite effect is observed on these markers in Otx2 conditional knock-out mice in which Otx2 presence in the visual cortex is strongly reduced (Sugiyama et al., 2008). In addition, in dark-rearing conditions that delay PV-cell maturation (Katagiri et al., 2007; Tropea et al., 2006), the direct infusion of Otx2 in the visual cortex restores normal levels of PV expression (Sugiyama et al., 2008). This effect of Otx2 is PV-cell specific, since the expression of calretinin and the development of calretinin-containing interneurons are not affected by Otx2 infusion or deletion.

Early cortical infusion of Otx2 triggers a precocious critical period before its natural onset (Sugiyama et al., 2008). Conversely, down-regulating *Otx2* expression in the retina prevents ocular dominance plasticity and the interception of extracellular Otx2 by antibody injection either in primary visual cortex or in the retina has similar effects (Sugiyama et al., 2008). Finally, *Otx2* conditional knock-out mice, which lack cortical Otx2, do not display ocular dominance plasticity during the critical period (Sugiyama et al., 2008; 2009) and plasticity is rescued by treatment with benzodiazepine, as in the *Gad65* knock-out mice (Hensch et al., 1998). This confirms that Otx2 is a crucial extra-cortical signal for the maturation of inhibitory circuits and the activation of critical period plasticity (Figure 14).

## **B. Otx2 transfer in the adult consolidated visual cortex**

Its preferential capture by PV-cells suggests the existence of Otx2 binding sites at the PV-cell surface. As PV-cells are gradually enwrapped by PNNs during critical period, there is a strong association between endogenous Otx2 and PNNs in layer IV of the adult visual cortex (Beurdeley et al., 2012). PNN hydrolysis with the enzyme ChABC, which reopens plasticity in the adult cortex (Pizzorusso et al., 2002), decreases endogenous Otx2 concentration in PV-



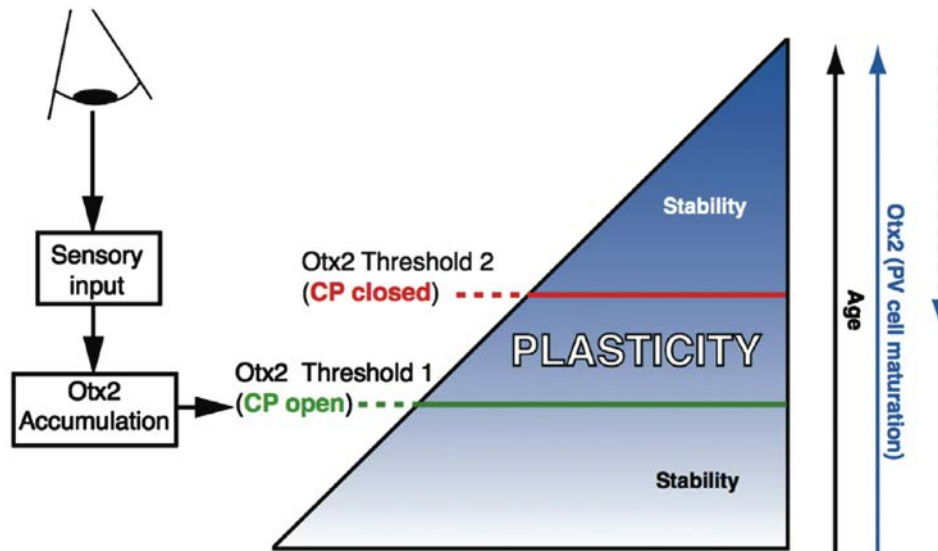


**Figure 17. A two-threshold model for Otx2 regulation of cortical plasticity**

Early sensory experience initiates the accumulation of Otx2 in PV-cells and induces their functional maturation that leads to plasticity onset. As the critical period proceeds, PNNs condense tightly around these PV-cells causing higher levels of Otx2 to accumulate and stabilize the local circuit. This process is reversible by knocking-down Otx2 at its source or blocking Otx2 transfer in the visual cortex (adapted from Spatazza et al., 2013b).

cells (Figure 15) (Beurdeley et al., 2012). Thus, it is likely that complex sugars of the PNNs participate in the specific recognition of Otx2 before its internalization.

A short motif within Otx2 sequence (RKQRRERTTFTRAQL), which partially overlaps with the beginning of the homeodomain, possesses consensus traits of a GAG-binding domain (Cardin and Weintraub, 1989). This RK motif is necessary for the preferential Otx2 recognition by PNNs. Indeed, while a full-length FITC-Otx2 protein injected in the visual cortex shows a preference towards PNN-enwrapped cells, FITC-Otx2-AA protein, in which the RK doublet is replaced by two alanines, is internalized by a larger range of cells (Figure 16). The RK motif shows a high affinity for chains of disulfated chondroitin sulfates CS-D and CS-E (Beurdeley et al., 2012) and a developmental increase in the 4-sulfation/6-sulfation (4S/6S) ratio of CS chains may be required for the accumulation of Otx2 (Miyata et al., 2012).

When a synthetic peptide (RK-peptide) corresponding to this GAG-binding motif is infused into the adult visual cortex, it competes with endogenous Otx2 and blocks its transfer into cells of the primary visual cortex. The amount of Otx2 captured by PV-cells is decreased, resulting in a down-regulation of PV expression and a clear decrease in PNN assembly, as if the maturational status of PV-cells was back to a critical period state. Indeed, this infusion in the adult cortex reactivates ocular dominance plasticity and allows recovery of visual acuity in amblyopic mice (Beurdeley et al., 2012). Both gain- and loss-of-function experiments (Beurdeley et al., 2012; Sugiyama et al., 2008) indicate that Otx2 internalization enhances several markers of PV-cell maturation, including PNN formation. The ongoing positive feedback of nascent PNNs attracting Otx2, thus triggering their own continued maintenance throughout life, may serve to prevent plasticity in adulthood (Beurdeley et al., 2012). Otx2 regulation of plasticity can therefore be explained by a two-threshold model: the critical period is triggered as Otx2 is first captured by PV-cells, but then closes as maturing PNNs condense and permit the constant accumulation of Otx2 in PV-cells (Figure 17). It is of note that Otx2 protein is present in PV-cells not only in the visual cortex, but also across various brain regions, including prefrontal, auditory, and somatosensory cortices, as well as the basolateral amygdala. Consequently, it has been speculated that this factor acts as a global regulator of PV-cell maturation and cerebral cortex plasticity during development and in the adult (Spatazza et al., 2013a).

A possible explanation for its widespread distribution is the existence of a global source of Otx2 synthesis and release. A distinct possibility for such a source is the choroid plexus, a structure present in the brain ventricles and responsible for the synthesis of the cerebrospinal fluid. Indeed, the choroid plexus is an established site of Otx2 expression throughout life (Johansson et al., 2013; Spatazza et al., 2013b). In the adult mouse, Otx2 is secreted by choroid plexus epithelial cells, as it is found both at the surface of the plexus and in the cerebrospinal fluid (Spatazza et al., 2013b). Knocking-down Otx2 in the adult choroid plexus decreases Otx2 cortical content, together with a parallel decrease in PV expression and PNN assembly. In agreement with the results obtained by a direct blockade of Otx2 transfer into adult cortex (Beurdeley et al., 2012), the knock-down of Otx2 in the adult choroid plexus leads to reactivation of cortical plasticity allowing both the installation of amblyopia and the restoration of visual acuity in adult amblyopic mice (Spatazza et al., 2013b).

These studies on Otx2 and cortical plasticity (Sugiyama et al., 2008; Beurdeley et al., 2012) are the foundation of my thesis project, which aims to understand how Otx2 interacts with the complex sugars at the surface of PV-cells for critical period regulation. The first approach is the analysis of a transgenic Otx2-AA mouse line, in which the interaction between Otx2 and GAGs should be disrupted. The studies described above suggest that CS GAG chains of the PNNs are involved in Otx2 binding and that specific sugar epitopes may be recognized by distinct homeoproteins according to a ‘sugar code’ (Holt and Dickson, 2005). The second, more biochemical, part of my project was therefore to identify whether there are specific GAG sequences that, in PNNs, are involved in Otx2 recognition. Finally, the third part of this thesis will describe models developed to interfere with Otx2 transduction in the adult using non-invasive techniques. These three aspects converge on the development of novel strategies to regulate plasticity in the adult cerebral cortex.





## **MATERIALS AND METHODS**



## I. PLASMID AND PROTEINS

### A. Single chain antibody plasmid

The single chain antibody plasmid was prepared from anti-Otx2 hybridoma cells (CD7) obtained from Eurogentec. Cloning was achieved as in (Barbas, 2001). The light and heavy chains were amplified through PCR from RNA extracted from the anti-Otx2 hybridoma cells. After selection of the proper sequences (Lefranc et al., 2003), the whole synthetic mini-gene was inserted into a vector for transgenic mouse generation. A similar preparation of single chain antibodies from anti-Pax6 and anti-Engrailed is described in (Lesaffre et al., 2007).

### B. Protein production

Recombinant CRE-Tat, NterOtx2 and Engrailed2 proteins were produced as described in (Beurdeley et al., 2012; Spatazza et al., 2013b). The protein coding sequences were inserted in a derivative of pSCherry2 (Eurogentec) and expressed in SE1 bacteria grown in MagicMedia Medium (Invitrogen). The proteins were purified by two successive steps of affinity chromatography, first on Nickel column and second on heparin column following removal of the polyhistidine tag by preScission proteolytic cleavage. The recombinant proteins were eluted on FPLC (AKTA, GE Healthcare), with a linear gradient of NaCl (ranging from 0.3 to 2 M), in 10mM phosphate buffer, pH 7.5.

The full-length Otx2 protein was purchased from PX'Therapeutics.

## II. ANIMALS

### A. Otx2-GFP and Otx2-AA mouse lines

Otx2-GFP and Otx2-AA mouse lines were generated by the laboratory of Antonio Simeone (CEINGE, Naples). In the Otx2-GFP mouse line, the Otx2 coding sequence and introns were replaced with the *GFP* gene (Acampora et al., 2009). *Otx2*<sup>+/GFP</sup> males were crossed with B6D2F1 females to obtain *Otx2*<sup>+/GFP</sup> heterozygous mice. *Otx2*<sup>+/AA</sup> males were crossed with B6D2F1 females to obtain *Otx2*<sup>+/AA</sup> heterozygous mice. *Otx2*<sup>+/AA</sup> males were crossed with *Otx2*<sup>+/AA</sup> females to obtain *Otx2*<sup>AA/AA</sup> homozygous mice. All animals have a B6D2 genetic



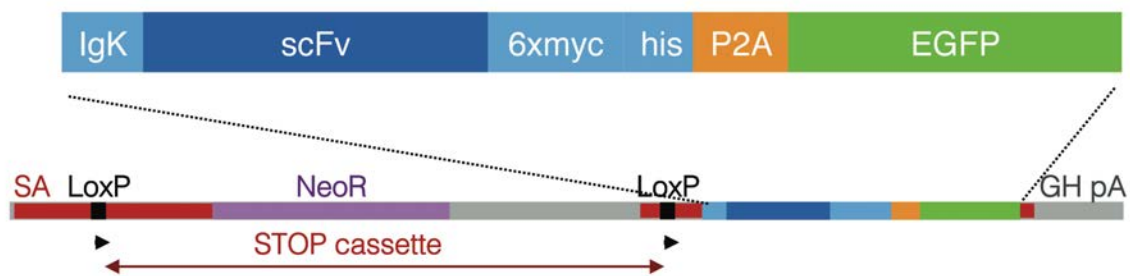


**Figure 18. Construct for single chain antibody knock-in mouse**

The anti-Otx2 single chain antibody (scFv) was knocked in the *ROSA26* locus of C57Bl6 mice. The scFv plasmid contains an IgK signal peptide for secretion, 6 myc tags for detection and a skipping peptide (P2A) before EGFP. A STOP cassette was inserted before the scFv construct, flanked with two LoxP sites.

**A**

	Mice	Fwd	Sequence	Rev	Sequence	Amplicon size (bp)
<b>GENOTYPING</b>	Otx2-GFP	Mal	ACT CCA GGC GAA TCG AGA CCG TC	GFP-Q	CTT GAA GAA GTC GTG CTG CTT CA	333
	Otx2-AA	AA Fwd	ACT TGC CAG AAT CCA GGG TGC AG	AA-Rev	CCA GGC TAA AAG ACC CTG GTT C	290
	scFvOtx2	Xf	CCT TTA AGC CTG CCC AGA AG	R1r	CTC GGC ATG GAC GAG CTG TAC AAG	597
	scFvPax6	Xf	CCT TTA AGC CTG CCC AGA AG	R1r	CTC GGC ATG GAC GAG CTG TAC AAG	597
	Mice	Fwd	Sequence	Rev	Sequence	Amplicon size (bp)
<b>RECOMBINATION</b>	scFvOtx2	Ef-Otx2	TGG AAG GGA TTC CAG AGA TAG A	Er2	AAA GTC GCT CTG AGT TGT TAT	757
	scFvPax6	Ef-Pax6	TCA ACA CAA TGT CGA GCT C	Er2	AAA GTC GCT CTG AGT TGT TAT	589

**B**

scFv mice		
temperature	time	cycles
95°C	5'	40 cycles
94°C	30"	
60°C	1'	
72°C	1'	
72°C	5'	
20°C	5'	
4°C	∞	

**C**

Otx2-AA and Otx2-GFP mice		
temperature	time	cycles
95°C	15'	35 cycles
96°C	30"	
62°C	1'30"	
72°C	1'	
72°C	7'	
4°C	∞	

**Table 1. Genotyping protocol**

(A) Primers used for genotyping Otx2-GFP, Otx2-AA and scFv mice. The lower part of the table presents the primers used to check the recombination in scFv mice.

(B) PCR protocol for scFv mice genotyping.

(C) PCR protocol for Otx2-AA and Otx2-GFP mice genotyping.

background. In all tests performed, there were no differences between wild-type animals from different litters.

### **B. scFv mouse lines**

scFvOtx2, scFvPax6 and scFvEn1/2 mouse lines were generated at the Institut Clinique de la Souris (ICS, Illkirch, France). The scFv construct, preceded by a LoxP-STOP-LoxP cassette, was inserted through a knock-in approach in the Rosa26 allele (Figure 18).

*scFvOtx2<sup>tg/o</sup>* males were crossed with C57Bl6/J females to obtain heterozygous mice. *scFvOtx2<sup>tg/o</sup>* males were crossed with *PV<sup>Cre/Cre</sup>* females to obtain *PV<sup>Cre/o</sup>;scFvOtx2<sup>o/o</sup>* and *PV<sup>Cre/o</sup>;scFvOtx2<sup>tg/o</sup>* mice. The same crossings were done with *scFvPax6<sup>tg/o</sup>* and *scFvEn1/2<sup>tg/o</sup>* males. In all tests performed, there were no differences between the wild-type animals from different litters.

### **C. Genotyping protocol**

Tail or ear biopsies were digested with 0.3 mg/ml proteinase K (#E195, Amresco) in 200 µl DirectPCR tail buffer (#101-T, Viagen) at 55°C for 16 h. After inactivation of the enzyme at 85°C for 45 min and centrifugation, 1 µl of the supernatant was analyzed by PCR (HotStarTaq *Plus* Master Mix Kit, #203646, Qiagen). The primer sequences and the PCR protocols are presented in Table 1. PCR products were loaded together with DNA loading dye (#R0611, Fermentas) on a gel with 1.5% agarose, 1X Sybr Safe (#S33102, Invitrogen) 20 mM Tris-acetate, 0.5 mM EDTA. The gel was run in 20 mM Tris-acetate, 0.5 mM EDTA buffer at 100 V for 15 min. DNA bands were imaged using a Safe Imager Blue-Light Transilluminator (#G6600, Invitrogen).

### **D. Cats**

The adult cats used for glycosaminoglycan extraction were a generous gift from Dr Milleret (Collège de France). They were all in good health and had no apparent malformations or pathologies.

## **E. Commercial mice and rats**

Conventionally raised (12:12 hour light:dark cycle) C57Bl/6 mice and Sprague Dawley rats were purchased from Janvier.

## **III. CELL CULTURE**

### **A. scFv ear fibroblast culture**

An ear punch was taken from adult *scFvPax6<sup>tg/o</sup>* and *scFvOtx2<sup>tg/o</sup>* mice, cut in small pieces in 0.5 ml HBSS (#24020-125, Invitrogen) and incubated 45 min at 37°C with collagenase (1000 U/ml, #C4785, Sigma-Aldrich). The sample was centrifuged 5 min at 1000 rpm, the supernatant discarded and the pellet was washed with HBSS and incubated with 0.05% trypsin (#15400-054, Gibco, Life Technologies) for 30 min at 37°C. The sample was centrifuged 5 min at 1000 rpm, the supernatant discarded and the pellet resuspended in 0.5 ml fibroblast culture medium (10% fetal calf serum (#16000-044, Invitrogen), 1% MEM Non essential amino acids (#11140-050, Invitrogen), 1% Penicillin/Streptomycin (#15240-122, Invitrogen) in DMEM Medium (#11965-092, Invitrogen)). After trituration to disrupt cell aggregates, the suspension was plated in a 3 cm culture dish in fibroblast culture medium and incubated in 37°C, 5% CO<sub>2</sub> humidified incubator.

After several days in culture, the fibroblasts were treated 1 hour with 10 µM Cre-TAT in DMEM added directly to the culture medium. Cells and supernatants were collected 48 hours later and protein extracts were processed for Western blot. The supernatants were also used as primary antibodies on Western blots for protein recognition specificity (the supernatants were incubated on the membrane overnight at 4°C).

### **B. Transfection and reporter assay**

The secreted alkaline phosphatase reporter construct Rbp3 prot/pSEAP2-Basic vector was a gift from Dr. Lamonerie (Université Nice Sophia Antipolis, France) (Chatelain et al., 2006). The reporter construct was co-transfected with Otx2 or Otx2-AA expression vector (pCL-Otx2 or pCL-Otx2-AA) into 293T human embryonic kidney cell line by Lipofectamine 2000. 48 hours post-transfection, secreted alkaline phosphatase was analyzed using the Great

EscAPe SEAP Chemiluminescence Assay (Clontech) according to the manufacturer's protocol.

## **IV. ANIMAL EXPERIMENTS**

### **A. Cortical infusion**

Eight week-old C57BL/6J mice were anesthetized with a mix of xylazine/ketamine (Imalgène 500 Virbac France, 80 mg/kg, Rompun 2% Bayer, 5 mg/kg) until pain reflexes were lost. Mice were mounted on a stereotaxic frame and a hole was made in the skull at right primary visual cortex coordinates (with respect to lambda:  $-0.65$  mm on the antero-posterior axis,  $-1.75$  mm laterally). A cannula linked to a micro-osmotic pump (Alzet, 1  $\mu$ L/h) was implanted at 400  $\mu$ m in depth. Mice were infused for 3 days into the right primary visual cortex with 0.4 nM of synthetic CS-E hexasaccharide. Control animals were infused with PBS. Animals were then processed for perfusion and immunohistochemistry.

### **B. CRE-Tat protein injection**

Adult mice were anesthetized with a mix of xylazine/ketamine (Imalgène 500 Virbac France, 80 mg/kg, Rompun 2% Bayer, 5 mg/kg) until pain reflexes were lost. Mice were mounted on a stereotaxic frame and a hole was made in the skull at lateral ventricle coordinates (with respect to bregma:  $-0.58$  mm on the A/P axis,  $\pm 1.28$  mm laterally and 2 mm in depth). CRE-Tat recombinant protein was injected bilaterally into the lateral ventricles, using a 10  $\mu$ l syringe (Hamilton) coupled to an electronic injection device, at a rate of 0.2  $\mu$ l/min. Five days after injection, the mice were processed for cerebrospinal fluid sampling.

### **C. Electroretinogram**

Mice were anesthetized with a mix of xylazine/ketamine (Imalgène 500 Virbac France, 80 mg/kg, Rompun 2% Bayer, 5 mg/kg), the iris dilated with tropicamide (Mydriaticum 0.5% Théa, France) and the cornea anesthetized locally with oxybuprocaine hydrochloride. Gold electrodes were placed in contact with each eye, reference electrodes were placed subcutaneously in the submandibular area, and a ground electrode was placed subcutaneously

on the back of the animal. ERG was performed in five animals of each genotype and each age with a mobile apparatus (SIEM Bio-Medicale, France) with LED lamps in a Ganzfeld chamber controlled by the VisioSystem software.

#### **D. Optomotor test**

Visual acuity was assessed by optomotor responses as described in (Abdeljalil et al., 2005; Torero Ibad et al., 2011). Mice adapted to ambient light were placed on a raised grid platform centered in a well-lit motorized drum with 100% contrast black and white vertical stripes. Different spatial frequencies were tested: 0.063, 0.125, 0.25, 0.375, 0.5 and 0.75 cycles per degree. The drum rotated at 2 rpm and the number of head turns was counted during clockwise and counter-clockwise rotation of the drum during 1 minute in each direction.

#### **E. Visual evoked potentials**

Electrophysiological recordings were performed under Nembutal/chlorprothixene anesthesia using standard techniques (Beurdeley et al., 2012). Transient visual evoked potentials in response to abrupt contrast reversal (100%, 1 Hz) over a range of spatial frequencies (0.01–0.6 cycles/degree) were band-pass filtered (0.1–100 Hz), amplified, and fed to a computer for analysis. At least 20 events were averaged in synchrony with the stimulus contrast reversal. Visual acuity was obtained by extrapolation to zero amplitude after correction of noise level. Monocular deprivation consisted of eyelid suture under isoflurane anesthesia; in some cases, the suture was reopened to test for recovery.

#### **F. Auditory cortex recordings**

Mice were placed in a sound-attenuating chamber and exposed from P16 to P19 to 7 kHz tones generated by Audacity software and amplified by speakers placed in two corners of the chamber. Mice were decapitated and acute auditory thalamocortical slices were prepared (Barkat et al., 2011) and incubated in artificial cerebrospinal fluid (ACSF) containing 5  $\mu\text{g/L}$  voltage-sensitive dye Di-4-ANEPPS (Invitrogen #D-1199) for at least 90 min. Slices were then transferred to an ACSF recording chamber and imaged using an Olympus MVX10 microscope. Fluorescence change was normalized to resting fluorescence ( $\Delta F/F_0$ ). The stimulating electrode was positioned on the rostral ventral medial geniculate body of the

thalamus at six discrete positions spaced at 100  $\mu\text{m}$  intervals along the medio-lateral axis. Cortical response amplitude was defined as maximum fluorescence change ( $\Delta F/F$ ) per trial at a given region of interest. Peak amplitude was defined as maximum response amplitude across all layer IV locations.

## **V. CEREBROSPINAL FLUID SAMPLING**

The cerebrospinal fluid sampling procedure was adapted from described methods in (Liu and Duff, 2008) and (Morrey et al., 2008). Mice were anesthetized with a mix of xylazine/ketamine (Imalgène 500 Virbac France, 80 mg/kg, Rompun 2% Bayer, 5 mg/kg) until pain reflexes were lost. Mice were mounted on a stereotaxic frame, the dura covering the cisterna magna was gently exposed, and the surrounding area was thoroughly cleaned using sterile saline-soaked cotton swabs. Cerebrospinal fluid was mechanically aspirated through a capillary connected to a sterile catheter tube and inserted into the cisterna magna. On average, 10  $\mu\text{l}$  of cerebrospinal fluid could be retrieved from an adult mouse. Samples contaminated with traces of blood were discarded. During the collection procedure, cerebrospinal fluid samples were kept on ice and then processed for immunoprecipitation or western blot detection.

## **VI. CELL SURFACE BIOTINYLATION**

Adult mouse choroid plexus from the fourth ventricle was rapidly extracted in cold PBS and two plexuses were pooled for one experimental sample. They were immediately processed for biotinylation with 0.5 M EZlink-SulfoNHS-Biotin (#21326, Thermoscientific) in PBS for 30 min at room temperature with gentle agitation. Following several washes in PBS 100 mM glycine, tissues were disrupted by sonication in PBS in the presence of protease inhibitors and nucleases. The samples were centrifuged 5min at 15 000 g and the supernatants were incubated with magnetic streptavidin beads (#65001, Dynabeads, Life Technologies) in PBS, 0.02% Tween and protease inhibitors, for 30 min at 4°C with gentle agitation. The beads were washed 4 times in PBS, 0.02% Tween and protease inhibitors and were directly resuspended in SDS-PAGE loading buffer, heated 10 min at 95°C and 1/5 of eluted biotinylated proteins was processed for western blot detection. Also, 1/4 of the flow-through from the beads was

**A PRIMARY ANTIBODIES**

Protein	Species	Origin/Reference	Dilution WB/DB	Dilution IHC
Brr3b	goat	Santa Cruz Biotechnologies (sc31989)	-	1/400
Calbindin	mouse monoclonal	Sigma-Aldrich (C9848)	-	1/500
CS-E	mouse monoclonal	laboratory of Linda Hsieh-Wilson, Caltech (USA)	1/5000	-
GFP	rabbit polyclonal	Life Technologies	1/1000	-
GPC6	mouse	Millipore (MABN531)	1/500	-
MYC	rabbit	Sigma-Aldrich (C3956)	1/4000	1/400
Otx2	rabbit monoclonal	Abcam (ab92326)	1/2000	-
Otx2	rabbit polyclonal	Millipore (AB9566)	-	1/400
Otx2	mouse monoclonal	in house (CD4)	-	1/50
Pax6	rabbit polyclonal	Covance (PRB-278P)	-	1/400
PV	rabbit polyclonal	Swant (PV25)	-	1/400
R/G opsin	rabbit polyclonal	Millipore (AB5405)	-	1/400
RhoA	mouse monoclonal	Santa Cruz Biotechnologies (sc418)	1/200	-
Sox2	goat	Santa Cruz Biotechnologies (sc17320)	-	1/200
Vsx2	mouse monoclonal	Santa Cruz Biotechnologies (sc365519)	-	1/300

**B SECONDARY ANTIBODIES**

IgG	Species	Origin/Reference	Dilution WB	Dilution IHC
anti-mouse, HRP-linked	horse	Cell Signalling Technology (7076)	1/2000	-
anti-rabbit, HRP-linked	goat	Cell Signalling Technology (7074)	1/4000	-
anti-goat, HRP-linked	rabbit	Abcam (ab6741)	1/4000	-
anti-mouse, Alexa fluor-conjugate	goat	Invitrogen (Life Technologies)	-	1/2000
anti-rabbit, Alexa fluor-conjugate	goat	Invitrogen (Life Technologies)	-	1/2000
anti-goat, Alexa fluor-conjugate	donkey	Invitrogen (Life Technologies)	-	1/2000

**C OTHERS**

	Origin/Reference	Dilution WB	Dilution IHC
WFA, biotin-conjugate	Sigma-Aldrich (L1516)	-	1/100
WFA, fluorescein-labeled	Vector (FL1351)	-	1/100
streptavidine, Alexa fluor-conjugate	Invitrogen (Life Technologies)	-	1/2000

**Table 2. Antibodies for Western blot, Dot blot and immunohistochemistry**

(A) Primary antibodies.

(B) Secondary antibodies.

(C) Other material used for PNN detection.

(WB: Western blot, DB: dot blot, IHC: immunohistochemistry)

concentrated by acetone precipitation (6 volumes acetone added at -20°C for 1 hour), resuspended in SDS-PAGE loading buffer, heated 10 min at 95°C and 1/5 of the total flow-through was processed for western blot detection.

## **VII. WESTERN BLOT**

Mice were killed by cervical dislocation, brain structures and retinas were manually dissected and homogenized in SDS-PAGE loading buffer according to tissue weight and heat 10 min at 95°C to denature proteins. Protein extracts were separated on NuPAGE 4%-12% Bis-Tris pre-casted gels (Invitrogen) for 1 hour at 200 V and transferred onto a methanol-activated PVDF membrane at 400 mA for 1 hour. The membrane was blocked in TBS, 0.2% Tween, 5% milk. Primary antibodies were incubated in blocking buffer overnight at 4°C and corresponding HRP-coupled secondary antibodies for 1 hour at room temperature. Membranes were imaged using a LAS-4000 gel imager (Fujifilm) and quantified by densitometry with ImageJ. The western blot primary and secondary antibodies are presented in Table 2.

## **VIII. RNA EXTRACTION AND DEEP SEQUENCING**

Mice were killed by cervical dislocation and cortical layers were manually dissected. RNA was extracted using the RNeasy Lipid Tissue Mini (#74804, Qiagen), according to manufacturer's instructions. For each sample processed for deep sequencing, layers from both cortices of 4 mice were pooled. From the extracted RNA, deep sequencing was performed and analyzed by the genomic platform of the École Normale Supérieure de Paris.

## **IX. IMMUNOHISTOCHEMISTRY**

Mice were anesthetized with a mix of xylazine/ketamine (Imalgène 500 Virbac France, 80 mg/kg, Rompun 2% Bayer, 5 mg/kg) until pain reflexes were lost and perfused transcardially with 15 ml of PBS followed by 10 ml of 4% paraformaldehyde prepared in PBS, at 160 ml/h. Their brains were dissected and post-fixed overnight at 4°C in 4% paraformaldehyde. Their eyes were dissected and post-fixed 1 hour at 4°C in 4% paraformaldehyde.



Immunohistochemistry was performed on free-floating sections (40  $\mu\text{m}$ ) encompassing the entire visual cortex or on cryo-sections (20  $\mu\text{m}$  for the brain, 12  $\mu\text{m}$  for the eyes). For the cryosections, the samples were cryoprotected in PBS 20% sucrose overnight at 4°C. Sections were permeabilized 30 min in PBS, 0.5% TritonX-100 and blocked in PBS, 0.5% TritonX-100, 10% normal goat serum for 1 hour at room temperature. Sections were incubated with primary antibodies overnight at 4°C, intensively washed in PBS at room temperature and further incubated with corresponding Alexa Fluor-conjugated secondary antibodies for 2 hours at room temperature. The immunohistochemistry primary and secondary antibodies are presented in Table 2. Biotinylated WFA (#L1516, Sigma-Aldrich, 1/100) was used to reveal perineuronal nets. Alexa Fluor-conjugated streptavidin (Molecular Probes, 1/2000) was used for its detection (Table 2C). Stained sections were mounted in Fluoromount medium (SouthernBiotech) and images were acquired with a SP5 confocal microscope (Leica). Images were analyzed (cell number and fluorescence) with ImageJ.

Hematoxylin and eosin staining on retinae was performed by Excalibur Pathology Inc. (Oklahoma City, USA).

## **X. GLYCOSAMINOGLYCAN EXPERIMENTS**

### **A. Glycosaminoglycan extraction and purification**

The animals were euthanized (rats with CO<sub>2</sub> and cats with a lethal dose of pentobarbital) and their posterior cortices were dissected. Cortices were either homogenized in acetone (to extract all cortical GAGs) or in 4 successive buffers (to differentially extract diffuse GAGs and PNNs). Cortical GAGs were extracted with acetone 30 min on ice, centrifuged 15 min at 2500g at 4°C and the pellet was washed in acetone once, dried using a Speedvac (SPD111V, Thermoscientific) and resuspended in pronase buffer (0.1 M Tris-HCl, pH 7.5). To extract the 4 types of GAGs, the cortices were homogenized in buffer 1 (50 mM TBS + protease inhibitors) then centrifuged 30 min at 15000 rpm at 4°C. The supernatant was kept and the pellet was re-extracted twice with buffer 1. The three supernatants from buffer 1 extractions were pooled. The pellet was extracted successively in the same way with buffer 2 (buffer 1 + 0.5% Triton X-100) and buffer 3 (buffer 2 + 1 M NaCl) and the supernatants for each buffer were pooled. The pellet was then extracted once with buffer 4 (buffer 2 + 6 M urea). The extracts were dialyzed against pronase buffer overnight. Pronase was added to the samples at

1:100 (enzyme:sample, w:w) 24 hours at 37°C. The pronase was inactivated by heating at 80°C 20 min. The samples were then digested with DNase 1 hour at 37°C in presence of 2.5 mM MgCl<sub>2</sub> and DNase was inactivated by heating at 75°C for 10 min. The samples were centrifuged 15 min at 4000 rpm and the supernatants were kept on ice. Proteins were precipitated overnight at 4°C with cold 10% trichloroacetic acid (TCA). The samples were centrifuged 15 min at 4000 rpm and the supernatants were incubated with cold 10% TCA for 1 hour on ice. The samples were centrifuged 15 min at 4000 rpm. The supernatants were washed with ether (1:1, v:v) 5 times and then neutralized with 1 M Na<sub>2</sub>CO<sub>3</sub>. GAGs were precipitated with 5% sodium acetate in 75% EtOH overnight at -20°C. The samples were centrifuged 15 min at 4000 rpm and the pellets washed with 100% EtOH. The pellets were resuspended in water and GAGs were quantified with Blyscan kit (#B1000, Biocolor).

## **B. Commercial GAGs and enzymes**

Chondroitin sulfate mix (#C4384), CS-A (#C9819), CS-B (#C3788) and CS-C (#C4384) were purchased from Sigma-Aldrich. Unsulfated chondroitin (#400640-1A), CS-D (#400676), CS-E (#AMS.CSR.NACS-2E.SQC-3) and HS (#AMS.GAG-HS01) were purchased from AMSBIO (former partnership with Seikagaku).

GAG-digesting enzymes: chondroitinase ABC (#C3667), heparinase II (#H6512) and hyaluronidase (#H4272) were purchased from Sigma-Aldrich.

## **C. Interaction between protein/peptides and GAGs**

### **Interaction on streptavidin beads**

Biotinylated RK-peptide (5 µg) was incubated on magnetic beads (#65001, Dynabeads, Life Technologies) in 100 mM ammonium acetate, for 1 hour at room temperature with gentle agitation. The beads were washed 3 times with 100 mM ammonium acetate. 10 µg of commercial GAGs were added on the beads together with 10 U hyaluronidase and incubated 30 min at 37°C with gentle agitation. The beads were washed 4 times with 100mM ammonium acetate and digested with 0.2 µg of trypsin 1 hour at 37°C with gentle agitation. The supernatant was recovered and trypsin was inactivated by heating 45 min at 85°C. GAGs were digested with 100 mU of ChABC overnight at 37°C and processed for FACE detection (see paragraph X.E).

### **Dot-blot**

Recombinant protein (1 µg) was incubated with commercial GAGs (10 µg) for 30 min at 37°C in 100 mM ammonium acetate. The samples were added on a PVDF membrane placed in a dot-blotting cassette and suction was applied. The wells were washed with 100 mM ammonium acetate. The membrane was blocked in TBS, 0.2% Tween, 300 mM NaCl, 1% BSA. Anti-CSE primary antibody was incubated in blocking buffer overnight at 4°C and the membrane was washed in TBS, 0.2% Tween, 300 mM NaCl. Anti-mouse HRP-coupled secondary antibody was incubated in blocking buffer for 1 hour at room temperature and the membrane was imaged using a LAS-4000 gel imager (Fujifilm).

### **Direct gel shift**

Otx2 protein (0.5 µg, PX'Therapeutics) was incubated at room temperature for 30 min with biotinylated synthetic CS-E hexasaccharide (3.4 nmol) in the presence of colominic acid (#C5762, Sigma-Aldrich) in 10 mM Tris, 100 mM NaCl and 2 mM EDTA. Complexes were separated on 6% native polyacrylamide gels at 100 V in migration buffer (90 mM Tris-borate, 2 mM EDTA; pre-run at 100 V for 30 min). After transfer onto a PVDF membrane at 380 mA for 30 min, the biotinylated sugar was detected using the LightShift Chemiluminescent EMSA Kit (#89880, Pierce), according to manufacturer's instructions. The membrane was then stripped with Restore Western Blot Stripping Buffer (#21063, ThermoScientific) and blotted with a primary anti-Otx2 antibody overnight at 4°C and a secondary anti-mouse-HRP antibody for 1 hour at room temperature. Membranes were imaged using a LAS-4000 gel imager (Fujifilm).

### **Competition gel shift**

Otx2 protein (0.5 µg, PX'Therapeutics) was incubated at room temperature for 30 min with 40 fmol of biotinylated *IRBP1* synthetic oligonucleotide (Chatelain et al, 2006) and sugars (4 pmol of commercial sugars, 4 pmol of synthetic CS-E hexasaccharide, 200 ng of purified cortical GAGs), in presence of 50 ng/µl dIdC in 10 mM Tris, 100 mM NaCl and 2 mM EDTA. For the digestion experiment, the cortical GAGs were pre-treated with 80 µU of GAG-digesting enzymes (ChABC, HepII, Hyaluronidase) for 1h30 at 37°C. Complexes were separated on 6% native polyacrylamide gels at 100 V in migration buffer (90 mM Tris-borate, 2 mM EDTA; pre-run at 100 V for 30 min). Samples were transferred onto a nylon membrane at 380 mA for 45 min, crosslinked with UV and detected using the LightShift Chemiluminescent EMSA Kit (#89880, Pierce), according to manufacturer's instructions.

Membranes were imaged using a LAS-4000 gel imager (Fujifilm) and quantified by densitometry with ImageJ.

### **Glycan arrays**

A poly-D-lysine-coated glass slide was prepared using a microarray printer, which deposits nanoliter volumes of carbohydrate solutions. Each carbohydrate was printed at five different concentrations: 0.5  $\mu$ M, 1  $\mu$ M, 5  $\mu$ M, 10  $\mu$ M and 15  $\mu$ M, with ten replicates per concentrations. The slide was blocked for 60 min with PBS 10% fetal bovine serum. 200  $\mu$ l of 1  $\mu$ M MYC-Engrailed2 or MYC-NterOtx2 in PBS 1% bovine serum albumin (blocking buffer) were spotted on the slide and incubated for 3 hours at room temperature. The slide was washed 3 times in PBS. Anti-MYC primary antibody was incubated in blocking buffer for 1 hour at room temperature and then washed three times in PBS. Anti-mouse Cy5-coupled secondary antibody was incubated in blocking buffer for 1 hour at room temperature, washed three times in PBS and one time in water. The slide was air-dried and scanned using an Agilent machine.

### **D. Sugar-ase protection protocol**

Commercial sugars (20  $\mu$ g) were incubated with Otx2 or Engrailed2 recombinant proteins for 20 min at room temperature in 100 mM ammonium acetate, 0.8% formaldehyde was added for 10 min at room temperature to cross-link the homeoprotein-GAG interactions and glycine (260 mM) was added for 5 min at room temperature to quench the formaldehyde. The samples were passed through a Zeba Spin Desalting Column (#89891, ThermoScientific) and digested overnight at 37°C with 100 mU of GAG-digesting enzymes. The samples were then passed through a 10 kD Amicon Centrifugal Filter (#UFC801024, Millipore) 4 times to remove the digested non-protected oligosaccharides. To remove the proteins, the recovered samples were digested with 20  $\mu$ g of proteinase K (#E195, Amresco) for 1 hour at 37°C, then inactivated for 45 min at 85°C. The samples were digested overnight at 37°C with 100 mU of GAG-digesting enzymes and processed for FACE detection.

### **E. Fluorophore Assisted Carbohydrate Electrophoresis**

GAGs (10  $\mu$ g) were digested with Chondroitinase ABC (100 mU) and/or Heparinase II (100 mU) and/or Hyaluronidase (10 U) overnight at 37°C. Proteins were precipitated with 80%

EtOH at -20°C for 1 hour, the sample was centrifuged 20 min at 10 000g at 4°C and the supernatant was dried using a Speedvacuum. The samples were resuspended in 12.5 mM AMAC (#06627, Sigma-Aldrich) in 85% DMSO/15% acetic acid and 1.25 M sodium cyanoborohydride (#156159, Sigma-Aldrich) in 100% DMSO for 16 hours at 37°C. 30% glycerol was added to the sample. 1 µl of sample was mixed with 20% DMSO and 10% glycerol and run on a 20% polyacrylamide native gel, in migration buffer (0.1 M glycine, 120 mM Tris, 0.1 M boric acid, pH 8.3) at 20 mA at 4°C for 1h30. The gel was imaged using a LAS-4000 gel imager (Fujifilm).

## **XI. STATISTICAL ANALYSIS**

Statistical analysis was performed with Prism software (version 5.0a). Pair wise comparison was done using Student t-test. A difference was considered significant at  $p < 0.05$ .





## **RESULTS AND DISCUSSION**



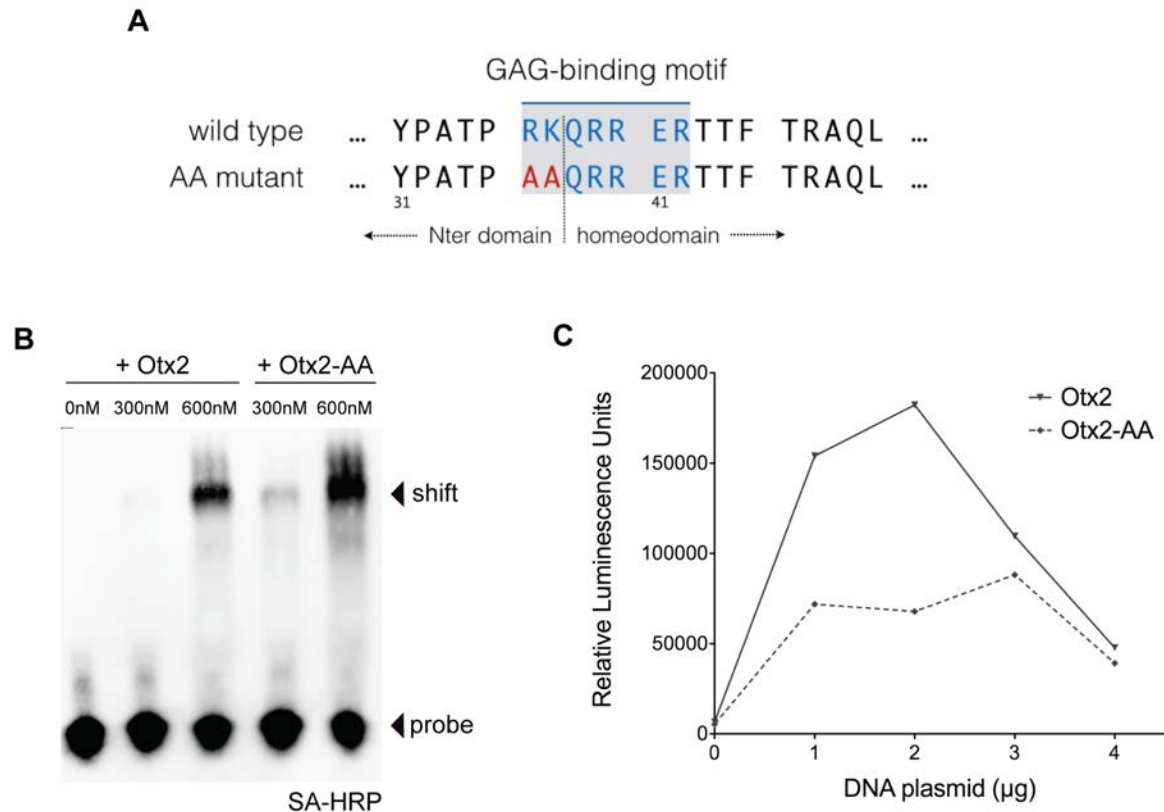


**Figure 19. Assessment of the transcriptional activity of Otx2-AA protein**

(A) Mutated amino acids in the Otx2 sequence. The mutated RK→AA doublet is located at the beginning of the GAG-binding motif.

(B) Gel shift assay with Otx2 and Otx2-AA recombinant proteins, using a *Rbp3* biotinylated DNA probe (revealed with streptavidin-HRP (SA-HRP)). The shift in DNA in presence of Otx2 and Otx2-AA shows that both proteins bind the DNA probe.

(C) To compare the transcriptional activities of Otx2 and Otx2-AA, HEK 293T cells were co-transfected with DNA constructs expressing secreted alkaline phosphatase under *Rbp3* promoter and increasing amounts of DNA expressing *Otx2* or *Otx2-AA*. Otx2-AA is a less active transactivator than Otx2 for the *Rbp3* promoter.

## **I. *Otx2* transgenic mice to investigate *Otx2* transfer roles in the visual system**

The discovery of a GAG-binding domain (RK motif) within *Otx2* sequence led us to develop a transgenic mouse line called *Otx2*-AA, in collaboration with Antonio Simeone and Dario Acampora (CEINGE, Naples). In this knock-in mouse, the RK doublet was replaced by two alanines (AA). Indeed, contrary to the RK-peptide, the AA-peptide did not show any measurable affinity for chondroitin sulfates in the isothermal titration calorimetry assay, nor had it the ability to compete with *Otx2* and to reactivate plasticity when infused in the adult visual cortex (Beurdeley et al., 2012). More importantly, the FITC-*Otx2*-AA protein did not show a preference towards the PNN-enwrapped cells when infused in the visual cortex (Beurdeley et al., 2012). We thus considered that in the *Otx2*-AA mouse where the RK was mutated into AA, transfer specificity into the PNN-enwrapped cells should be severely diminished, due to a decrease in specific GAG recognition by *Otx2*.

In addition to *Otx2*-AA mutants (the heterozygous *Otx2*<sup>+/AA</sup> and the homozygous *Otx2*<sup>AA/AA</sup> mice), we studied an *Otx2*-GFP mouse line. In this knock-in mouse, the *GFP* gene is inserted in one *Otx2* allele, making the *Otx2*<sup>+/GFP</sup> mouse heterozygous for *Otx2*.

### **A. *Otx2*-AA protein activity**

#### ***Otx2*-AA binds to DNA**

The *Otx2* GAG-binding motif spans the junction between the N-terminal domain and the homeodomain (Figure 19A). As both transfer sequences, penetratin and  $\Delta 1$ , are located within the homeodomain, mutations of these motifs also interfere with cell autonomous functions, and especially with DNA binding (Joliot and Prochiantz, 2004). Our first concern was to assess the activity of the *Otx2*-AA protein. Previous *in vivo* experiments (Beurdeley et al., 2012) indicated that exogenous *Otx2*-AA protein is still able to enter cortical cells, which suggests that the RK→AA mutation does not alter *Otx2* internalization properties.

To examine if the RK to AA mutation modifies *Otx2* DNA-binding properties, we compared the ability of *Otx2*-AA and *Otx2* recombinant proteins to bind the *Rpb3* promoter DNA sequence, an *Otx2* target (Chatelain et al., 2006). In a gel shift assay, both *Otx2* and *Otx2*-AA proteins were able to bind the DNA probe. The binding of *Otx2*-AA seemed even greater than the binding of the wild-type protein (Figure 19B).

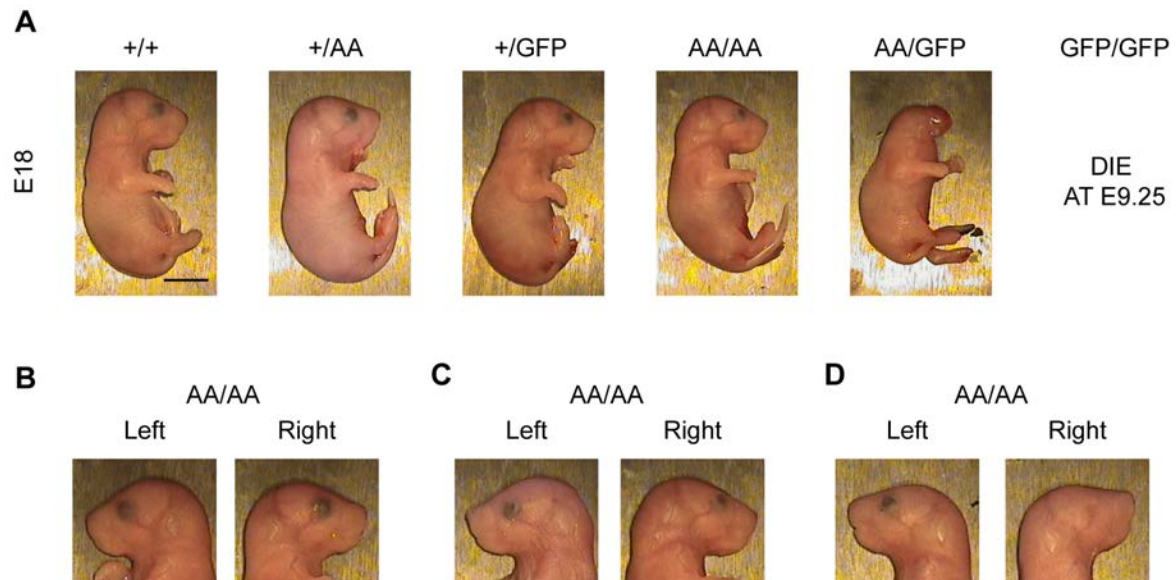


**Figure 20. *Otx2* mutants gross head and eye phenotypes**

(A) E18 embryos of the various genotypes. *Otx2*<sup>+/AA</sup>, *Otx2*<sup>+/GFP</sup> and *Otx2*<sup>AA/AA</sup> mice resemble *Otx2*<sup>+/+</sup> mice. The *Otx2*<sup>AA/GFP</sup> embryo is lacking the nasal half of the head but the rest of the body appears largely normal (scale bar: 0.5 cm).

(B-D) Left and right sides of *Otx2*<sup>AA/AA</sup> E18 embryos showing either normal sized eyes (B), a microphthalmic right eye (C) or anophthalmia on the right side (D). These images show the variable expressivity and incomplete penetrance of the phenotypes.

### **Otx2-AA transcriptional activity is reduced**

We also assessed the transcriptional activity of Otx2-AA in cultured mammalian cells expressing secreted alkaline phosphatase under the control of the *Rbp3* promoter. Transfection of Otx2 or Otx2-AA plasmids in this cell line showed that Otx2-AA was a less active trans-activator than Otx2 for the *Rbp3* promoter (Figure 19C). Similar experiments were done using *PKCα* and *Crx* promoters (Koike et al., 2007; Nishida et al., 2003) driving the expression of luciferase. In these experiments, transcriptional activity of Otx2-AA protein corresponded to 71 and 60%, respectively, of that of Otx2.

These *in vitro* results suggest that Otx2-AA is not only a transfer specificity mutant, but also present perturbed cell-autonomous activities. This precludes a precise discrimination of the two aspects of Otx2 activity (cell autonomous and transfer) in the Otx2-AA mutant mouse. In the rest of this study, the term “activity” will therefore include both cell autonomous and non-cell autonomous activities.

## **B. Otx2 activity in eye development and maintenance**

### **Gross phenotypes leading to eye investigation**

The altered activity of Otx2-AA was confirmed by the comparison of *Otx2*<sup>+/GFP</sup> mice (with one wild-type allele) with *Otx2*<sup>AA/GFP</sup> mice (with only one AA allele). The former mice have a grossly normal morphology, whereas the latter ones have a truncated head and die at birth (Figure 20A). *Otx2* null mice show a complete deletion of the early *Otx2* expression domain and are thus headless (Acampora et al., 1995; Ang et al., 1996). *Otx2*<sup>AA/GFP</sup> mice develop a hindbrain but only rudiments of the forebrain and midbrain, suggesting that one AA allele is insufficient for normal brain development. Similar to *Otx2*<sup>+/GFP</sup> mice, heterozygous *Otx2*<sup>+/AA</sup> and homozygous *Otx2*<sup>AA/AA</sup> mice were viable with an apparently normal head development (Figure 20A).

The most striking gross phenotype observed in the Otx2-AA mice was microphthalmia and anophthalmia in some *Otx2*<sup>AA/AA</sup> mice, with variable penetrance (Figure 20C-D). This was observed in 15% of the *Otx2*<sup>AA/AA</sup> mice, the others showing apparently normal eyes (Figure 2B). Among the *Otx2*<sup>AA/AA</sup> mice showing anophthalmia or microphthalmia, two mice out of 30 were affected bilaterally. The expression of these phenotypes was mostly asymmetric,

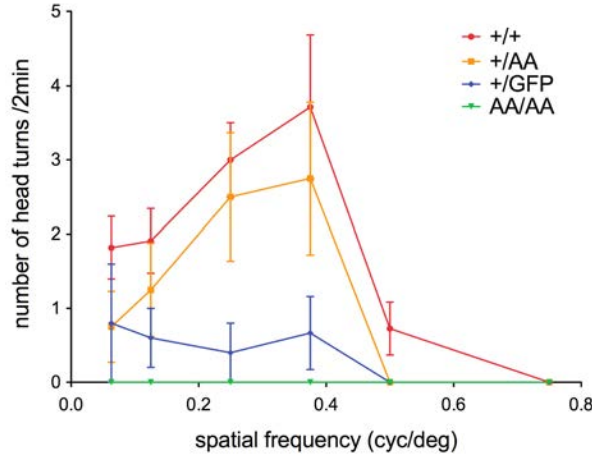
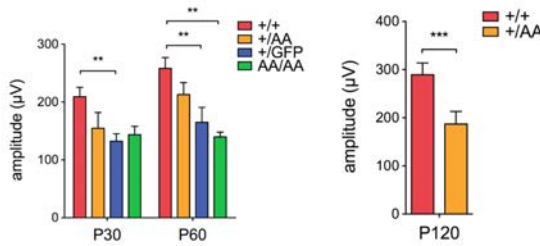
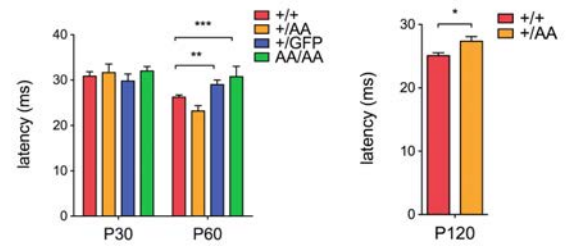


**Figure 21. *Otx2* mutants visual acuity**  
Visual acuity of *Otx2*<sup>+/-AA</sup> mice tested at P60 with the optomotor test is indistinguishable from visual acuity of *Otx2*<sup>+/+</sup> mice. The visual acuity of *Otx2*<sup>+/-GFP</sup> mice is significantly reduced at all spatial frequencies tested. All contrast gratings fail to elicit any head turns in *Otx2*<sup>AA/AA</sup> mice (error bars indicate SEM).

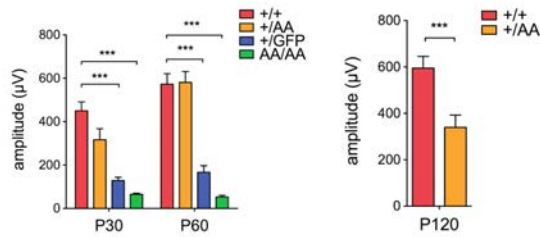
**A scotopic a-wave amplitude**



**B scotopic a-wave latency**



**C scotopic b-wave amplitude**



**D scotopic b-wave latency**

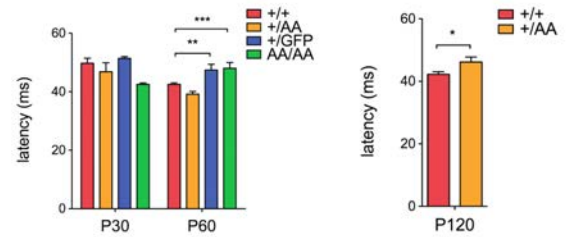


**Figure 22. *Otx2* mutants show functional deficits of photoreceptors and bipolar cells**

(A) Quantifications of a-wave ERG amplitudes at P30, P60 and P120. There is already a significant reduction of the a-wave amplitude at P30 in *Otx2*<sup>+/-GFP</sup> mice. The difference became significant for *Otx2*<sup>AA/AA</sup> mice at P60 and for *Otx2*<sup>+/-AA</sup> mice at P120.

(B) Quantifications of a-wave latencies. Both *Otx2*<sup>+/-GFP</sup> and *Otx2*<sup>AA/AA</sup> mice exhibit a significant increase in their a-wave latency at P60, observed only at P120 for *Otx2*<sup>+/-AA</sup> mice.

(C) Quantifications of b-wave ERG amplitudes. *Otx2*<sup>+/-GFP</sup> and *Otx2*<sup>AA/AA</sup> mice show a significant decrease in the b-wave amplitude at P30 and P60, observed only at P120 for *Otx2*<sup>+/-AA</sup> mice.

(D) Quantifications of b-wave ERG latencies. *Otx2*<sup>+/-GFP</sup> and *Otx2*<sup>AA/AA</sup> mice show significant increases in latencies at P60, observed only at P120 for *Otx2*<sup>+/-AA</sup> mice (\*p<0.05, \*\*p<0.01, \*\*\*p<0.001, error bars indicate SEM, Student t-test compared to wild-type littermates).

suggesting a lack of robustness in eye development. The absence of such major phenotypes in *Otx2*<sup>+/AA</sup> and *Otx2*<sup>+/GFP</sup> mice indicates that a single wild-type allele is sufficient to generate normal eye structure at a gross level. This, and the well-known importance of *Otx2* in eye development, led us to collaborate with the group of Jin Woo Kim (KAIST, Korea) to investigate eye development and maintenance in *Otx2*-AA mice, compared to their wild-type littermates and to heterozygous *Otx2*<sup>+/GFP</sup> mice. In order to simplify interpretation, we only studied *Otx2*<sup>AA/AA</sup> mice with externally normal eyes.

### ***Otx2* mutants have reduced visual acuity**

To evaluate the visual acuity of the *Otx2*-GFP and *Otx2*-AA mice, we chose the optomotor test (Prusky and Douglas, 2003). The mouse is placed in a rotating drum with vertical black and white stripes of different spatial frequencies. The number of head turns measures the ability of the mouse to distinguish the rotating stimulus. As the spatial frequency of the stripes increases (from 0.125 to 0.75 cycles per degree), the ability to separate them decreases with a parallel decrease in the number of head turns. When measured at P60, no significant difference in visual acuity was observed between the *Otx2*<sup>+/AA</sup> and *Otx2*<sup>+/+</sup> mice at all spatial frequencies tested (Figure 21). By contrast, *Otx2*<sup>+/GFP</sup> mice made significantly fewer head turns than their wild-type littermates at all spatial frequencies (principally  $0.67 \pm 0.49$  versus  $3.71 \pm 0.97$  at 0.375 cycles per degree and  $0.40 \pm 0.40$  versus  $3.00 \pm 0.50$  at 0.25 cycles per degree, respectively). Strikingly, *Otx2*<sup>AA/AA</sup> mice failed to respond to any spatial frequency tested (Figure 21). This behavioral test allowed us to rank the four genotypes according to their vision performance at P60, from normal to most severe: *Otx2*<sup>+/+</sup> = *Otx2*<sup>+/AA</sup> < *Otx2*<sup>+/GFP</sup> < *Otx2*<sup>AA/AA</sup>.

### ***Otx2* mutants have functional deficits in the retina**

Retinal physiological function was assessed by electroretinogram (ERG) measurements under dark adapted (scotopic) and light adapted (photopic) conditions at P30, P60 and P120. The ERG recordings were performed in collaboration with Serge Picaud (Institut de la vision, Paris). In the following description of our data, all changes observed in mutants are described in comparison with wild-type mice from the same litter.

A-wave amplitude and latency are two indexes of photoreceptor number and physiological activity, respectively. Photoreceptor function in the outer nuclear layer of the retina can therefore be monitored by measuring the a-wave responses (Figure 22A-B). Under scotopic

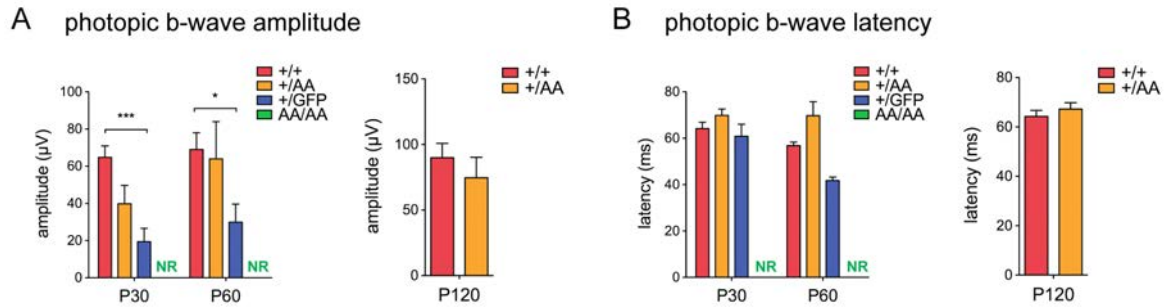


**Figure 23. *Otx2* mutants show functional deficits in the cone pathway**

(A) Quantifications of photopic ERG amplitudes at P30, P60 and P120. Photopic ERGs are not measurable in *Otx2*<sup>AA/AA</sup> mice already at P30 (NR: non responsive). In *Otx2*<sup>+GFP</sup> mice, the photopic ERG is significantly reduced at P30. No difference is detected for *Otx2*<sup>+AA</sup> mice. (B) Quantification of photopic ERG latencies. (\*p<0.05, \*\*\*p<0.001, error bars indicate SEM, Student t-test compared to wild-type littermates).

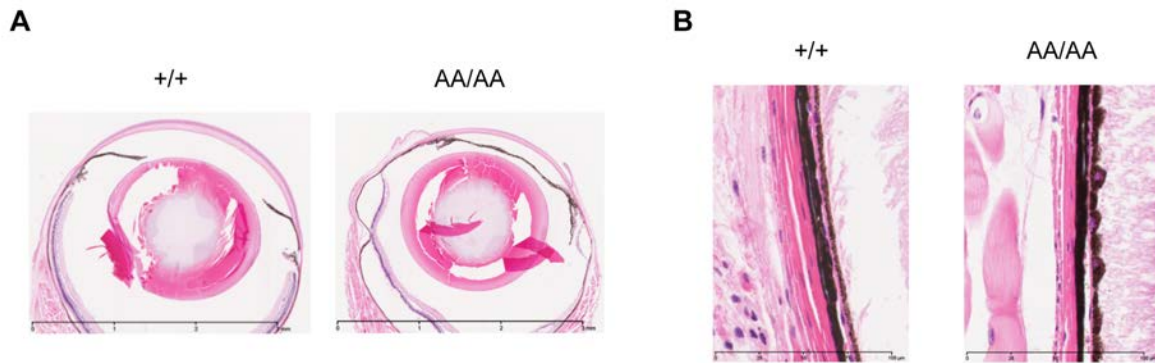


**Figure 24. Eye and retina defects in *Otx2*<sup>AA/AA</sup> mice**

Despite externally normal eyes, all *Otx2*<sup>AA/AA</sup> mice present eye and retina defects: for instance, 46% of *Otx2*<sup>AA/AA</sup> mice show iris defects (A, scale bar: 3 mm) and 46% of *Otx2*<sup>AA/AA</sup> mice show a festooned retinal pigment epithelium (B, scale bar: 100 μm). No similar defects were observed in the eye and retinal structures in *Otx2*<sup>+/+</sup>, *Otx2*<sup>+AA</sup> and *Otx2*<sup>+GFP</sup> animals.

conditions, the *Otx2<sup>+GFP</sup>* mice showed a statistically significant decrease in the a-wave amplitude at P30 and P60 when stimulated with an intense flash (Figure 22A). The decrease in a-wave amplitude became statistically significant for the *Otx2<sup>AA/AA</sup>* mice at P60. In contrast, the a-wave amplitudes measured for the *Otx2<sup>+AA</sup>* mice remained indistinguishable from those of their wild-type littermates until P120 when the difference became statistically significant (Figure 22A). When considering a-wave latencies, their differences were not statistically significant at P30, whereas the values increased significantly at P60 for the *Otx2<sup>+GFP</sup>* and *Otx2<sup>AA/AA</sup>* mice (Figure 22B). A similar increase in latency was observed for *Otx2<sup>+AA</sup>* mice but only at P120 (Figure 22B). These changes in the latencies are likely to be related to the photoreceptor dysfunction indicated by the a-wave amplitude decreases. However, the change in b-wave (see below) could also induce such effects. These results are consistent with graded alterations in photoreceptor function for these various genotypes with a greater effect in *Otx2<sup>+GFP</sup>* and *Otx2<sup>AA/AA</sup>* mice.

To investigate inner retinal layer function, b-wave amplitude was measured for all genotypes. The b-wave is often attributed to bipolar cell activity because it is suppressed when blocking metabotropic glutamate receptors 6 that are specific to these cells (Figure 22C-D). B-wave amplitudes were strongly decreased in *Otx2<sup>+GFP</sup>* and *Otx2<sup>AA/AA</sup>* mice as early as P30, the differences being even greater at P60 for both genotypes (Figure 22C). At P120, the *Otx2<sup>+AA</sup>* mice also exhibited diminished b-wave amplitudes (Figure 22C). These decreases in b-wave amplitudes were relatively greater than the decrease in a-wave amplitude leading to a further decrease in the b/a amplitude ratio for the different genotypes considered. Therefore, these ERGs indicated a major dysfunction of the inner retina and most likely of bipolar cells. The b-wave latencies were similar in all genotypes at P30 but increased significantly at P60 for the *Otx2<sup>+GFP</sup>* and *Otx2<sup>AA/AA</sup>* mice in agreement with bipolar cell dysfunction (Figure 22D). A small increase in b-wave latency was also seen in *Otx2<sup>+AA</sup>* mice at P120 (Figure 22D).

To examine further the cone pathway, we recorded photopic ERGs by saturating rods with a background light (Figure 23). We found that *Otx2<sup>AA/AA</sup>* mice had a non-measurable photopic ERG as early as P30 whereas *Otx2<sup>+GFP</sup>* mice displayed a statistically significant decrease in photopic ERG amplitude at P30 (Figure 23A). In contrast, *Otx2<sup>+AA</sup>* mice showed normal photopic ERG responses. These data suggested a strong deficit of the cone circuit in *Otx2<sup>AA/AA</sup>* mice and a milder dysfunction of this cone pathway in *Otx2<sup>+GFP</sup>* mice.



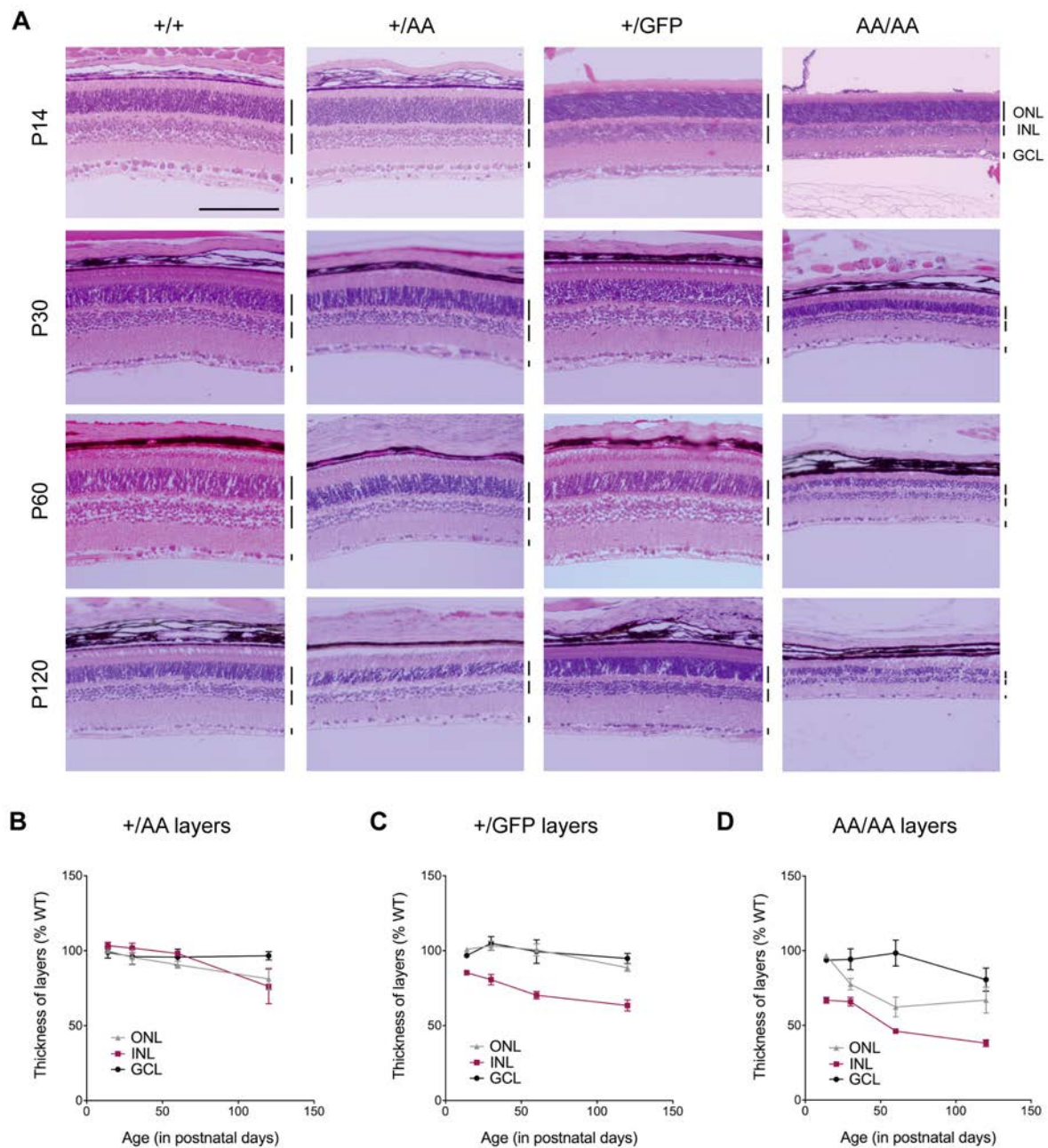


**Figure 25. *Otx2* dose- and age-related retinal thickness differences**

(A) Hematoxyline and eosin stained paraffin sections of retina from the four *Otx2* genotypes at P14, P30, P60 and P120. At P14, the inner retinal layer of *Otx2*<sup>+/-GFP</sup> and *Otx2*<sup>AA/AA</sup> mice is thinner compared to compared to *Otx2*<sup>+/+</sup> retina. With increasing ages, the thinning of the retina increases in *Otx2*<sup>+/-AA</sup>, *Otx2*<sup>+/-GFP</sup> and *Otx2*<sup>AA/AA</sup> mice.

(B-D) Quantification of layers thickness in percentage of wild-type from P14 to P120, in *Otx2*<sup>+/-AA</sup> retina (B), in *Otx2*<sup>+/-GFP</sup> retina (C), and in *Otx2*<sup>AA/AA</sup> retina (D) (ONL: outer nuclear layer, INL: inner nuclear layer, GCL: ganglion cell layer; scale bar: 100μm; error bars indicate SEM).

The latter functional measurements demonstrate a graded retinal physiological dysfunction in the different genotypes with a ranking similar to that observed in eye development analysis and in the optomotor test. In addition, they also strongly suggest that a decrease in *Otx2* activity leads to a progressive decrease in the number and/or activity of cone pathway neurons, such as cone photoreceptors and cone bipolar cells, correlated with a diminished physiological performance.

### ***Otx2* mutants have morphological defects in the retina**

Hematoxylin and eosin staining of retinal sections at P14, P30, P60 and P120 showed no major disorganization or deformation of the eye and retinal structures in *Otx2*<sup>+/+</sup>, *Otx2*<sup>+/AA</sup> and *Otx2*<sup>+GFP</sup> animals. On the contrary, *Otx2*<sup>AA/AA</sup> mice with externally normal eyes could present various defects with variable expressivity: iris defects (46%), rosette-like structures in the outer nuclear layer (23%), festooned retinal pigment epithelium (46%) and a disorganized optic nerve (31%) (Figure 24). The images of retinas analyzed below did not contain gross deformities and the following results are always presented in percentage of wild-type littermates.

At P14, P30, and P60, the thickness of the different retinal layers of *Otx2*<sup>+/AA</sup> mice appeared similar to that of wild-type siblings. At P120, both the inner and outer nuclear layers were reduced in thickness (76.2±11.5% and 81.2±7.3%, respectively) (Figure 25A-B). The inner nuclear layer in the retina of *Otx2*<sup>+GFP</sup> mice was already thinner at P14 (85.4±1.2%) and this progressively worsened at P30, P60 and P120 (Figure 25C). The *Otx2*<sup>AA/AA</sup> mice also showed a thinner inner nuclear layer at P14 (66.9±2.0%) that worsened with age (38.1±2.3% at P120). The outer nuclear layer thickness in *Otx2*<sup>AA/AA</sup> retina was comparable to wild-type at P14 and was reduced in thickness from P30 (77.6±1.5%) (Figure 25D). In the ganglion cell layer, the number of cells was comparable between the four genotypes at P14, P30 and P60. At ages greater than 10 months the number of cells in this layer was significantly reduced in *Otx2*<sup>+/AA</sup> (77.9±1.5) and *Otx2*<sup>AA/AA</sup> (74.8±0.6%) mice.

These results show that retinal morphology is affected in *Otx2* dose-dependent and age-dependent manners. Layer thinning occurs earlier in the inner nuclear layer of *Otx2*<sup>+GFP</sup> and *Otx2*<sup>AA/AA</sup> mice compared to *Otx2*<sup>+/AA</sup> mice and the ganglion cell layer is affected at later ages only in the *Otx2*<sup>+/AA</sup> and *Otx2*<sup>AA/AA</sup> mice.

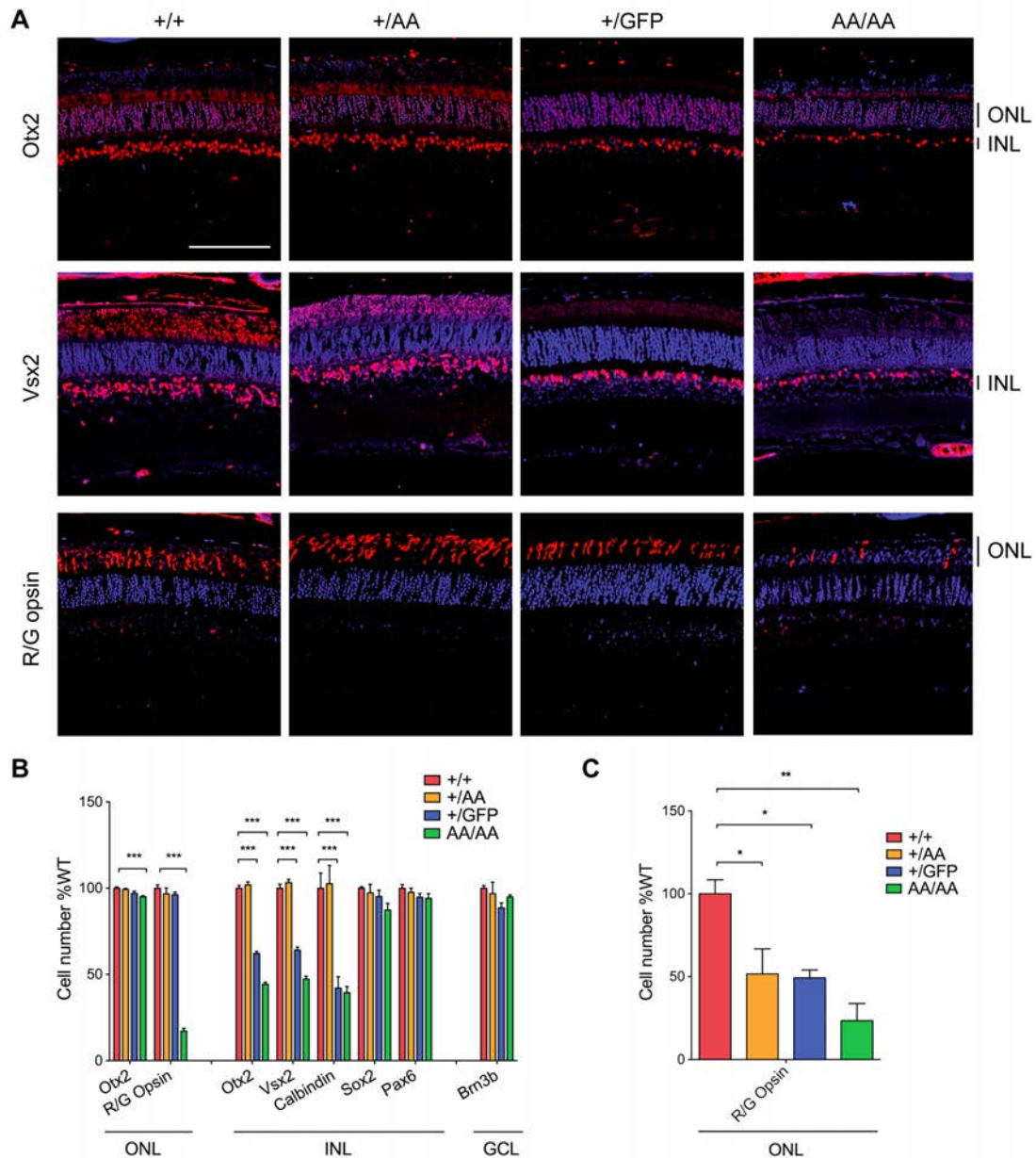


**Figure 26. Cell loss in the retina of *Otx2* mutants**

(A) Representative images of Otx2, Vsx2 and R/G-opsin immunofluorescence in the four genotypes.

(B) Cell counting at P30 of retinal cell types identified by immunohistochemistry. In the outer nuclear layer of *Otx2*<sup>AA/AA</sup> mice, there are significantly fewer Otx2- and R/G opsin-positive cone cells. In the inner nuclear layer, the number of Otx2-expressing bipolar cells is decreased in *Otx2*<sup>+GFP</sup> and *Otx2*<sup>AA/AA</sup> retina. Similarly, there are fewer Vsx2-positive bipolar cells in *Otx2*<sup>+GFP</sup> and *Otx2*<sup>AA/AA</sup> retina. Calbindin-expressing horizontal cells are fewer in *Otx2*<sup>+GFP</sup> and *Otx2*<sup>AA/AA</sup> retina while there are no differences in Brn3b-positive ganglion cells between the genotypes at this age.

(C) Cell counting of cone photoreceptors at P365. In all three mutant mice, there are significantly fewer R/G opsin-positive cells.

(ONL: outer nuclear layer, INL: inner nuclear layer, GCL: ganglion cell layer; scale bar: 100μm; \*p<0.05, \*\*p<0.01, \*\*\*p<0.001, error bars indicate SEM, Student t-test compared to wild-type littermates)

### ***Otx2* mutants have fewer photoreceptors, bipolar and horizontal cells in the retina**

We next examined specific cell losses by using immunofluorescence for *Otx2* (marker for photoreceptors and bipolar cells), R/G opsin (marker for red/green sensitive cones), *Vsx2* (marker for bipolar cells), calbindin (marker for horizontal cells), *Sox2* (marker for Müller glia), *Pax6* (marker for amacrine cells) and *Brn3b* (marker for retinal ganglion cells). At P30, there was a significant decrease in the number of *Otx2*-expressing photoreceptors in the outer nuclear layer of *Otx2*<sup>AA/AA</sup> retina (Figure 26A-B). In terms of photoreceptor type, red/green sensitive cones were already reduced over 70% in the retina of *Otx2*<sup>AA/AA</sup> at P30 (Figure 26A-B). Cone photoreceptors could therefore account for most of the cell loss in the outer nuclear layer at P30. This loss of cone cells is consistent with the decrease or disappearance of the photopic ERG response in this genotype.

At P30, the number of *Vsx2*-positive bipolar cells was reduced by 35.9% in *Otx2*<sup>+/*GFP*</sup> retina and by 62.6% in *Otx2*<sup>AA/AA</sup> retina (Figure 26A-B). *Otx2*-positive cells in the inner nuclear layer were reduced to a similar extent (i.e. 37.8% in *Otx2*<sup>+/*GFP*</sup> retina and 62.9% in *Otx2*<sup>AA/AA</sup> retina). This loss of bipolar cells is consistent with the reduction in b-wave amplitudes. Calbindin-positive horizontal cells in the inner nuclear layer were reduced by about 60% in *Otx2*<sup>+/*GFP*</sup> and *Otx2*<sup>AA/AA</sup> mice retinas. The number of *Sox2*- and *Pax6*-expressing cells did not significantly differ among the four genotypes at P30 (Figure 26B). At P30, in the ganglion cell layer, the numbers of *Brn3b*-positive cells were similar in the three *Otx2* mutants and in the wild-type mice (Figure 26B). These results show that, in the outer nuclear layer, there are fewer cones in *Otx2*<sup>AA/AA</sup> mice at P30. In the inner nuclear layer, there are fewer bipolar cells in *Otx2*<sup>+/*GFP*</sup> retina, even less in *Otx2*<sup>AA/AA</sup> retina and fewer horizontal cells in both genotypes. Thus, the reduced number of cells in the retina at P30 is most severe in *Otx2*<sup>AA/AA</sup>, intermediate in *Otx2*<sup>+/*GFP*</sup> mice, while *Otx2*<sup>+/*AA*</sup> are indistinguishable from *Otx2*<sup>+/*+*</sup> mice at this age.

At ages older than P30, compared to wild-type littermates, the number of R/G-opsin cone photoreceptors was reduced not only in *Otx2*<sup>AA/AA</sup> but also in *Otx2*<sup>+/*GFP*</sup> mice by 50.7% and in *Otx2*<sup>+/*AA*</sup> mice by 48.4% compared to wild-type littermates (Figure 26C). These results suggest that mice with a higher dose of *Otx2* activity (*Otx2*<sup>+/*AA*</sup> mice) lose retinal cells later than mice with a lower dose of *Otx2* activity (*Otx2*<sup>AA/AA</sup> mice).

The data on the loss of specific subtypes in the three *Otx2* mutants suggest that the ERG perturbation observed in the *Otx2* mutant mice might be caused by the loss of bipolar cells

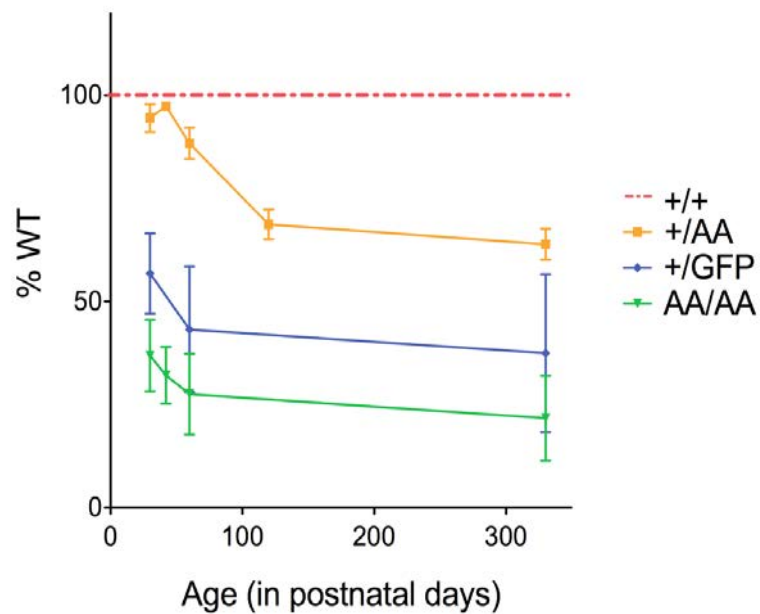


### Figure 27. Overall phenotype ranking

Data at a given age are determined in percentage of the wild-type response. All percentages are plotted together on one graph from P30 to P365. One point on the graph represents the mean of all experiments (gross phenotypes, ERG, IHC, ...) done at one age for one genotype. This illustrates the age- and dose-dependence of *Otx2* activity in the three *Otx2* mutants compared to wild-type mice (error bars indicate SEM).

and cone photoreceptors. More precisely, it can be argued that the cone pathway, composed of cone photoreceptors, cone-bipolar cells, and horizontal cells, is most severely affected by the decrease in Otx2 activity. The less Otx2 activity there is, the earlier the loss of retinal cells and changes in retinal physiological activity. Pooling the results from all experiments (Figure 27) thus confirms the severity ranking  $Otx2^{+/+} < Otx2^{+/AA} < Otx2^{+/GFP} < Otx2^{AA/AA}$  and establishes that the observed phenotypes are both Otx2 activity-dependent and age-dependent.

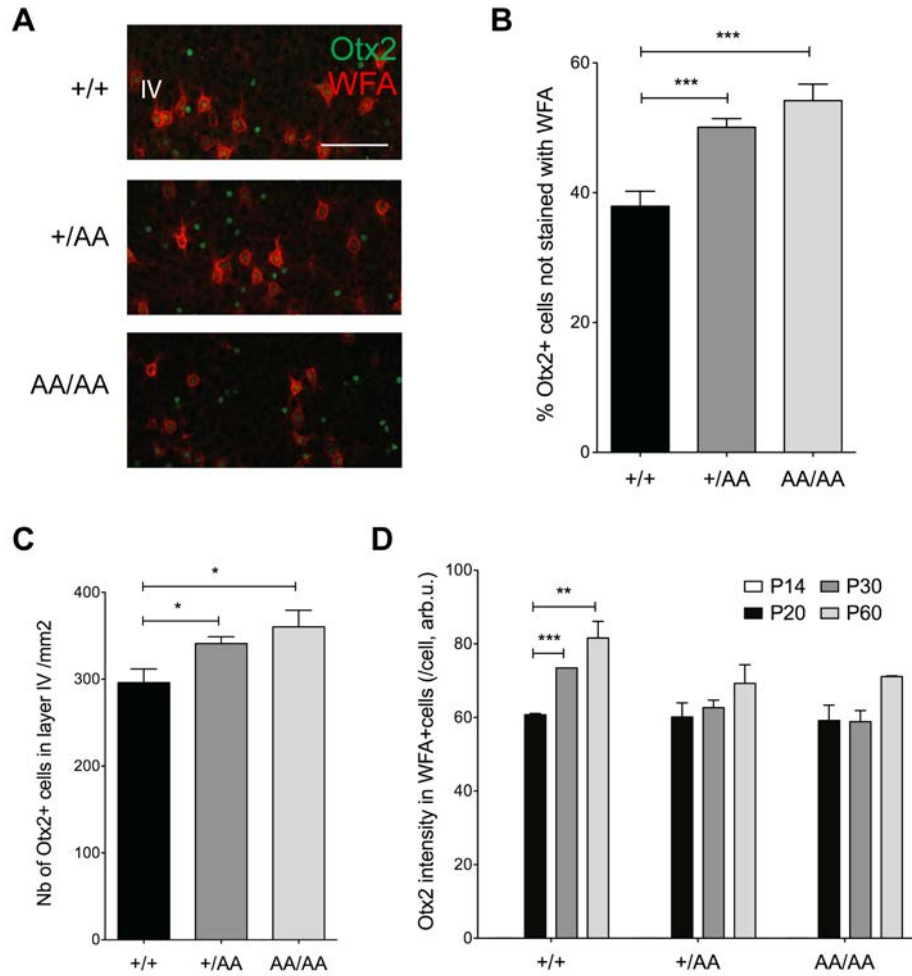


**Figure 28. Mis-localisation of Otx2 protein in the visual cortex of Otx2-AA mice**

(A) Co-staining of WFA and Otx2 in layer IV of the visual cortex of P30 *Otx2*<sup>+/+</sup>, *Otx2*<sup>+/-AA</sup> and *Otx2*<sup>AA/AA</sup> mice (scale bar: 100  $\mu$ m).

(B) Quantification of WFA and Otx2 co-staining in layer IV of the visual cortex of *Otx2*<sup>+/+</sup>, *Otx2*<sup>+/-AA</sup> and *Otx2*<sup>AA/AA</sup> mice, from P20 to P40. The number of Otx2-positive cells not surrounded by PNNs is increased in Otx2-AA mutants.

(C) Number of Otx2-positive cells in layer IV of the visual cortex of *Otx2*<sup>+/+</sup>, *Otx2*<sup>+/-AA</sup> and *Otx2*<sup>AA/AA</sup> mice, from P20 to P40. Otx2 is present in a larger number of cells in the Otx2-AA mutants compared to wild-type mice.

(D) Quantification of the mean intensity of Otx2 staining in WFA-positive cells in layer IV of the visual cortex of *Otx2*<sup>+/+</sup>, *Otx2*<sup>+/-AA</sup> and *Otx2*<sup>AA/AA</sup> mice, from P14 to P60. While Otx2 staining intensity increases with time in wild-type mice, there is no significant increase in the Otx2-AA mutants from P20 to P60.

(arb.u.: arbitrary units; \* $p < 0.05$ , \*\* $p < 0.01$ , \*\*\* $p < 0.001$ , error bars indicate SEM, Student t-test; 700x200 $\mu$ m)



### C. Otx2 GAG-binding motif has a role in critical period timing

During postnatal development, Otx2 homeoprotein is present not only in the retina but also at several levels of the optic trail, especially in the visual cortex in a non-cell autonomous manner (Sugiyama et al., 2008). We therefore used the Otx2-AA mouse line to explore the role of the GAG-binding motif in Otx2 preferential transfer into PNN-expressing cells, in collaboration with the laboratory of Takao Hensch (Harvard Medical School, Boston, USA).

#### Otx2 protein localization is altered in the visual cortex of Otx2-AA mice

We first assessed the localization of Otx2 protein in the visual cortex of *Otx2*<sup>+/-AA</sup> mice by immunostaining for Otx2 and PNNs (recognized by the WFA lectin). In juvenile Otx2-AA mice (from P20 to P40), we observed a significant increase in Otx2 accumulation in cells not surrounded by PNNs (Figure 28A-B). In layer IV of the primary visual cortex of Otx2-AA mice, approximately 50% of Otx2 was found outside WFA-positive cells ( $50.07 \pm 1.34\%$  in *Otx2*<sup>+/-AA</sup> mice and  $54.19 \pm 2.54\%$  in *Otx2*<sup>AA/AA</sup> mice, compared to  $37.90 \pm 2.34\%$  in wild-type littermates). This reflects a 20 % increase in the number of Otx2-positive cells ( $341.0 \pm 7.88$  cells/mm<sup>2</sup> for *Otx2*<sup>+/-AA</sup> mice and  $360.3 \pm 19.12$  cells/mm<sup>2</sup> for *Otx2*<sup>AA/AA</sup> mice compared to  $291.1 \pm 13.77$  cells/mm<sup>2</sup> for wild-type mice) (Figure 28C) while the number of WFA-positive cells containing Otx2 did not change. In other words, Otx2-AA protein is internalized by a wider range of cells.

If the amount of Otx2 arriving in the cortex is unchanged, one would expect the amount of Otx2 in each cell to be reduced in Otx2-AA mice, due to its wider distribution, thus dilution. Indeed, this is what we observed (Figure 28D). At P30, less Otx2 protein was present in WFA-positive cells in Otx2-AA mice (Otx2 intensity in WFA-positive cells was  $62.65 \pm 2.04$  arbitrary units (arb. units) in *Otx2*<sup>+/-AA</sup> mice and  $58.84 \pm 3.05$  arb. units in *Otx2*<sup>AA/AA</sup> mice, compared to  $73.47 \pm 0.10$  arb. units in wild-type animals). Strikingly, up to P60, Otx2-AA protein did not effectively accumulate in WFA-positive cells (Figure 28D). In wild-type mice, PNN assembly intensifies during this period and is thought to help consolidate plasticity changes and eventually to close the critical period for binocular vision (Köppe et al., 1997a). Concomitantly, Otx2 protein significantly increases in WFA-positive cells (in wild-type mice, from  $60.74 \pm 0.34$  arb. units at P20 to  $81.60 \pm 4.53$  arb. units at P60). This is consistent with the idea that, as maturing PNNs condense, they permit higher levels of Otx2 to accumulate. Since



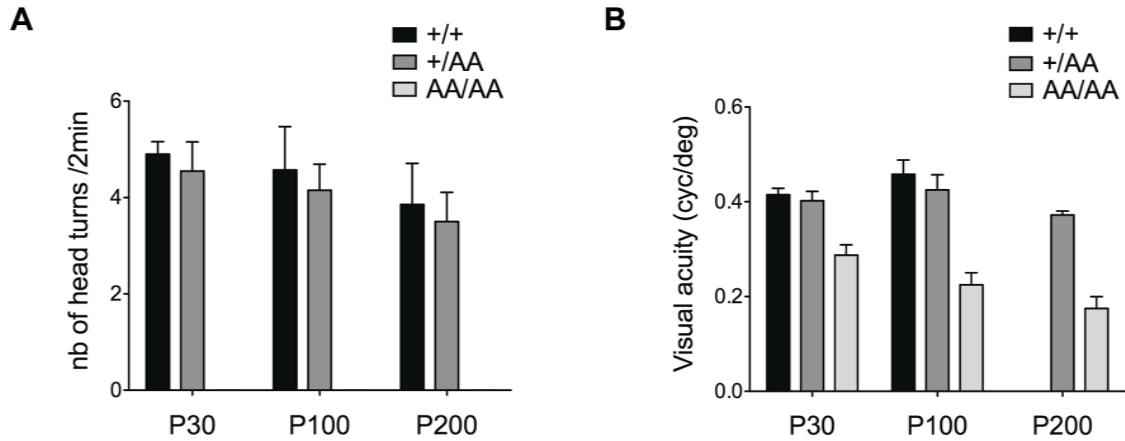


**Figure 29. Visual acuity of *Otx2*-AA mutants**

Visual acuity of *Otx2*-AA mutants assessed by the optomotor test (A) and visual evoked potentials (B). In both tests, visual acuity of *Otx2*<sup>+/-AA</sup> mice is indistinguishable from that of *Otx2*<sup>+/+</sup> littermates at P30, P100 and P200, while *Otx2*<sup>AA/AA</sup> mice have significantly reduced visual acuity (error bars indicate SEM).

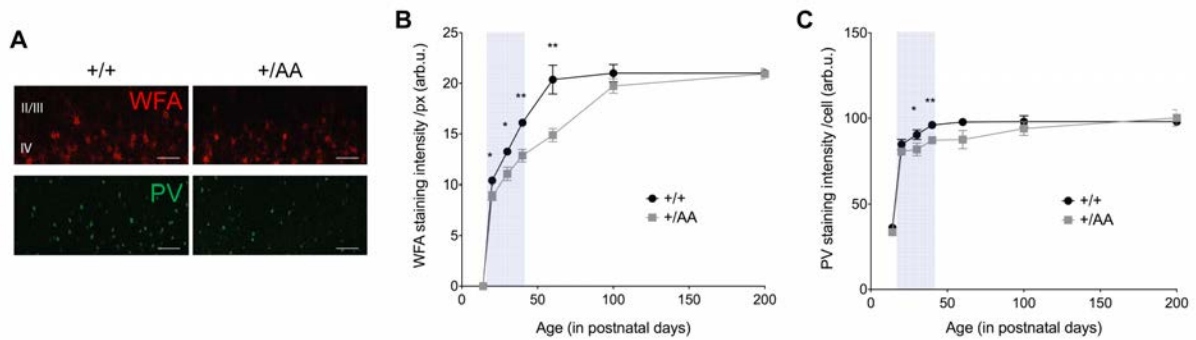


**Figure 30. Delayed PV and PNN expression in the visual cortex of *Otx2*<sup>+/-AA</sup> mice**

(A) WFA and PV immunostaining in supragranular layers of the visual cortex of *Otx2*<sup>+/+</sup> and *Otx2*<sup>+/-AA</sup> mice at P40 (scale bar: 100  $\mu$ m).

(B) Quantification of the mean intensity of WFA staining per pixel in supragranular layers of the visual cortex of *Otx2*<sup>+/+</sup> and *Otx2*<sup>+/-AA</sup> mice, from P14 to P200. WFA staining intensity is significantly lower in *Otx2*<sup>+/-AA</sup> mice than in wild-type littermates from P14 to P60. The blue shaded area indicates the wild-type critical period for ocular dominance plasticity.

(C) Quantification of the mean intensity of PV staining per cell in supragranular layers of the visual cortex of *Otx2*<sup>+/+</sup> and *Otx2*<sup>+/-AA</sup> mice, from P14 to P200. PV staining intensity is significantly lower in *Otx2*<sup>+/-AA</sup> mice than in wild-type littermates at P30 and P40. The blue shaded area indicates the wild-type critical period for ocular dominance plasticity.

(arb.u.: arbitrary units; \* $p < 0.05$ , \*\* $p < 0.01$ , error bars indicate SEM, Student t-test; 700x450 $\mu$ m)

Otx2 transfer regulates PNN expression (Beurdeley et al., 2012; Sugiyama et al., 2008), it is possible that a positive feedback loop is responsible for their concomitant increase. However, the levels of both PNNs and Otx2 are activity-dependent at normal critical period onset (Sugiyama et al., 2008; Ye and Miao, 2013). Therefore, in Otx2-AA mice, we needed to evaluate if a compromised retinal activity was in part responsible for the reduced accumulation of Otx2-AA in PNN-expressing cells.

### ***Otx2*<sup>+AA</sup> mice retain normal visual acuity**

In our study on Otx2-AA eye development presented above, we showed that heterozygous *Otx2*<sup>+AA</sup> mice did not show any difference in visual acuity at P60 compared to wild-type littermates. We confirmed these results in older mice. By using the optomotor test at 0.375 cycles per degree, we found similar visual acuities at all ages between wild-type and *Otx2*<sup>+AA</sup> mice (Figure 29A). The *Otx2*<sup>AA/AA</sup> mice did not respond to this test whatever their age.

By measuring visual evoked potentials to assess visual acuity, we again found no significant difference between wild-type and heterozygous *Otx2*<sup>+AA</sup> mice from P30 to P200 (for instance at P100, 0.46±0.03 cycles/degree for *Otx2*<sup>+/+</sup> and 0.43±0.03 cycles/degree for *Otx2*<sup>+AA</sup> mice), while homozygous *Otx2*<sup>AA/AA</sup> mice had significantly reduced acuity (already at P30, 0.28±0.02 cycles/degree for *Otx2*<sup>AA/AA</sup>) (Figure 29B). We therefore chose to restrict further analysis (see below) to heterozygous *Otx2*<sup>+AA</sup> mice. Indeed, in these mice, molecular and physiological consequences of the AA mutation were more likely to be due to non-cell autonomous functions of Otx2-AA protein in the cortex rather than to an altered retinal activity. Clearly, for the homozygous *Otx2*<sup>AA/AA</sup> mice, we could not rule out an influence of defective retina on cortical morphology and function.

### **Delayed PV and PNN expression in the visual cortex of *Otx2*<sup>+AA</sup> mice**

Since the Otx2 protein content failed to increase in WFA-positive cells of the visual cortex of heterozygous *Otx2*<sup>+AA</sup> mice, it was possible that PV-cells could be modified in their maturation, thus in PNN assembly and PV expression. We examined the staining intensity of WFA and PV in the supragranular layers of primary visual cortex of wild-type and *Otx2*<sup>+AA</sup> mice at 7 different ages ranging from P14 to P200 (Figure 30). The intensity of WFA staining was significantly reduced in *Otx2*<sup>+AA</sup> mice between P20 and P60 (for example at P40, 12.85±0.62 arb. units for *Otx2*<sup>+AA</sup> compared to 16.10±0.37 arb. units for wild-type littermates) but reached wild-type levels by P100 (Figure 30B). The intensity of PV staining was also

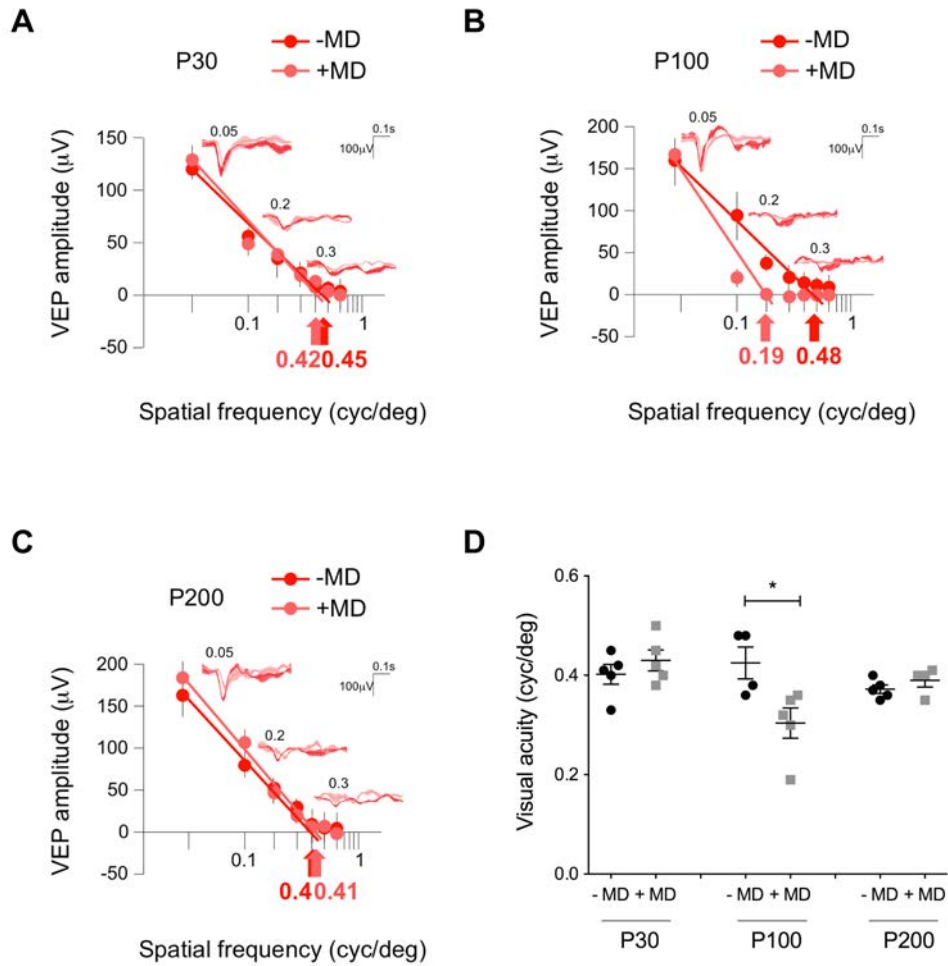


**Figure 31. Delayed onset and closure of critical period for ocular dominance plasticity in *Otx2*<sup>+/AA</sup> mice**

(A-C) Visual evoked potential amplitudes in *Otx2*<sup>+/AA</sup> mice with and without monocular deprivation (MD) at P30 (A), P100 (B) and P200 (C).

(D) Visual acuity of *Otx2*<sup>+/AA</sup> assessed by visual evoked potential recordings, after a short MD of 4 days, at P30, P100 and P200. Visual acuity is decreased by monocular deprivation only at P100 in *Otx2*<sup>+/AA</sup> mice (\*p<0.05, error bars indicate SEM, Student t-test).

reduced in heterozygous *Otx2*<sup>+AA</sup> mice prior to P100, with significant differences measured at P30 (81.69±2.8 arb. units for *Otx2*<sup>+AA</sup> and 90.31±2.8 arb. units for wild-type mice) and P40 (87.09±2.26 arb. units for *Otx2*<sup>+AA</sup> and 95.99±1.73 arb. units for wild-type mice) (Figure 30C). While intensities for both markers reach a plateau at around P60 in wild-type mice, they do not reach this plateau until P100 in *Otx2*<sup>+AA</sup> mice. Taken together, it appears that the RK→AA mutation delays the maturation of fast-spiking PV-cells.

### **Delayed onset and closure of critical period for ocular dominance plasticity in *Otx2*<sup>+AA</sup> mice**

Reduced inhibition shifts the excitatory/inhibitory balance in the visual cortex during postnatal development and leads to a delay in the onset of the critical period for ocular dominance (Hensch et al., 1998). To assess critical period timing, short-term monocular deprivation followed by visual evoked potential recordings was performed at P30, P100 and P200 (Figure 31). As expected, wild-type mice experienced a reduction in visual acuity only at P30. Indeed, during normal critical period for ocular dominance, a short-term monocular deprivation (4 days) impairs visual acuity (Wiesel and Hubel, 1963), indicating cortical plasticity. In contrast, monocular deprivation at this age failed to impair vision in *Otx2*<sup>+AA</sup> mice (*Otx2*<sup>+AA</sup>: 0.43±0.02 cycles/degree). However, at P100, *Otx2*<sup>+AA</sup> visual acuity was decreased by short-term monocular deprivation (*Otx2*<sup>+AA</sup>: 0.30±0.03 cycles/degree). At P200, a short-term monocular deprivation did not change visual acuity in *Otx2*<sup>+/+</sup> nor in *Otx2*<sup>+AA</sup> mice (*Otx2*<sup>+AA</sup>: 0.39±0.01 cycles/degree) (Figure 31D). These recordings show that the onset and the closure of the critical period for ocular dominance plasticity are delayed in *Otx2*<sup>+AA</sup> mice.

### **Modified critical period for tonotopic map refinement in *Otx2*<sup>+AA</sup> mice**

Otx2 protein is present in a non-cell autonomous fashion in PV-cells of many cerebral cortices (Spatazza et al., 2013b). Otx2 transfer could therefore be a more general regulator of critical period plasticity across several brain regions. We therefore tested, still in collaboration with the groupe of Takao Hensch, the timing of a critical period for tonotopic map plasticity in the auditory cortex of *Otx2*<sup>+AA</sup> mice. Tonotopy, similarly to retinotopy in the visual system, corresponds to the topographic organization of sounds of different frequencies from the cochlea to the ventral medial geniculate body (MGBv) in the auditory thalamus and from there to the auditory cortex (Hackett et al., 2011; Winer et al., 2005). Onset of critical periods is not the same across cortices, and in mouse auditory cortex, critical period for tonotopic map

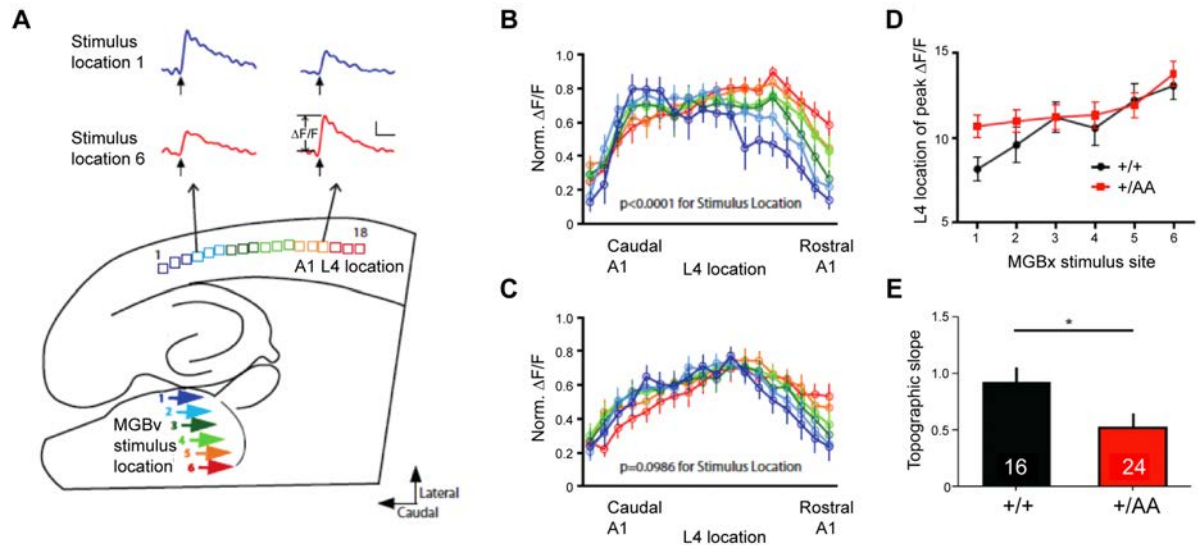


**Figure 32. Critical period for tonotopic plasticity in auditory cortex of *Otx2*<sup>+/AA</sup> mice**

(A) Schematic representation of the six ventral medial geniculate body (MGBv) stimulus sites (colored arrows) and of the 18 recorded spots in layer IV (L4) of the auditory cortex (A1). Sample traces of fluorescent response amplitude ( $\Delta F/F$ ) at two different L4 locations (4 and 15) as a function of time following a stimulus to MGBv site 1 (blue) or site 6 (red) (scale bars: 100ms and 0.1%  $\Delta F/F$ ).

(B-C) Normalized (norm.) maximal  $\Delta F/F$  across layer IV locations in response to different MGBv stimulus sites for P20 wild-type (B) and *Otx2*<sup>+/AA</sup> mice (C), after a 7 kHz exposure from P16 to P19.

(D) Peak  $\Delta F/F$  location in layer IV, defined as the maximum  $\Delta F/F$  amplitude across all L4 locations, as a function of MGBv stimulus site, for wild-type (black) and *Otx2*<sup>+/AA</sup> (red) mice at P20, after a 7 kHz exposure from P16 to P19.

(E) Topographic slope for wild-type (black) and *Otx2*<sup>+/AA</sup> (red) mice. The topographic slope is flattened in P20 *Otx2*<sup>+/AA</sup> mice exposed to 7 kHz at P16-19 compared to wild-type mice (\* $p < 0.05$ , error bars indicate SEM).

reorganization happens early during postnatal development, from P12 to P15 (Barkat et al., 2011).

The thalamic MGBv was stimulated at six different loci in brain slices that preserve the thalamocortical connection to auditory cortex (Figure 32A). The subsequent recording of layer IV responses in the auditory cortex, using voltage-sensitive dye imaging, allowed the establishment of a map of peak amplitudes as function of stimulus sites (Figure 32B-D). This relation between MGBv input and peak position in layer IV is presented as a topographic slope (Figure 32E). Outside of the critical period, the topographic slope is around 1, indicating an orderly spatial layout of the thalamocortical pathway (Barkat et al., 2011). If the mouse is exposed to an abnormal acoustic environment (7 kHz) during critical period, the thalamocortical topography (assessed by the topographic slope) is markedly altered. A 7 kHz exposure after the critical period, between P16 and P19, did not impact the topographic slope of wild-type littermate. However, this exposure clearly flattened the topographic slope in *Otx2*<sup>+/-AA</sup> mice (Figure 32E). This suggests that *Otx2*<sup>+/-AA</sup> mice are plastic for tonotopic map reorganization at P16, when the wild-type critical period is closed. Similarly to the critical period for ocular dominance, the timing of this critical period is thus modified in *Otx2*<sup>+/-AA</sup> mice compared to wild-type littermates.

Our *Otx2*-AA cortical analysis showed that plasticity onset is delayed in *Otx2*<sup>+/-AA</sup> mice, which have a broader distribution of *Otx2* protein in visual cortex cells and attenuated *Otx2* accumulation in PV-cells. Therefore, a slight reduction in *Otx2* concentration within WFA-positive cells results in delay of critical period timing, concomitant with reduced PNN assembly and PV expression. A similar effect on the critical period for tonotopic map reorganization in the auditory cortex supports the hypothesis of *Otx2* as a general regulator of critical period plasticity. This is in agreement with our two-threshold model for *Otx2* cortical activity, in which accumulation of *Otx2* protein in PV-cells opens critical period by crossing a first concentration threshold then closes critical period at a second threshold (Figure 17 p.38, (Spatazza et al., 2013b)).

A

	P100 vs P30
Otx2 <sup>+/+</sup>	⬇ 260 genes ⬆ 130 genes
Otx2 <sup>+/AA</sup>	⬇ 532 genes ⬆ 303 genes
Otx2 <sup>+/GFP</sup>	⬇ 351 genes ⬆ 374 genes

B

	P30	P100
Otx2 <sup>+/AA</sup> vs Otx2 <sup>+/+</sup>	⬇ 5 genes ⬆ 2 genes	⬇ 1 gene ⬆ 17 genes
Otx2 <sup>+/GFP</sup> vs Otx2 <sup>+/+</sup>	⬇ 225 genes ⬆ 69 genes	⬇ 113 genes ⬆ 156 genes
Otx2 <sup>+/AA</sup> vs Otx2 <sup>+/GFP</sup>	⬇ 235 genes ⬆ 417 genes	⬇ 143 genes ⬆ 126 genes

**Figure 33. General observation of layer IV deep sequencing in *Otx2* mutants**

(A) Number of up- and down-regulated genes between P30 and P100, in wild-type, *Otx2*<sup>+/AA</sup> and *Otx2*<sup>+/GFP</sup> mice ( $p_{\text{adj}} < 0.05$ ).

(B) Number of up- and down-regulated genes between wild-type mice and *Otx2* mutants (*Otx2*<sup>+/AA</sup> and *Otx2*<sup>+/GFP</sup>) at P30 and P100 ( $p_{\text{adj}} < 0.05$ ).

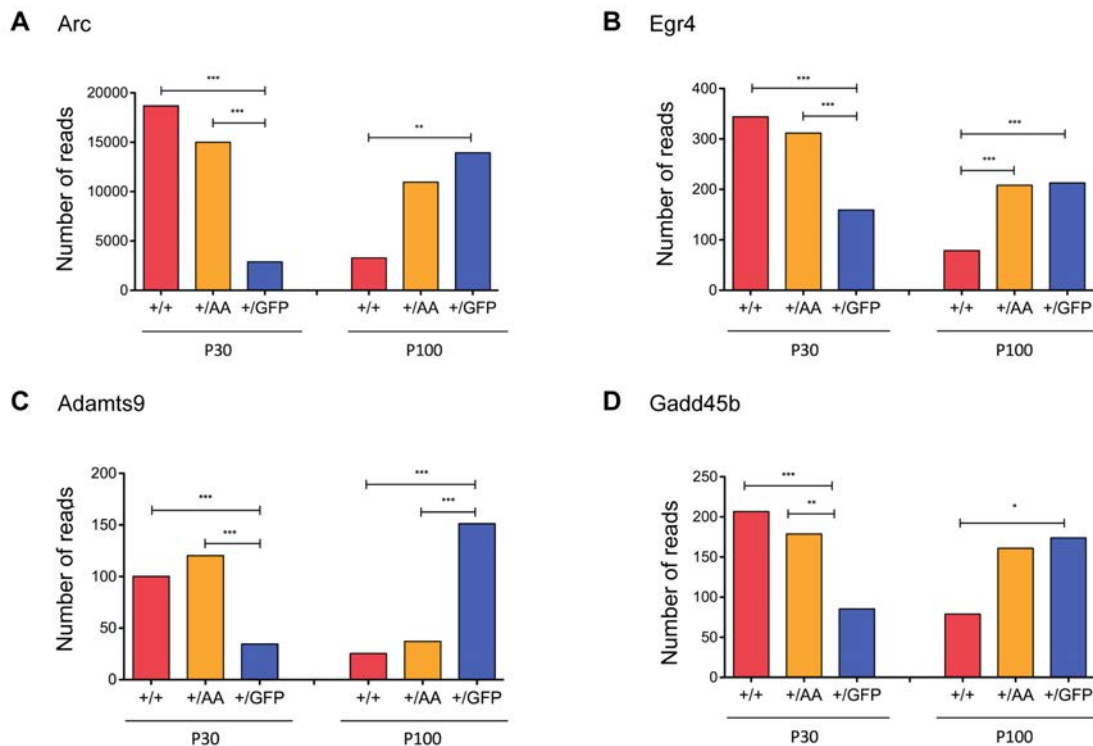


**Figure 34. Examples of differentially regulated genes at P30 and P100 in *Otx2* mutants**

Number of reads for *Arc* RNA (A), *Egr4* RNA (B), *Adamts9* RNA (C) and *Gadd45b* RNA (D) in layer IV of visual cortex of wild-type, *Otx2*<sup>+/AA</sup> and *Otx2*<sup>+/GFP</sup> mice (\* $p < 0.05$ , \*\* $p < 0.01$ , \*\*\* $p < 0.001$ , Student t-test).

## D. Towards the identification of targets of Otx2 in the visual cortex

Otx2 arrival in the visual cortex and its accumulation in WFA-positive cells after eye opening is crucial for the onset of critical period. However, we do not know which genes are regulated by Otx2 in the PV-cells and therefore how Otx2 transfer regulates PV-cell maturation and the timing of critical period for ocular dominance plasticity. To start investigating Otx2 putative targets in PV-cells, we analyzed by deep sequencing (RNA-seq) the RNAs present in layer IV of the visual cortex of our two mutant mouse lines (Otx2-GFP and Otx2-AA) and of their wild-type littermates.

### Manual dissection of layer IV and broad observation of RNA-seq data

The layer IV of the visual cortex of Otx2 mutant (*Otx2*<sup>+/GFP</sup>, *Otx2*<sup>+/AA</sup>) and wild-type mice was manually dissected at two ages (P30 and P100). The visual cortex was dissected and sliced in two across its height. The upper part, corresponding to the supragranular layers (I, II, III and IV) was again sliced in two, and the resulting lower part was considered as layer IV. Four mice were pooled per RNA sample and the experiment was performed in duplicates. RNA-seq was performed by the genomic platform at the Ecole Normale Supérieure (Paris).

The RNA-seq data allowed us to compare gene expression in layer IV between the three genotypes at P30 and P100. We performed two sorts of analysis of this data: a comparison between P30 and P100 for each genotype (Figure 33A) and a comparison between genotypes at both ages (Figure 33B). We then limited our analysis to the genes for which the adjusted p-value ( $p_{\text{adj}}$ ) was inferior to 0.05. It is striking that, whereas many genes are up- or down-regulated between *Otx2*<sup>+/+</sup> and *Otx2*<sup>+/GFP</sup> at P30 (294 genes) and at P100 (169 genes), only very few genes are significantly up- or down-regulated in *Otx2*<sup>+/AA</sup> compared to *Otx2*<sup>+/+</sup> (at P30, 7 genes; at P100, 18 genes). This suggests that, at both ages, the cortical state of *Otx2*<sup>+/AA</sup> mice is closer to that of wild-type mice than to that of *Otx2*<sup>+/GFP</sup> mice. This observation fits well with our previous “eye study”, in which *Otx2*<sup>+/AA</sup> phenotypes were often undistinguishable from wild-type phenotypes.

### Plasticity genes are differentially regulated between P30 and P100 in Otx2 mutants

When comparing genotypes at P30 and P100, we observed that some genes that were up-regulated in wild-type mice at P30 were similarly up-regulated in *Otx2*<sup>+/GFP</sup> mice at P100.



Gene symbol		Gene name	P30			+/AA vs +/-			+/GFP vs +/-		
			+/+	+/AA	+/GFP	log2FC	p <sub>adj</sub>		log2FC	p <sub>adj</sub>	
Adams9		a disintegrin-like and metalloproteinase with thrombospondin type 1 motif, 9	100.07	120.32	34.62	0.27	1.00		-1.53	0.00	
Arc		activity regulated cytoskeletal-associated protein	18889.15	14989.14	2877.21	-0.32	1.00		-2.70	0.00	
Arid3b		AT rich interactive domain 3B (BRIGHT-like)	247.14	223.02	117.03	-0.15	1.00		-1.08	0.01	
Arl4d		ADP-ribosylation factor-like 4D	634.77	382.88	178.60	-0.73	1.00		-1.83	0.00	
Csmpl		cysteine-serine-rich nuclear protein 1	255.65	159.71	99.15	-0.68	1.00		-1.37	0.05	
Dyrk3		dual-specificity tyrosine-(Y)-phosphorylation regulated kinase 3	267.43	223.33	100.84	-0.26	1.00		-1.41	0.00	
Egr1		early growth response 1	5375.85	4855.17	2375.33	-0.15	1.00		-1.18	0.01	
Egr2		early growth response 2	1430.82	782.74	291.08	-0.87	1.00		-2.30	0.00	
Egr3		early growth response 3	601.69	727.98	279.38	0.27	1.00		-1.11	0.00	
Egr4		early growth response 4	343.96	311.98	159.22	-0.14	1.00		-1.11	0.00	
Fosb		FBJ osteosarcoma oncogene B	329.02	307.55	97.52	-0.10	1.00		-1.75	0.01	
Fosl2		fos-like antigen 2	1607.18	1701.63	584.02	0.08	1.00		-1.46	0.04	
Frmf6		FERM domain containing 6	856.35	771.31	331.41	-0.15	1.00		-1.37	0.00	
Gadd45b		growth arrest and DNA-damage-inducible 45 beta	206.66	178.78	85.42	-0.21	1.00		-1.27	0.00	
Gadd45g		growth arrest and DNA-damage-inducible 45 gamma	315.20	182.90	144.37	-0.79	1.00		-1.13	0.00	
Homer1		homer homolog 1 (Drosophila)	13874.39	14490.29	7181.12	0.08	1.00		-0.93	0.00	
Map3k14		mitogen-activated protein kinase kinase kinase 14	109.37	96.50	47.56	-0.18	1.00		-1.20	0.05	
Nr4a1		nuclear receptor subfamily 4, group A, member 1	3696.22	1558.78	817.73	-1.25	0.10		-2.18	0.00	
Nr4a2		nuclear receptor subfamily 4, group A, member 2	670.08	520.83	255.61	-0.36	1.00		-1.39	0.00	
Per1		period circadian clock 1	1267.69	1081.59	604.06	-0.26	1.00		-1.07	0.00	
Ptgs2		prostaglandin-endoperoxide synthase 2	464.57	479.75	190.50	0.05	1.00		-1.29	0.03	
Tmem252		transmembrane protein 252	60.85	52.59	5.78	-0.21	1.00		-3.40	0.00	
Trib1		tribbles homolog 1 (Drosophila)	681.36	428.56	179.43	-0.67	1.00		-1.92	0.00	

Gene symbol		Gene name	P100			+/AA vs +/-			+/GFP vs +/-		
			+/+	+/AA	+/GFP	log2FC	p <sub>adj</sub>		log2FC	p <sub>adj</sub>	
Adams9		a disintegrin-like and metalloproteinase with thrombospondin type 1 motif, 9	25.44	37.19	151.28	0.55	1.00		2.57	0.00	
Arc		activity regulated cytoskeletal-associated protein	3278.11	10950.24	13933.39	1.74	0.41		2.09	0.00	
Arid3b		AT rich interactive domain 3B (BRIGHT-like)	99.27	117.23	211.81	0.24	1.00		1.09	0.01	
Arl4d		ADP-ribosylation factor-like 4D	163.21	384.63	335.18	1.24	0.02		1.04	0.02	
Csmpl		cysteine-serine-rich nuclear protein 1	91.94	175.22	211.57	0.93	0.89		1.20	0.00	
Dyrk3		dual-specificity tyrosine-(Y)-phosphorylation regulated kinase 3	101.02	129.66	166.74	0.36	1.00		0.72	0.05	
Egr1		early growth response 1	1304.99	3327.58	3329.32	1.35	0.09		1.35	0.01	
Egr2		early growth response 2	68.31	807.37	642.92	3.56	0.00		3.23	0.00	
Egr3		early growth response 3	320.58	376.67	747.76	0.23	1.00		1.22	0.00	
Egr4		early growth response 4	78.88	208.31	212.88	1.40	0.00		1.43	0.00	
Fosb		FBJ osteosarcoma oncogene B	120.22	238.15	350.08	0.99	1.00		1.54	0.01	
Fosl2		fos-like antigen 2	476.82	784.92	1455.66	0.72	1.00		1.61	0.00	
Frmf6		FERM domain containing 6	377.48	471.57	701.70	0.32	1.00		0.89	0.00	
Gadd45b		growth arrest and DNA-damage-inducible 45 beta	79.04	161.02	173.89	1.03	1.00		1.14	0.04	
Gadd45g		growth arrest and DNA-damage-inducible 45 gamma	83.85	183.34	157.06	1.13	0.00		0.91	0.01	
Homer1		homer homolog 1 (Drosophila)	6305.25	8785.30	13689.26	0.48	1.00		1.12	0.01	
Map3k14		mitogen-activated protein kinase kinase kinase 14	53.73	73.18	111.97	0.45	1.00		1.06	0.04	
Nr4a1		nuclear receptor subfamily 4, group A, member 1	647.59	2547.84	1762.86	1.98	0.00		1.44	0.01	
Nr4a2		nuclear receptor subfamily 4, group A, member 2	166.42	402.00	751.40	1.27	0.12		2.17	0.00	
Per1		period circadian clock 1	439.51	861.93	867.98	0.97	0.00		0.98	0.00	
Ptgs2		prostaglandin-endoperoxide synthase 2	203.17	251.49	406.52	0.31	1.00		1.00	0.04	
Tmem252		transmembrane protein 252	2.00	16.02	18.64	3.00	0.37		3.22	0.02	
Trib1		tribbles homolog 1 (Drosophila)	121.77	322.27	405.51	1.40	1.00		1.74	0.02	

**Table 3. List of differentially regulated genes at P30 and P100 in *Otx2* mutants**

Average number of reads, log2FoldChange (log2FC) and adjusted probability (p<sub>adj</sub>) for genes differentially regulated between P30 (A) and P100 (B) in layer IV of visual cortex of wild-type, *Otx2*<sup>+/AA</sup> and *Otx2*<sup>+/GFP</sup> mice (p<sub>adj</sub><0.05 and log2FC<-1 and >1).

Putting thresholds at  $p_{adj} < 0.05$  and  $\log_2FC < -1$  and  $> 1$ , we obtained a list of 23 genes (Table 3). The majority of these genes showing an opposite regulation between P30 and P100 were known “plasticity genes”: for instance, the average number of reads for *Arc* was 18689.15 for the wild-type and 2877.21 for *Otx2*<sup>+/GFP</sup> at P30, while 3278.11 for wild-type and 13933.39 for *Otx2*<sup>+/GFP</sup> at P100 (Figure 34A). Some of them, like *Arc* and *Fosb*, are immediate early genes, that have been implicated in cortical plasticity (Andreasson and Kaufmann, 2002; Kaczmarek and Chaudhuri, 1997; Shepherd and Bear, 2011) (Figure 34A and Table 3). Others have been involved in synaptic plasticity: *Gadd45b* (Sultan et al., 2012), *Homer1* (Gerstein et al., 2012), *Egr4* (Li et al., 2005) (Figure 34B, 34D and Table 3). Another one of these genes, *Adamts9*, is of particular interest considering the link between *Otx2* and PNNs in the visual cortex (Figure 34C). Indeed, *Adamts9* is part of a family of enzymes that degrade chondroitin sulfate proteoglycans in the central nervous system (Demircan et al., 2013; Lemarchant et al., 2013).

Although this list of genes is only an indication of putative *Otx2* targets in PV-cells, the up-regulation of known “plasticity genes” at P100 in *Otx2*<sup>+/GFP</sup> samples strongly suggests that the visual cortex of *Otx2*<sup>+/GFP</sup> mice is plastic at P100, in agreement with a delayed critical period for ocular dominance in *Otx2*<sup>+/GFP</sup> mice. We examined WFA staining intensity in the supragranular layers of the visual cortex of wild-type and *Otx2*<sup>+/GFP</sup> mice from P14 to P120 (Figure 35). The intensity of WFA staining was significantly reduced in *Otx2*<sup>+/GFP</sup> compared to wild-type mice, from P14 to P35 (for example at P35,  $11.03 \pm 1.11$  arbitrary units for *Otx2*<sup>+/GFP</sup> compared to  $30.2 \pm 1.55$  arbitrary units for wild-type littermates). This decrease is similar to what we observed with *Otx2*<sup>+/AA</sup> mice. However, at P120, WFA staining intensity in *Otx2*<sup>+/GFP</sup> cortex has not yet reached the wild-type levels, suggesting that, in *Otx2*<sup>+/GFP</sup> mice, critical period for ocular dominance is even more delayed than in *Otx2*<sup>+/AA</sup> mice.

All in all, these data support the hypothesis that *Otx2*<sup>+/GFP</sup> mice open their critical period for ocular dominance after *Otx2*<sup>+/AA</sup> mice (Figure 36). Again, this fits in with our two-threshold model (Spatazza et al., 2013b). In the *Otx2*<sup>+/AA</sup> mutants, the accumulation of *Otx2* protein in PV-cells is delayed due to the mutation in *Otx2* GAG-binding domain and therefore the absence of specific recognition between *Otx2* and the PNNs. This causes a delay in cortical maturation because it takes longer to reach the first *Otx2* threshold that opens the critical period. In the *Otx2*<sup>+/GFP</sup> mice, *Otx2* protein levels are at 50% of wild-type, therefore only half as much of the *Otx2* should reach the cortex as compared to wild-type. This would explain

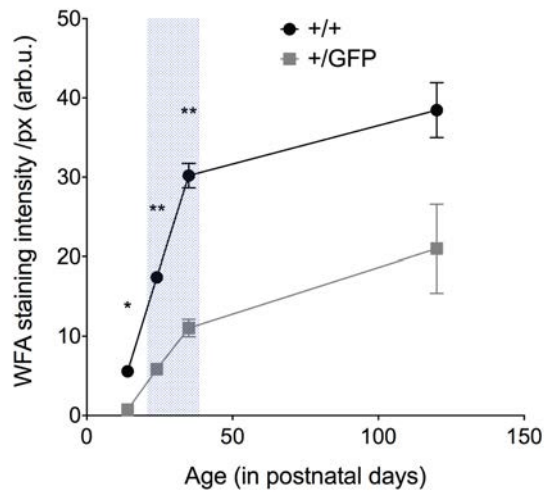


**Figure 35. Delayed PNN expression in the visual cortex of  $Otx2^{+/GFP}$  mice**

Quantification of the mean intensity of WFA staining per pixel in supragranular layers of visual cortex of  $Otx2^{+/+}$  and  $Otx2^{+/GFP}$ , from P14 to P120. WFA staining intensity is significantly lower in  $Otx2^{+/GFP}$  mice than in wild-type littermates from P14 to P35. The blue shaded area indicates the wild-type critical period for ocular dominance plasticity. (arb.u.: arbitrary units; \* $p < 0.05$ , \*\* $p < 0.01$ , error bars indicate SEM, Student t-test;  $700 \times 450 \mu\text{m}$ ).

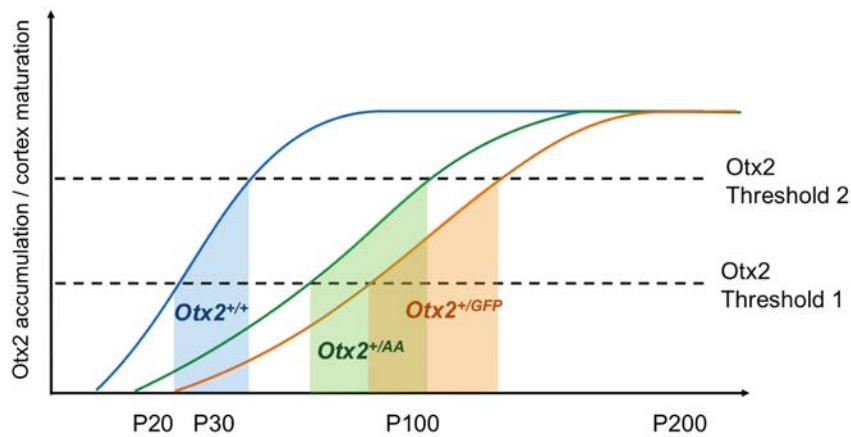


**Figure 36. Critical period model for  $Otx2$  mutants**

The normal critical period (in blue) for ocular dominance in the mouse binocular visual cortex opens at P20 and closes at P40. A decrease in the  $Otx2$  accumulation/cortical maturation slope leads to a change in both thresholds as a function of time. In the  $Otx2^{+/AA}$  mice (in green), the opening and closure of the critical period is delayed, as their visual cortex is plastic at P100 but not at P30 or P200. We hypothesize that the critical period of  $Otx2^{+/GFP}$  mice should be delayed even further in time.

both RNA-seq data and WFA immunostaining suggest that critical period onset is even more delayed in these heterozygous mice.

## Discussion

Our analyses of the eye and retina of *Otx2* mutant mice, *Otx2*-AA and *Otx2*-GFP, show an *Otx2* dose- and age-dependence for the development and maintenance of the retina. In studying visual cortex postnatal development of these mice, we find that *Otx2* binding to glycans in the PNNs is essential for the proper accumulation of *Otx2* in the PV-cells and therefore for the proper timing of the critical period for ocular dominance plasticity.

The striking eye phenotypes observed in the *Otx2*<sup>AA/AA</sup> mice are reminiscent of phenotypes associated with *OTX2* mutations in humans (Ashkenazi-Hoffnung et al., 2010; Ragge et al., 2005; Schilter et al., 2011). We show that small differences in gene dosage can have dramatic consequences, such as microphthalmia and anophthalmia. *OTX2* mutations in humans can lead to such abnormal eye phenotypes. To this date, no mutations in *Otx2* GAG-binding motif has been reported in human cases. However, in humans, expressivity is highly variable and penetrance of these phenotypes is incomplete. This variable expressivity can even be observed within an individual: in one cohort, three of eight patients were reported with asymmetric phenotypes such as asymmetric anophthalmia, anterior segment dysgenesis or optic nerve size (Ragge et al., 2005). In a more recent cohort, four of eight cases manifested asymmetric microphthalmia or anophthalmia (Wyatt et al., 2008). We observed this asymmetry in some *Otx2*<sup>AA/AA</sup> mice and the highly variable phenotype expressivity observed in humans is well represented in the phenotypes of our *Otx2* mutant mice. These results suggest that transcription factor dysfunction is not an all or none issue. This can lead to a better understanding of pathologies associated with a deregulation of transcription factors: small differences in the range of 10 to 20% can be significant in terms of phenotype expressivity and/or severity of the pathology as well as the timing of its appearance.

Most of this work has been done using the *Otx2*-AA mouse line. This genetic model was generated to look at non-cell autonomous phenotypes of *Otx2* without interfering with cell autonomous activities of the homeoprotein. Indeed, the only amino acids that are modified in this mouse line are the arginine and lysine (RK doublet) at the beginning of the GAG-binding

domain. The GAG-binding domain encompasses the N-terminus and the homeodomain of Otx2, but the RK doublet is located outside of the homeodomain. Therefore the RK→AA mutation does not alter the homeodomain sequence. However, our transcriptional activity results show that Otx2-AA is a less active transactivator for three promoters tested (*Rbp3*, *PKCα* and *Crx*). Consequently, although this mouse line was intended for studying non-cell autonomous Otx2 activities, we cannot exclude cell autonomous defects. This is why, in the retina study, we combined the two aspects (cell and non-cell autonomous) under the generic term of “activity”.

Other “activities” of Otx2 should also be taken into account. Homeoproteins, once internalized by a target cell, can play a role not only on transcription in the nucleus but also at the translation level in the cytoplasm (Prochiantz, 2013). Regulation of translation has been established for homeoprotein Bicoid in *Drosophila* (Rivera-Pomar et al., 1996) and also for some vertebrate homeoproteins, such as Engrailed (Brunet et al., 2005) and HoxA9 (Topisirovic and Borden, 2005). This regulation requires a direct interaction with the eukaryotic translation initiation factor 4E (eIF4E) through a motif conserved in over 200 homeoproteins (Topisirovic and Borden, 2005). Otx2, as Engrailed and Emx2, has been shown to interact with eIF4E (Nédélec et al., 2004), suggesting that it regulates translation. Therefore, we cannot preclude that the phenotype associated with Otx2-AA could be in part explained by changes in the regulation of translation by this transcription factor.

The RK→AA mutation is unlikely to impact on the transport of the protein across the membrane. Indeed, full-length FITC-Otx2-AA protein injected in the adult visual cortex is internalized by a wide range of cells (Beurdeley et al., 2012). Moreover, in *Otx2<sup>AA/AA</sup>* visual cortex, the protein is found inside many cells, suggesting that the internalization properties of the homeoprotein are not strongly modified. However, the internalization mechanisms for homeoproteins are not yet entirely understood. The penetratin sequence, that corresponds to the third helix of the homeodomain, is necessary and sufficient for internalization of homeodomains and homeoproteins (Derossi et al., 1994; Le Roux et al., 1993). *In vivo*, the cell surface binding sites, such as glycans chains, can trap the proteins and could regulate their local concentration with obvious consequences on their internalization rate. Cell surface GAGs may be involved in penetratin capture, as the removal of GAGs reduced the internalization of penetratin peptides (Alves et al., 2011; Bechara et al., 2013; Yang et al., 2010). We speculate that GAGs play a role in homeoprotein transduction through their ability

to trap the proteins at the cell surface with an element of specificity (the existence of a possible sugar code) as suggested by our studies.

The rest of this discussion will be focused on the cortex. A full discussion on the eye study can be found in the paper “Graded Otx2 activities demonstrate dose-sensitive eye and retina phenotypes” (Bernard et al., 2014).

In the retina, many cell types produce Otx2, making it impossible to differentiate between cell autonomous and non-cell autonomous phenotypes. However, in the cortex, the mRNA for Otx2 is absent (Spatazza et al., 2013b; Sugiyama et al., 2008) and Otx2 protein presence has been confirmed by immunohistochemistry (Beurdeley et al., 2012; Spatazza et al., 2013b; Sugiyama et al., 2008), Western blot (Spatazza et al., 2013b) and mass spectrometry (Kim et al., in preparation). This implies that the effect observed on visual cortex maturation in the Otx2-AA mice is purely non-cell autonomous. However, there could be a link between retinal defects and cortical phenotypes. Indeed, retinal activity is needed for postnatal development of the visual cortex: dark-rearing delays the maturation of the inhibitory circuits (Katagiri et al., 2007; Tropea et al., 2006) and the transfer of Otx2 in the cortex (Sugiyama et al., 2008). Retinal dysfunction could therefore account for the delayed maturation observed in *Otx2*<sup>+/-AA</sup> visual cortex. In the *Otx2*<sup>+/-AA</sup> mice, we did not observe morphological, histological or functional defects in the eye before P120. Even then, the defects are quite small and the *Otx2*<sup>+/-AA</sup> eye phenotypes are very close to that of the wild-type. Therefore, the absence of ocular dominance plasticity observed at P30 in the *Otx2*<sup>+/-AA</sup> visual cortex is most likely due to a cortical transfer defect and not to a problem in retinal development. This is also supported by the normal visual acuity of *Otx2*<sup>+/-AA</sup> observed at P200 by two different methods (optomotor test and visual evoked potentials). We cannot however exclude that, in older mice (P100 and P200), there might be subtle changes in retinal activity sufficient to alter thalamocortical activity and cortical plasticity.

In *Otx2*<sup>+/-AA</sup> visual cortex, the mis-localization of Otx2 can be accounted for the slower maturation of PV-cells in these mice. However, we have shown that Otx2-AA transcriptional activity is not equal to that of the wild-type and we therefore cannot exclude that the maturation phenotype is in part due to transcription changes. The identification of direct cortical targets of Otx2 will allow us to test the transcriptional activity of Otx2-AA in PV-cells.

PV expression and PNN assembly are delayed in the visual cortex of *Otx2*<sup>+/-AA</sup> mice. Otx2 arrival in the cortex impacts on the maturational state of PV-cells, either during development (Sugiyama et al., 2008) or after Otx2 loss of function in the adult (Beurdeley et al., 2012; Spatazza et al., 2013b). PV expression is affected by Otx2 transfer in visual cortex (Beurdeley et al., 2012; Spatazza et al., 2013b; Sugiyama et al., 2008). However, PV mRNA is not differentially regulated between *Otx2* mutants and wild-type littermates in our RNA-seq data. This had already been observed on microarrays of FACS-isolated PV-cells from PV-GFP mice: PV mRNA was not modified in PV-cells of mice injected with Otx2 in visual cortex at P20, compared to mice injected with vehicle (Spatazza, Di Nardo and colleagues, unpublished results). This suggests that Otx2 possibly regulates PV at other levels, such as mRNA/protein stability or protein translation. As mentioned earlier, homeoproteins can be translation regulators: for instance, Engrailed1/2 regulates the translation of mitochondrial mRNAs (primarily Ndufs1 and Ndufs3) (Alvarez-Fischer et al., 2011; Stettler et al., 2012). The absence of modification of PNN-related genes in the RNA-seq data, apart from *Adamts9*, also suggests that the regulation by Otx2 of PNN assembly could be due to protein stability and trafficking or translation regulation. Indeed, the reduced WFA staining in the visual cortex of *Otx2*<sup>+/-AA</sup> mice supports the hypothesis that PNN assembly is regulated by Otx2. There appears to be a feedback loop between PNNs accumulating Otx2 (Beurdeley et al., 2012) and Otx2 increasing PNN assembly (Sugiyama et al., 2008). Deep sequencing of polysome-associated mRNAs in PV-cells will provide a list of putative translation targets. Interestingly, preliminary data show an increased number of WFA-labeled cells in the visual cortex of one year old *Otx2*<sup>+/-AA</sup> and *Otx2*<sup>AA/AA</sup> mice. This suggests that the broader distribution of cortical Otx2 protein in Otx2-AA mice could eventually induce PNN expression in these additional cells.

We chose the ages P30 and P100 for layer IV RNA-seq because of our observation that *Otx2*<sup>+/-AA</sup> mice are physiologically plastic for ocular dominance at P100 and not at P30. More differences between *Otx2*<sup>+/-AA</sup> mice and their wild-type littermates could therefore be expected. However, for most of the 23 genes that are differentially regulated in *Otx2* mutants at P30 and P100, the average number of reads for *Otx2*<sup>+/-AA</sup> is often close to that of *Otx2*<sup>+/+</sup> at P30, when the wild-type mice are plastic for ocular dominance. This suggests that there might be several gene regulation steps in the establishment of plasticity. The RNA-seq data could therefore give insight into subtle timing of plasticity gene regulation. Indeed, we do not know when the

peak of plasticity occurs in the visual cortex of *Otx2*<sup>+/AA</sup> mice. Some (early plasticity) genes could already be up-regulated at P30 (such as *Arc* and *Egr4*) but this would not be yet translated into a physiological response to monocular deprivation. Genes like *Adamts9*, *Egr3* and *Fosl2* have a number of reads in *Otx2*<sup>+/AA</sup> P100 mice closer to that of wild-type P100 mice. This would indicate that P100 is probably not the peak of plasticity for *Otx2*<sup>+/AA</sup> mice but rather towards the end of their critical period for ocular dominance: while some genes are still up-regulated (*Gadd45b*), others are already at levels similar to wild-type mice (non plastic at P100).

This RNA-seq data also gives an insight into *Otx2*<sup>+/GFP</sup> mice critical period timing. *Otx2* conditional knock-down mice (CamKII-Cre x *Otx2*<sup>+/floxed</sup>) have a delayed onset for their ocular dominance critical period: they are not plastic at P28 (Sugiyama et al., 2008). In *Otx2*<sup>+/GFP</sup> mice, only 50% of *Otx2* is synthesized, therefore a smaller amount of *Otx2* protein should reach the cortex, compared to wild-type mice. WFA staining indicates that PNN assembly is delayed in *Otx2*<sup>+/GFP</sup> visual cortex and that it does not reach the wild-type level at P100, contrary to what is observed in *Otx2*<sup>+/AA</sup> mice. Our hypothesis is therefore that *Otx2*<sup>+/GFP</sup> mutants should reach their critical period after *Otx2*<sup>+/AA</sup> mice. Our observation that “known plasticity” genes, that are up-regulated at the critical period peak (P30) in wild-type mice, are up-regulated at P100 in *Otx2*<sup>+/GFP</sup> mice supports this hypothesis. Physiological plasticity data, such as recording visual evoked potentials in *Otx2*<sup>+/GFP</sup> mice after monocular deprivation, will be required to address this question.

We are currently examining which of the RNA-seq targets are actually expressed in PV-cells. Indeed, our RNA-seq was performed on layer IV samples, containing various cell types, and in the search for *Otx2* direct targets, we are primarily interested in genes expressed by PV-cells. Among these PV-cell genes, we will need to validate their differential expression in *Otx2* mutants, but direct transcriptional regulation of these genes by *Otx2* will nevertheless be confirmed only by chromatin immunoprecipitation (ChIP) experiments. The validated genes will then be tested in physiological experiments to examine the functional outcome of their regulation by *Otx2*. This can be achieved by shRNA experiments or with knock-down mouse lines (if available), followed by rescue with *Otx2*.

Once validated in PV-cells of the visual cortex, it will be most interesting to examine whether these targets are also regulated by *Otx2* in other cortices. Non-cell autonomous *Otx2* is



present throughout the adult cortex (Spatazza et al., 2013b) and its transfer seems to regulate the timing of critical periods for other cortices. This is illustrated by our data showing that *Otx2*<sup>+AA</sup> mice have extended tonotopic critical period in the auditory cortex. The critical periods for various cortices are spread during postnatal development and Otx2 transfer could then be a more general regulator of cortical plasticity. Indeed, some of our RNA-seq data overlap with genome-wide studies in other models of cortical plasticity. For instance, in the rat barrel cortex, induction of plasticity through an enriched environment reveals differential expression of genes such as *Arc*, *Egr1-4*, *Nr4a1-2*, *Gadd45b-g*, *Arl4d* and *Cyr61* (Vallès et al., 2011).

It will also be exciting to examine which genes are regulated after reactivation of plasticity in the adult. Indeed, reducing cortical Otx2 levels by recombining *Otx2* in adult choroid plexus reactivates plasticity (Spatazza et al., 2013b). Deep sequencing of the layer IV mRNA of mice recombined – or not – for *Otx2* in the choroid plexus will inform us on differentially regulated cortical genes. Some gene expression studies have already been done using other techniques to reactivate adult plasticity: fluoxetine treatment (a serotonergic transmission modulator) followed by monocular deprivation restores plasticity in the adult visual cortex (Maya Vetencourt et al., 2008) and leads to changes in chromatin structure remodeling, synaptic plasticity molecules, extracellular matrix and inhibitory transmission (as assessed by gene expression changes on DNA microarrays, (Tiraboschi et al., 2013)). Comparing our results with this list should deepen our understanding of the mechanism by which Otx2 maintains a non-plastic state in the adult cortex. Beyond the understanding of plasticity mechanisms during postnatal development, identifying these adult plasticity targets of Otx2 could lead to the development of precise tools to reopen windows of plasticity in the adult.





## **II. Identifying Otx2-binding GAGs**

Otx2 accumulation in PV-cells driven by sensory experience triggers a critical period for plasticity, which eventually closes as PNNs condense around PV-cells. This, in turn, maintains a stable post-critical period state by attracting Otx2 throughout life in a positive feedback loop (Beurdeley et al., 2012). We therefore wondered which glycans present in the PNNs bind specifically to Otx2 in order to capture the homeoprotein. Previous isothermal titration calorimetry experiments with commercial chondroitin sulfates (CS) showed that a peptide mimicking Otx2 GAG-binding domain (RK-peptide) bound strongly to CS-D and CS-E, had a lower affinity for CS-C and heparin, and showed no measurable binding to CS-A (Beurdeley et al., 2012). We wanted to confirm the affinity of the full-length Otx2 protein for this subtype of commercial CS, but also to identify which cortical GAGs are binding to Otx2.

### **A. Otx2-binding GAGs in the cortex**

#### **Otx2 has a greater affinity for commercial CS-E**

To further investigate the GAGs binding to this small Otx2 fragment (RK-peptide: RKQRRERTTFTRAQL), we used a biotinylated RK-peptide and tested its interaction with two commercial CS, CS-A and CS-E. The peptide was immobilized on streptavidin beads and then incubated with GAGs. The fraction retained by the streptavidin beads, i.e. GAGs bound to the RK-peptide, was analysed by using Fluorophore Assisted Carbohydrate Electrophoresis (FACE). This technique allows the visualization of disaccharides by tagging them with a fluorophore, before running them into a native polyacrylamide gel. Each band on the FACE gel corresponds to a disaccharide (tagged with fluorophore 2-aminoacridone (AMAC)) with a specific sulfation pattern: the more sulfated a disaccharide, the quicker it runs in the gel. In Figure 37A, the first lane shows the fluorescence of AMAC, corresponding to the background noise of the experiment. The second lane shows all disaccharides present in the commercial CS-E preparation and the lowest band corresponds to the CS-E disaccharide. No specific signal was observed on the third lane, indicating that commercial CS-E on its own did not bind to streptavidin beads, whereas the CS-E incubated with RK-peptide was found on the beads (fourth lane). This was not observed with commercial CS-A. Commercial CS-E, like other commercial glycans, does not contain only CS-E polysaccharides: it is quite obvious from the FACE gel of commercial CS-E (second lane) that other types of glycans are present

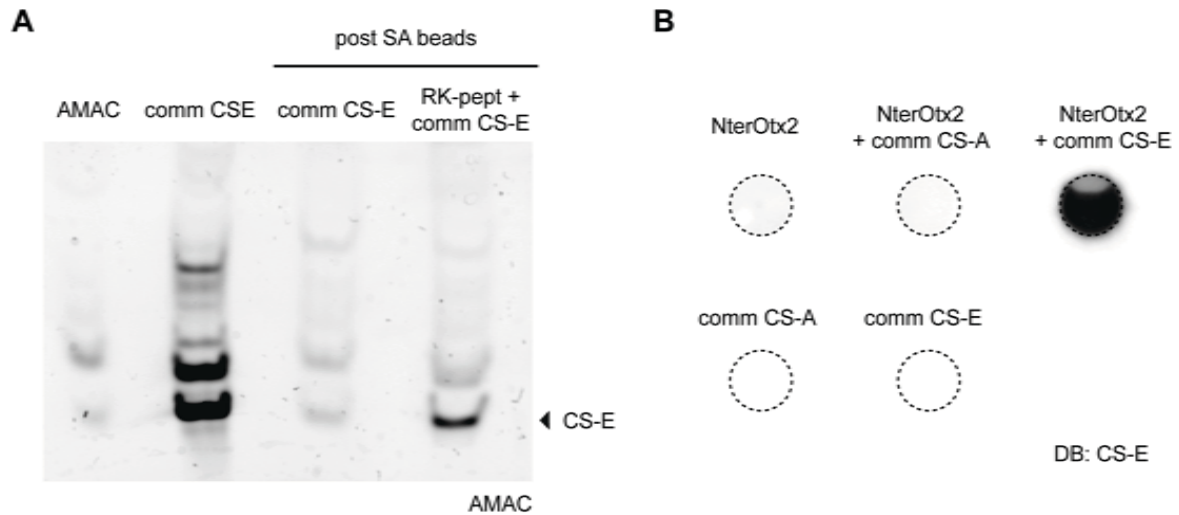


**Figure 37. Both the RK-peptide and NterOtx2 protein bind to commercial CS-E**

(A) FACE gel showing interaction between biotinylated RK-peptide and commercial CS-E: commercial CSs digested into disaccharides are tagged with 2-aminoacridone (AMAC) fluorophore and revealed using its fluorescence. Commercial CS-E is applied to streptavidin (SA) beads with or without biotinylated RK-peptide: a fraction of CS-E is retained by the beads when RK-peptide is present.

(B) Dot-blot (DB) with NterOtx2 protein and commercial CS-A and CS-E. The membrane is revealed using an anti-CS-E antibody. Commercial CS-E is held on the PVDF membrane due to its binding to NterOtx2 protein.

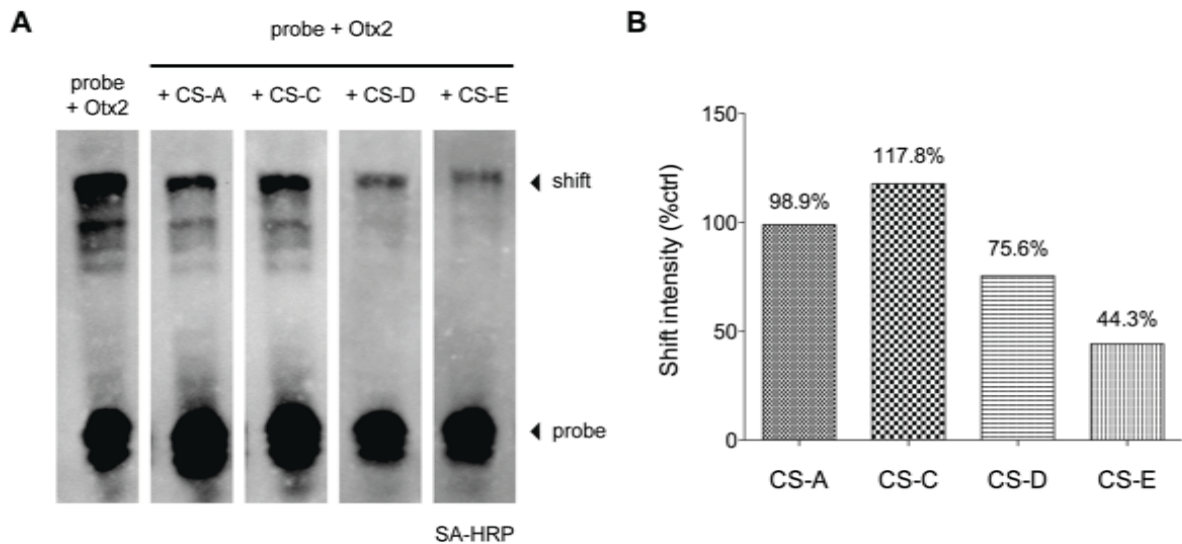


**Figure 38. Full-length Otx2 binds preferentially to commercial CS-E**

(A) Competition gel shift assay using a biotinylated DNA probe (*Rbp3*, revealed by streptavidin-HRP (SA-HRP)). The reduction in the intensity of the DNA shift shows the competition ability of commercial chondroitin sulfates for Otx2 binding.

(B) Quantification of the DNA shift intensity, compared to control (probe + Otx2). Commercial CS-E presents the highest competing activity.

(according to the manufacturer's information, this includes unsulfated CS, CS-A and CS-C). It is interesting to note that, among all these glycans, only the CS-E was retained on the beads by the RK-peptide (Figure 37A), confirming that RK-peptide binds to CS-E with greater affinity than to other glycans.

The kind gift of an anti-CSE antibody by the laboratory of Linda Hsieh-Wilson (CalTech, California, USA) (Brown et al., 2012) allowed us to investigate the binding of Otx2 protein to CS-E. Otx2 full-length recombinant protein is difficult to produce in large amounts, and seems to lose its activity after some time (usually 2-3 months at -80°C, R. Torero Ibad, personal communication). Therefore, we primarily used a 12 kD NterOtx2 protein, which encompasses the N-terminus and the homeodomain of Otx2. This NterOtx2 had been used previously for binding experiments on fresh frozen sections of the cortex (Beurdeley et al., 2012), showing not only that the NterOtx2 construct binds cortical sections, but also that the full-length Otx2 protein is able to disrupt this binding. This justifies the use of the NterOtx2 for some experiments since even though the binding may be less specific, due to the absence of Otx2 C-terminus, we would not get false positive binding. We incubated NterOtx2 protein with the same two commercial CS, CS-A and CS-E, and blotted the samples on a PVDF membrane using a dot-blot cassette, so that only the GAGs bound to NterOtx2 would stay on the membrane. The membrane was then probed with the anti-CS-E antibody. Commercial CS-A and CS-E were not held on the membrane without the protein: a signal was observed only when the NterOtx2 had been incubated with the commercial CS-E (Figure 37B). The membrane was also probed with an anti-Otx2 antibody, to check that the protein had stayed on the membrane. This experiment performed with the full-length Otx2 protein gave the same results.

Finally, we wanted to assess the affinity of the full-length Otx2 recombinant protein for an array of commercial chondroitin sulfates. In order to do this, we developed a competition gel shift assay. The GAG-binding domain of Otx2 corresponds to the first helix of its DNA-binding domain (homeodomain) plus the RK doublet upstream of the helix. We thus formed the hypothesis that a CS recognized by Otx2 could antagonize its binding to specific DNA promoter sequences. Using a gel shift assay with a biotinylated *Rbp3* DNA probe that binds specifically to Otx2 (Chatelain et al., 2006), we tested the competing activities of 4 different commercial chondroitin sulfates. At 4 pmol, CS-E almost entirely displaced the transcription factor from its binding site (DNA shift intensity reduced by 55.7%) (Figure 38). CS-D was

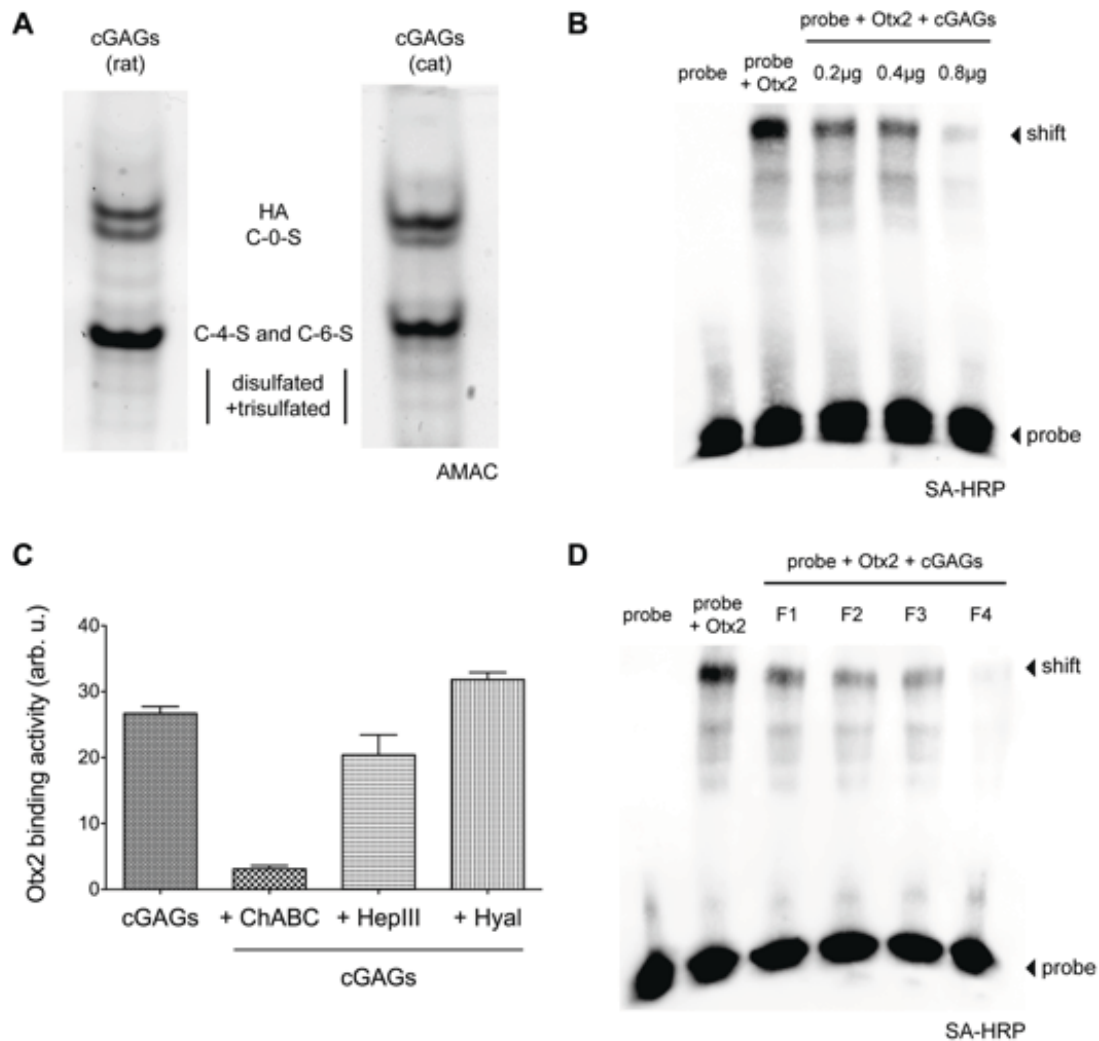


**Figure 39. Full-length Otx2 binds to purified cortical GAGs**

(A) FACE gel with purified cortical GAGs (cGAGs) extracted from rat or cat cortices. GAGs digested into disaccharides are tagged with 2-aminoacridone (AMAC) fluorophore and revealed using its fluorescence. These GAGs contain mainly CS-A (C-4-S) and CS-C (C-6-S), with a smaller amount of unsulfated chondroitin sulfate (C-0-S) and hyaluronan (HA). Disulfated CS-D and CS-E are present in very low amounts.

(B) Competition gel shift assay using a biotinylated DNA probe (*Rbp3*, revealed by streptavidin-HRP (SA-HRP)). The reduction in the intensity of the DNA shift shows the competition ability of purified cortical GAGs for Otx2 binding. Cortical GAGs are able to compete with DNA for Otx2 binding in a dose-dependent manner.

(C) Quantification of Otx2-binding activity of cortical GAGs assessed by competition gel shift assay, before and after treatment with GAG-digesting enzymes: chondroitinase ABC (ChABC), heparinase II (HepII) or hyaluronidase (Hyal). Only treatment with ChABC decreases the binding of the cortical GAGs to Otx2 (arb.u.: arbitrary units, error bars indicate SEM).

(D) Competition gel shift assay using a biotinylated DNA probe (*Rbp3*, revealed by SA-HRP). The reduction in the intensity of the DNA shift shows the competition ability of four successive fractions of purified cortical GAGs (F1-4) for Otx2 binding. The fourth PNN-containing fraction (F4) presents the highest competing activity.

slightly less active (DNA shift intensity reduced by 24.4%) and CS-A and CS-C were devoid of competing activity. All in all, these experiments confirm the highest affinity of Otx2 for the highly sulfated CS-E.

### **Otx2 binds to purified cortical PNN GAGs**

In order to work with cortical GAGs, we extracted and purified GAGs from the posterior cortex of mice, rats and cats, according to the protocol developed in James Fawcett's laboratory (Deepa et al., 2006). The use of rats and cats allowed us to obtain bigger amounts of GAGs. We verified by FACE that the respective amounts of CS disaccharides were the same as described in (Deepa et al., 2006) (Figure 39A). The main CS present in the adult cortex is CS-A (CS-A and CS-C disaccharide bands are very close, making it difficult to distinguish between A and C). Unsulfated chondroitine sulfate (C-0-S) and hyaluronan (HA) were also present, and disulfated CS-D and CS-E were found in very small amounts. We obtained the same patterns with GAGs extracted from either mouse, rat or cat cortex (Figure 39A).

By using the competition gel shift assay with the *Rbp3* probe, we tested Otx2 binding to GAGs purified from posterior cortex. The DNA shift was gradually lost when increasing amounts of GAGs were added to the samples, showing that, like the commercial CS-E, cortical GAGs can compete with DNA for full-length Otx2 binding (Figure 39B). The higher amount of cortical GAGs needed to completely displace Otx2 from DNA (compared with commercial CS polysaccharides) suggests that the Otx2-binding GAGs are present in small quantities in purified cortical GAG preparation.

Injecting chondroitinase ABC in the visual cortex leads to a reduction in the number of Otx2-positive cells, whereas injecting heparinase II has no effect on the cortical Otx2 staining (Beurdeley et al., 2012). To determine whether these results could be recapitulated in vitro, we pre-digested the purified cortical GAGs with chondroitinase ABC, heparinase II and/or hyaluronidase before the gel shift assay. Competition properties of the cortical GAGs were only lost when treated with chondroitinase ABC (Figure 39C). No difference was observed when the GAGs were pre-digested with heparinase II and/or hyaluronidase. This confirmed that cortical Otx2 binds chondroitin sulfates with a high specificity.



	<u>GAG-binding motif</u>
Arx	RKQRRYRTTFTSYQL
Chx10	RKKRRHRTIFTSYQL
Crx	RKQRRERTTFTRS QL
Dlx1	KKIRKPRTIYSSLQL
Dlx4	RKLRKPRTIYSSLQL
Dmbx1	RKQRRSRTAFTAQQL
En2	KEDKRPRTAFTAQQL
Gsc	RRKRRHRTIFTDEQL
HoxA13	RRGRKKRVPYTKVQL
Nkx2.5	RRRRKPRVLFSSQAQV
Otx1	RKQRRERTTFTRS QL
Otx2	RKQRRERTTFTRAQL
Pax3	RKQRRSRTTFTAEQL
Pax7	RKQRRSRTTFTAEQL
Phox2a	RKQRRIRTTFTSAQL
Phox2b	RKQRRIRTTFTSAQL
Prrx11	RKQRRNRTTFTLQQL
Prrx1	RKQRRNRTTFNSSQL
Pitx1	KKQRRQRTHTFSQQL
Pitx2	KKQRRQRTHTFSQQL
Pitx3	KKQRRQRTHTFSQQL
Prrx2	KKQRRNRTTFNSSQL
Prx2	KKKQRRNRTTFNSSQ

#### Figure 40. RK motif in homeoproteins

A consensus GAG-binding motif is found in many homeoproteins. The equivalent of Otx2 basic amino acids are highlighted in green.

We also purified the cortical GAGs using 4 successive extraction buffers in order to separate the condensed PNNs from the diffuse extracellular glycans (Deepa et al., 2006). This technique allows one to differentially extract diffuse and membrane-bound GAGs (fractions 1-3) and PNN-associated GAGs (fraction 4). In a competition gel shift assay, all 4 fractions were able to compete with DNA for Otx2 binding, however the PNN fraction (fraction 4) almost entirely displaced Otx2 from the DNA probe (the DNA shift intensity was reduced by 75.4% in experiments using GAGs from three different extractions) (Figure 39D). This suggests that Otx2 has a stronger affinity for GAGs within the PNNs rather than for glycans present in the diffuse extracellular matrix.

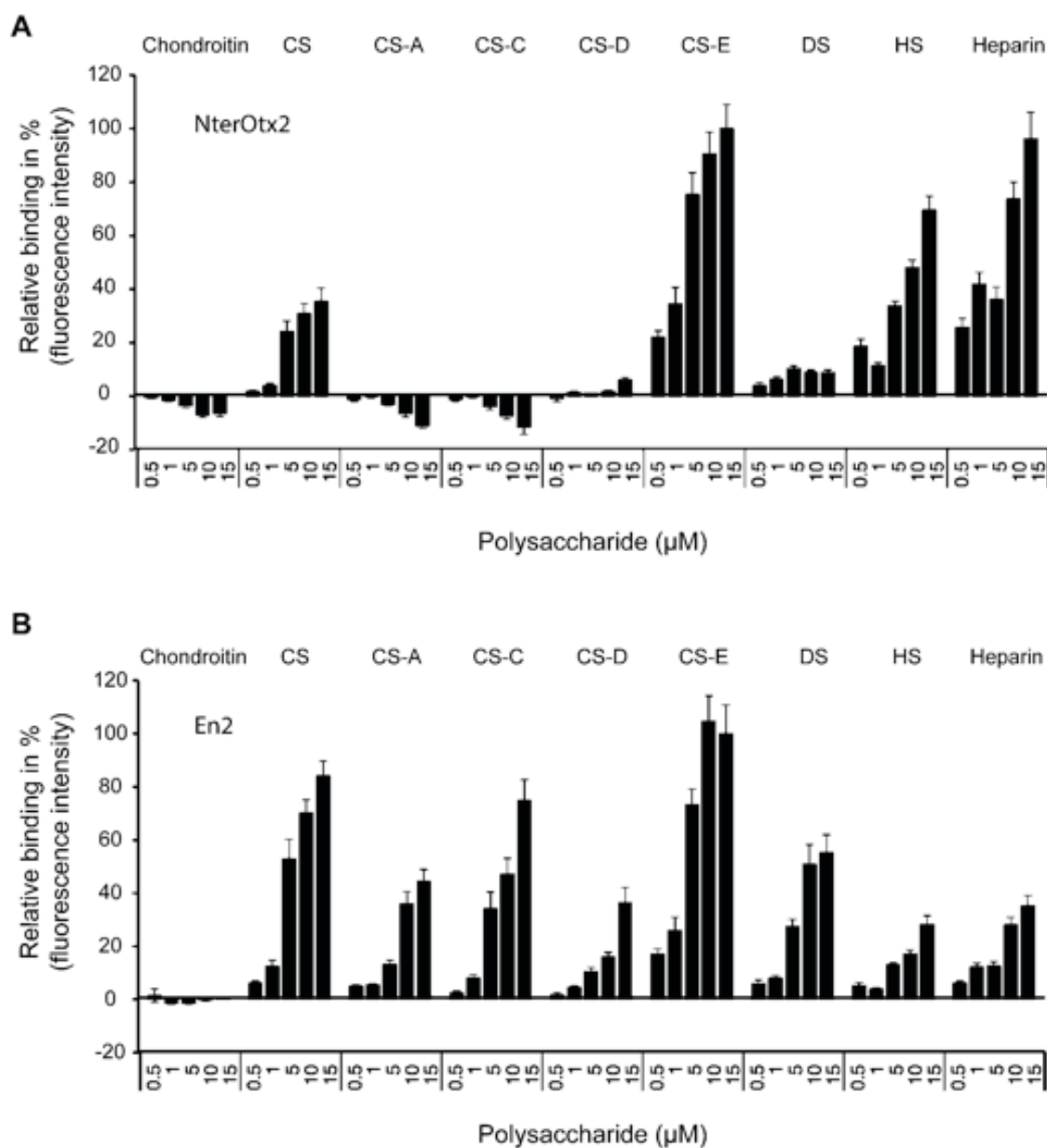


**Figure 41. NterOtx2- and Engrailed2-binding GAGs on glycan microarrays**

Microarrays containing increasing concentrations (0.5, 1, 5, 10, 15 $\mu\text{M}$ ) of the indicated commercial GAGs were incubated with either Myc-NterOtx2 (A) or Myc-Engrailed2 (B) and revealed using an anti-Myc antibody followed by a fluorescence secondary antibody. NterOtx2 binds selectively to CS-E, HS and heparin. Engrailed2 (En2) shows less binding selectivity than NterOtx2 (error bars indicate SEM).

## **B. GAG-binding homeoproteins: Engrailed2 versus Otx2**

### **Sugar code hypothesis**

Homeoproteins all share the highly conserved DNA-binding homeodomain. The identification of Otx2 GAG-binding motif just upstream of the homeodomain led us to look for putative GAG-binding sites in other homeoproteins. Indeed, sequences homologous to the GAG-binding domain identified in Otx2 are present upstream of the homeodomain of many homeoproteins (some examples are presented in Figure 40).

Whereas FITC-Otx2 showed a preference towards PNN-enwrapped cells when infused in the visual cortex, in contrast, FITC-Engrailed2, although it has a similar internalization (penetratin) sequence, was not preferentially captured by these cells (Beurdeley et al., 2012). This raises the issue of the presence of specific surface binding sites for homeoproteins and of a glycan code for homeoprotein recognition.

### **Homeoproteins-binding commercial GAGs**

To start the identification of homeoprotein-binding GAGs, we collaborated with the group of Linda Hsieh-Wilson. They have developed a glycan microarray that allows direct comparison of protein binding across diverse GAG subtypes enriched in specific sulfation motifs (Shipp and Hsieh-Wilson, 2007). We tested the binding of both Engrailed2 and NterOtx2 with various CS GAGs, as well as dermatan sulfate (DS), heparan sulfate (HS) and heparin, with glycan concentrations ranging from 0.5 $\mu$ M to 15 $\mu$ M. The results presented here are the average of four different experiments. NterOtx2 exhibited a strong, concentration-dependent binding to CS-E, HS and heparin (Figure 41A). A weaker binding was observed with CS, a GAG preparation that contains multiple sulfation motifs. NterOtx2 bound very little to dermatan sulfate and not at all to CS-A, CS-C or CS-D. Engrailed2 protein showed a more promiscuous behavior: even if the highest binding was observed for CS-E, Engrailed2 appeared to be less selective since it bound to all the sulfated motifs on the array (Figure 41B).

### **A sugar-ase protection protocol to identify homeoproteins-binding GAGs**

The commercial GAG preparations are not entirely purified and contain many different polysaccharides. In order to have access to the sugar code, our aim was to isolate the GAGs

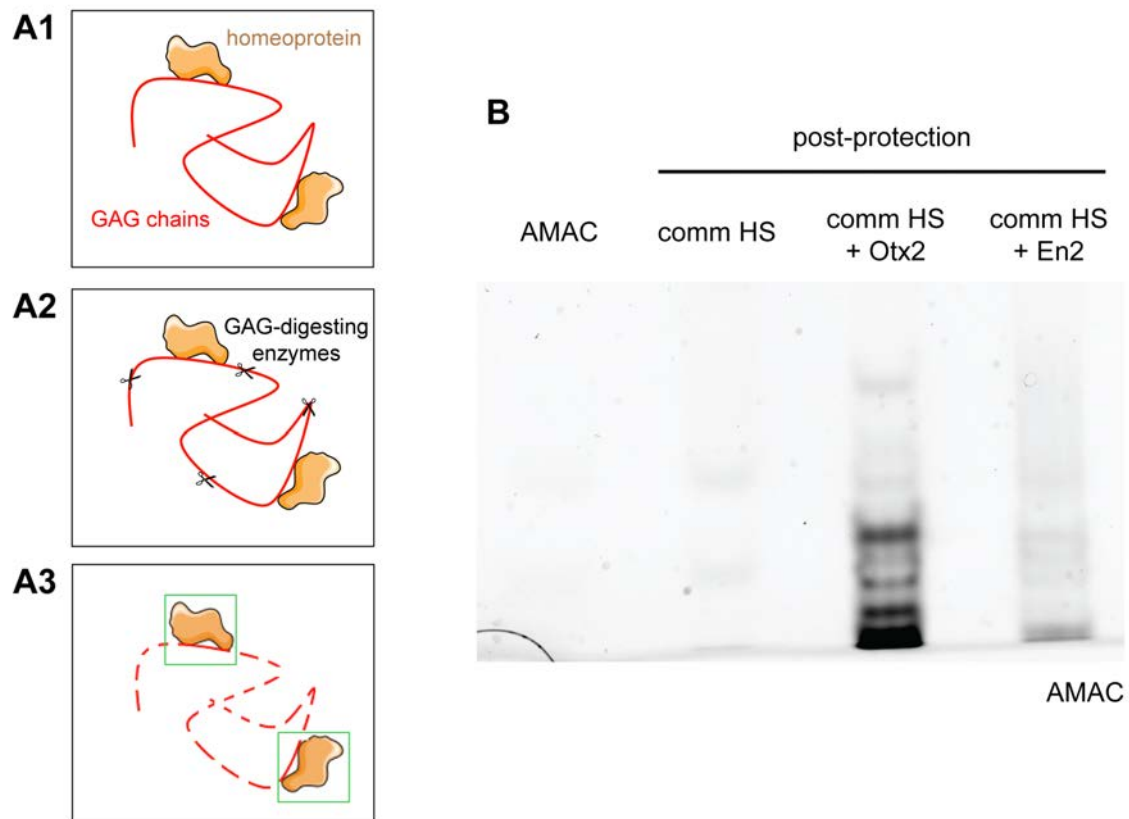


**Figure 42. Homeoprotein-binding protects GAGs from digestion**

(A) Sugar-ase protection protocol. Homeoprotein and GAG chains are incubated (A1) and the samples are digested with GAG-digesting enzymes, chondroitinase ABC, heparinase II or hyaluronidase (A2). The glycan motif bound to the homeoprotein is protected from digestion and can then be isolated and analyzed (A3).

(B) FACE gel with commercial heparan sulfate (HS) sugar-ase protection samples. GAGs digested into disaccharides are tagged with 2-aminoacridone (AMAC) fluorophore and revealed using its fluorescence. Otx2, and Engrailed2 (En2) to a lesser extent, can protect some HS chains from digestion.

that are binding to each homeoprotein. We developed a sugar-ase protection assay, based on the DNase protection protocol, in which DNA and protein are incubated and treated with DNase. Only the DNA sequence bound to the protein is protected from digestion. In our sugar-ase protection assay, we incubate homeoprotein and GAGs, then digest the samples with GAG-digesting enzymes (chondroitinase ABC, heparinase II and/or hyaluronidase). The glycan motif binding to the homeoprotein should be protected from digestion, as would be a DNA sequence (Figure 42A).

Among the GAGs tested on the glycan microarray, HS was bound both by NterOtx2 and Engrailed2, with a higher binding by NterOtx2. We therefore decided to validate our protection assay using Otx2, Engrailed2 and commercial HS (Figure 42B). After incubation of the homeoprotein and the GAGs, the samples were digested with heparinase II overnight. The digested oligosaccharides were filtered through a centrifugal filter device and the sample was recovered. The protein was digested with proteinase K and precipitated before processing the glycans for FACE (a fully described protocol can be found in the material and methods section of the thesis, p.57). In the absence of protein, no disaccharide was found after protection (lane 2 of Figure 42B), suggesting that the HS were completely digested. However, in the presence of Otx2, certain HS seemed to be protected (lane 3). Each band on the FACE gel corresponds to an HS disaccharide with a specific sulfation pattern. To a lesser extent, Engrailed2 could also protect some glycans from heparinase digestion (lane 4).

These experiments confirmed that homeoproteins have different binding affinities and selectivity towards glycans. Otx2 and Engrailed2 do not show the same binding for commercial GAGs and they do not protect the same disaccharides to the same extent in the sugar-ase protection assay.

## **Discussion**

These results confirm that Otx2 protein binds preferentially to commercial CS-E. We have used several Otx2 constructs to study Otx2 binding to glycans, from the RK-peptide of 15 amino acids to the full-length recombinant protein. In the isothermal titration calorimetry experiments performed with commercial polysaccharides and the RK-peptide, the RK-peptide shows the highest affinity for CS-E (dissociation constant of 54 nM) and CS-D (dissociation

constant of 18 nM) (Beurdeley et al., 2012). However, in the glycan microarrays, there is almost no binding activity of NterOtx2 to CS-D (even with 15 $\mu$ M of polysaccharide), while a binding to CS-E is already detectable at 0.5 $\mu$ M of polysaccharide. It is not unexpected that by increasing the size from a 15 amino acid peptide to a 12kD protein, changes are observed in terms of specificity. Not only the size but also the three dimensional structure of the protein has to be considered. Following up this point, one has to be careful in comparing NterOtx2 and Engrailed2 bindings in the glycan microarray results. Indeed, Engrailed2 is a full-length recombinant protein while NterOtx2 is missing the C-terminus of Otx2. It is doubtless that the three-dimensional structure of the full-length protein is different from that of NterOtx2 and this could impact GAG-binding selectivity. The absence of a crystal structure of the whole homeoprotein makes it difficult to assess the role played by the C-terminal domain of Otx2 in GAG binding (only the homeodomain is available (Ohnishi et al., 2006, PDB ID: 2DMS)).

Testing Otx2 interaction with commercial polysaccharides is informative, but it can never be representative of the GAG combination present in the extracellular matrix to which Otx2 binds *in vivo*. We have shown, by extracting and purifying GAGs from the cortex, that Otx2 binds to purified cortical GAGs. Among these GAGs, Otx2 seems to bind with higher affinity to PNN-associated GAGs. However, we have not yet managed to show whether Otx2 binds preferentially to the CS-E fraction of the PNNs. Indeed, CS-E accounts for a very small part of the total chondroitin sulfate GAGs of the PNNs (about 2%, (Deepa et al., 2006)), making it difficult to observe a direct interaction between Otx2 and the cortical CS-E. Moreover, the three-dimensional structure of the PNNs and the distribution of chondroitin sulfate chains in the PNNs are not known, and there might be an accessibility issue to take into account in our biochemical experiments. The easiest way to observe an interaction between the PNN CS-E and Otx2 would be through a blocking/interfering experiment. The anti-CS-E antibody given by Linda Hsieh-Wilson has been shown to have blocking properties (Brown et al., 2012; Dick et al., 2013). We will therefore test if its infusion into adult visual cortex can impact Otx2 transfer to PNN-surrounded cells.

PNN glycans are getting more and more attention from neurobiologists. In addition to preventing neuronal plasticity (Pizzorusso et al., 2002) in various parts of the brain, they may play a role in stabilizing the extracellular milieu, by maintaining water and cation homeostasis (Costa et al., 2007; Härtig et al., 1999). They recently have been shown to protect cells against oxidative stress (Cabungcal et al., 2013; Suttkus et al., 2014). Their relatively easy

local manipulation using the enzyme chondroitinase ABC makes PNNs good targets in plasticity reopening experiments, for instance in injured spinal cord regeneration experiments (Bradbury et al., 2002; Burnside and Bradbury, 2014; Wang et al., 2011). However, only few proteins have been found to directly interact with PNNs. Basic fibroblast growth factor (bFGF), which is responsible for neuronal survival and neurite extension, is present in PNNs (Celio and Blümcke, 1994; Flaumenhaft and Rifkin, 1991). More recently, Semaphorin3A (Sema3A), a chemorepulsive axon guidance protein that binds to chondroitin sulfate chains, has been shown to be a constituent of PNNs in the adult rodent brain (Vo et al., 2013). Similarly to Otx2, Sema3A binds PNNs via chondroitin sulfate E (Dick et al., 2013). Interestingly, Sema3A has also been tested for various polysaccharides binding on glycan microarrays. The strong specific binding of Sema3A to CS-E and heparin parallels the results obtained with NterOtx2, with the exception of heparan sulfate binding (Dick et al., 2013).

Glycan microarrays with NterOtx2 show that the protein has a high binding capacity for heparan sulfates, although lower than the binding to CS-E. Even if many proteins that recognize heparan sulfate also recognize CS-E (Shipp and Hsieh-Wilson, 2007), Otx2-heparan sulfate binding is of particular interest. When exogenous Otx2 is infused in the cortex, it has to be pre-incubated with polysialic acid (Beurdeley et al., 2012), otherwise the homeoprotein cannot diffuse and is immediately taken up by cells at the infusion site. The presence of polysialic acid thus allows the diffusion of the protein until it meets the PNN-enwrapped neurons. This suggests that endogenous traveling Otx2 is associated with low-affinity glycans and, once in the cortex, transfers from the latter low-affinity glycans to high-affinity PNN-associated glycans. Otx2 binding to HS observed with glycan microarrays suggests that heparan sulfate chains could be these low-affinity GAGs. The laboratory has previously shown that the choroid plexus is one of the sources of cortical Otx2: Otx2 is produced by the plexus and secreted in the cerebrospinal fluid. A part of Otx2 (5%) is therefore at the surface of the choroid plexus (Spatazza et al., 2013b). We hypothesize that Otx2 could be kept on the surface of the plexus by glycans. Preliminary results (RNA-seq data of adult mouse choroid plexus and surface biotinylation assays) show that most of the known proteoglycan types are expressed by the plexus: interestingly, the highly expressed proteoglycans are bearing heparan sulfate chains rather than chondroitin sulfate chains: 9738.23 reads for syndecan-2 and 2110.13 reads for glypican-6, compared to 57.56 reads for versican and 2.52 reads for aggrecan. Otx2 could therefore be bound to low-affinity glycans (perhaps heparan sulfates) on the surface of the plexus, then released in the cerebrospinal



fluid attached to these GAGs. As proposed above, once in the cortex, it could be transferred from these low-affinity glycans to the high-affinity glycans of the PNNs. Identifying which distinct sulfation motifs in heparan sulfate bind to Otx2 will increase our understanding of Otx2 transfer mechanism.

Extracellular GAGs mediate the specificity of Otx2 transfer. Complex sugars are accurately distributed in the postnatal brain suggesting the existence of a sugar code for specific protein recognition. Many homeoproteins contain sequences homologous to the GAG-binding domain identified in Otx2 suggesting the existence of a sugar code for target cell recognition. We developed the sugar-ase protection protocol to confirm the existence of such a code and eventually to “crack” it. GAG binding sites are often not conserved between proteins of the same family, as observed in the case of chemokines, which have high structural similarities but do not share common GAG-binding regions (Johnson et al., 2004). This allows specificity and selectivity of GAG binding across chemokines (Gandhi and Mancera, 2008). We have not yet managed to test the purified cortical GAGs on our sugar-ase protection protocol. Using a commercial mix of heparan sulfates, heparinase was the obvious option for a GAG-digesting enzyme. But cortical GAGs present various GAG chains: chondroitin sulfates, heparan sulfates and hyaluronan. Moreover, GAG-digesting enzymes have overlapping digesting capacities: for instance, most hyaluronidases have a hydrolytic activity towards CS-A comparable to that for hyaluronan (Gushulak et al., 2012; Honda et al., 2012). Therefore, the appropriate types and amounts of GAG-digesting enzymes for the digestion of cortical GAGs in our sugar-ase protection assay need to be carefully tested.

The read-out of this sugar-ase protection protocol is the main issue. Even if the FACE method is considered reliable to monitor the sulfation and amount of chondroitin sulfates in biological samples (Karousou et al., 2014), we will eventually need a more precise analysis of our protected glycans. Techniques for the identification of a sequence of disaccharides are rare, due to considerable heterogeneity in average molecular mass, molecular mass range, disaccharide composition, content and position of sulfate groups. Electrospray ionization mass spectrometry has recently been developed for detection and characterization of sulfated oligosaccharides. GAGs are treated with various enzymes to obtain disaccharides that are labeled with AMAC (similarly to the FACE experiment) and resolved by different liquid chromatography systems for high-sensitivity detection by fluorescence. These disaccharides can then be characterized by mass spectrometry (Volpi et al., 2014). This technique has now

been set up for CS/DS samples (Volpi and Linhardt, 2010), HS oligosaccharides (Galeotti and Volpi, 2011), GAG mixtures (Yang et al., 2012a) and with extracts from cell culture (Mizumoto and Sugahara, 2012), tissue (Volpi, 2010) and biological fluids (Zhang et al., 2006).

Once these many technical questions are resolved, it will be interesting to examine whether Otx2 recognizes the same GAG sequence in different brain structures. Indeed, signaling molecules can require distinct GAG modification in different cellular contexts, which adds an additional level of complexity to signaling specificity in the nervous system (Bülow and Hobert, 2004). Otx2 is transferred in many cerebral cortices, where it is internalized preferentially by PV-cells (Spatazza et al., 2013b). In these cases, we can expect the Otx2-binding surface GAGs to be very similar to those of the visual cortex. To further (and more widely) investigate homeoprotein-binding GAGs, we would also like to test GAGs extracted from various parts of the brain where homeoproteins display non-cell autonomous functions. Engrailed2 plays a crucial role in guiding retinal axons during embryonic development (Brunet et al., 2005). To discover which GAGs are at the surface of these axons and if Engrailed2 binds to these GAGs would be a second demonstration of homeoprotein-GAG recognition in non-cell autonomous homeoprotein functions.

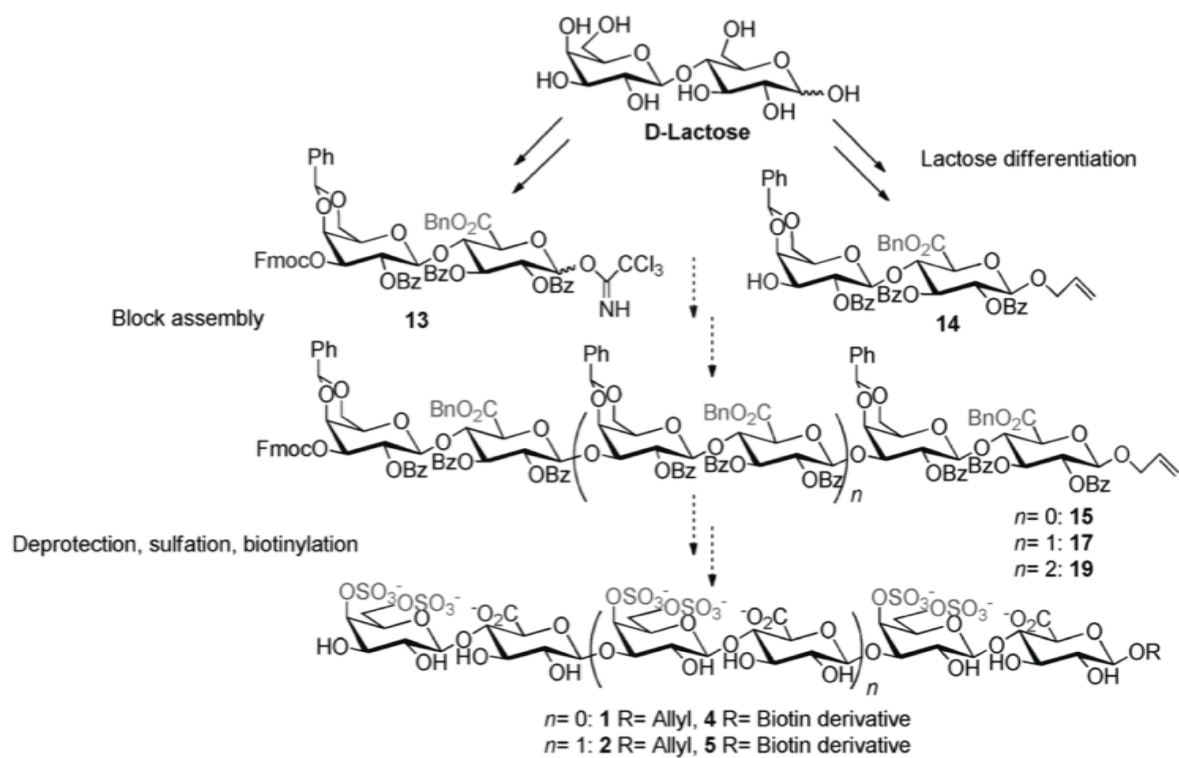


**Figure 43. CS-E analog synthesis plan**

This diagram presents the various steps for the synthesis of biotinylated or non-biotinylated oligosaccharide analogs of CS-E, obtained from D-Lactose.

### **III. Tools for disrupting Otx2 transfer in the visual cortex**

Interaction of Otx2 with glycans at the surface of cells plays an important role in the specificity of its transfer into PV-cells. A proper understanding of the molecular basis of this specificity would give us tools to control Otx2 transfer, spatially and temporally. Previous experiments have shown that modulating the amount of cortical Otx2 in the adult by blocking its secretion by the choroid plexus or its internalization by PV-cells leads to re-activation of visual cortex plasticity. This renewed adult plasticity allowed us to cure amblyopia in the mouse (Beurdeley et al., 2012; Spatazza et al., 2013b). Considering that Otx2 may have a role in regulating plasticity in other cerebral cortex regions, setting up new strategies to block its transfer could have a therapeutic potential beyond visual acuity. We first took advantage of the high affinity binding between Otx2 and CS-E to explore the blocking potential of a synthetic CS-E hexasaccharide analogue. The second strategy was the generation of a mouse line expressing a secreted single chain antibody against Otx2, in an inducible manner, to trap extracellular Otx2.

#### **A. A synthetic CS-E hexasaccharide interferes with Otx2 cortical transfer**

##### **Brief presentation of hexasaccharide CS-E synthesis**

The sulfation pattern of glycan chains is thought to encode information for the binding of growth factors and morphogens. Chemical synthesis of glycosaminoglycans is a very laborious task. Therefore, only small oligosaccharides have been generated so far (Lopin and Jacquinet, 2006). Jean-Maurice Mallet and his colleagues (Ecole Normale Supérieure, Paris) succeeded to prepare very close analogues of CS-E, in which the sulfation and charge patterns are completely preserved. They only modified an uncharged residue: the 2-acetamido (2-NHAc) group was replaced by a hydroxyl group (2-OH), as previously done for heparin and ganglioside synthesis (Bastide et al., 2011; Petitou and van Boeckel, 2004). This modification reduced by half the chemical steps needed for the synthesis.

CS-E hexasaccharide analog was prepared from lactose. Disaccharide blocks, obtained from peracetylated allyl  $\beta$ -lactose, were oligomerized to obtain an octosaccharide. CS analogs were sulfated to eventually recover CS-E disaccharide, tetrasaccharide and hexasaccharide analogues. Our chemist colleagues then took advantage of the presence of an allyl group to

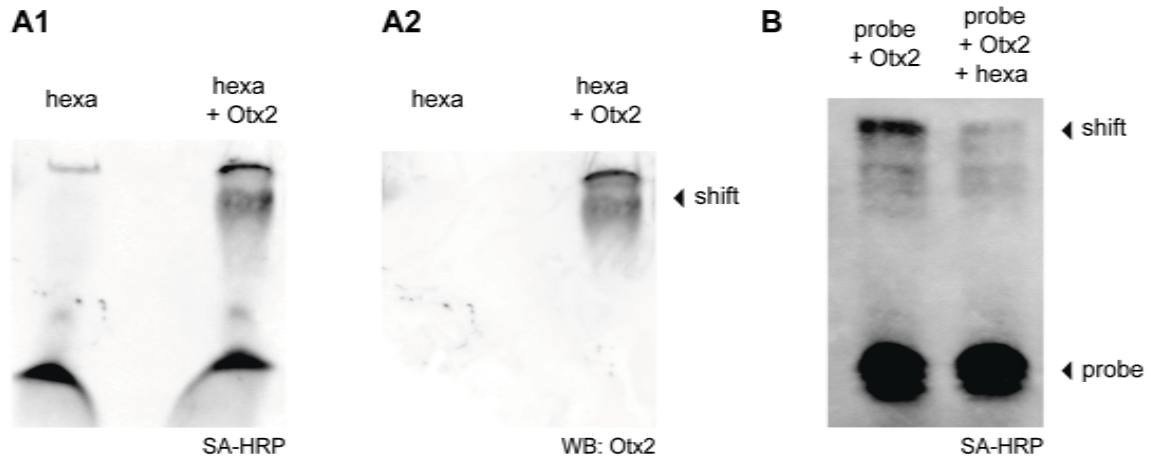


**Figure 44. Otx2 binds to synthetic CS-E hexasaccharide**

(A) Gel shift assay with the biotinylated CS-E hexasaccharide (hexa). Biotinylated hexasaccharide is revealed by streptavidin-HRP (SA-HRP, A1) and Otx2 protein by a Western blot (BW) with an anti-Otx2 antibody (A2). The shift in hexasaccharide in presence of Otx2 shows that Otx2 binds the synthetic CS-E analogue.

(B) Competition gel shift assay using a biotinylated DNA probe (*Rbp3*, revealed by SA-HRP). The reduction in the intensity of the DNA shift shows the competition ability of the synthetic hexasaccharide for Otx2 binding.

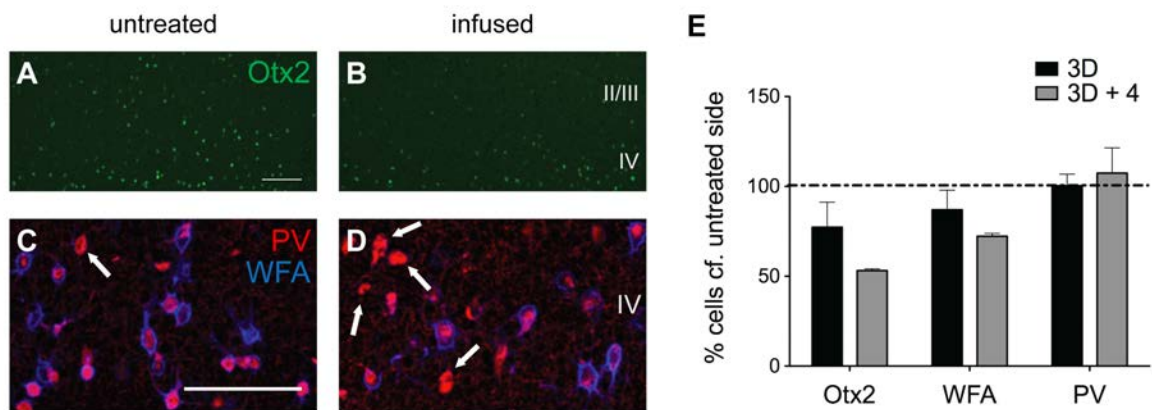


**Figure 45. Otx2 binding to hexasaccharide interferes with Otx2 transfer *in vivo***

(A-D) Otx2, PV and WFA immunostainings in supragranular layers of visual cortex of untreated (A, C) and hexasaccharide-infused (B, D) adult mice (scale bar: 100µm; arrows: PV-cells not surrounded by WFA staining).

(E) Percentage of Otx2, WFA and PV-positive cells in the supragranular layers of visual cortex (infused side compared to contralateral, untreated side), 3 days or 7 days post-infusion. Hexasaccharide infused by osmotic minipumps for 3 days in adult cortex decreases the number of Otx2-stained cells. It also decreases the number of WFA-stained cells, but not that of PV-positive cells (error bars indicate SEM; 700x450µm).

develop a click biotinylation, through its transformation into a 2-azido-2-hydroxyl-propyl group in two steps (epoxidation and sodium azide epoxide opening). The synthesis is summarized in Figure 43.

### **Otx2 binds to hexasaccharide CSE**

We first examined if Otx2 recognizes this synthetic CS-E hexasaccharide analogue. We used the biotinylated form of the hexasaccharide in a gel shift assay. In this direct gel shift assay, the biotinylated DNA probe was replaced by the biotinylated hexasaccharide. As illustrated in Figure 44A1, incubating the hexasaccharide with Otx2 recombinant protein led to a shift in its migration. Blotting the membrane with an antibody against Otx2 confirmed that the observed shift is due to the interaction of the hexasaccharide with Otx2 (Figure 44A2). Interestingly, Engrailed2 protein was also able to induce a shift in the biotinylated hexasaccharide migration. The shift was not observed using disaccharide or tetrasaccharide forms of the CS-E analogue, suggesting that six monosaccharide units is the minimum chain length for homeoprotein binding.

Using the competition gel shift assay with the *Rbp3* DNA probe, we tested the competing activity of the hexasaccharide. Strikingly, the synthetic hexasaccharide CS-E almost entirely displaced the transcription factor from its DNA binding site (Figure 44B). Compared to the commercial chondroitin sulfates (see II.A and Figure 38, p.98), for equal molar amounts of GAGs, the CS-E hexasaccharide presented the highest competing activity. The two gel shift experiments demonstrate that Otx2 binds the synthetic CS-E analogue.

### **Infusion of hexasaccharide CS-E blocks Otx2 transfer in primary visual cortex**

The preferential internalization of endogenous Otx2 by PV-cells is mediated by its specific binding to complex glycans present at the surface of the cells. Accordingly, Otx2 internalization is antagonized by the infusion of the GAG-binding domain and severely decreased following the injection of chondroitinase ABC into the visual cortex (Wizenmann et al., 2009). We investigated if the CS-E hexasaccharide could modify the amount of endogenous Otx2 internalized by PV-cells following its infusion into the adult mouse visual cortex for 3 days. As illustrated in Figure 45A-B and quantified in Figure 45E, a marked decrease in the number of Otx2-positive cells was observed in cortical supragranular layers of infused hemispheres, compared to the untreated hemispheres (at 3 days:  $77.3 \pm 13.9\%$  of control; at 7 days:  $53.1 \pm 0.8\%$  of control). Thus, Otx2 localization in the visual cortex was

disrupted by the presence of the hexasaccharide analogue. In addition, blocking Otx2 transfer induced a significant loss of PNN staining by the WFA lectin (Figure 45C-D, at 3 days:  $87\pm10.9\%$ ; at 7 days:  $72.2\pm1.3\%$ ). Indeed, the persistent accumulation of Otx2 is needed to maintain the PNNs around the PV-cells in the visual cortex (Beurdeley et al., 2012). PV expression was not modified at 3 days ( $100.3\pm6.5\%$ ) nor at 7 days ( $107.3\pm11.5\%$ ). This was unexpected but at least showed an absence of cell death (Figure 45C-D).

These results show that this synthetic hexasaccharide analogue of CS-E binds to Otx2 and can be used as an inhibitor of Otx2 cortical transfer *in vivo*.

### **B. Blocking Otx2 transfer *in vivo* in a single chain antibody mouse**

Studying Otx2 transfer, beyond its putative therapeutic potential, also provides a better understanding of homeoprotein transfer physiological functions. The best model for this would be a transgenic mouse line in which an extracellular homeoprotein would be blocked without altering its cell autonomous functions. We could not manipulate genetically the homeoprotein itself, as the transfer sequences are in the DNA-binding domain, thus precluding the production of a cell autonomous only mouse. In addition, even mutations outside the homeodomain may lead to modified transcriptional activities. We therefore turned to single chain antibody technology. Single chain antibodies (single chain fragment variable, scFv) exist under natural forms in camelids and sharks (Greenberg et al., 1995; Muyldermans et al., 1994), but we opted for their production by fusing the heavy and light variable chains extracted from a hybridoma, with a short peptidic linker. scFvs retain the antigen-binding capacity and specificity of the original antibodies, despite the removal of the constant regions (Ahmad et al., 2012). Single chain antibodies have previously been used with success for blocking extracellular homeoproteins, such as Pax6 in zebrafish (Lesaffre et al., 2007) and chick (Di Lullo et al., 2011) and Engrailed in chick, xenopus (Wizenmann et al., 2009) and drosophila (Layalle et al., 2011). We obtained the anti-Otx2 scFv by directly sub-cloning heavy and light chains derived from hybridoma cells secreting anti-Otx2 mouse monoclonal antibody. This anti-Otx2 monoclonal antibody recognizes a sequence in the homeodomain of Otx2. We then generated three conditional knock-in mouse lines, with the scFv directed against three homeoproteins (Otx2, Pax6 and Engrailed). We studied the knock-in mouse for anti-Otx2 scFv and used the knock-in mouse for anti-Pax6 scFv as a control.

### **A stop-lox knock-in mouse for spatio-temporal control of scFv expression**

The plasmids for anti-Otx2 and anti-Pax6 single chain antibodies were knocked in the *ROSA26* locus of C57Bl6 mice (Figure 18, in the Material and methods section of the thesis, p.46). The scFv plasmid contains a signal peptide for secretion of the scFv, allowing enough scFv secretion to catch the homeoprotein in the extracellular space. The scFv construct also contains 6 Myc tags for detection and a skipping peptide (P2A) before a GFP reporter sequence. A skipping peptide is introduced as a linker between two proteins to allow autonomous intra-ribosomal self-processing: the small 2A peptide, during its translation, interacts with the exit tunnel of the ribosome to induce the “skipping” of its last amino acid. The same ribosomal structure is then able to continue translating the downstream gene (in this case, GFP), after releasing the first protein (de Felipe, 2004). This normally results in the production of two proteins from a single vector, here the scFv (tagged with Myc) and the GFP (for visualization of scFv-producing cells). The presence of a STOP cassette, inserted before the scFv construct and flanked with two LoxP sites, is meant to spatio-temporally control the scFv expression. Due to the STOP cassette, the scFv will only be expressed upon recombination, following the injection or expression the Cre-recombinase. An obvious strategy is to cross the scFv mice with mice expressing Cre-recombinase under various promoters (inducible or not). We have worked with heterozygous *scFvOtx2<sup>tg/o</sup>* and *scFvPax6<sup>tg/o</sup>* mice, hereafter named *scFvOtx2* and *scFvPax6* mice, respectively.

### **Both anti-Otx2 and anti-Pax6 scFv are expressed and secreted *in vitro***

We first examined the expression of the scFv *in vitro*, by culturing ear fibroblasts from *scFvOtx2* and *scFvPax6* mice. Recombination was induced by adding a cell-permeable recombinase, Cre-TAT (obtained by the fusion of the bacterial Cre enzyme to the TAT peptide vector), directly in the culture medium for 1 hour. Forty-eight hours later, we examined by Western blot with an anti-Myc antibody whether the scFv was expressed (cell protein extract) and secreted (supernatant) by the cells (Figure 46A). No signal was observed in cells not treated with Cre-TAT. In the extracts and supernatants of cells treated with Cre-TAT, we observed two bands: one just above the 55kD marker (that is the expected weight of the single chain antibody) and a higher band above the 70kD marker (Figure 46A). The molecular weight of this upper band corresponds to that of a fusion protein, comprising both the scFv and the GFP, suggesting the P2A skipping peptide was not 100% efficient. A



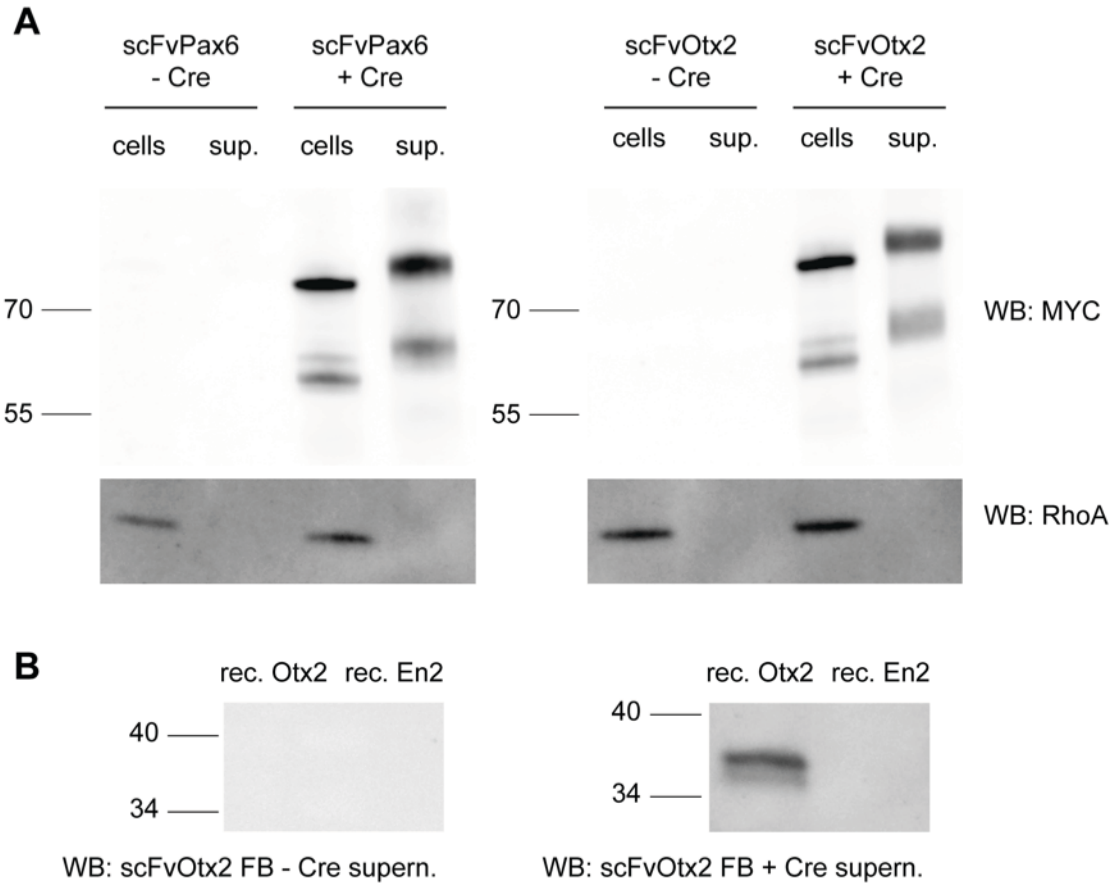


**Figure 46. *scFvOtx2* and *scFvPax6* ear fibroblasts express and secrete scFv *in vitro***

(A) Western blots (WB) of cell and supernatant protein extracts from *scFvOtx2* and *scFvPax6* ear fibroblasts treated or not with Cre-TAT. Anti-Otx2 scFv and anti-Pax6 scFv (revealed with anti-Myc antibody) are expressed and secreted only by fibroblasts treated with Cre-TAT. RhoA serves as an intracellular protein control.

(B) Western blots (WB) of recombinant (rec.) Otx2 and Engrailed2 (En2) proteins, revealed by using supernatants of *scFvOtx2* ear fibroblasts (FB) treated or not with Cre-TAT. Recombinant Otx2 is specifically recognized by the supernatant of fibroblasts treated with Cre-TAT.

Western blot analysis of the same extracts with an anti-GFP antibody confirmed this hypothesis: a signal was detected only for the upper band. Therefore, in both mice, there were two versions of the scFv, one corresponding to the antibody only and another corresponding to the antibody fused to GFP. The observation of both bands in the supernatant indicated that the presence of the GFP did not prevent secretion (RhoA was used as an intracellular control, showing that only secreted proteins were present in supernatant samples) (Figure 46A). Incidentally, the anti-Myc bands in the supernatant samples are slightly higher than those in the cell extract samples (Figure 46A). This may be due to post-translational modifications before secretion of the scFvs. In the rest of the experiments, the Myc antibody was used for blotting and staining both anti-Otx2 and anti-Pax6 scFv.

Previous *in vitro* work with the anti-Otx2 scFv plasmid had shown that the single chain antibody recognizes Otx2. To verify that the single chain antibody from the knock-in mouse was also able to bind Otx2, we collected the supernatant of cultured ear fibroblasts from *scFvOtx2* mice, treated or not with Cre-TAT and used it as an antibody to detect the recombinant Otx2 protein on a Western blot. Recombinant Engrailed2 protein was used as a negative control. Otx2 was recognized by the supernatant of cells treated with Cre-TAT but not Engrailed2, confirming specificity (Figure 46B).

In order to study the ability of the anti-Otx2 scFv to interfere with Otx2 transfer *in vivo*, we studied induced its expression by the choroid plexus of *scFvOtx2* mice, a strategy aimed at blocking Otx2 just after its secretion in the cerebrospinal fluid. A second strategy involved the crossing of *scFvOtx2* mice with *PV<sup>Cre/Cre</sup>* mice, in order to block Otx2 in the visual cortex, just before its internalization by PV-cells. The resulting mice, *PV<sup>Cre/o</sup>*, *PV<sup>Cre/o</sup>;scFvPax6<sup>tg/o</sup>* and *PV<sup>Cre/o</sup>;scFvOtx2<sup>tg/o</sup>* are hereafter named *PVCre*, *PVCrexscFvPax6* and *PVCrexscFvOtx2* mice, respectively.

### **Choroid plexus expresses and secretes scFv into cerebrospinal fluid**

To test the *in vivo* scFv production and secretion, we used a choroid plexus recombination method developed previously (Spatazza et al., 2013b). The cell-permeable Cre-TAT, injected into the lateral ventricles, leads to a very high recombination efficiency in the choroid plexus, as shown for the ROSA locus and *Otx2* (Spatazza et al., 2013b). Cre-TAT access to the choroid plexus is very specific and recombination is not observed in other brain structures.

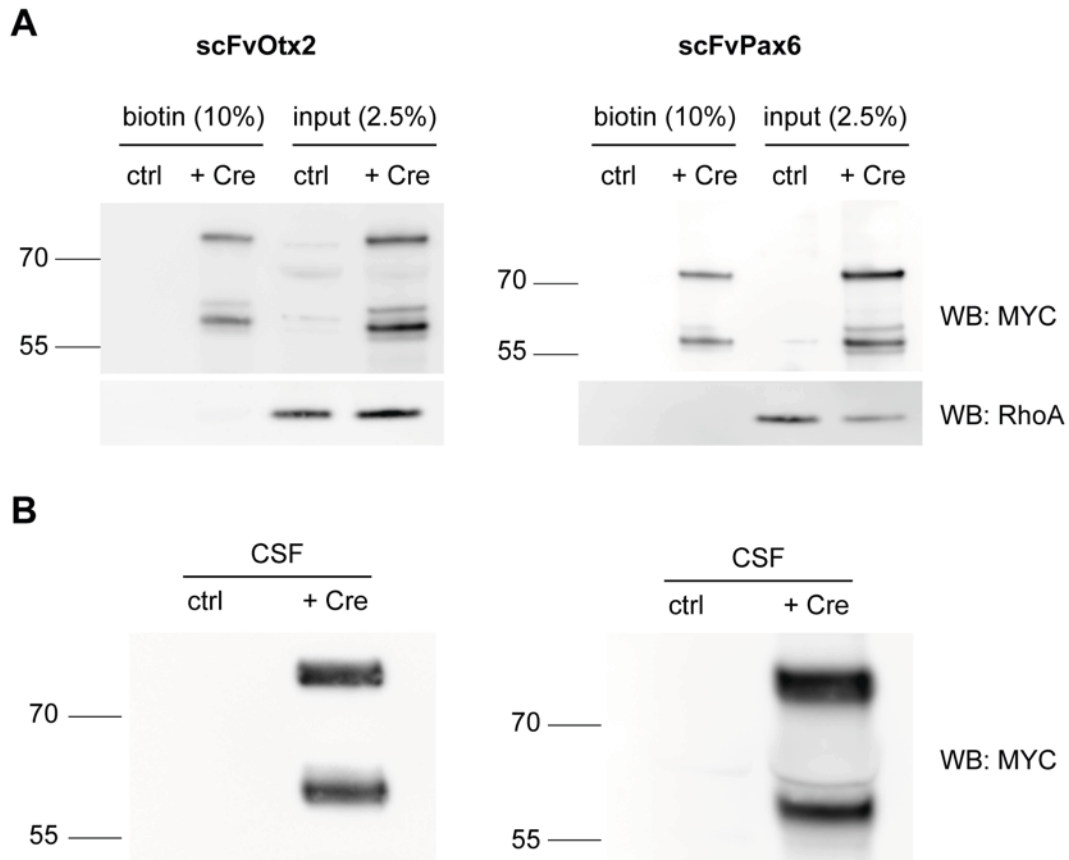


**Figure 47. Both scFv are expressed and secreted upon recombination *in vivo***

(A) Detection by Western blot (WB) of choroid plexus cell surface proteins with surface biotinylation assay. Biotinylation of choroid plexus allows the identification of surface protein (biotin) and intracellular proteins (input). Upon plexus recombination after Cre-TAT injection in lateral ventricles of *scFvOtx2* and *scFvPax6* adult mice, anti-Otx2 scFv and anti-Pax6 scFv (revealed with anti-MYC antibody) are expressed (input) and secreted (biotin) by the choroid plexus. Control mice (ctrl) are not injected with Cre-TAT. RhoA serves as an intracellular (input) protein control.

(B) Western blots (WB) of cerebrospinal fluid (CSF) protein extracts from *scFvOtx2* and *scFvPax6* mice injected (+ Cre) or not (ctrl) with Cre-TAT in lateral ventricles. Anti-Otx2 scFv and anti-Pax6 scFv (revealed with anti-MYC antibody) are secreted in the CSF upon choroid plexus recombination.

Cre-TAT was injected into the lateral ventricles of adult *scFvOtx2* and *scFvPax6* mice. 5 days later, the cerebrospinal fluid was collected and the 4<sup>th</sup> ventricle choroid plexus was dissected. We processed the dissected choroid plexus for surface biotinylation, a secretion assay already used with homeoproteins Engrailed (Wizenmann et al., 2009), Pax6 (Di Lullo et al., 2011) and Otx2 (Spatazza et al., 2013b). This assay, based on the biotinylation of cell surface proteins, showed that both anti-Otx2 scFv and anti-Pax6 scFv are present at the surface of recombined plexuses (Figure 47A). RhoA protein was used as an intracellular control.

Strikingly, both scFvs were also highly present in the cerebrospinal fluid of recombined mice (Figure 47B), showing efficient secretion. No scFv was detected in the cerebrospinal fluid of control mice (scFv mice not injected with Cre-TAT).

### **Functional outcome in cortex: local blocking with scFv expression in PV-cells**

To study the interfering ability of the anti-Otx2 scFv for Otx2 transfer at the level of the target PV-cells, we turned to *PV<sup>Cre/Cre</sup>* mice. In these mice, the Cre recombinase is under the promoter of PV, which allows a specific expression of Cre in PV-cells. PV expression starts at around P8-P10 in cortical interneurons (Endo et al., 1985; Solbach and Celio, 1991). Crossing *PV<sup>Cre/Cre</sup>* mice with *scFvOtx2* and *scFvPax6* mice should induce the expression and secretion of the scFv specifically by PV-cells, prior to normal critical period onset.

We first checked scFv production in the cortex of adult *PVCrexscFvPax6* and *PVCrexscFvOtx2* mice. Western blots of posterior cortex extracts of *PVCre*, *PVCrexscFvPax6* and *PVCrexscFvOtx2* mice show that both anti-Otx2 scFv and anti-Pax6 scFv were expressed in the cortex of *PVCrexscFvOtx2* and *PVCrexscFvPax6* mice, respectively (Figure 48A). We examined the localization of the scFv by immunostaining for Myc and PV in the visual cortex of *PVCre*, *PVCrexscFvPax6* and *PVCrexscFvOtx2* mice at P30. At P30, Myc staining was co-detected with PV in all layers of the cortex (Figure 48B). Very few cells were not co-stained with both PV and Myc. In both Western blot and immunostaining experiments, no Myc signal was detected in the cortex of control *PVCre* mice. Both Western blot and immunohistochemistry show that anti-Pax6 and anti-Otx2 scFv are produced in similar amounts in *PVCrexscFvOtx2* and *PVCrexscFvPax6* mice, respectively.

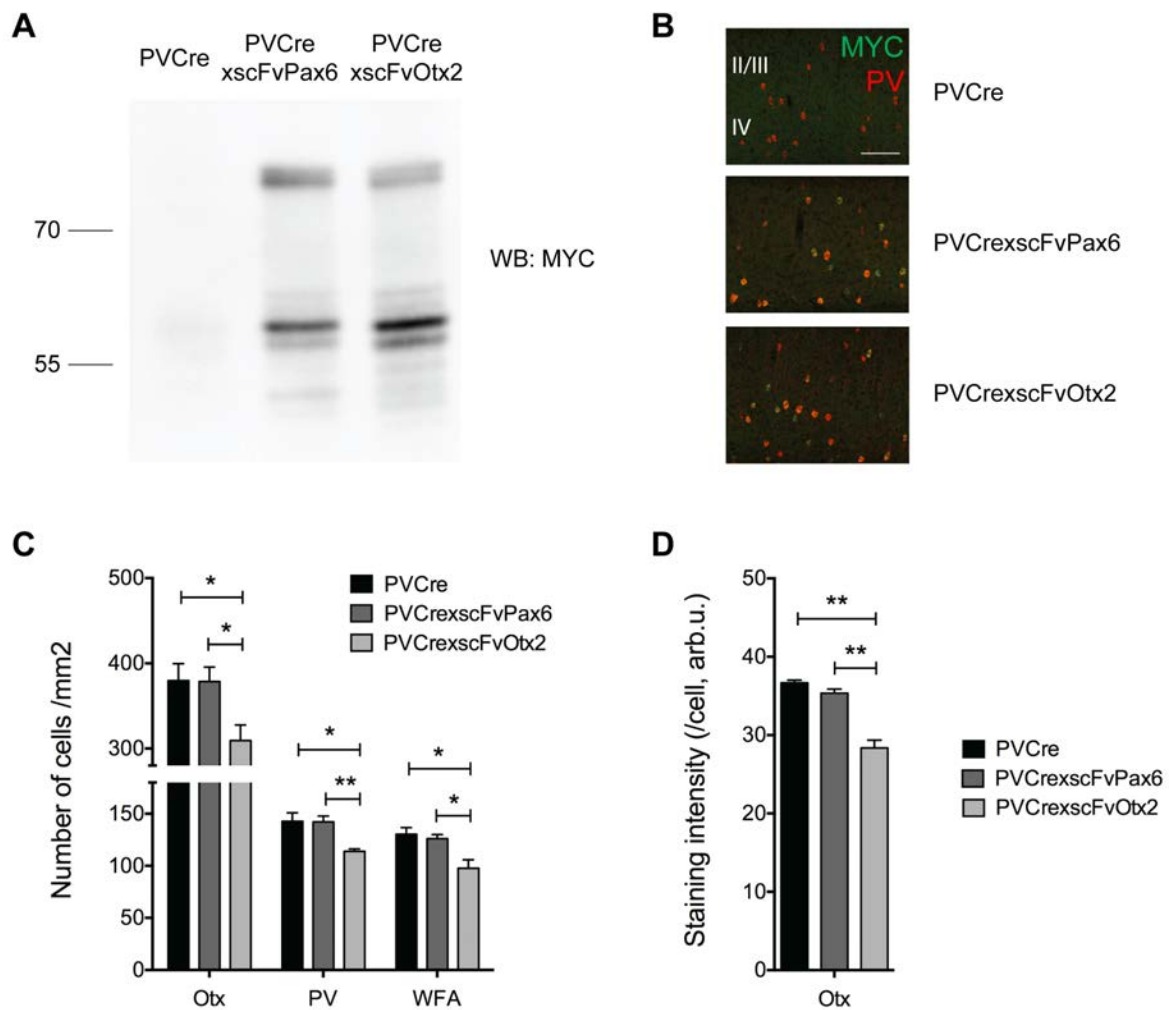


**Figure 48. Anti-Otx2 scFv interferes with Otx2 transfer in visual cortex**

(A) Western blot (WB) of posterior cortex protein extracts from adult *PVCre*, *PVxscFvPax6* and *PVxscFvOtx2* mice. Anti-Otx2 scFv and anti-Pax6 scFv (revealed with anti-MYC antibody) are expressed in the cortex of *PVxscFvPax6* and *PVxscFvOtx2* mice.

(B) Myc and PV immunostainings in supragranular layers of visual cortex *PVCre*, *PVxscFvPax6* and *PVxscFvOtx2* mice at P30 (scale bar: 100  $\mu$ m). Anti-Otx2 scFv and anti-Pax6 scFv are expressed by PV-cells in the cortex of *PVxscFvPax6* and *PVxscFvOtx2* mice.

(C) Number of Otx-, PV- and WFA-positive cells in supragranular layers of the visual cortex of P30 *PVCre*, *PVxscFvPax6* and *PVxscFvOtx2* mice. The number of cells is reduced in *PVxscFvOtx2* mice compared to *PVCre* and *PVxscFvPax6* mice.

(D) Quantification of the mean intensity of Otx2 staining in supragranular layers of the visual cortex of P30 *PVCre*, *PVxscFvPax6* and *PVxscFvOtx2* mice. Otx2 staining intensity is reduced in *PVxscFvOtx2* mice compared to *PVCre* and *PVxscFvPax6* mice.

To assess if the anti-Otx2 scFv can interfere with Otx2 transfer in the visual cortex, we examined the staining of Otx2, PV and WFA in visual cortex supragranular layers of *PVCre*, *PVCrexscFvPax6* and *PVCrexscFvOtx2* mice at P30. A decrease in the number and in the intensity of Otx2-positive cells was observed: the number of Otx2-positive cells was significantly reduced in *PVCrexscFvOtx2* cortex ( $309.3 \pm 18.4$  cells/mm<sup>2</sup>) compared to *PVCre* littermates ( $379.7 \pm 19.9$  cells/mm<sup>2</sup>) and *PVCrexscFvPax6* mice ( $378.5 \pm 16.9$  cells/mm<sup>2</sup>) (Figure 48C). Otx2 staining intensity per cell was lower in *PVCrexscFvOtx2* cortex ( $28.4 \pm 1.0$  arb. units) compared to *PVCre* littermates ( $36.7 \pm 0.3$  arb. units) and *PVCrexscFvPax6* mice ( $35.4 \pm 0.5$  arb. units) (Figure 48D).

Otx2 transfer is needed for the maturation of PV-cells in the visual cortex (Sugiyama et al., 2008). The reduction in Otx2 cortical amount observed in the visual cortex of *PVCrexscFvOtx2* mice could therefore impact the maturation of PV-cells. Indeed, a decrease in the number of cells visualized with the PV antibody and the WFA lectin was observed in *PVCrexscFvOtx2* visual cortex (for instance, for PV:  $113.8 \pm 2.5$  cells/mm<sup>2</sup> in *PVCrexscFvOtx2* mice compared to  $142.8 \pm 8.1$  cells/mm<sup>2</sup> in *PVCre* and  $142.1 \pm 5.7$  cells/mm<sup>2</sup> cells in *PVCrexscFvPax6* mice) (Figure 48C).

These results obtained with *PVCrexscFvOtx2* mice suggest that Otx2 transfer in the visual cortex is disrupted by the presence of the anti-Otx2 scFv, 20 days after induction of scFv expression by PV-cells. They also highlight the specificity of the interference, as the anti-Pax6 scFv has no effect on the number of Otx2-positive cells.

## Discussion

We have used two approaches to block Otx2 transfer in the visual cortex. A first tool was a synthetic CS-E hexasaccharide analogue that binds Otx2 and interferes with its transfer in the adult cortex. The second was the generation of mouse lines knocked-in for a single chain antibody against Otx2. Expression and secretion of the scFv by the PV-cells decreases Otx2 transfer in the visual cortex during postnatal development.

The high affinity of Otx2 protein for commercial CS-E led us to examine the binding between Otx2 and synthetic CS-E analogues. While binding is observed between Otx2 and the

hexasaccharide, this is not the case for di- and tetra-saccharides. This is in agreement with what is known of growth factor interaction with GAGs: the minimum GAG chain length required for binding is typically 4-12 monosaccharide units (Gandhi and Mancera, 2008). This was also observed for the binding of other proteins to the CS-E analogue. Two isoforms of CXCL12, a known GAG-binding chemokine, were tested for binding to CS-E oligosaccharide analogues. CXCL12 $\alpha$  exclusively binds to heparan sulfate, whereas CXCL12 $\gamma$  interacts with both heparan sulfate and chondroitin sulfate (Laguri et al., 2007; Lortat-Jacob, 2009). Indeed, CXCL12 $\alpha$  does not bind to any of the CS-E oligosaccharide analogues. On the contrary, CXCL12 $\gamma$  shows a strong binding to the hexasaccharide but no, or barely no binding to tetrasaccharides (Despras et al., 2013). Engrailed2 protein also binds to the CS-E hexasaccharide in a direct gel shift assay, which is consistent with the Engrailed2 binding to commercial CS-E polysaccharides on glycan microarrays.

Synthetic CS-E mimetics have been shown to have biological activity. For instance, a synthetic tetrasaccharide bearing CS-E sulfation pattern stimulates the neuronal growth and differentiation in primary culture of hippocampal neurons (Tully et al., 2004). In our study, infusing the CS-E hexasaccharide analogue into the visual cortex of adult mice decreases the number of Otx2-positive cells in supragranular layers. Given that, after critical period closure, Otx2 internalization is necessary to maintain a non-plastic state of the cortex, it will be interesting to test whether the synthetic CS-E hexasaccharide can be used to reactivate plasticity in the adult, as is the case for the RK-peptide (Beurdeley et al., 2012). There is a feedback loop between PNNs concentrating Otx2 at the cell surface and Otx2 increasing PNN expression. Our infusion experiment does not establish whether the CS-E hexasaccharide disrupts the PNNs, therefore decreasing Otx2 transfer in the PNN-enwrapped cells, or whether the hexasaccharide directly binds to Otx2, interfering with its specific recognition of PNNs. Moreover, other proteins, including proteins within the PNNs, bind to CS-E (Dick et al., 2013; Shipp and Hsieh-Wilson, 2007). The observed decrease in the number of Otx2- and WFA-positive cells could therefore be a secondary effect of a disruption of endogenous CS-E interaction with other proteins. This is another reason why the identification of the exact glycan sequence for Otx2 recognition in the PNNs is of interest as this glycan sequence could be synthesized and used *in vivo* to block specifically Otx2 transfer.

The other tool developed to block Otx2 cortical transfer is the scFv mouse. The scFv mouse lines are the first mouse genetic models that allow extracellular blocking of homeoproteins and therefore disruption of homeoprotein transfer without interfering with cell autonomous functions.

The anti-Otx2 and anti-Pax6 single chain antibodies are produced and secreted upon recombination *in vitro* and *in vivo*. However, the P2A skipping peptide is not 100% efficient in *scFvOtx2* and *scFvPax6* mouse lines, as shown by Western blot. Indeed, in *scFvOtx2* ear fibroblast cell culture, 65% of the Myc signal corresponds to the fusion protein (scFv + GFP) while 35% corresponds to the scFv alone. *In vivo*, both in the recombined *scFvOtx2* choroid plexus and in the *PVCrexscFvOtx2* cortex, the upper band represents between 45 and 50% of the total Myc signal. Very similar proportions were observed with *scFvPax6* mice. The proportions between the two proteins are similar inside and outside the cells (as shown in the cell culture Western blots and in the surface biotinylation experiments on recombined plexus). This suggests that the fusion protein is secreted like the scFv and that the GFP sequence does not interfere with secretion. This is important since the retention of the fusion protein within an organelle could be deleterious to the cell. On another hand, the GFP may participate in scFv stability. Whatsoever, the results obtained on the amount of Otx2 in PV-cells expressing the anti-Otx2 scFv (discussed in the next section) demonstrate that the strategy works. Another *scFvOtx2* mouse line without P2A skipping peptide and GFP is currently being generated at the Institut Clinique de la Souris (ICS, Illkirch, France). Comparing the phenotypes of the new mouse line with the current one will hopefully answer these questions.

At P30, in *PVCrexscFvOtx2* mice, we observe a decrease in the number of Otx2-positive cells and in Otx2 staining intensity in the supragranular layers of the binocular zone of the visual cortex. We hypothesize that this is due to a direct capture of Otx2 protein by anti-Otx2 scFv in the extracellular space. Indeed, the phenotypes observed in *PVCrexscFvOtx2* mice are necessarily due to an extracellular interaction between the homeoprotein and the single chain antibody: as the PV-cells do not synthesize Otx2 protein, the scFv and the homeoprotein are not produced by the same cells. The overall reduction of Otx2 staining intensity in the visual cortex can have two explanations that are not mutually exclusive. The first one is that there is a very good diffusion of scFv in the extracellular milieu allowing the scFv to trap Otx2 around many cell types and not only around PV-cells. A second possibility is that Otx2 is trapped by the scFv before its arrival in the visual cortex. Indeed, PV is expressed at around



P10 in many cells all along the optic pathway (in the ganglion cells of the retina, in the thalamus, etc.) (Endo et al., 1985; Solbach and Celio, 1991) and we know that retinal activity and Otx2 local transfer in the retina are crucial for PNN assembly and Otx2 capture by PV-cells (Sugiyama et al., 2008). We have tested the *PVCrexscFv* mice on the optomotor test: *PVCrexscFvOtx2* have a reduced visual acuity already at P28, compared to *PVCre* and *PVCrexscFvOtx2* mice. This suggests that Otx2 could be trapped by the scFv already at the level of the retina leading to the observed reduced Otx2 capture at the level of the visual cortex. To better distinguish between the two alternatives, we are presently analyzing other cortical regions.

In the *PVCrexscFvOtx2* visual cortex at P30, there is a decrease in the number of PV- and WFA-positive cells, two markers for the maturation of PV-cells. Indeed, Otx2 transfer during postnatal development is necessary and sufficient to trigger the maturation of PV-cells in the visual cortex. We observed a reduction of only 20% in the number of Otx2-, PV- and WFA-positive cells in *PVCrexscFvOtx2* cortex at P30. This, along with the fact that we still observe co-staining between Otx2 and PV in the visual cortex of *PVCrexscFvOtx2* mice, suggests that the scFv-Otx2 interaction is probably weaker than the Otx2-PNN interaction. Immunostainings for Otx2, PV and WFA at older ages, such as P60, will tell us whether Otx2 uptake by PV-cells is more efficiently blocked after 50 days of continuous production of scFv by PV cells. In any event, we have shown with other experimental paradigms (Beurdeley et al., 2012; Spatazza et al., 2013b) that a 20% reduction in PV-cell Otx2 content is sufficient to reopen plasticity in the adult. Recording the visual evoked potentials of these mice after monocular deprivation during their postnatal development should indicate whether blocking Otx2 transfer and accumulation in the PV-cells using the scFv can modify the critical period timing.

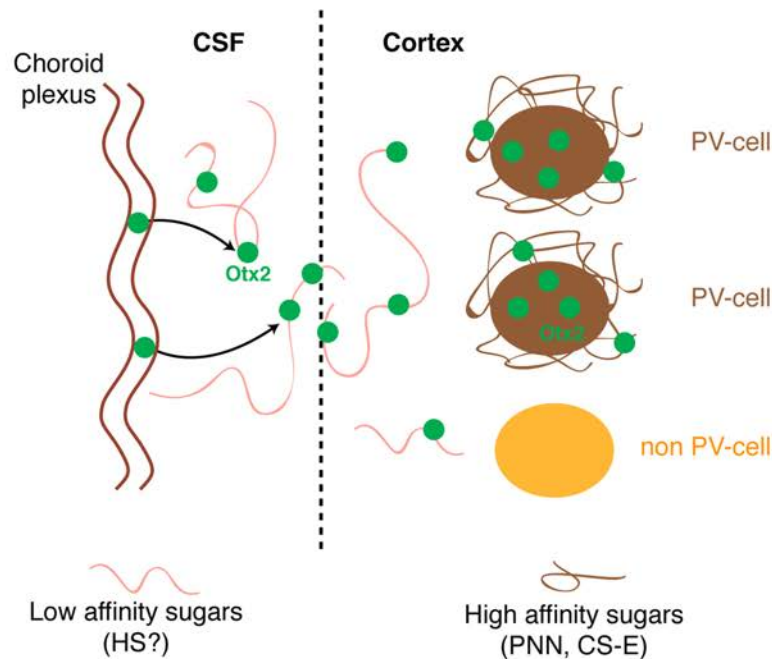
To confirm the *in vivo* capture of Otx2 by its scFv and discard possible developmental issues, Otx2 can also be trapped at the source rather than at the level of target cells. We have shown that recombining the choroid plexus of adult *scFvOtx2* and *scFvPax6* mice by injecting Cre-TAT in the lateral ventricles induces expression and very efficient secretion of the antibody in the cerebrospinal fluid. scFv expression by the choroid plexus will therefore be used to capture Otx2 at the plexus surface and in the cerebrospinal fluid and to block its transport into the cerebral cortices.





## **CONCLUSION AND PERSPECTIVES**

A. At P30, in wild-type mice



B. At P30, in Otx2-AA mutants

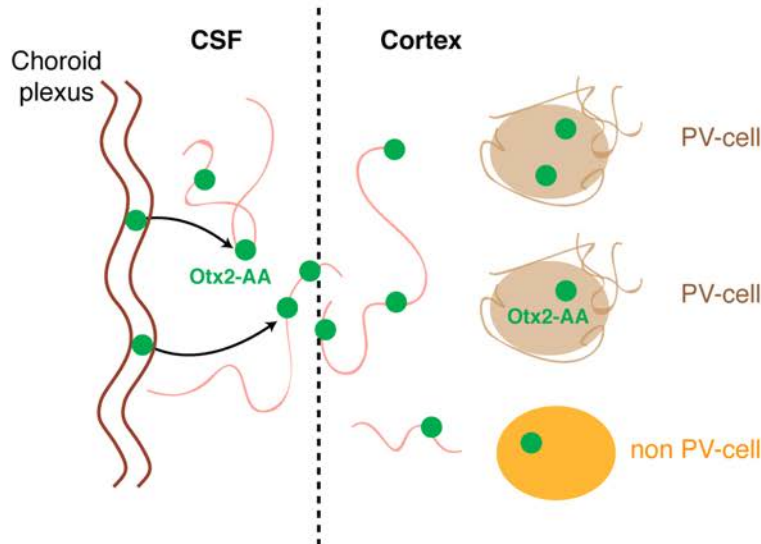


**Figure 49. Otx2 transfer, from choroid plexus to cortex, to regulate cortical plasticity**

(A) Otx2 transfer in wild-type mouse at P30, at the peak of the critical period for ocular dominance plasticity. One of the main sources of cortical Otx2 is the choroid plexus, which secretes the homeoprotein in the cerebrospinal fluid (CSF). Once in the cortex, Otx2 is preferentially captured by PV-cells, enwrapped by PNNs. Otx2 transfer during the critical period regulates PV-cell maturation and PNN assembly.

(B) Otx2 transfer in Otx2-AA mutants at P30. Otx2-AA protein is mutated for glycan recognition and is internalized by a wider range of cortical cells. PV-cell maturation, and therefore critical period timing, is delayed in Otx2-AA mice.

## **I. Otx2, a master regulator of cortical plasticity?**

### **Otx2 non-cell autonomous role for visual cortex plasticity**

The role and importance of Otx2 transfer in the mouse visual cortex are now well established. During postnatal development, Otx2 protein is preferentially transferred to the fast-spiking GABAergic PV-cells that are surrounded by the GAG-enriched perineuronal nets (PNNs) (Sugiyama et al., 2008). This transfer is activity-dependent: dark-rearing delays Otx2 cortical transfer until eye opening (Sugiyama et al., 2008). Once internalized by the PV-cells, Otx2 regulates their maturation, including PNN assembly (Sugiyama et al., 2008). This triggers the onset of a critical period for ocular dominance plasticity in the visual cortex at around P20, a critical period that closes 20 days later (Figure 49A).

Interfering with Otx2 transfer to reduce the amount of Otx2 protein in PV-cells during postnatal development impacts on critical period timing. *Otx2* conditional knock-down mice (CamKII-Cre x *Otx2*<sup>+/*flox*</sup>) have a delayed onset for their ocular dominance critical period and are not plastic at P28, suggesting that a 50% reduction in Otx2 protein is sufficient to alter PV-cell maturation (Sugiyama et al., 2008). These observations have been further strengthened with our Otx2-AA mutants. These mice are mutated in the GAG-recognition motif and our results show that this mutation also affects critical period timing. Indeed, Otx2-AA protein is diluted between target and non-target cells, leading to a reduced amount of Otx2 in PNN-enwrapped PV-cells. This delays the maturation of PV-cells during postnatal development. The Otx2-AA mice are not plastic for ocular dominance at the peak of the natural critical period (P30) (Figure 49B). Accumulation of Otx2-AA in the visual cortex of *Otx2*<sup>+/*AA*</sup> mice eventually catches up with the wild-type and *Otx2*<sup>+/*AA*</sup> mice are plastic at P100, and not plastic at P200. Thus both onset and closure of the ocular dominance critical period are delayed in *Otx2*<sup>+/*AA*</sup> mice.

### **Otx2 non-cell autonomous role in other cortices: the example of auditory cortex**

One of the main sources of cortical Otx2 in the adult is the choroid plexus (Spatazza et al., 2013b). Otx2 protein is present in a non-cell autonomous fashion in PV-cells of many cerebral cortices, including the auditory cortex (Spatazza et al., 2013b). The choroid plexus, *via* the secretion of Otx2 in the cerebrospinal fluid and its transport to the cortex, may be a general regulator of critical period plasticity, in brain structures with critical periods different from that observed in the visual cortex (of different duration and/or onset and closure).

Indeed, maturation of GABA circuits is heterogeneous across brain regions, paralleling the heterogeneous onset/duration of various critical periods (Takesian and Hensch, 2013). In the mouse auditory cortex, the critical period for tonotopic map reorganization opens at P12 and closes at P15 (Barkat et al., 2011). Similar to the visual cortex, we have shown that *Otx2*<sup>+/AA</sup> mice display plasticity in the auditory cortex at a time when the critical period is normally closed. *Otx2* may therefore function in a similar manner in the auditory cortex, by triggering the maturation of PV-cells: the diagram presented in Figure 49 could thus be valid at least for the visual and auditory cortex, the only difference being the timing of the critical periods.

In the post-critical period visual cortex and in the adult, the constant arrival of *Otx2* in the PV-cells is required to maintain the mature, consolidated, non-plastic state of the adult cortex. Interfering with *Otx2* transfer in the adult visual cortex decreases the maturational state of PV-cells and reopen a window of plasticity for ocular dominance (Beurdeley et al., 2012; Spatazza et al., 2013b). We have developed several tools and techniques (Figure 50) to block *Otx2* transfer in the adult visual cortex, which could be applied to other cortices. If *Otx2* plays a similar role in the establishment of the tonotopic critical period in the auditory cortex, blocking *Otx2* transfer in the adult auditory cortex could also open a window of plasticity in the adult and potentially correct developmental defects in tonotopic map organization.

*Otx2* mRNA and proteins are present during embryonic development in the peripheral organs of at least three sensory systems: the retina (Koike et al., 2007; Larsen et al., 2009; Martinez-Morales et al., 2001), the inner ear (Hidalgo-Sánchez et al., 2000; Miyazaki et al., 2006; Sánchez-Calderón et al., 2004) and the olfactory epithelium (Mallamaci et al., 1996; Matsuo et al., 1995; Veilleux et al., 2013). Moreover, *Otx2* protein is found in a non-cell autonomous fashion in the corresponding cortices: visual cortex, auditory cortex and piriform cortex ((Spatazza et al., 2013b) and unpublished observations). *Otx2* transfer could therefore possibly have a wide role in regulating sensory experience during postnatal development. In the visual pathway, *Otx2* transfer is activity-dependent and as shown by its injection in the eye, the protein can travel along the visual pathway to end in PV-cells of the visual cortex (Sugiyama et al., 2008). Injecting *Otx2* in the peripheral structures of other sensory pathways would indicate whether *Otx2* transport from the periphery to the corresponding cortex could take place. This raises the question of how activity (for instance in the visual pathway, the opening of the eyes) operates. Indeed, activity-dependent critical periods open following the initial activity of the corresponding peripheral sensory organs. Because the choroid plexus

provides a continuous supply of Otx2 throughout postnatal development, Otx2 accumulation in the cortex is probably triggered by sensory activity. We speculate that sensory activity regulates the initial PNN assembly allowing for the accumulation of Otx2 en route from the choroid plexus. Whether the sensory trigger requires Otx2 transport along sensory pathway is an interesting hypothesis even if PNN initial assembly could involve another molecular mechanism. Later on and throughout adulthood, the choroid plexus would serve as a general source of Otx2 protein to maintain the non-plastic adult state.

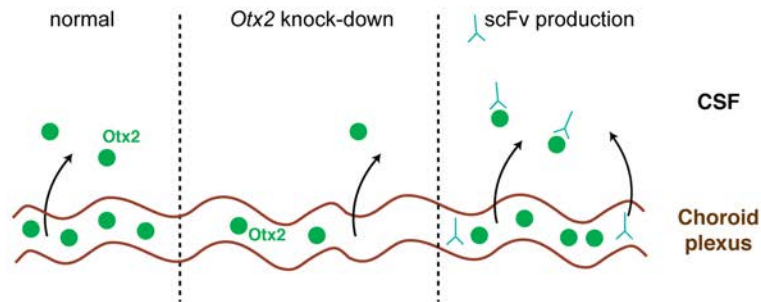
### **Otx2 non-cell autonomous role in other cortices: the hypothesis of amygdala**

Otx2 has been found not only in PV-cells of sensory cortices, but also in structures governing more complex systems, such as the amygdala, cingulate and limbic cortices ((Spatazza et al., 2013b) and unpublished observations). Critical periods have been proposed for these regions in mice, for fear extinction in the amygdala (Gogolla et al., 2009), for acoustic preference (Yang et al., 2012b) and for schizophrenia-related symptoms (Belforte et al., 2010), that can all be linked to the emotional and anxiety state of the animal. Interestingly, Otx2 heterozygous mice (*Otx2*<sup>+/*GFP*</sup> mice) show a hypo-anxiety behavior at P30 and in the adult, compared to wild-type littermates (C. Vincent and colleagues, unpublished observations).

Several reports propose that some psychiatric diseases may find their origin, at least in part, in cortical dysfunctions that occur in a period that precedes the onset of puberty (Dobbs, 2010; Fagiolini et al., 2009; Insel, 2010; Rubenstein, 2010). Defective maturation of PV-cells has been reported in cortex of subjects with schizophrenia (Akbarian et al., 1995; Hashimoto et al., 2003) and has been proposed as one of the causes of psychiatric phenotypes (Caballero et al., 2014; Fine et al., 2014; Gandal et al., 2012; Marín, 2012; Volk et al., 2012). PNN assembly has also been linked to schizophrenia (Bitanhirwe and Woo, 2014): PNN density is reduced in the amygdala and the entorhinal and prefrontal cortices of subjects with schizophrenia (Mauney et al., 2013; Pantazopoulos et al., 2010). Confirming the regions implicated in the hypo-anxious phenotype observed in *Otx2*<sup>+/*GFP*</sup> mice could support a role for Otx2 in their postnatal development. Identifying the non-cell autonomous roles of Otx2 in these brain regions can now be assessed with the use of the anti-Otx2 single chain antibody (scFv) mouse line, which allows to trap the extracellular Otx2 in a spatio-temporal manner. We have shown that, by using the scFv mice, Otx2 transfer can be trapped at its source (choroid plexus, Figure 50A) or intercepted before its capture by the target cells (PV-cells, Figure 50B). In addition to the scFv mice, we plan to work with adeno-associated viruses or



### A. Block Otx2 at the source



### B. Block Otx2 at the target

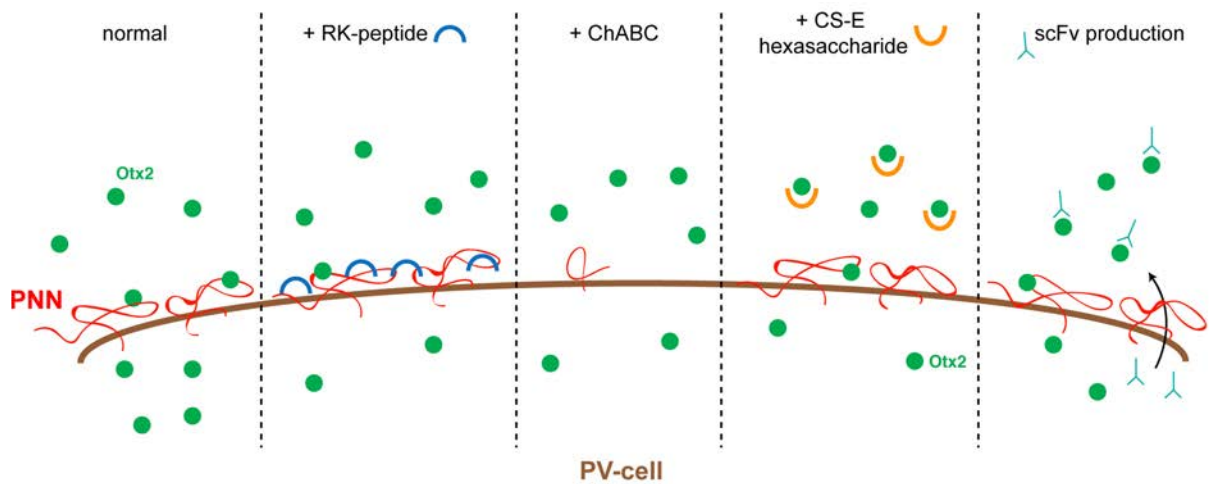


### Figure 50. Tools and techniques to block Otx2 transfer

Constant arrival of Otx2 in the adult cortex is required to maintain a mature, consolidated, non-plastic state of the cortex. Blocking Otx2 cortical transfer can reactivate plasticity in the adult.

(A) Otx2 transfer can be blocked at one of its sources. This can be achieved in the choroid plexus 1) by knocking-down Otx2 genetically by injecting Cre-TAT in *Otx2<sup>flox/flox</sup>* mice; 2) by transiently knocking-down Otx2 by using morpholinos or siRNAs against *Otx2*; or 3) by inducing the production of anti-Otx2 single chain antibodies (scFv) in the choroid plexus (by injecting Cre-TAT in *scFvOtx2* mice).

(B) Otx2 transfer can be blocked at its arrival at the target (PV) cells. Under normal conditions, Otx2 binds to the PNNs before being internalized by PV-cells. Infusing the RK-peptide in the adult cortex competes with Otx2 for the binding to PNNs. Injecting the chondroitinase ABC (ChABC) in the adult cortex digests the glycan chains in the PNNs. Infusing the synthetic CS-E hexasaccharide analogue competes with the PNNs for the binding to Otx2. The anti-Otx2 single chain antibody (scFv) expressed and secreted by PV-cells in *PVCrexscFvOtx2* mice traps Otx2 in the extracellular milieu. All of these tools reduce the amount of Otx2 in PV-cells and therefore alter the maturational state of these cells.

lentiviruses expressing the secreted single chain antibodies. This approach will permit the expression and secretion of the antibodies in all structures of interest and in any animal model. This scFv strategy will thus be helpful to identify the sources and target regions of Otx2 transfer in the hypo-anxious phenotype.

### **Otx2 non-cell autonomous targets in the cortex**

The deep sequencing data on the layer IV of the visual cortex suggest that the cortical state of the *Otx2* mutants is quite different from that of the wild-type mice at P30 and P100. Beyond the list of putative targets, direct Otx2 target genes or gene pathways modified by Otx2 transfer in PV-cells must now be identified. If Otx2 is a more general regulator of critical period plasticity across the cerebral cortex (as discussed above), these genes/pathways may also be modified at other time points in other cortices (for instance, between P12-15 in the auditory cortex). Blocking Otx2 transfer in the adult (Figure 50) can reopen a window of plasticity in the cortex: examining changes in gene expression in reactivated adult plasticity might provide new strategies to reopen plasticity in the adult cortex.

PV-cells are fast-spiking GABAergic interneurons that are highly sensitive to oxidative stress (Do et al., 2009) and may be protected by PNNs (Cabungcal et al., 2013; Suttikus et al., 2014). We intend to explore if, in addition to promoting PNN assembly, Otx2 could protect against oxidative stress by decreasing the formation of superoxide-inducible double strand breaks (DSBs). This hypothesis is based on the role of Otx2 and Engrailed homeoproteins in midbrain dopaminergic neurons survival (Alvarez-Fischer et al., 2011; Di Salvio et al., 2010; Sonnier et al., 2007). It was recently established that Engrailed protects midbrain dopaminergic neurons from the substantia nigra pars compacta against DSB formation (H. Rekaik, FX de Thé and colleagues in preparation). In the course of these studies, it was shown that *Engrailed1* heterozygous mice are very sensitive to oxidative stress and that one mode of action of Engrailed could be to maintain the perinucleolar and perinuclear heterochromatin. As a result, in the *Engrailed1* heterozygote, relaxation of the heterochromatin leads to illegitimate transcription, with the activation of transposable elements, in particular from the Long Intersped Nuclear Elements (LINE) family. The ability of Engrailed to down-regulate LINE transcription seems to involve both heterochromatin maintenance and a direct repression of LINE transcription. This activity, although highly hypothetical, is reinforced by preliminary experiments showing that Engrailed from midbrain is co-immunoprecipitated with piRNAs, a class of small non-coding RNAs implicated in LINE silencing (Huang et al.,

2013; Tushir et al., 2009), thus protecting against transposon-induced DNA damage (Reilly et al., 2013; Siomi et al., 2011). Given the similarities between Otx2 and Engrailed in their ability to protect midbrain dopaminergic neurons, it would be interesting to verify if Otx2 also regulates chromatin structure and the expression of transposable elements, not only in a cell autonomous way (as shown for Engrailed), but also in a non-cell autonomous one. Experiments are in progress to identify small non-coding RNAs associated with Otx2 in and outside the choroid plexus. This novel aspect of homeoprotein physiology may open a new angle to better understand the link between epigenetic regulation and cortical plasticity (Fagiolini et al., 2009).

## **II. Otx2-GAG interaction, from the source to the cortex?**

### **Otx2 binds to glycans at the surface of target cells**

The PNN-associated glycans assemble and mature in the binocular zone of the visual cortex during the critical period for ocular dominance plasticity (Köppe et al., 1997a). They have been mainly involved in synaptic stabilization and limitation of plasticity: digestion of the PNNs reactivates ocular dominance plasticity in the adult (Pizzorusso et al., 2002). In layer IV of the adult visual cortex, there is a strong colocalization between Otx2 and PNNs and digestion of the PNNs in the adult cortex decreases the number of Otx2-positive cells (Beurdeley et al., 2012), suggesting that binding of Otx2 to surface GAGs is necessary for Otx2 accumulation inside PV-cells. Accordingly, our results with the Otx2-AA mice, in which the GAG recognition motif is impaired, show a reduced accumulation of Otx2 in the PNN-enwrapped PV-cells. This reduced accumulation is accompanied by a delay in PNN assembly maturation, supporting the hypothesis of a positive feedback loop between Otx2 and PNNs (Figure 49). We also establish by biochemical experiments that Otx2 binds to purified cortical GAGs and has the highest affinity for PNN-associated chondroitin sulfate GAGs. Previous experiments have shown that a peptide mimicking Otx2 GAG-binding domain (RK-peptide) presents high affinity for disulfated chondroitin sulfates CS-D and CS-E (Beurdeley et al., 2012). We show, using several techniques (pull-down, dot-blot, gel shift assay and glycan arrays), that Otx2 protein binds with high affinity to commercial chondroitin sulfate CS-E. We therefore hypothesize that the GAG sequence binding to Otx2 in the PNNs contains CS-E disaccharides.

In the adult visual cortex, blocking Otx2 transfer can be achieved by interfering with its interaction with surface GAGs. Infusing the GAG-binding RK-peptide in the adult visual cortex competes with Otx2 for the binding to PNNs and thus decreases the number of Otx2-positive cells (Beurdeley et al., 2012) (Figure 50B). We show that a synthetic CS-E hexasaccharide analogue binds to Otx2 and interferes with its transfer when infused in the adult visual cortex (Figure 50B). Infusing an anti-CS-E antibody should hopefully corroborate our hypothesis of Otx2 binding to CS-E chains at the surface of the PV-cells.

Otx2 protein is present in PV-cells of other cerebral cortex regions (Spatazza et al., 2013b), where colocalization between Otx2 and PNNs has to be confirmed. It has been reported that modification of the sulfation pattern of PNNs (using transgenic mice with a low 4S/6S ratio) reduces Otx2 accumulation in the PNNs of the visual cortex (Miyata et al., 2012). Examining Otx2 localization in other cortices of these transgenic mice should indicate whether the concept of Otx2-PNN interaction could be generalized to other cerebral cortices. Whether Otx2 regulates PNN assembly in other brain regions should also be investigated. As PNNs have been involved in several neuronal functions (Cabungcal et al., 2013; Härtig et al., 1999; Pizzorusso et al., 2002), Otx2, *via* its regulation of PNN assembly and maintenance, could maintain some PNN functions such as protection against oxidative stress (already discussed) and water and cation homeostasis.

### **Otx2 could travel attached to glycans**

The choroid plexus is one of the main sources of cortical Otx2 in the adult: it expresses Otx2 and secretes the homeoprotein in the cerebrospinal fluid (Spatazza et al., 2013b). Otx2 can thus be seen as a growth factor or a morphogen and, as such, is unlikely to travel on its own in the cerebrospinal fluid. Infusion of homeoproteins in the brain parenchyma requires a co-infusion of polysialic acid to allow their diffusion (Beurdeley et al., 2012; Sonnier et al., 2007; Sugiyama et al., 2008). Endogenous Otx2 could therefore also be bound to glycans chains during its transfer until it meets the high-affinity GAGs of the PNNs (Figure 49A). The choroid plexus expresses many types of proteoglycans, mainly heparan sulfate proteoglycans (unpublished results); glycans and glycoproteins have also been reported in the cerebrospinal fluid (Halim et al., 2013; Perosa et al., 2002; Zhang et al., 2011). We shall investigate whether Otx2 interacts with GAG chains present in these proteoglycans at the surface of the choroid plexus before being released in the cerebrospinal fluid. This will be done through co-

immunoprecipitation experiments and by experiments aiming at releasing Otx2 from the surface of the plexus with GAG-digesting enzymes.

In keeping with these ideas, Otx2 could also travel from the plexus to the cortex within complexes encompassing not only sugars and lipids but also other proteins. Immunoprecipitations from choroid plexus samples show that Otx2 binds to bone morphogenic proteins (BMP4 and BMP6, N. Kim and colleagues, unpublished results). This opens discussion to a possible cooperation between homeoprotein transduction and classical signaling pathways. For example, Engrailed, EphrinA5 and Adenosine pathways act in synergy for axon guidance (Stettler et al., 2012; Wizenmann et al., 2009). Similarly, Pax6 homeoprotein interacts with Netrin signaling pathway to regulate oligodendrocyte precursor migration (Di Lullo et al., 2011). Another example is Engrailed association with Decapentaplegic signaling (DPP, the drosophila homolog of vertebrate BMPs), for the formation of the anterior cross vein in the *Drosophila* wing disk (Layalle et al., 2011). BMPs are part of the transforming growth factor beta (TGF $\beta$ ) family. TGF $\beta$ /BMP signaling has been implicated in cortical plasticity through regulation of innate immunity (Berke et al., 2013; Bialas and Stevens, 2013; Datwani et al., 2009; Takao et al., 2013) and BMP signaling has been shown to act on PV-cell differentiation (Mukhopadhyay et al., 2009). TGF $\beta$ /BMP pathway is known to cross-talk with other signaling pathways (Guo and Wang, 2009) and a functional interaction between BMP4 and Otx2 has been proposed in two different models (Acampora et al., 2013; Gammill and Sive, 2000). Otx2 signaling could therefore cooperate with BMP signaling to regulate PV-cell maturation during postnatal development and in the adult. Examining the phosphorylation of downstream effectors of BMP in PV-cells in the absence or presence of Otx2 will assess the possible synergy between these two pathways. This interaction includes the possibility that BMPs, Otx2 and GAGs (not excluding other partners) travel together from the choroid plexus to PV-cells. Indeed, BMP proteins also bind to GAGs, mainly heparan sulfates (Dani et al., 2012; Gandhi and Mancera, 2012; Yan and Lin, 2009).

The choroid plexus is one of the sources of Otx2 in the adult visual cortex, but other sources of Otx2 might exist in the brain and at its “periphery”. The retina is possibly one of them since it was shown that biotinylated Otx2 injected in the eye is transported to PV-cells through the passage of several synapses (Sugiyama et al., 2008). The pineal gland, a small endocrine gland, is another established site of Otx2 expression (Nishida et al., 2003; Rath et

al., 2006) and could be a source of Otx2. The deep pineal gland is attached to the third ventricle: it is therefore in direct contact with the cerebrospinal fluid (Welsh et al., 1989), into which it may secrete hormones (Reiter et al., 2014; Tricoire et al., 2003). Incidentally, heparan sulfate proteoglycans have been described in the pineal gland (Kuberan et al., 2004). An adeno-associated virus expressing a tagged Otx2 (AAV-Otx2-HA) will confirm the identification of sources and target structures. Injecting the AAV-Otx2-HA in the choroid plexus will allow us to trace the Otx2-HA protein to its target brain structures. This could also establish the choroid plexus as a general source of cortical Otx2 (not only in the visual cortex). In the pineal gland, injecting the AAV-Otx2-HA or inducing the expression of the anti-Otx2 scFv could assess the role of this structure in the secretion of Otx2. The use of AAV-Otx2-HA could also shed light on Otx2 interactors during its transport. For example, the immunoprecipitation of Otx2-HA could be used to verify the interaction between Otx2 and BMP proteins and identify other transport partners, including proteoglycans.

The results reported in this thesis confirm an *in vivo* role for Otx2-GAG interaction, both in the timing of critical periods during postnatal development and in the maintenance of the non-plastic state of the cortex in the adult. They open perspectives on strategies to interfere with Otx2 transfer, by disrupting PNNs or by trapping extracellular Otx2. This work can also be extended to homeoprotein transduction in general. Otx2-GAG interaction study provides insight on the possibility of a sugar code for homeoprotein recognition. More generally, scFv mouse lines characterized in this thesis will be of help to assess the *in vivo* roles of homeoprotein transfer during development through to the adult.



## **REFERENCES**





- Abdeljalil, J., Hamid, M., Abdel-mouttalib, O., Stéphane, R., Raymond, R., Johan, A., José, S., Pierre, C., and Serge, P. (2005). The optomotor response: a robust first-line visual screening method for mice. *Vision Res* 45, 1439–1446.
- Acampora, D., Gulisano, M., Broccoli, V., and Simeone, A. (2001). Otx genes in brain morphogenesis. *Prog. Neurobiol.* 64, 69–95.
- Acampora, D., Mazan, S., Lallemand, Y., Avantaggiato, V., Maury, M., Simeone, A., and Brûlet, P. (1995). Forebrain and midbrain regions are deleted in Otx2<sup>-/-</sup> mutants due to a defective anterior neuroectoderm specification during gastrulation. *Development* 121, 3279–3290.
- Acampora, D., Di Giovannantonio, L.G., and Simeone, A. (2013). Otx2 is an intrinsic determinant of the embryonic stem cell state and is required for transition to a stable epiblast stem cell condition. *Development* 140, 43–55.
- Acampora, D., Di Giovannantonio, L.G., Di Salvio, M., Mancuso, P., and Simeone, A. (2009). Selective inactivation of Otx2 mRNA isoforms reveals isoform-specific requirement for visceral endoderm anteriorization and head morphogenesis and highlights cell diversity in the visceral endoderm. *Mech Dev* 126, 882–897.
- Ahmad, Z.A., Yeap, S.K., Ali, A.M., Ho, W.Y., Alitheen, N.B.M., and Hamid, M. (2012). scFv antibody: principles and clinical application. *Clin. Dev. Immunol.* 2012, 980250.
- Akbadian, S., Kim, J.J., Potkin, S.G., Hagman, J.O., Tafazzoli, A., Bunney, W.E., and Jones, E.G. (1995). Gene expression for glutamic acid decarboxylase is reduced without loss of neurons in prefrontal cortex of schizophrenics. *Arch. Gen. Psychiatry* 52, 258–266.
- Ali, A.B., and Thomson, A.M. (2008). Synaptic alpha 5 subunit-containing GABAA receptors mediate IPSPs elicited by dendrite-preferring cells in rat neocortex. *Cerebral Cortex* 18, 1260–1271.
- Alvarez-Fischer, D., Fuchs, J., Castagner, F., Stettler, O., Massiani-Beaudoin, O., Moya, K.L., Bouillot, C., Oertel, W.H., Lombès, A., Faigle, W., et al. (2011). Engrailed protects mouse midbrain dopaminergic neurons against mitochondrial complex I insults. *Nature Publishing Group* 14, 1260–1266.
- Alves, I.D., Bechara, C., Walrant, A., Zaltsman, Y., Jiao, C.-Y., and Sagan, S. (2011). Relationships between membrane binding, affinity and cell internalization efficacy of a cell-penetrating peptide: penetratin as a case study. *PLoS ONE* 6, e24096.
- Andreasson, K.I., and Kaufmann, W.E. (2002). Role of immediate early gene expression in cortical morphogenesis and plasticity. *Results Probl Cell Differ* 39, 113–137.
- Ang, S.L., Conlon, R.A., Jin, O., and Rossant, J. (1994). Positive and negative signals from mesoderm regulate the expression of mouse Otx2 in ectoderm explants. *Development* 120, 2979–2989.
- Ang, S.L., Jin, O., Rhinn, M., Daigle, N., Stevenson, L., and Rossant, J. (1996). A targeted mouse Otx2 mutation leads to severe defects in gastrulation and formation of axial mesoderm and to deletion of rostral brain. *Development* 122, 243–252.

- Antonini, A., Fagiolini, M., and Stryker, M.P. (1999). Anatomical correlates of functional plasticity in mouse visual cortex. *J. Neurosci.* *19*, 4388–4406.
- Ashkenazi-Hoffnung, L., Lebenthal, Y., Wyatt, A.W., Ragge, N.K., Dateki, S., Fukami, M., Ogata, T., Phillip, M., and Gat-Yablonski, G. (2010). A novel loss-of-function mutation in OTX2 in a patient with anophthalmia and isolated growth hormone deficiency. *Hum. Genet.* *127*, 721–729.
- Atwal, J.K., Pinkston-Gosse, J., Syken, J., Stawicki, S., Wu, Y., Shatz, C., and Tessier-Lavigne, M. (2008). PirB is a functional receptor for myelin inhibitors of axonal regeneration. *Science* *322*, 967–970.
- Balmer, T.S., Carels, V.M., Frisch, J.L., and Nick, T.A. (2009). Modulation of perineuronal nets and parvalbumin with developmental song learning. *J. Neurosci.* *29*, 12878–12885.
- Barbas, C.F. (2001). Phage display (Cold Spring Harbor Laboratory Pr).
- Barkat, T.R., Polley, D.B., and Hensch, T.K. (2011). A critical period for auditory thalamocortical connectivity. *Nature Publishing Group* *14*, 1189–1194.
- Bassett, E.A., and Wallace, V.A. (2012). Cell fate determination in the vertebrate retina. *Trends Neurosci* *35*, 565–573.
- Bastide, L., Priem, B., and Fort, S. (2011). Chemo-bacterial synthesis and immunoreactivity of a brain HNK-1 analogue. *Carbohydr Res* *346*, 348–351.
- Bavelier, D., Levi, D.M., Li, R.W., Dan, Y., and Hensch, T.K. (2010). Removing brakes on adult brain plasticity: from molecular to behavioral interventions. *J. Neurosci.* *30*, 14964–14971.
- Bechara, C., Pallerla, M., Zaltsman, Y., Burlina, F., Alves, I.D., Lequin, O., and Sagan, S. (2013). Tryptophan within basic peptide sequences triggers glycosaminoglycan-dependent endocytosis. *Faseb J* *27*, 738–749.
- Bekku, Y., Saito, M., Moser, M., Fuchigami, M., Maehara, A., Nakayama, M., Kusachi, S., Ninomiya, Y., and Oohashi, T. (2012). Bral2 is indispensable for the proper localization of brevican and the structural integrity of the perineuronal net in the brainstem and cerebellum. *J Comp Neurol* *520*, 1721–1736.
- Bekku, Y., Su, W.-D., Hirakawa, S., Fässler, R., Ohtsuka, A., Kang, J.S., Sanders, J., Murakami, T., Ninomiya, Y., and Oohashi, T. (2003). Molecular cloning of Bral2, a novel brain-specific link protein, and immunohistochemical colocalization with brevican in perineuronal nets. *Mol Cell Neurosci* *24*, 148–159.
- Belforte, J.E., Zsiros, V., Sklar, E.R., Jiang, Z., Yu, G., Li, Y., Quinlan, E.M., and Nakazawa, K. (2010). Postnatal NMDA receptor ablation in corticolimbic interneurons confers schizophrenia-like phenotypes. *Nature Publishing Group* *13*, 76–83.
- Berardi, N., Pizzorusso, T., and Maffei, L. (2000). Critical periods during sensory development. *Curr Opin Neurobiol* *10*, 138–145.
- Berardi, N., Pizzorusso, T., Ratto, G.M., and Maffei, L. (2003). Molecular basis of plasticity

in the visual cortex. *Trends Neurosci* 26, 369–378.

Berke, B., Wittnam, J., McNeill, E., Van Vactor, D.L., and Keshishian, H. (2013). Retrograde BMP signaling at the synapse: a permissive signal for synapse maturation and activity-dependent plasticity. *J. Neurosci.* 33, 17937–17950.

Berlose, J.P., Convert, O., Derossi, D., Brunissen, A., and Chassaing, G. (1996). Conformational and associative behaviours of the third helix of antennapedia homeodomain in membrane-mimetic environments. *Eur J Biochem* 242, 372–386.

Beurdeley, M., Spatazza, J., Lee, H.H.C., Sugiyama, S., Bernard, C., Di Nardo, A.A., Hensch, T.K., and Prochiantz, A. (2012). Otx2 binding to perineuronal nets persistently regulates plasticity in the mature visual cortex. *J. Neurosci.* 32, 9429–9437.

Bialas, A.R., and Stevens, B. (2013). TGF- $\beta$  signaling regulates neuronal C1q expression and developmental synaptic refinement. *Nature Publishing Group* 16, 1773–1782.

Billeter, M., Qian, Y.Q., Otting, G., Müller, M., Gehring, W., and Wüthrich, K. (1993). Determination of the nuclear magnetic resonance solution structure of an Antennapedia homeodomain-DNA complex. *Journal of Molecular Biology* 234, 1084–1093.

Billeter, M., Qian, Y., Otting, G., Müller, M., Gehring, W.J., and Wüthrich, K. (1990). Determination of the three-dimensional structure of the Antennapedia homeodomain from *Drosophila* in solution by  $^1\text{H}$  nuclear magnetic resonance spectroscopy. *Journal of Molecular Biology* 214, 183–197.

Binette, F., Cravens, J., Kahoussi, B., Haudenschild, D.R., and Goetinck, P.F. (1994). Link protein is ubiquitously expressed in non-cartilaginous tissues where it enhances and stabilizes the interaction of proteoglycans with hyaluronic acid. *J Biol Chem* 269, 19116–19122.

Bitanhirwe, B.K.Y., and Woo, T.-U.W. (2014). Perineuronal nets and schizophrenia: The importance of neuronal coatings. *Neuroscience and Biobehavioral Reviews* 45C, 85–99.

Bradbury, E.J., Moon, L.D.F., Popat, R.J., King, V.R., Bennett, G.S., Patel, P.N., Fawcett, J.W., and McMahon, S.B. (2002). Chondroitinase ABC promotes functional recovery after spinal cord injury. *Nature* 416, 636–640.

Brown, J.M., Xia, J., Zhuang, B., Cho, K.-S., Rogers, C.J., Gama, C.I., Rawat, M., Tully, S.E., Uetani, N., Mason, D.E., et al. (2012). A sulfated carbohydrate epitope inhibits axon regeneration after injury. *Proceedings of the National Academy of Sciences* 109, 4768–4773.

Brunet, I., Weinl, C., Piper, M., Trembleau, A., Volovitch, M., Harris, W., Prochiantz, A., and Holt, C. (2005). The transcription factor Engrailed-2 guides retinal axons. *Nature* 438, 94–98.

Brunet, I., Di Nardo, A.A., Sonnier, L., Beurdeley, M., and Prochiantz, A. (2007). The topological role of homeoproteins in the developing central nervous system. *Trends Neurosci* 30, 260–267.s

Brückner, G., Morawski, M., and Arendt, T. (2008). Aggrecan-based extracellular matrix is an integral part of the human basal ganglia circuit. *Neuroscience* 151, 489–504.

Burnside, E.R., and Bradbury, E.J. (2014). Manipulating the extracellular matrix and its role

in brain and spinal cord plasticity and repair. *Neuropathol. Appl. Neurobiol.* *40*, 26–59.

Bülow, H.E., and Hobert, O. (2004). Differential sulfations and epimerization define heparan sulfate specificity in nervous system development. *Neuron* *41*, 723–736.

Bülow, H.E., and Hobert, O. (2006). The molecular diversity of glycosaminoglycans shapes animal development. *Annu. Rev. Cell Dev. Biol.* *22*, 375–407.

Caballero, A., Flores-Barrera, E., Cass, D.K., and Tseng, K.Y. (2014). Differential regulation of parvalbumin and calretinin interneurons in the prefrontal cortex during adolescence. *Brain Struct Funct* *219*, 395–406.

Cabelli, R.J., Shelton, D.L., Segal, R.A., and Shatz, C.J. (1997). Blockade of endogenous ligands of trkB inhibits formation of ocular dominance columns. *Neuron* *19*, 63–76.

Cabungcal, J.-H., Steullet, P., Morishita, H., Kraftsik, R., Cuenod, M., Hensch, T.K., and Do, K.Q. (2013). Perineuronal nets protect fast-spiking interneurons against oxidative stress. *Proceedings of the National Academy of Sciences* *110*, 9130–9135.

Capila, I., and Linhardt, R.J. (2002). Heparin-protein interactions. *Angew. Chem. Int. Ed. Engl.* *41*, 391–412.

Cardin, A.D., and Weintraub, H.J. (1989). Molecular modeling of protein-glycosaminoglycan interactions. *Arteriosclerosis* *9*, 21–32.

Carrasco, A.E., McGinnis, W., Gehring, W.J., and De Robertis, E.M. (1984). Cloning of an *X. laevis* gene expressed during early embryogenesis coding for a peptide region homologous to *Drosophila* homeotic genes. *Cell* *37*, 409–414.

Carulli, D., Pizzorusso, T., Kwok, J.C.F., Putignano, E., Poli, A., Forostyak, S., Andrews, M.R., Deepa, S.S., Glant, T.T., and Fawcett, J.W. (2010). Animals lacking link protein have attenuated perineuronal nets and persistent plasticity. *Brain* *133*, 2331–2347.

Carulli, D., Rhodes, K.E., and Fawcett, J.W. (2007). Upregulation of aggrecan, link protein 1, and hyaluronan synthases during formation of perineuronal nets in the rat cerebellum. *J Comp Neurol* *501*, 83–94.

Carulli, D., Rhodes, K.E., Brown, D.J., Bonnert, T.P., Pollack, S.J., Oliver, K., Strata, P., and Fawcett, J.W. (2006). Composition of perineuronal nets in the adult rat cerebellum and the cellular origin of their components. *J Comp Neurol* *494*, 559–577.

Castren, E., Zafra, F., Thoenen, H., and Lindholm, D. (1992). Light regulates expression of brain-derived neurotrophic factor mRNA in rat visual cortex. *Proc Natl Acad Sci USA* *89*, 9444–9448.

Celio, M.R., and Blümcke, I. (1994). Perineuronal nets--a specialized form of extracellular matrix in the adult nervous system. *Brain Res. Brain Res. Rev.* *19*, 128–145.

Chang, M.C., Park, J.M., Pelkey, K.A., Grabenstatter, H.L., Xu, D., Linden, D.J., Sutula, T.P., Mcbain, C.J., and Worley, P.F. (2010). Narp regulates homeostatic scaling of excitatory synapses on parvalbumin-expressing interneurons. *Nature Publishing Group* *13*, 1090–1097.

- Chatelain, G., Fossat, N., Brun, G., and Lamonerie, T. (2006). Molecular dissection reveals decreased activity and not dominant negative effect in human OTX2 mutants. *J. Mol. Med.* 84, 604–615.
- Chatelin, L., Volovitch, M., Joliot, A.H., Perez, F., and Prochiantz, A. (1996). Transcription factor *hoxa-5* is taken up by cells in culture and conveyed to their nuclei. *Mech Dev* 55, 111–117.
- Christiaens, B., Symoens, S., Verheyden, S., Engelborghs, Y., Joliot, A., Prochiantz, A., Vandekerckhove, J., Rosseneu, M., Vanloo, B., and Vanderheyden, S. (2002). Tryptophan fluorescence study of the interaction of penetratin peptides with model membranes. *Eur J Biochem* 269, 2918–2926.
- Cohen, S., and Jürgens, G. (1991). *Drosophila* headlines. *Trends Genet* 7, 267–272.
- Costa, C., Tortosa, R., Domènech, A., Vidal, E., Pumarola, M., and Bassols, A. (2007). Mapping of aggrecan, hyaluronic acid, heparan sulphate proteoglycans and aquaporin 4 in the central nervous system of the mouse. *Journal of Chemical Neuroanatomy* 33, 111–123.
- Dani, N., Nahm, M., Lee, S., and Broadie, K. (2012). A Targeted Glycan-Related Gene Screen Reveals Heparan Sulfate Proteoglycan Sulfation Regulates WNT and BMP Trans-Synaptic Signaling. *PLoS Genet* 8, e1003031.
- Datwani, A., McConnell, M.J., Kanold, P.O., Micheva, K.D., Busse, B., Shamloo, M., Smith, S.J., and Shatz, C.J. (2009). Classical MHCI molecules regulate retinogeniculate refinement and limit ocular dominance plasticity. *Neuron* 64, 463–470.
- de Felipe, P. (2004). Skipping the co-expression problem: the new 2A “CHYSEL” technology. *Genet Vaccines Ther* 2, 13.
- Deepa, S.S., Carulli, D., Galtrey, C., Rhodes, K., Fukuda, J., Mikami, T., Sugahara, K., and Fawcett, J.W. (2006). Composition of perineuronal net extracellular matrix in rat brain: a different disaccharide composition for the net-associated proteoglycans. *J Biol Chem* 281, 17789–17800.
- del Río, J.A., de Lecea, L., Ferrer, I., and Soriano, E. (1994). The development of parvalbumin-immunoreactivity in the neocortex of the mouse. *Brain Res. Dev. Brain Res.* 81, 247–259.
- Demircan, K., Yonezawa, T., Takigawa, T., Topcu, V., Erdogan, S., Ucar, F., Armutcu, F., Yigitoglu, M.R., Ninomiya, Y., and Hirohata, S. (2013). ADAMTS1, ADAMTS5, ADAMTS9 and aggrecanase-generated proteoglycan fragments are induced following spinal cord injury in mouse. *Neurosci Lett* 544, 25–30.
- Derossi, D., Calvet, S., Trembleau, A., Brunissen, A., Chassaing, G., and Prochiantz, A. (1996). Cell internalization of the third helix of the Antennapedia homeodomain is receptor-independent. *J Biol Chem* 271, 18188–18193.
- Derossi, D., Joliot, A.H., Chassaing, G., and Prochiantz, A. (1994). The third helix of the Antennapedia homeodomain translocates through biological membranes. *J Biol Chem* 269, 10444–10450.

- Despras, G., Bernard, C., Perrot, A., Cattiaux, L., Prochiantz, A., Lortat-Jacob, H., and Mallet, J.-M. (2013). Toward Libraries of Biotinylated Chondroitin Sulfate Analogues: From Synthesis to In Vivo Studies. *Chemistry* *19*, 531–540.
- Di Cristo, G., Berardi, N., Cancedda, L., Pizzorusso, T., Putignano, E., Ratto, G.M., and Maffei, L. (2001). Requirement of ERK activation for visual cortical plasticity. *Science* *292*, 2337–2340.
- Di Cristo, G., Chattopadhyaya, B., Kuhlman, S.J., Fu, Y., Bélanger, M.-C., Wu, C.Z., Rutishauser, U., Maffei, L., and Huang, Z.J. (2007). Activity-dependent PSA expression regulates inhibitory maturation and onset of critical period plasticity. *Nat Neurosci* *10*, 1569–1577.
- Di Lullo, E., Haton, C., Le Poupon, C., Volovitch, M., Joliot, A., Thomas, J.-L., and Prochiantz, A. (2011). Paracrine Pax6 activity regulates oligodendrocyte precursor cell migration in the chick embryonic neural tube. *Development* *138*, 4991–5001.
- Di Salvio, M., Di Giovannantonio, L.G., Acampora, D., Prosperi, R., Omodei, D., Prakash, N., Wurst, W., and Simeone, A. (2010). Otx2 controls neuron subtype identity in ventral tegmental area and antagonizes vulnerability to MPTP. *Nature Publishing Group* *13*, 1481–1488.
- Dick, G., Tan, C.L., Alves, J.N., Ehlert, E.M.E., Miller, G.M., Hsieh-Wilson, L.C., Sugahara, K., Oosterhof, A., van Kuppevelt, T.H., Verhaagen, J., et al. (2013). Semaphorin 3A binds to the perineuronal nets via chondroitin sulfate type E motifs in rodent brains. *Journal of Biological Chemistry* *288*, 27384–27395.
- Do, K.Q., Cabungcal, J.H., Frank, A., Steullet, P., and Cuenod, M. (2009). Redox dysregulation, neurodevelopment, and schizophrenia. *Curr Opin Neurobiol* *19*, 220–230.
- Dobbs, D. (2010). Schizophrenia: The making of a troubled mind. *Nature* *468*, 154–156.
- Dupont, E., Prochiantz, A., and Joliot, A. (2007). Identification of a signal peptide for unconventional secretion. *J Biol Chem* *282*, 8994–9000.
- Endo, T., Kobayashi, S., and Onaya, T. (1985). Parvalbumin in rat cerebrum, cerebellum and retina during postnatal development. *Neurosci Lett* *60*, 279–282.
- Esko, J.D., and Lindahl, U. (2001). Molecular diversity of heparan sulfate. *J. Clin. Invest.* *108*, 169–173.
- Fagiolini, M., and Hensch, T.K. (2000). Inhibitory threshold for critical-period activation in primary visual cortex. *Nature* *404*, 183–186.
- Fagiolini, M., Pizzorusso, T., Berardi, N., Domenici, L., and Maffei, L. (1994). Functional postnatal development of the rat primary visual cortex and the role of visual experience: dark rearing and monocular deprivation. *Vision Res* *34*, 709–720.
- Fagiolini, M., Fritschy, J.-M., Löw, K., Möhler, H., Rudolph, U., and Hensch, T.K. (2004). Specific GABAA circuits for visual cortical plasticity. *Science* *303*, 1681–1683.
- Fagiolini, M., Jensen, C.L., and Champagne, F.A. (2009). Epigenetic influences on brain

development and plasticity. *Curr Opin Neurobiol* 19, 207–212.

Fine, R., Zhang, J., and Stevens, H.E. (2014). Prenatal stress and inhibitory neuron systems: implications for neuropsychiatric disorders. *Mol Psychiatry* 19, 641–651.

Finkelstein, R., and Perrimon, N. (1990). The orthodenticle gene is regulated by bicoid and torso and specifies *Drosophila* head development. *Nature* 346, 485–488.

Flaumenhaft, R., and Rifkin, D.B. (1991). Extracellular matrix regulation of growth factor and protease activity. *Curr. Opin. Cell Biol.* 3, 817–823.

Forsberg, E., and Kjellen, L. (2001). Heparan sulfate: lessons from knockout mice. *J. Clin. Invest.* 108, 175–180.

Fossat, N., Le Greneur, C., Beby, F., Vincent, S., Godement, P., Chatelain, G., and Lamonerie, T. (2007). A new GFP-tagged line reveals unexpected Otx2 protein localization in retinal photoreceptors. *BMC Dev Biol* 7, 122.

Frantz, G.D., Weimann, J.M., Levin, M.E., and McConnell, S.K. (1994). Otx1 and Otx2 define layers and regions in developing cerebral cortex and cerebellum. *J. Neurosci.* 14, 5725–5740.

Galeotti, F., and Volpi, N. (2011). Online reverse phase-high-performance liquid chromatography-fluorescence detection-electrospray ionization-mass spectrometry separation and characterization of heparan sulfate, heparin, and low-molecular weight-heparin disaccharides derivatized with 2-aminoacridone. *Anal Chem* 83, 6770–6777.

Galtrey, C.M., and Fawcett, J.W. (2007). The role of chondroitin sulfate proteoglycans in regeneration and plasticity in the central nervous system. *Brain Res Rev* 54, 1–18.

Galtrey, C.M., Kwok, J.C.F., Carulli, D., Rhodes, K.E., and Fawcett, J.W. (2008). Distribution and synthesis of extracellular matrix proteoglycans, hyaluronan, link proteins and tenascin-R in the rat spinal cord. *Eur J Neurosci* 27, 1373–1390.

Gammill, L.S., and Sive, H. (2000). Coincidence of otx2 and BMP4 signaling correlates with *Xenopus* cement gland formation. *Mech Dev* 92, 217–226.

Gandal, M.J., Nesbitt, A.M., McCurdy, R.M., and Alter, M.D. (2012). Measuring the maturity of the fast-spiking interneuron transcriptional program in autism, schizophrenia, and bipolar disorder. *PLoS ONE* 7, e41215.

Gandhi, N.S., and Mancera, R.L. (2008). The structure of glycosaminoglycans and their interactions with proteins. *Chem Biol Drug Des* 72, 455–482.

Gandhi, N.S., and Mancera, R.L. (2012). Prediction of heparin binding sites in bone morphogenetic proteins (BMPs). *Biochim Biophys Acta* 1824, 1374–1381.

Gehring, W. (1967). Clonal analysis of determination dynamics in cultures of imaginal disks in *Drosophila melanogaster*. *Dev Biol* 16, 438–456.

Gehring, W.J., Qian, Y.Q., Billeter, M., Furukubo-Tokunaga, K., Schier, A.F., Resendez-Perez, D., Affolter, M., Otting, G., and Wüthrich, K. (1994). Homeodomain-DNA



recognition. *Cell* 78, 211–223.

Gerstein, H., O'Riordan, K., Osting, S., Schwarz, M., and Burger, C. (2012). Rescue of synaptic plasticity and spatial learning deficits in the hippocampus of Homer1 knockout mice by recombinant Adeno-associated viral gene delivery of Homer1c. *Neurobiol Learn Mem* 97, 17–29.

Giamanco, K.A., and Matthews, R.T. (2012). Deconstructing the perineuronal net: cellular contributions and molecular composition of the neuronal extracellular matrix. *Neuroscience* 218, 367–384.

Giamanco, K.A., Morawski, M., and Matthews, R.T. (2010). Perineuronal net formation and structure in aggrecan knockout mice. *Neuroscience* 170, 1314–1327.

Gogolla, N., Caroni, P., Luthi, A., and Herry, C. (2009). Perineuronal Nets Protect Fear Memories from Erasure. *Science* 325, 1258–1261.

Gordon, J.A., and Stryker, M.P. (1996). Experience-dependent plasticity of binocular responses in the primary visual cortex of the mouse. *J. Neurosci.* 16, 3274–3286.

Greenberg, A.S., Avila, D., Hughes, M., Hughes, A., McKinney, E.C., and Flajnik, M.F. (1995). A new antigen receptor gene family that undergoes rearrangement and extensive somatic diversification in sharks. *Nature* 374, 168–173.

Greenberg, M.E., Xu, B., Lu, B., and Hempstead, B.L. (2009). New insights in the biology of BDNF synthesis and release: implications in CNS function. *J. Neurosci.* 29, 12764–12767.

Grobe, K., Ledin, J., Ringvall, M., Holmborn, K., Forsberg, E., Esko, J.D., and Kjellén, L. (2002). Heparan sulfate and development: differential roles of the N-acetylglucosamine N-deacetylase/N-sulfotransferase isozymes. *Biochim Biophys Acta* 1573, 209–215.

Gu, Y., Huang, S., Chang, M.C., Worley, P., Kirkwood, A., and Quinlan, E.M. (2013). Obligatory role for the immediate early gene NARP in critical period plasticity. *Neuron* 79, 335–346.

Guerrini, M., Agulles, T., Bisio, A., Hricovini, M., Lay, L., Naggi, A., Poletti, L., Sturiale, L., Torri, G., and Casu, B. (2002). Minimal heparin/heparan sulfate sequences for binding to fibroblast growth factor-1. *Biochem Biophys Res Commun* 292, 222–230.

Guo, X., and Wang, X.-F. (2009). Signaling cross-talk between TGF-beta/BMP and other pathways. *Cell Res.* 19, 71–88.

Gushulak, L., Hemming, R., Martin, D., Seyrantepe, V., Pshezhetsky, A., and Triggs-Raine, B. (2012). Hyaluronidase 1 and  $\beta$ -hexosaminidase have redundant functions in hyaluronan and chondroitin sulfate degradation. *Journal of Biological Chemistry* 287, 16689–16697.

Hackett, T.A., Barkat, T.R., O'Brien, B.M.J., Hensch, T.K., and Polley, D.B. (2011). Linking topography to tonotopy in the mouse auditory thalamocortical circuit. *J. Neurosci.* 31, 2983–2995.

Halim, A., Rüetschi, U., Larson, G., and Nilsson, J. (2013). LC-MS/MS Characterization of O-Glycosylation Sites and Glycan Structures of Human Cerebrospinal Fluid Glycoproteins. *J.*

Proteome Res. 12, 573–584.

Hanover, J.L., Huang, Z.J., Tonegawa, S., and Stryker, M.P. (1999). Brain-derived neurotrophic factor overexpression induces precocious critical period in mouse visual cortex. *J. Neurosci.* 19, RC40.

Hashimoto, T., Volk, D.W., Eggan, S.M., Mirnics, K., Pierri, J.N., Sun, Z., Sampson, A.R., and Lewis, D.A. (2003). Gene expression deficits in a subclass of GABA neurons in the prefrontal cortex of subjects with schizophrenia. *J. Neurosci.* 23, 6315–6326.

Härtig, W., Brauer, K., and Brückner, G. (1992). Wisteria floribunda agglutinin-labelled nets surround parvalbumin-containing neurons. *NeuroReport* 3, 869–872.

Härtig, W., Derouiche, A., Welt, K., Brauer, K., Grosche, J., Mäder, M., Reichenbach, A., and Brückner, G. (1999). Cortical neurons immunoreactive for the potassium channel Kv3.1b subunit are predominantly surrounded by perineuronal nets presumed as a buffering system for cations. *Brain Res* 842, 15–29.

Härtig, W., Singer, A., Grosche, J., Brauer, K., Ottersen, O.P., and Brückner, G. (2001). Perineuronal nets in the rat medial nucleus of the trapezoid body surround neurons immunoreactive for various amino acids, calcium-binding proteins and the potassium channel subunit Kv3.1b. *Brain Res* 899, 123–133.

He, H.-Y., Ray, B., Dennis, K., and Quinlan, E.M. (2007). Experience-dependent recovery of vision following chronic deprivation amblyopia. *Nat Neurosci* 10, 1134–1136.

Hensch, T.K., Fagiolini, M., Mataga, N., Stryker, M.P., Baekkeskov, S., and Kash, S.F. (1998). Local GABA circuit control of experience-dependent plasticity in developing visual cortex. *Science* 282, 1504–1508.

Hensch, T.K. (2004). Critical period regulation. *Annu Rev Neurosci* 27, 549–579.

Hensch, T.K. (2005). Critical period plasticity in local cortical circuits. *Nat Rev Neurosci* 6, 877–888.

Hidalgo-Sánchez, M., Alvarado-Mallart, R., and Alvarez, I.S. (2000). Pax2, Otx2, Gbx2 and Fgf8 expression in early otic vesicle development. *Mech Dev* 95, 225–229.

Hide, T., Hatakeyama, J., Kimura-Yoshida, C., Tian, E., Takeda, N., Ushio, Y., Shiroishi, T., Aizawa, S., and Matsuo, I. (2002). Genetic modifiers of otocephalic phenotypes in Otx2 heterozygous mutant mice. *Development* 129, 4347–4357.

Hirth, F., Therianos, S., Loop, T., Gehring, W.J., Reichert, H., and Furukubo-Tokunaga, K. (1995). Developmental defects in brain segmentation caused by mutations of the homeobox genes orthodenticle and empty spiracles in *Drosophila*. *Neuron* 15, 769–778.

Holt, C.E., and Dickson, B.J. (2005). Sugar codes for axons? *Neuron* 46, 169–172.

Honda, T., Kaneiwa, T., Mizumoto, S., Sugahara, K., and Yamada, S. (2012). Hyaluronidases Have Strong Hydrolytic Activity toward Chondroitin 4-Sulfate Comparable to that for Hyaluronan. *Biomolecules* 2, 549–563.

- Huang, X.A., Yin, H., Sweeney, S., Raha, D., Snyder, M., and Lin, H. (2013). A major epigenetic programming mechanism guided by piRNAs. *Dev Cell* 24, 502–516.
- Huang, Z.J., Kirkwood, A., Pizzorusso, T., Porciatti, V., Morales, B., Bear, M.F., Maffei, L., and Tonegawa, S. (1999). BDNF regulates the maturation of inhibition and the critical period of plasticity in mouse visual cortex. *Cell* 98, 739–755.
- Hwang, H.-Y., Olson, S.K., Esko, J.D., and Horvitz, H.R. (2003). *Caenorhabditis elegans* early embryogenesis and vulval morphogenesis require chondroitin biosynthesis. *Nature* 423, 439–443.
- Insel, T.R. (2010). Rethinking schizophrenia. *Nature* 468, 187–193.
- Iozzo, R.V. (1998). Matrix proteoglycans: from molecular design to cellular function. *Annu. Rev. Biochem.* 67, 609–652.
- Itano, N., Sawai, T., Yoshida, M., Lenas, P., Yamada, Y., Imagawa, M., Shinomura, T., Hamaguchi, M., Yoshida, Y., Ohnuki, Y., et al. (1999). Three isoforms of mammalian hyaluronan synthases have distinct enzymatic properties. *J Biol Chem* 274, 25085–25092.
- Iwai, Y., Fagiolini, M., Obata, K., and Hensch, T.K. (2003). Rapid critical period induction by tonic inhibition in visual cortex. *J. Neurosci.* 23, 6695–6702.
- Izumikawa, T., Kanagawa, N., Watamoto, Y., Okada, M., Saeki, M., Sakano, M., Sugahara, K., Sugihara, K., Asano, M., and Kitagawa, H. (2010). Impairment of embryonic cell division and glycosaminoglycan biosynthesis in glucuronyltransferase-I-deficient mice. *Journal of Biological Chemistry* 285, 12190–12196.
- Izumikawa, T., Kitagawa, H., Mizuguchi, S., Nomura, K.H., Nomura, K., Tamura, J.-I., Gengyo-Ando, K., Mitani, S., and Sugahara, K. (2004). Nematode chondroitin polymerizing factor showing cell-/organ-specific expression is indispensable for chondroitin synthesis and embryonic cell division. *J Biol Chem* 279, 53755–53761.
- Jiao, C.-Y., Delaroche, D., Burlina, F., Alves, I.D., Chassaing, G., and Sagan, S. (2009). Translocation and endocytosis for cell-penetrating peptide internalization. *Journal of Biological Chemistry* 284, 33957–33965.
- Jiao, Y., Zhang, C., Yanagawa, Y., and Sun, Q.-Q. (2006). Major effects of sensory experiences on the neocortical inhibitory circuits. *J. Neurosci.* 26, 8691–8701.
- Johansson, P.A., Irmeler, M., Acampora, D., Beckers, J., Simeone, A., and Götz, M. (2013). The transcription factor *Otx2* regulates choroid plexus development and function. *Development* 140, 1055–1066.
- Johnson, Z., Power, C.A., Weiss, C., Rintelen, F., Ji, H., Ruckle, T., Camps, M., Wells, T.N.C., Schwarz, M.K., Proudfoot, A.E.I., et al. (2004). Chemokine inhibition--why, when, where, which and how? *Biochem. Soc. Trans* 32, 366–377.
- Joliot, A.H., Triller, A., Volovitch, M., Pernelle, C., and Prochiantz, A. (1991a). alpha-2,8-Polysialic acid is the neuronal surface receptor of antennapedia homeobox peptide. *New Biol.* 3, 1121–1134.

- Joliot, A., Maizel, A., Rosenberg, D., Trembleau, A., Dupas, S., Volovitch, M., and Prochiantz, A. (1998). Identification of a signal sequence necessary for the unconventional secretion of Engrailed homeoprotein. *Curr Biol* 8, 856–863.
- Joliot, A., Pernelle, C., Deagostini-Bazin, H., and Prochiantz, A. (1991b). Antennapedia homeobox peptide regulates neural morphogenesis. *Proc Natl Acad Sci USA* 88, 1864–1868.
- Joliot, A., Trembleau, A., Raposo, G., Calvet, S., Volovitch, M., and Prochiantz, A. (1997). Association of Engrailed homeoproteins with vesicles presenting caveolae-like properties. *Development* 124, 1865–1875.
- Joliot, A., and Prochiantz, A. (2004). Transduction peptides: from technology to physiology. *Nat Cell Biol* 6, 189–196.
- Kaczmarek, L., and Chaudhuri, A. (1997). Sensory regulation of immediate-early gene expression in mammalian visual cortex: implications for functional mapping and neural plasticity. *Brain Res. Brain Res. Rev.* 23, 237–256.
- Kamimura, K., Rhodes, J.M., Ueda, R., McNeely, M., Shukla, D., Kimata, K., Spear, P.G., Shworak, N.W., and Nakato, H. (2004). Regulation of Notch signaling by *Drosophila* heparan sulfate 3-O sulfotransferase. *J Cell Biol* 166, 1069–1079.
- Kaneko, M., Stellwagen, D., Malenka, R.C., and Stryker, M.P. (2008). Tumor necrosis factor- $\alpha$  mediates one component of competitive, experience-dependent plasticity in developing visual cortex. *Neuron* 58, 673–680.
- Karetko, M., and Skangiel-Kramska, J. (2009). Diverse functions of perineuronal nets. *Acta Neurobiol Exp (Wars)* 69, 564–577.
- Karousou, E., Asimakopoulou, A., Monti, L., Zafeiropoulou, V., Afratis, N., Gartaganis, P., Rossi, A., Passi, A., and Karamanos, N.K. (2014). FACE Analysis as a Fast and Reliable Methodology to Monitor the Sulfation and Total Amount of Chondroitin Sulfate in Biological Samples of Clinical Importance. *Molecules* 19, 7959–7980.
- Katagiri, H., Fagiolini, M., and Hensch, T.K. (2007). Optimization of somatic inhibition at critical period onset in mouse visual cortex. *Neuron* 53, 805–812.
- Kitagawa, H., Tsutsumi, K., Tone, Y., and Sugahara, K. (1997). Developmental regulation of the sulfation profile of chondroitin sulfate chains in the chicken embryo brain. *J Biol Chem* 272, 31377–31381.
- Koike, C., Nishida, A., Ueno, S., Saito, H., Sanuki, R., Sato, S., Furukawa, A., Aizawa, S., Matsuo, I., Suzuki, N., et al. (2007). Functional roles of Otx2 transcription factor in postnatal mouse retinal development. *Mol Cell Biol* 27, 8318–8329.
- Kotak, V.C., Takesian, A.E., and Sanes, D.H. (2008). Hearing loss prevents the maturation of GABAergic transmission in the auditory cortex. *Cerebral Cortex* 18, 2098–2108.
- Köppe, G., Brückner, G., Brauer, K., Härtig, W., and Bigl, V. (1997a). Developmental patterns of proteoglycan-containing extracellular matrix in perineuronal nets and neuropil of the postnatal rat brain. *Cell Tissue Res* 288, 33–41.

- Köppe, G., Brückner, G., Härtig, W., Delpech, B., and Bigl, V. (1997b). Characterization of proteoglycan-containing perineuronal nets by enzymatic treatments of rat brain sections. *Histochem. J.* 29, 11–20.
- Kuberan, B., Lech, M., Borjigin, J., and Rosenberg, R.D. (2004). Light-induced 3-O-sulfotransferase expression alters pineal heparan sulfate fine structure. A surprising link to circadian rhythm. *J Biol Chem* 279, 5053–5054.
- Kusche-Gullberg, M., and Kjellén, L. (2003). Sulfotransferases in glycosaminoglycan biosynthesis. *Curr Opin Struct Biol* 13, 605–611.
- Kwok, J.C.F., Carulli, D., and Fawcett, J.W. (2010). In vitro modeling of perineuronal nets: hyaluronan synthase and link protein are necessary for their formation and integrity. *J Neurochem* 114, 1447–1459.
- Kwok, J.C.F., Dick, G., Wang, D., and Fawcett, J.W. (2011). Extracellular matrix and perineuronal nets in CNS repair. *Devel Neurobio* 71, 1073–1089.
- Laguri, C., Sadir, R., Rueda, P., Baleux, F., Gans, P., Arenzana-Seisdedos, F., and Lortat-Jacob, H. (2007). The novel CXCL12gamma isoform encodes an unstructured cationic domain which regulates bioactivity and interaction with both glycosaminoglycans and CXCR4. *PLoS ONE* 2, e1110.
- Lamanna, W.C., Kalus, I., Padva, M., Baldwin, R.J., Merry, C.L.R., and Dierks, T. (2007). The heparanome--the enigma of encoding and decoding heparan sulfate sulfation. *J. Biotechnol.* 129, 290–307.
- Larsen, K.B., Lutterodt, M., Rath, M.F., and Møller, M. (2009). Expression of the homeobox genes PAX6, OTX2, and OTX1 in the early human fetal retina. *Int J Dev Neurosci* 27, 485–492.
- Laughon, A., and Scott, M.P. (1984). Sequence of a *Drosophila* segmentation gene: protein structure homology with DNA-binding proteins. *Nature* 310, 25–31.
- Layalle, S., Volovitch, M., Mugat, B., Bonneaud, N., Parmentier, M.-L., Prochiantz, A., Joliot, A., and Maschat, F. (2011). Engrailed homeoprotein acts as a signaling molecule in the developing fly. *Development* 138, 2315–2323.
- Le Roux, I., Joliot, A.H., Bloch-Gallego, E., Prochiantz, A., and Volovitch, M. (1993). Neurotrophic activity of the Antennapedia homeodomain depends on its specific DNA-binding properties. *Proc Natl Acad Sci USA* 90, 9120–9124.
- Lee, H., Leamey, C.A., and Sawatari, A. (2012). Perineuronal nets play a role in regulating striatal function in the mouse. *PLoS ONE* 7, e32747.
- Lefranc, M.-P., Pommié, C., Ruiz, M., Giudicelli, V., Foulquier, E., Truong, L., Thouvenin-Contet, V., and Lefranc, G. (2003). IMGT unique numbering for immunoglobulin and T cell receptor variable domains and Ig superfamily V-like domains. *Dev. Comp. Immunol.* 27, 55–77.
- Lemarchant, S., Pruvost, M., Montaner, J., Emery, E., Vivien, D., Kanninen, K., and Koistinaho, J. (2013). ADAMTS proteoglycanases in the physiological and pathological

central nervous system. *J Neuroinflammation* 10, 133.

Lensink, M.F., Christiaens, B., Vandekerckhove, J., Prochiantz, A., and Rosseneu, M. (2005). Penetratin-membrane association: W48/R52/W56 shield the peptide from the aqueous phase. *Biophys. J.* 88, 939–952.

Lesaffre, B., Joliot, A., Prochiantz, A., and Volovitch, M. (2007). Direct non-cell autonomous Pax6 activity regulates eye development in the zebrafish. *Neural Dev* 2, 2.

Lewis, E.B. (1978). A gene complex controlling segmentation in *Drosophila*. *Nature* 276, 565–570.

Lewis, T.L., and Maurer, D. (2009). Effects of early pattern deprivation on visual development. *Optom Vis Sci* 86, 640–646.

Li, L., Carter, J., Gao, X., Whitehead, J., and Tourtellotte, W.G. (2005). The neuroplasticity-associated arc gene is a direct transcriptional target of early growth response (Egr) transcription factors. *Mol Cell Biol* 25, 10286–10300.

Lin, R., Rosahl, T.W., Whiting, P.J., Fawcett, J.W., and Kwok, J.C.F. (2011). 6-Sulphated chondroitins have a positive influence on axonal regeneration. *PLoS ONE* 6, e21499.

Lin, X., and Perrimon, N. (1999). Dally cooperates with *Drosophila* Frizzled 2 to transduce Wingless signalling. *Nature* 400, 281–284.

Lin, X., Wei, G., Shi, Z., Dryer, L., Esko, J.D., Wells, D.E., and Matzuk, M.M. (2000). Disruption of gastrulation and heparan sulfate biosynthesis in EXT1-deficient mice. *Dev Biol* 224, 299–311.

Lin, X. (2004). Functions of heparan sulfate proteoglycans in cell signaling during development. *Development* 131, 6009–6021.

Liu, L., and Duff, K. (2008). A Technique for Serial Collection of Cerebrospinal Fluid from the Cisterna Magna in Mouse. *J Vis Exp* e960.

Lopin, C., and Jacquinet, J.-C. (2006). From polymer to size-defined oligomers: an expeditious route for the preparation of chondroitin oligosaccharides. *Angew. Chem. Int. Ed. Engl.* 45, 2574–2578.

Lortat-Jacob, H. (2009). The molecular basis and functional implications of chemokine interactions with heparan sulphate. *Curr Opin Struct Biol* 19, 543–548.

Maeda, N., Ishii, M., Nishimura, K., and Kamimura, K. (2011). Functions of chondroitin sulfate and heparan sulfate in the developing brain. *Neurochem. Res.* 36, 1228–1240.

Maizel, A., Tassetto, M., Filhol, O., Cochet, C., Prochiantz, A., and Joliot, A. (2002). Engrailed homeoprotein secretion is a regulated process. *Development* 129, 3545–3553.

Mallamaci, A., Di Blas, E., Briata, P., Boncinelli, E., and Corte, G. (1996). OTX2 homeoprotein in the developing central nervous system and migratory cells of the olfactory area. *Mech Dev* 58, 165–178.

- Marín, O. (2012). Interneuron dysfunction in psychiatric disorders. *Nat Rev Neurosci* 13, 107–120.
- Martinez-Morales, J.R., Signore, M., Acampora, D., Simeone, A., and Bovolenta, P. (2001). Otx genes are required for tissue specification in the developing eye. *Development* 128, 2019–2030.
- Mataga, N., Mizuguchi, Y., and Hensch, T.K. (2004). Experience-dependent pruning of dendritic spines in visual cortex by tissue plasminogen activator. *Neuron* 44, 1031–1041.
- Mataga, N., Nagai, N., and Hensch, T.K. (2002). Permissive proteolytic activity for visual cortical plasticity. *Proc Natl Acad Sci USA* 99, 7717–7721.
- Matsuo, I., Kuratani, S., Kimura, C., Takeda, N., and Aizawa, S. (1995). Mouse Otx2 functions in the formation and patterning of rostral head. *Genes & Development* 9, 2646–2658.
- Matthews, R.T., Kelly, G.M., Zerillo, C.A., Gray, G., Tiemeyer, M., and Hockfield, S. (2002). Aggrecan glycoforms contribute to the molecular heterogeneity of perineuronal nets. *J. Neurosci.* 22, 7536–7547.
- Mauney, S.A., Athanas, K.M., Pantazopoulos, H., Shaskan, N., Passeri, E., Berretta, S., and Woo, T.-U.W. (2013). Developmental pattern of perineuronal nets in the human prefrontal cortex and their deficit in schizophrenia. *Biological Psychiatry* 74, 427–435.
- Maya Vetencourt, J.F., Sale, A., Viegi, A., Baroncelli, L., De Pasquale, R., O'Leary, O.F., Castrén, E., and Maffei, L. (2008). The antidepressant fluoxetine restores plasticity in the adult visual cortex. *Science* 320, 385–388.
- McGinnis, W., Garber, R.L., Wirz, J., Kuroiwa, A., and Gehring, W.J. (1984a). A homologous protein-coding sequence in *Drosophila* homeotic genes and its conservation in other metazoans. *Cell* 37, 403–408.
- McGinnis, W., Hart, C.P., Gehring, W.J., and Ruddle, F.H. (1984b). Molecular cloning and chromosome mapping of a mouse DNA sequence homologous to homeotic genes of *Drosophila*. *Cell* 38, 675–680.
- McLaughlin, T., and O'Leary, D.D.M. (2005). Molecular gradients and development of retinotopic maps. *Annu Rev Neurosci* 28, 327–355.
- McRae, P.A., Rocco, M.M., Kelly, G., Brumberg, J.C., and Matthews, R.T. (2007). Sensory deprivation alters aggrecan and perineuronal net expression in the mouse barrel cortex. *J. Neurosci.* 27, 5405–5413.
- Mikami, T., and Kitagawa, H. (2013). Biosynthesis and function of chondroitin sulfate. *Biochim Biophys Acta* 1830, 4719–4733.
- Mikami, T., Yasunaga, D., and Kitagawa, H. (2009). Contactin-1 is a functional receptor for neuroregulatory chondroitin sulfate-E. *J Biol Chem* 284, 4494–4499.
- Mitsunaga, C., Mikami, T., Mizumoto, S., Fukuda, J., and Sugahara, K. (2006). Chondroitin sulfate/dermatan sulfate hybrid chains in the development of cerebellum. *Spatiotemporal*

regulation of the expression of critical disulfated disaccharides by specific sulfotransferases. *J Biol Chem* 281, 18942–18952.

Miyata, S., Nishimura, Y., Hayashi, N., and Oohira, A. (2005). Construction of perineuronal net-like structure by cortical neurons in culture. *Neuroscience* 136, 95–104.

Miyata, S., Komatsu, Y., Yoshimura, Y., Taya, C., and Kitagawa, H. (2012). Persistent cortical plasticity by upregulation of chondroitin 6-sulfation. *Nature Publishing Group* 15, 414–22–S1–2.

Miyazaki, H., Kobayashi, T., Nakamura, H., and Funahashi, J.-I. (2006). Role of Gbx2 and Otx2 in the formation of cochlear ganglion and endolymphatic duct. *Dev Growth Differ* 48, 429–438.

Mizuguchi, S., Uyama, T., Kitagawa, H., Nomura, K.H., Dejima, K., Gengyo-Ando, K., Mitani, S., Sugahara, K., and Nomura, K. (2003). Chondroitin proteoglycans are involved in cell division of *Caenorhabditis elegans*. *Nature* 423, 443–448.

Mizumoto, S., and Sugahara, K. (2012). Glycosaminoglycan chain analysis and characterization (glycosylation/epimerization). *Methods Mol. Biol.* 836, 99–115.

Morales, B., Choi, S.-Y., and Kirkwood, A. (2002). Dark rearing alters the development of GABAergic transmission in visual cortex. *J. Neurosci.* 22, 8084–8090.

Morrey, J.D., Olsen, A.L., Siddharthan, V., Motter, N.E., Wang, H., Taro, B.S., Chen, D., Ruffner, D., and Hall, J.O. (2008). Increased blood-brain barrier permeability is not a primary determinant for lethality of West Nile virus infection in rodents. *J. Gen. Virol.* 89, 467–473.

Morris, N.P., and Henderson, Z. (2000). Perineuronal nets ensheath fast spiking, parvalbumin-immunoreactive neurons in the medial septum/diagonal band complex. *Eur J Neurosci* 12, 828–838.

Mukhopadhyay, A., McGuire, T., Peng, C.-Y., and Kessler, J.A. (2009). Differential effects of BMP signaling on parvalbumin and somatostatin interneuron differentiation. *Development* 136, 2633–2642.

Muyldermans, S., Atarhouch, T., Saldanha, J., Barbosa, J.A., and Hamers, R. (1994). Sequence and structure of VH domain from naturally occurring camel heavy chain immunoglobulins lacking light chains. *Protein Eng.* 7, 1129–1135.

Nakielnny, S., and Dreyfuss, G. (1997). Nuclear export of proteins and RNAs. *Curr. Opin. Cell Biol.* 9, 420–429.

Nédélec, S., Foucher, I., Brunet, I., Bouillot, C., Prochiantz, A., and Trembleau, A. (2004). Emx2 homeodomain transcription factor interacts with eukaryotic translation initiation factor 4E (eIF4E) in the axons of olfactory sensory neurons. *Proc Natl Acad Sci USA* 101, 10815–10820.

Nishida, A., Furukawa, A., Koike, C., Tano, Y., Aizawa, S., Matsuo, I., and Furukawa, T. (2003). Otx2 homeobox gene controls retinal photoreceptor cell fate and pineal gland development. *Nat Neurosci* 6, 1255–1263.



- Nothias, F., Fishell, G., and Ruiz i Altaba, A. (1998). Cooperation of intrinsic and extrinsic signals in the elaboration of regional identity in the posterior cerebral cortex. *Curr Biol* 8, 459–462.
- Ohira, K., Takeuchi, R., Iwanaga, T., and Miyakawa, T. (2013). Chronic fluoxetine treatment reduces parvalbumin expression and perineuronal nets in gamma-aminobutyric acidergic interneurons of the frontal cortex in adult mice. *Mol Brain* 6, 43.
- Oray, S., Majewska, A., and Sur, M. (2004). Dendritic spine dynamics are regulated by monocular deprivation and extracellular matrix degradation. *Neuron* 44, 1021–1030.
- Otting, G., Qian, Y.Q., Billeter, M., Müller, M., Affolter, M., Gehring, W.J., and Wüthrich, K. (1990). Protein--DNA contacts in the structure of a homeodomain--DNA complex determined by nuclear magnetic resonance spectroscopy in solution. *Embo J* 9, 3085–3092.
- Pantazopoulos, H., Woo, T.-U.W., Lim, M.P., Lange, N., and Berretta, S. (2010). Extracellular matrix-glia abnormalities in the amygdala and entorhinal cortex of subjects diagnosed with schizophrenia. *Arch. Gen. Psychiatry* 67, 155–166.
- Pellegrini, L., Burke, D.F., Delft, von, F., Mulloy, B., and Blundell, T.L. (2000). Crystal structure of fibroblast growth factor receptor ectodomain bound to ligand and heparin. *Nature* 407, 1029–1034.
- Perosa, S.R., Porcionatto, M.A., Cukiert, A., Martins, J.R.M., Amado, D., Nader, H.B., Cavalheiro, E.A., Leite, J.P., and Naffah-Mazzacoratti, M.G. (2002). Extracellular matrix components are altered in the hippocampus, cortex, and cerebrospinal fluid of patients with mesial temporal lobe epilepsy. *Epilepsia* 43 Suppl 5, 159–161.
- Petitou, M., and van Boeckel, C.A.A. (2004). A synthetic antithrombin III binding pentasaccharide is now a drug! What comes next? *Angew. Chem. Int. Ed. Engl.* 43, 3118–3133.
- Pizzorusso, T., Medini, P., Berardi, N., Chierzi, S., Fawcett, J.W., and Maffei, L. (2002). Reactivation of ocular dominance plasticity in the adult visual cortex. *Science* 298, 1248–1251.
- Pizzorusso, T., Medini, P., Landi, S., Baldini, S., Berardi, N., and Maffei, L. (2006). Structural and functional recovery from early monocular deprivation in adult rats. *Proc Natl Acad Sci USA* 103, 8517–8522.
- Prabhakar, V., Capila, I., Bosques, C.J., Pojasek, K., and Sasisekharan, R. (2005). Chondroitinase ABC I from *Proteus vulgaris*: cloning, recombinant expression and active site identification. *Biochem J* 386, 103–112.
- Prochiantz, A. (2013). Signaling with homeoprotein transcription factors in development and throughout adulthood. *Curr. Genomics* 14, 361–370.
- Prochiantz, A., and Joliot, A. (2003). Can transcription factors function as cell-cell signalling molecules? *Nat Rev Mol Cell Biol* 4, 814–819.
- Prusky, G.T., and Douglas, R.M. (2003). Developmental plasticity of mouse visual acuity. *Eur J Neurosci* 17, 167–173.

- Putignano, E., Lonetti, G., Cancedda, L., Ratto, G., Costa, M., Maffei, L., and Pizzorusso, T. (2007). Developmental downregulation of histone posttranslational modifications regulates visual cortical plasticity. *Neuron* 53, 747–759.
- Qian, Y.Q., Billeter, M., Otting, G., Müller, M., Gehring, W.J., and Wüthrich, K. (1989). The structure of the Antennapedia homeodomain determined by NMR spectroscopy in solution: comparison with prokaryotic repressors. *Cell* 59, 573–580.
- Ragge, N.K., Brown, A.G., Poloschek, C.M., Lorenz, B., Henderson, R.A., Clarke, M.P., Russell-Eggitt, I., Fielder, A., Gerrelli, D., Martinez-Barbera, J.P., et al. (2005). Heterozygous mutations of OTX2 cause severe ocular malformations. *Am. J. Hum. Genet.* 76, 1008–1022.
- Raman, R., Raguram, S., Venkataraman, G., Paulson, J.C., and Sasisekharan, R. (2005). Glycomics: an integrated systems approach to structure-function relationships of glycans. *Nat Meth* 2, 817–824.
- Rath, M.F., Muñoz, E., Ganguly, S., Morin, F., Shi, Q., Klein, D.C., and Møller, M. (2006). Expression of the Otx2 homeobox gene in the developing mammalian brain: embryonic and adult expression in the pineal gland. *J Neurochem* 97, 556–566.
- Rauch, U. (2004). Extracellular matrix components associated with remodeling processes in brain. *Cell. Mol. Life Sci.* 61, 2031–2045.
- Reese, B.E. (2011). Development of the retina and optic pathway. *Vision Res* 51, 613–632.
- Reilly, M.T., Faulkner, G.J., Dubnau, J., Ponomarev, I., and Gage, F.H. (2013). The role of transposable elements in health and diseases of the central nervous system. *J. Neurosci.* 33, 17577–17586.
- Reiter, R.J., Tan, D.X., Kim, S.J., and Cruz, M.H.C. (2014). Delivery of pineal melatonin to the brain and SCN: role of canaliculi, cerebrospinal fluid, tanycytes and Virchow-Robin perivascular spaces. *Brain Struct Funct.*
- Rivera-Pomar, R., Niessing, D., Schmidt-Ott, U., Gehring, W.J., and Jäckle, H. (1996). RNA binding and translational suppression by bicoid. *Nature* 379, 746–749.
- Rubenstein, J.L., Shimamura, K., Martinez, S., and Puelles, L. (1998). Regionalization of the prosencephalic neural plate. *Annu Rev Neurosci* 21, 445–477.
- Rubenstein, J.L.R. (2010). Three hypotheses for developmental defects that may underlie some forms of autism spectrum disorder. *Curr. Opin. Neurol.* 23, 118–123.
- Rusnati, M., Tulipano, G., Spillmann, D., Tanghetti, E., Oreste, P., Zoppetti, G., Giacca, M., and Presta, M. (1999). Multiple interactions of HIV-I Tat protein with size-defined heparin oligosaccharides. *J Biol Chem* 274, 28198–28205.
- Sale, A., Maya Vetencourt, J.F., Medini, P., Cenni, M.C., Baroncelli, L., De Pasquale, R., and Maffei, L. (2007). Environmental enrichment in adulthood promotes amblyopia recovery through a reduction of intracortical inhibition. *Nat Neurosci* 10, 679–681.
- Sasisekharan, R., and Venkataraman, G. (2000). Heparin and heparan sulfate: biosynthesis, structure and function. *Curr Opin Chem Biol* 4, 626–631.

- Sánchez-Calderón, H., Martín-Partido, G., and Hidalgo-Sánchez, M. (2004). *Otx2*, *Gbx2*, and *Fgf8* expression patterns in the chick developing inner ear and their possible roles in otic specification and early innervation. *Gene Expr. Patterns* 4, 659–669.
- Schilter, K.F., Schneider, A., Bardakjian, T., Soucy, J.-F., Tyler, R.C., Reis, L.M., and Semina, E.V. (2011). OTX2 microphthalmia syndrome: four novel mutations and delineation of a phenotype. *Clin Genet* 79, 158–168.
- Schlessinger, J., Plotnikov, A.N., Ibrahimi, O.A., Eliseenkova, A.V., Yeh, B.K., Yayon, A., Linhardt, R.J., and Mohammadi, M. (2000). Crystal structure of a ternary FGF-FGFR-heparin complex reveals a dual role for heparin in FGFR binding and dimerization. *Molecular Cell* 6, 743–750.
- Shatz, C.J., and Stryker, M.P. (1978). Ocular dominance in layer IV of the cat's visual cortex and the effects of monocular deprivation. *J Physiol (Lond)* 281, 267–283.
- Shepherd, J.C., McGinnis, W., Carrasco, A.E., De Robertis, E.M., and Gehring, W.J. (1984). Fly and frog homoeo domains show homologies with yeast mating type regulatory proteins. *Nature* 310, 70–71.
- Shepherd, J.D., and Bear, M.F. (2011). New views of Arc, a master regulator of synaptic plasticity. *Nature Publishing Group* 14, 279–284.
- Shipp, E.L., and Hsieh-Wilson, L.C. (2007). Profiling the sulfation specificities of glycosaminoglycan interactions with growth factors and chemotactic proteins using microarrays. *Chem Biol* 14, 195–208.
- Silbert, J.E., and Sugumaran, G. (2002). Biosynthesis of chondroitin/dermatan sulfate. *IUBMB Life* 54, 177–186.
- Silingardi, D., Scali, M., Belluomini, G., and Pizzorusso, T. (2010). Epigenetic treatments of adult rats promote recovery from visual acuity deficits induced by long-term monocular deprivation. *Eur J Neurosci* 31, 2185–2192.
- Simeone, A., Acampora, D., Gulisano, M., Stornaiuolo, A., and Boncinelli, E. (1992). Nested expression domains of four homeobox genes in developing rostral brain. *Nature* 358, 687–690.
- Simeone, A., Acampora, D., Mallamaci, A., Stornaiuolo, A., D'Apice, M.R., Nigro, V., and Boncinelli, E. (1993). A vertebrate gene related to orthodenticle contains a homeodomain of the bicoid class and demarcates anterior neuroectoderm in the gastrulating mouse embryo. *Embo J* 12, 2735–2747.
- Siomi, M.C., Sato, K., Pezic, D., and Aravin, A.A. (2011). PIWI-interacting small RNAs: the vanguard of genome defence. *Nat Rev Mol Cell Biol* 12, 246–258.
- Solbach, S., and Celio, M.R. (1991). Ontogeny of the calcium binding protein parvalbumin in the rat nervous system. *Anat. Embryol.* 184, 103–124.
- Sonnier, L., Le Pen, G., Hartmann, A., Bizot, J.-C., Trovero, F., Krebs, M.-O., and Prochiantz, A. (2007). Progressive loss of dopaminergic neurons in the ventral midbrain of adult mice heterozygote for *Engrailed1*. *J. Neurosci.* 27, 1063–1071.

Southwell, D.G., Froemke, R.C., Alvarez-Buylla, A., Stryker, M.P., and Gandhi, S.P. (2010). Cortical plasticity induced by inhibitory neuron transplantation. *Science* 327, 1145–1148.

Spatazza, J., Di Lullo, E., Joliot, A., Dupont, E., Moya, K.L., and Prochiantz, A. (2013a). Homeoprotein signaling in development, health, and disease: a shaking of dogmas offers challenges and promises from bench to bed. *Pharmacol. Rev.* 65, 90–104.

Spatazza, J., Lee, H.H.C., Di Nardo, A.A., Tibaldi, L., Joliot, A., Hensch, T.K., and Prochiantz, A. (2013b). Choroid-plexus-derived Otx2 homeoprotein constrains adult cortical plasticity. *Cell Rep* 3, 1815–1823.

Spicer, A.P., Olson, J.S., and McDonald, J.A. (1997). Molecular cloning and characterization of a cDNA encoding the third putative mammalian hyaluronan synthase. *J Biol Chem* 272, 8957–8961.

Stettler, O., Joshi, R.L., Wizenmann, A., Reingruber, J., Holcman, D., Bouillot, C., Castagner, F., Prochiantz, A., and Moya, K.L. (2012). Engrailed homeoprotein recruits the adenosine A1 receptor to potentiate ephrin A5 function in retinal growth cones. *Development* 139, 215–224.

Sugahara, K., Mikami, T., Uyama, T., Mizuguchi, S., Nomura, K., and Kitagawa, H. (2003). Recent advances in the structural biology of chondroitin sulfate and dermatan sulfate. *Curr Opin Struct Biol* 13, 612–620.

Sugiyama, S., Di Nardo, A.A., Aizawa, S., Matsuo, I., Volovitch, M., Prochiantz, A., and Hensch, T.K. (2008). Experience-dependent transfer of Otx2 homeoprotein into the visual cortex activates postnatal plasticity. *Cell* 134, 508–520.

Sugiyama, S., Prochiantz, A., and Hensch, T.K. (2009). From brain formation to plasticity: insights on Otx2 homeoprotein. *Dev Growth Differ* 51, 369–377.

Sultan, F.A., Wang, J., Tront, J., Liebermann, D.A., and Sweatt, J.D. (2012). Genetic deletion of Gadd45b, a regulator of active DNA demethylation, enhances long-term memory and synaptic plasticity. *J. Neurosci.* 32, 17059–17066.

Sur, M., Garraghty, P.E., and Roe, A.W. (1988). Experimentally induced visual projections into auditory thalamus and cortex. *Science* 242, 1437–1441.

Suttkus, A., Rohn, S., Weigel, S., Glöckner, P., Arendt, T., and Morawski, M. (2014). AggreCAN, link protein and tenascin-R are essential components of the perineuronal net to protect neurons against iron-induced oxidative stress. *Cell Death Dis* 5, e1119.

Syken, J., Grandpre, T., Kanold, P.O., and Shatz, C.J. (2006). PirB restricts ocular-dominance plasticity in visual cortex. *Science* 313, 1795–1800.

Taha, S., and Stryker, M.P. (2002). Rapid ocular dominance plasticity requires cortical but not geniculate protein synthesis. *Neuron* 34, 425–436.

Takao, K., Kobayashi, K., Hagihara, H., Ohira, K., Shoji, H., Hattori, S., Koshimizu, H., Umemori, J., Toyama, K., Nakamura, H.K., et al. (2013). Deficiency of schnurri-2, an MHC enhancer binding protein, induces mild chronic inflammation in the brain and confers molecular, neuronal, and behavioral phenotypes related to schizophrenia. *Neuropsychopharmacology* 38, 1409–1425.

- Takesian, A.E., and Hensch, T.K. (2013). Balancing plasticity/stability across brain development. *Prog. Brain Res.* 207, 3–34.
- Takesian, A.E., Kotak, V.C., and Sanes, D.H. (2010). Presynaptic GABA(B) receptors regulate experience-dependent development of inhibitory short-term plasticity. *J. Neurosci.* 30, 2716–2727.
- Tam, P.P., and Behringer, R.R. (1997). Mouse gastrulation: the formation of a mammalian body plan. *Mech Dev* 68, 3–25.
- Tamura, J.-I., Tsutsumishita-Nakai, N., Nakao, Y., Kawano, M., Kato, S., Takeda, N., Nadanaka, S., and Kitagawa, H. (2012). Synthesis and interaction with midline of biotinylated chondroitin sulfate tetrasaccharides. *Bioorg. Med. Chem. Lett.* 22, 1371–1374.
- Tiraboschi, E., Guirado, R., Greco, D., Auvinen, P., Maya Vetencourt, J.F., Maffei, L., and Castrén, E. (2013). Gene expression patterns underlying the reinstatement of plasticity in the adult visual system. *Neural Plasticity* 2013, 605079.
- Topisirovic, I., and Borden, K.L.B. (2005). Homeodomain proteins and eukaryotic translation initiation factor 4E (eIF4E): an unexpected relationship. *Histol. Histopathol.* 20, 1275–1284.
- Torero Ibad, R., Rheey, J., Mrejen, S., Forster, V., Picaud, S., Prochiantz, A., and Moya, K.L. (2011). Otx2 promotes the survival of damaged adult retinal ganglion cells and protects against excitotoxic loss of visual acuity in vivo. *J. Neurosci.* 31, 5495–5503.
- Trachtenberg, J.T., and Stryker, M.P. (2001). Rapid anatomical plasticity of horizontal connections in the developing visual cortex. *J. Neurosci.* 21, 3476–3482.
- Tricoire, H., Malpoux, B., and Møller, M. (2003). Cellular lining of the sheep pineal recess studied by light-, transmission-, and scanning electron microscopy: morphologic indications for a direct secretion of melatonin from the pineal gland to the cerebrospinal fluid. *J Comp Neurol* 456, 39–47.
- Tropea, D., Kreiman, G., Lyckman, A., Mukherjee, S., Yu, H., Horng, S., and Sur, M. (2006). Gene expression changes and molecular pathways mediating activity-dependent plasticity in visual cortex. *Nat Neurosci* 9, 660–668.
- Tully, S.E., Mabon, R., Gama, C.I., Tsai, S.M., Liu, X., and Hsieh-Wilson, L.C. (2004). A chondroitin sulfate small molecule that stimulates neuronal growth. *J Am Chem Soc* 126, 7736–7737.
- Turrigiano, G.G., and Nelson, S.B. (2004). Homeostatic plasticity in the developing nervous system. *Nat Rev Neurosci* 5, 97–107.
- Tushir, J.S., Zamore, P.D., and Zhang, Z. (2009). SnapShot: mouse piRNAs, PIWI proteins, and the ping-pong cycle. *Cell* 139, 830–830.e831.
- Vallès, A., Boender, A.J., Gijsbers, S., Haast, R.A.M., Martens, G.J.M., and de Weerd, P. (2011). Genomewide analysis of rat barrel cortex reveals time- and layer-specific mRNA expression changes related to experience-dependent plasticity. *J. Neurosci.* 31, 6140–6158.
- Veilleux, H.D., Van Herwerden, L., Cole, N.J., Don, E.K., De Santis, C., Dixon, D.L.,

- Wenger, A.S., and Munday, P.L. (2013). Otx2 expression and implications for olfactory imprinting in the anemonefish, *Amphiprion percula*. *Biol Open* 2, 907–915.
- Vo, T., Carulli, D., Ehlert, E.M.E., Kwok, J.C.F., Dick, G., Mecollari, V., Moloney, E.B., Neufeld, G., de Winter, F., Fawcett, J.W., et al. (2013). The chemorepulsive axon guidance protein semaphorin3A is a constituent of perineuronal nets in the adult rodent brain. *Mol Cell Neurosci* 56, 186–200.
- Volk, D.W., Matsubara, T., Li, S., Sengupta, E.J., Georgiev, D., Minabe, Y., Sampson, A., Hashimoto, T., and Lewis, D.A. (2012). Deficits in transcriptional regulators of cortical parvalbumin neurons in schizophrenia. *American Journal of Psychiatry* 169, 1082–1091.
- Volovitch, M., Le Roux, I., Joliot, A.H., Bloch-Gallego, E., and Prochiantz, A. (1993). Control of neuronal morphogenesis by homeoproteins: consequences for the making of neuronal networks. *Perspect Dev Neurobiol* 1, 133–138.
- Volpi, N. (2010). High-performance liquid chromatography and on-line mass spectrometry detection for the analysis of chondroitin sulfates/hyaluronan disaccharides derivatized with 2-aminoacridone. *Anal Biochem* 397, 12–23.
- Volpi, N., and Linhardt, R.J. (2010). High-performance liquid chromatography-mass spectrometry for mapping and sequencing glycosaminoglycan-derived oligosaccharides. *Nat Protoc* 5, 993–1004.
- Volpi, N., Galeotti, F., Yang, B., and Linhardt, R.J. (2014). Analysis of glycosaminoglycan-derived, precolumn, 2-aminoacridone-labeled disaccharides with LC-fluorescence and LC-MS detection. *Nat Protoc* 9, 541–558.
- Wang, D., Ichiyama, R.M., Zhao, R., Andrews, M.R., and Fawcett, J.W. (2011). Chondroitinase combined with rehabilitation promotes recovery of forelimb function in rats with chronic spinal cord injury. *J. Neurosci.* 31, 9332–9344.
- Wang, H., Katagiri, Y., McCann, T.E., Unsworth, E., Goldsmith, P., Yu, Z.-X., Tan, F., Santiago, L., Mills, E.M., Wang, Y., et al. (2008). Chondroitin-4-sulfation negatively regulates axonal guidance and growth. *J Cell Sci* 121, 3083–3091.
- Weber, P., Bartsch, U., Rasband, M.N., Czaniera, R., Lang, Y., Bluethmann, H., Margolis, R.U., Levinson, S.R., Shrager, P., Montag, D., et al. (1999). Mice deficient for tenascin-R display alterations of the extracellular matrix and decreased axonal conduction velocities in the CNS. *J. Neurosci.* 19, 4245–4262.
- Wegner, F., Härtig, W., Bringmann, A., Grosche, J., Wohlfarth, K., Zuschratter, W., and Brückner, G. (2003). Diffuse perineuronal nets and modified pyramidal cells immunoreactive for glutamate and the GABA(A) receptor alpha1 subunit form a unique entity in rat cerebral cortex. *Exp Neurol* 184, 705–714.
- Weimann, J.M., Zhang, Y.A., Levin, M.E., Devine, W.P., Brûlet, P., and McConnell, S.K. (1999). Cortical neurons require Otx1 for the refinement of exuberant axonal projections to subcortical targets. *Neuron* 24, 819–831.
- Welsh, M.G., Sheridan, M.N., and Rollag, M.D. (1989). Cerebrospinal fluid-contacting area of the deep pineal: effects of photoperiod. *J. Pineal Res.* 7, 365–380.

- Wiesel, T.N., and Hubel, D.H. (1963). Single-cell responses in striate cortex of kittens deprived of vision in one eye. *J. Neurophysiol.* 26, 1003–1017.
- Winer, J.A., Miller, L.M., Lee, C.C., and Schreiner, C.E. (2005). Auditory thalamocortical transformation: structure and function. *Trends Neurosci* 28, 255–263.
- Wizenmann, A., Brunet, I., Lam, J.S.Y., Sonnier, L., Beurdeley, M., Zarbalis, K., Weisenhorn-Vogt, D., Weinl, C., Dwivedy, A., Joliot, A., et al. (2009). Extracellular Engrailed participates in the topographic guidance of retinal axons in vivo. *Neuron* 64, 355–366.
- Wolberger, C., Vershon, A.K., Liu, B., Johnson, A.D., and Pabo, C.O. (1991). Crystal structure of a MAT alpha 2 homeodomain-operator complex suggests a general model for homeodomain-DNA interactions. *Cell* 67, 517–528.
- Wyatt, A., Bakrania, P., Bunyan, D.J., Osborne, R.J., Crolla, J.A., Salt, A., Ayuso, C., Newbury-Ecob, R., Abou-Rayyah, Y., Collin, J.R.O., et al. (2008). Novel heterozygous OTX2 mutations and whole gene deletions in anophthalmia, microphthalmia and coloboma. *Hum Mutat* 29, E278–E283.
- Yamada, J., and Jinno, S. (2013). Spatio-temporal differences in perineuronal net expression in the mouse hippocampus, with reference to parvalbumin. *Neuroscience* 253, 368–379.
- Yamaguchi, Y. (2000). Leticans: organizers of the brain extracellular matrix. *Cell. Mol. Life Sci.* 57, 276–289.
- Yan, D., and Lin, X. (2009). Shaping morphogen gradients by proteoglycans. *Cold Spring Harb Perspect Biol* 1, a002493.
- Yang, B., Chang, Y., Weyers, A.M., Sterner, E., and Linhardt, R.J. (2012a). Disaccharide analysis of glycosaminoglycan mixtures by ultra-high-performance liquid chromatography-mass spectrometry. *J Chromatogr A* 1225, 91–98.
- Yang, E.-J., Lin, E.W., and Hensch, T.K. (2012b). Critical period for acoustic preference in mice. *Proceedings of the National Academy of Sciences* 109 Suppl 2, 17213–17220.
- Yang, H., Liu, S., Cai, H., Wan, L., Li, S., Li, Y., Cheng, J., and Lu, X. (2010). Chondroitin sulfate as a molecular portal that preferentially mediates the apoptotic killing of tumor cells by penetratin-directed mitochondria-disrupting peptides. *Journal of Biological Chemistry* 285, 25666–25676.
- Ye, Q., and Miao, Q.-L. (2013). Experience-dependent development of perineuronal nets and chondroitin sulfate proteoglycan receptors in mouse visual cortex. *Matrix Biol* 32, 352–363.
- Yoon, B.C., Jung, H., Dwivedy, A., O'Hare, C.M., Zivraj, K.H., and Holt, C.E. (2012). Local translation of extranuclear lamin B promotes axon maintenance. *Cell* 148, 752–764.
- Zhang, F., Moniz, H.A., Walcott, B., Moremen, K.W., Linhardt, R.J., and Wang, L. (2013). Characterization of the interaction between Robo1 and heparin. *Biochimie* 95, 2345–2353.
- Zhang, F., Sun, P., Muñoz, E., Chi, L., Sakai, S., Toida, T., Zhang, H., Mousa, S., and Linhardt, R.J. (2006). Microscale isolation and analysis of heparin from plasma using an

anion-exchange spin column. *Anal Biochem* 353, 284–286.

Zhang, H., Young, S.P., Auray-Blais, C., Orchard, P.J., Tolar, J., and Millington, D.S. (2011). Analysis of glycosaminoglycans in cerebrospinal fluid from patients with mucopolysaccharidoses by isotope-dilution ultra-performance liquid chromatography-tandem mass spectrometry. *Clin. Chem.* 57, 1005–1012.



